UNIVERSITY OF LONDON THESIS

Degree PhD Year 2008 Name of Author WARD, JORDAN, DAVID.

Insight into homologous recombination at replication blocking lesions through analysis of the *C. elegans* RAD-51 paralog, RFS-1.

Jordan David Ward

DNA Damage Response Laboratory

Clare Hall Laboratories

London Research Institute

Cancer Research UK

London

A thesis submitted for the degree of

Doctor of Philosophy

at the University of London

2008

ProQuest LLC
789 East Eisenhower Parkway
P.O. Box 1346
Ann Arbor, MI 48106-1346

I, Jordan Ward, declare that the work presented in this thesis is my own, except where acknowledged.

Abstract

The ability to sense and repair replication blocking DNA damage is a critical task for a cell, as evidenced by the embryonic lethality or cancer predisposition caused by mutation in any of these processes. Recent work has implicated homologous recombinational repair (HRR) as a key player in promoting genome stability in response to stalled replication forks, in addition to its well documented role of in the error-free repair of DNA double-strand breaks (DSBs). Although the five paralogs of the mammalian recombinase, Rad51, have been suggested to be general mediators of HRR, genetic evidence fails to support this hypothesis and their exact roles have remained elusive.

Here it is shown that the single *C. elegans* RAD-51 paralog, RFS-1, plays a specific role in promoting HRR at replication forks blocked by DNA cross-linking agents or camptothecin, but is dispensable for HRR at both meiotic and ionizing radiation-induced DSBs. Strikingly, RFS-1 is also dispensable for RAD-51 loading at forks collapsed by hydroxyurea or by the absence of the S-phase checkpoint, indicating that these lesions may resemble a conventional HRR substrate. *rfs-1* mutations suppress mitotic catastrophe in a *him-6*; *top-3(RNAi)* mutant background and accelerate polyG/C tract deletion in *dog-1* mutants, demonstrating that these genetic backgrounds drive the formation of replication blocking lesions, a notion that had been previously suggested but never validated. These data suggest that RFS-1 is not a general HRR mediator, but instead specifically promotes RAD-51 loading at replication fork barriers (RFBs).

Yeast two-hybrid (Y2H) screening identified a novel RFS-1-interacting protein, RIP-1, mutants of which phenocopied *rfs-1* mutants with respect to embryonic lethality, elevated apoptosis and the RAD-51 loading defect in response to replication fork blocking lesions. Use of Y2H analysis of RFS-1 fragments, followed by RFS-1 peptide

arrays, fine-mapped the interaction with RAD-51 to a single 30mer and interaction with RIP-1 to two distinct 30mers. Substitution peptide array analysis of RIP-1 has further refined the interaction surfaces; in the case of the RIP-1 binding peptides, two residues are critical for binding in each 30mer. These interaction studies, combined with promising attempts at purification of RFS-1 and RIP-1, open the possibility of detailed biochemical analysis of the role of these proteins in HRR at RFBs.

Preliminary work has explored the potential role of RFS-1 in aging and meiosis. Although the IGF-1 pathway transcriptional factor DAF-16 and the HRR factors HIM-6 and RFS-1 impact on spontaneous mutation rate, the mechanism behind this effect on mutation rate and interrelation between these proteins, is currently unclear. *rfs-1* and *rip-1* mutants both have an increased percentage of male progeny, indicating an elevation in X chromosome non-disjunction during meiosis. Additionally, loss of *rfs-1* suppresses RAD-51 accumulation in *mus-81; him-9/xpf-1* double mutants and evidence suggests that these recombination intermediates arise from meiotic DSBs as opposed to mitotic lesions. Elucidating how RFS-1, and presumably RIP-1, impact on meiotic recombination and whether this role is mechanistically distinct from a role in promoting HRR at RFBs will be an important avenue of future study.

Acknowledgements

First, an immense thank you to my supervisor, Simon Boulton, who took a chance on a skinny microbiologist from Red Deer. His passion and enthusiasm for science have proved infectious, and I am indebted to him for all of his encouragement and support. Thank you as well to my thesis committee members Dale Wigley and Vincenzo Costanzo for invaluable guidance; to Steve West for helpful advice; and to Tim Hunt for those enjoyable bacon breakfasts early in my PhD.

Thank you to all members of the Boulton lab, past and present, for making these four years so enjoyable: Julie Martin, Nicole Winkelmann, Usha Viveganantha n, Tati Garcia-Muse, Mark Petalcorin, the cross-link club members Spencer Collis and Louise Barber, Dragana Ahel, Zuzanna Horejsi, Visnja Pavicic-Kaltenbrunner, and Jill Youds. Special thanks to Tati for being such a good friend and desk neighbour, and for teaching me that the lab microwave is not for reheating food, like it was in my old lab; to Julie for her technical advice and for ensuring that the lab ran so smoothly; to Lou for teaching me so much about ICLs and for her company during those long worm counting sessions; to Spen for matching my low brow sense of humour and for three years of beer and curry following the GSN meeting in Cambridge (the only other Boulton lab member to ever partake in this); to Mark for his legendary stories and technical advice; and to Jill for her tireless effort in editing this work!

Big thanks to all of the people at Clare Hall over the past four years. They made me look forward to work every weekday morning. A special thanks to Christian Zierhut, Peter O'Donovan, Alberto Ciccia, Kristina Trenz, Luke Selth, Dirk Remus, Barbara Schuwirth, Thomas Wechsler, and the members of my PhD intake Eloise Smith and Diana Huttner.

I am grateful for the privilege of having so many superb friends outside of work: Seamus Heffernan, Jon Leslie, Mary Wu, Grant Otto, Megan Cully, Ditte Andersen, Inbal Ringel, Tim Schmidt, Aphro Bilioni, François Giudicelli, Joana Novais, Bruno Contreras-Moreira and Nadja Muncke. Thanks are in order for too many good times to count.

This work has been successful through the help of some phenomenal collaborators. Recognition must go to Nigel O'Neil and Ann Rose, Kiyotaka Kawaguche, Judith Yanowitz, Diego Muzzini and Federica Marini, Melissa Grabowski and Heidi Tissenbaum, Adriana LaVolpe, Susi Sigrid-Kaitna and Monique Zetka for their contributions.

The research infrastructure and services at the London Research Institute have greatly aided in this work. Much credit is due to the Fermentation, Equipment Park, Media services, the Bioinformatic and Biostatistics group (Mike Miller in particular), Nicola O'Reilly and the Peptide synthesis group, and to Erin Fortin and Sally Leevers for making life as a grad student so much easier.

Although I may joke about Red Deer, a huge acknowledgement goes to my family and friends for making me the man I am today. Thanks to my mom, dad, sister, brother-in-law, and Grannie, for their love, friendship, and support.

Finally, last but unquestionably not least, a massive thank you goes to my best friend and wife, Liz, for her love, encouragement and support. These four years have been among the best of my life, and I have learned so much (eg. clothes go in drawers, NOT on the floor, don't end sentences with prepositions, etc.). Additionally, she has helped this work immeasurably with her suggestions on organisation and grammar. A colossal acknowledgement must be made for her relentless work editing the first draft, where she learned more about DNA damage and homologous recombination than she cares to remember. Thanks Liz!

Table of Contents

Title Page 1
Declaration 2
Abstract 3
Acknowledgements 5
Table of Contents 6
List of Figures 10
List of Tables 12
List of Abbreviations 13

1 Chapter 1: Introduction 16
1.1 The DNA damage response 16
1.1.1 Sources of DNA damage 16
1.1.1.1 Ultraviolet light 16
1.1.1.2 Ionizing radiation 17
1.1.1.3 Chemical exposure 17
1.1.1.4 Endogenous damage 19
1.1.2 DNA repair 20
1.1.2.1 Direct damage reversal 20
1.1.2.2 Single-strand damage repair (BER, MMR, NER) 20
1.1.2.3 Double-strand break repair (HRR, NHEJ) 24
1.1.2.4 Damage tolerance 25
1.2 Homologous recombinational repair 26
1.2.1 HRR and DSB repair 26
1.2.1.1 Prokaryotic HRR 26
1.2.1.2 Eukaryotic HRR 28
1.2.2 Rad51 paralogs 37
1.2.2.1 Metazoan Rad51 paralogs 37
1.2.2.2 Rad51 paralogs in yeast 39
1.2.3 HRR and DNA replication 39
1.2.3.1 RecBCD and fork restart 39
1.2.3.2 HRR at non-DSB substrates in prokaryotes and eukaryotes 43
1.3 Replication fork barriers (RFBs) and genomic instability 44
1.3.1 Endogenous RFBs 44
1.3.1.1 DNA secondary structure 44
1.3.1.2 Intersection of replication and transcriptional machineries 45
1.3.1.3 Non-histone DNA-protein complexes 46
1.3.2 Genotoxic agents that induce RFBs 46
1.4 Interstrand cross-link (ICL) repair 47
1.4.1 Models of ICL repair 47
1.4.1.1 ICL repair in bacteria and yeast 47
1.4.1.2 ICL repair in mammals 51
1.5 *C. elegans* as a DNA repair model 56
1.5.1 Meiotic HRR 58
1.5.2 Mitotic HRR 59
1.5.3 RFB repair 60
1.6 The Biological question 62
1.6.1 RFS-1 plays a specific role at impeded replication forks 62

1.6.2 A novel RFS-1 interacting protein, RIP-1, also specifically responds to RFBs 63
1.6.3 RFS-1 and oxidative stress 63
1.6.4 RFS-1 and meiosis 64

2 Chapter 2: Materials and Method 66
2.1 *C. elegans* stocks and genetics 66
2.1.1 General *C. elegans* culturing 66
2.1.1.1 Culture conditions 66
2.1.1.2 Staging and sexing of animals 66
2.1.1.3 *C. elegans* strains used 67
2.1.2 DNA damage sensitivity assays 67
2.1.3 Scoring apoptosis 72
2.1.4 Cell cycle arrest assay 73
2.1.5 RNA interference 74
2.1.5.1 dsRNA generation and injection 74
2.1.5.2 RNAi by feeding 74
2.1.6 *C. elegans* neutral comet assay 75
2.2 Molecular biological techniques 76
2.2.1 PCR 76
2.2.1.1 PCR for cloning 76
2.2.1.2 PCR for *C. elegans* genotyping 77
2.2.1.3 PCR to monitor polyG/C tract stability 79
2.2.2 DNA sequencing 80
2.2.3 Gateway recombinational cloning 81
2.3 Bacterial strains and plasmids 81
2.4 Immunofluorescence 81
2.5 Microscopy 85
2.5.1 DeltaVision microscopy 85
2.6 Biochemical techniques 87
2.6.1 Protein expression 87
2.6.1.1 Protein expression using *E. coli* 87
2.6.2 Protein analysis 88
2.6.2.1 SDS-PAGE 88
2.6.2.2 Immuno-blotting 88
2.6.2.3 Immunoprecipitation from 293T cells 89
2.6.3 Protein purification 92
2.6.3.1 MBP tagged protein affinity purification 92
2.6.4 Peptide array analysis 93
2.6.4.1 Peptide array stripping 94
2.7 Antibody generation 94
2.7.1.1 Generation of anti-MRE-11 antibody 94
2.7.1.2 Generation of anti-RFS-1 antibodies 95
2.7.1.3 Generation of anti-RIP-1 antibodies 95
2.8 Yeast two-hybrid (Y2H) assays 96
2.8.1 Yeast transformation 96
2.8.2 Genome wide yeast two-hybrid screening 97
2.8.3 Small scale interaction matrices 99

3 Chapter 3: RFS-1 plays a specific role in promoting homologous recombination at impeded replication forks 101
3.1 Phenotypic analysis of *rfs-1(ok1372)* 101

3.1.1 RFS-1 appears to be the single *C. elegans* RAD-51 paralog 101
3.1.2 Description of *ok1372* allele of *rfs-1* 101
3.1.3 RFS-1 is dispensable for repair of meiotic DNA double-strand breaks.... 104
3.2 RFS-1 is required for repair of lesions that impede DNA replication 107
3.2.1 Lesions that impede replication forks cause increased progeny lethality, apoptosis, and chromosomal fragmentation in *rfs-1* mutants 107
3.2.2 *rfs-1* mutants are defective in RAD-51 loading at impeded replication forks 111
3.2.3 Mutations in *rfs-1* are responsible for the sensitivity to replication blocking lesions and a defect in RAD-51 loading at these lesions 115
3.3 Nature of the substrate onto which RFS-1 promotes RAD-51 loading 118
3.3.1 RFS-1 is dispensable for promoting homologous recombination at collapsed replication forks 118
3.3.2 Processed DSBs as a substrate at impeded forks 121
3.3.2.1 MUS-81 and XPF-1 are involved in HRR substrate generation at CDDP-induced lesions. 121
3.3.2.2 DSB generation in *rfs-1* mutants following CDDP treatment 125
3.3.3 RFS-1 promotes RAD-51 loading onto ssDNA 129
3.4 Endogenous substrates at which RFS-1 promotes HRR 129
3.4.1 RFS-1 is required for polyG/C tract stability in the absence of the DOG-1 helicase 129
3.4.2 Loss of RFS-1 suppresses mitotic catastrophe in the absence of HIM-6 and TOP-3 132
3.5 Discussion and Conclusions 136

4 Chapter 4: Characterization of R01H10.5, a novel RFS-1 interacting protein 145
4.1 Identification of R01H10.5 as an interacting partner of RFS-1 145
4.1.1 Y2H screening for RFS-1 interacting proteins 145
4.1.2 Reciprocal yeast two-hybrid screening to identify RIP-1 interacting proteins 147
4.2 Biological role of RIP-1 150
4.2.1 Phenotypic analysis of *rip-1(tm2948)* 150
4.2.2 Sensitivity to DNA damaging agents 153
4.2.3 RAD-51 focus formation following treatment with DNA damaging agents 153
4.3 Characterization of RFS-1-RIP-1 interaction domains 157
4.3.1 RAD-51 and RIP-1 bind to the same fragment of RFS-1 157
4.3.2 Peptide array analysis of RAD-51 and RIP-1 binding to RFS-1 159
4.4 Preliminary purification of RFS-1 and RIP-1 164
4.5 Discussion 171

5 Chapter 5: Work in progress 180
5.1 RFS-1 and oxidative stress 180
5.1.1 *daf-16* mutations increase mutation rates in *clk-2* and *him-6* mutants, but not in *rfs-1* mutants 181
5.1.2 *daf-16* mutations do not cause increased apoptosis or mitotic RAD-51 foci in *him-6* or *rfs-1* mutants 185
5.1.3 Conclusions 187

5.2 RFS-1 and meiosis 189
5.2.1 Him phenotype 189
5.2.2 Meiotic DSB repair through intersister HRR 190
5.2.3 *rfs-1* suppression of *mus-81; him-9/xpf-1* meiotic catastrophe 191
5.2.4 Conclusions 202

6 Chapter 6: Conclusions and Future Work 210
Published work 216
References 221
Appendix 209
Oligonucleotides used for this study (see following pages) 246
Reprints of papers to which this author has contributed (see following pages): 255

List of Figures

Figure 1.1. DSB repair model 30
Figure 1.2. Alternate eukaryotic DSBR models 36
Figure 1.3. HRR pathways and DNA replication in *E. coli* 41
Figure 1.4. Proposed mammalian ICL repair model 52
Figure 1.5. Features of *C. elegans* germ line. 57

Figure 3.1. Cladogram of the RAD-51 protein family 102
Figure 3.2. Alignment of RFS-1 with human, mouse, Arabidopsis and Drosophila RAD51D proteins 103
Figure 3.3. Gene, deletion, and domain architecture of RFS-1 105
Figure 3.4. RFS-1 is dispensable for meiotic recombination and crossing over. 106
Figure 3.5. Lesions that impede replication forks cause increased progeny lethality in *rfs-1* mutants 108
Figure 3.6. Replication blocking lesions caused increased apoptosis and chromosome fragmentation in *rfs-1* mutants 110
Figure 3.7. RFS-1 mutants are defective for RAD-51 focus formation specifically following ICL-induced DNA damage 112
Figure 3.8. CDDP-induced RAD-51 focus formation is defective, not delayed in *rfs-1* mutants 113
Figure 3.9. RFS-1 is dispensable for cell cycle arrest following HU treatment. 114
Figure 3.10. *eDf25* is a deficiency that deletes the entire coding region of *rfs-1* 116
Figure 3.11. *ok1372/eDf25* transheterozygotes display a similar sensitivity to DNA damaging agents as *rfs-1(ok1372)* homozygotes and also are defective for RAD-51 focus formation after CDDP but not IR 117
Figure 3.12. Potential HR substrates generated at fork blocking lesions 119
Figure 3.13. RFS-1 is not required for RAD-51 loading at collapsed replication forks 120
Figure 3.14. Gene, deletion, and domain architecture of MUS-81 122
Figure 3.15. MUS-81 and XPF-1 are involved in HRR substrate generation at CDDP-induced lesions 123
Figure 3.16. MRE-11 responds to both DSBs and replicative stress 127
Figure 3.17. RFS-1 is required for RAD-51 loading at UVC-induced lesions, but not for repair. 130
Figure 3.18. RFS-1 is required for stability of polyG/C/ tracts in the absence of DOG-1 133
Figure 3.19. *rfs-1* mutants suppress RAD-51 focus formation and mitotic catastrophe caused by the combined loss of HIM-6 and TOP-3 134

Figure 4.1. Yeast two-hybrid identification of RFS-1 interactors. 146
Figure 4.2. Verification of RFS-1-RIP-1 interaction by GST pull-down 148
Figure 4.3. RIP-1 is a true phylogenetic orphan protein. 149
Figure 4.4. Schematic of *rip-1* deletion 151
Figure 4.5. RIP-1 is dispensable for meiotic recombination and crossing over. 152
Figure 4.6. *rip-1* mutants are moderately sensitive to IR and HN2 but only exhibit increased apoptosis in response to HN2 154
Figure 4.7. RIP-1 mutants are also defective for RAD-51 focus formation specifically following replication blocking damage 155
Figure 4.8. RIP-1 is dispensable for the S-phase checkpoint and RAD-51 loading at collapsed forks 156

Figure 4.9. Mapping of RAD-51 and RIP-1 binding to RFS-1 by Y2H fragment analysis....158
Figure 4.10. Peptide array fine mapping of RAD-51 and RIP-1 binding sites on ..... RFS-1....161
Figure 4.11. Identification of RIP-1 interacting domains in RFS-1....163
Figure 4.12. Substitution analysis of RAD-51 binding to RFS-1....165
Figure 4.13. Development of RFS-1 and RIP-1 antibodies....167
Figure 4.14. Preliminary partial purification of RFS-1 and RIP-1. 170

Figure 5.1 Effect of *clk-2, daf-16,* and *him-6* mutations on spontaneous mutations rates....182
Figure 5.2. RAD-51 foci and apoptosis in *daf-16, him-6, rfs-1* single, double, and triple mutants....186
Figure 5.3. RFS-1 does not appear to play a role in the inter-sister pathway of meiotic DSB repair. 192
Figure 5.4. *rfs-1* mutations suppress RAD-51 accumulation in *mus-81; him-9/xpf-1* animals....194
Figure 5.5. Elevation of late pachytene RAD-51 levels in *mus-81, him-9/xpf-1, rfs-1,* and *mus-81; him-9/xpf-1* animals....196
Figure 5.6. RAD-51 accumulation in *mus-81; him-9/xpf-1* animals appears to arise from meiotic DSBs, but not through a defect in chromosome pairing 200

List of Tables

Table 1. Comparison of prokaryotic and eukaryotic DSBR factors 35
Table 2. *C. elegans* strains used in this study. 68
Table 3. Bacterial strains used in this study 82
Table 4. Plasmids used in this study. 83
Table 5. Antibodies used for immunofluorescence 86
Table 6. Antibodies used for immuno-blotting 90
Table 7. Brood size analysis of *daf-16, him-6, rfs-1* single, double, and triple mutants. 184
Table 8. Oligonucleotides used in this study. 247

List of Abbreviations

3AT	3-Aminotriazole
AD	Gal4p activation domain
Amp	Ampicillin
BCDX2	Complex consisting of RAD51B, RAD51C, RAD51D, XRCC2
BER	Base excision repair
BIR	Break-induced replication
BME	β-mercaptoethanol
bp	Base pair(s)
BSA	Bovine serum albumin
Cam	Chloramphenicol
CDDP	Cisplatin
CGC	*Caenorhabditis* genetics centre
CO	Crossover
CPD	Cyclobutane pyrimidine dimers
CPT	Camptothecin
CX3	RAD51C-XRCC3 complex
DAPI	4',6'-diamidino-2-phenylindole
DB	Gal4p DNA binding domain
dHJ	Double Holliday junction
DNA	Deoxyribonucleic acid
dNTP	Deoxyribonucleoside triphosphates
DOG-1	Deletions of guanine rich DNA
dRP	Deoxyribose phosphate
DSB	DNA double-strand break
dsDNA	Double-stranded DNA
dsRNA	Double-stranded RNA
DTC	Distal tip cell
DTT	Dithiothreitol
EDTA	Ethylenediaminetetraacetic acid
Emb	Embryonic lethality
FA	Fanconi anaemia
FRAXA	Fragile site on X chromosome-A
γH2AX	Phosphorylated variant histone H2AX
GST	Glutathione-S-transferase
Him	High incidence of males
His	Histidine
HJ	Holliday junction
HN2	Nitrogen mustard
HRP	Horseradish peroxidase
HRR	Homologous recombinational repair
HU	Hydroxyurea
ICL	Interstrand cross-link
IDL	Insertion-deletion loop

List of Abbreviations

IGF1	Insulin-like growth factor 1
IPTG	Isopropyl-beta-D-thiogalactopyranoside
IR	Ionizing radiation
Kan	Kanamycin
kb	kilobase pair(s)
kDa	kiloDalton
L4	*C. elegans* stage four larva
LB	Luria broth
Leu	Leucine
LiAc	Lithium acetate
MBP	Maltose-binding protein
MMC	Mitomycin C
MMR	Mismatch repair
*Mos*TIC	*MosI* excision-induced transgene instructed gene conversion
MRN	Complex consisting of Mre11-Rad50-Nbs1
MRX	Complex consisting of Mre11-Rad50-Xrs2
MutLα	MSH1-PMS2 heterodimer
MutSα	MSH2-MSH6 heterodimer
MutSβ	MSH2-MSH3 heterodimer
NER	Nucleotide excision repair
NHEJ	Non-homologous end joining
NMR	Nuclear magnetic resonance
O/N	Overnight
PBS	Phosphate buffered saline
PCNA	Proliferating cell nuclear antigen
PCR	Polymerase chain reaction
PEG	Polyethylene glycol
PFA	Paraformaldehyde
PFGE	Pulsed field gel electrophoresis
PI3K	Phosphoinositide 3-kinase
Polβ	DNA Polymerase beta
PolI	*E. coli* DNA polymerase I
rDNA	Ribosomal RNA gene repeats
RFB	Replication fork barrier
RFC	Replication factor C
RFS-1	RAD-51 short
RIP-1	RFS-1 interacting protein
RNA	Ribonucleic acid
RNAi	RNA interference
ROS	Reactive oxygen species
RPA	Replication protein A
rpm	Revolutions per minute
RT	Room temperature
S.E.M.	Standard error of the mean
S/N	Supernatant
SC	Synaptonemal complex

List of Abbreviations

SC-Leu	Synthetic complete dropout medium lacking leucine
SC-Leu,-Trp,-His,-Ura	Synthetic complete dropout medium lacking leucine, tryptophan, histidine, and uracil
SDSA	Synthesis-dependent strand annealing
SSA	Single-strand annealing
SSB	DNA single-strand break
SSB	*E. coli* DNA single stranded binding protein
ssDNA	Single-stranded DNA
std. dev.	Standard deviation
Strep	Streptomycin
TBS	Tris buffered saline
TBSB	Tris buffered saline-0.5% BSA
TBST	TBS+0.1% Tween-20
TBST-M	TBS+0.1% Tween-20+5% milk
TE	Tris-HCl-EDTA buffer
Tet	Tetracycline
TILLING	Targeting Induced Local Lesions IN Genomes
TLS	Translesion DNA synthesis
TMP	Trimethylpsoralen
TopI	Topoisomerase I
TopoIIIα	TopoisomeraseIIIα
Trp	Tryptophan
TUNEL	Terminal deoxynucleotidyl transferase-mediated dUTP-biotin nick end labeling
TZ	Transition zone
Ura	Uracil
UV	Ultraviolet radiation
UVA	Ultraviolet radiation-A (400-315 nm)
UVC	Ultraviolet radiation-C (254 nm)
Wt	Wild type
X-Gal	5-bromo-4-chloro-3-indolyl- beta-D-galactopyranoside
XP	Xeroderma pigmentosum
XP-V	Xeroderma pigmentosum -variant
Y2H	Yeast two-hybrid

1 Chapter 1: Introduction

1.1 The DNA damage response

The staggering number of human cancer predisposition syndromes caused by either loss or haploinsuffiency of DNA repair or checkpoint factors highlights the importance of genome instability as a driving factor in cancer development. The DNA damage response involves activation of a checkpoint to transiently halt the cell cycle, allowing time for repair factors to correct the damage or, should the damage be insurmountable, to induce apoptotic destruction of the cell.

1.1.1 Sources of DNA damage

DNA is an extremely reactive molecule that is subject to both spontaneous and environmental damage. Endogenous damage can arise from replicative errors, spontaneous alterations to base chemistry, loss of bases, or oxidative damage to bases (Friedberg *et al.* 1995). Environmental factors such as exposure to UV or ionizing radiation, or a wide array of chemical mutagens also pose a significant threat to DNA. As the work detailed in this thesis involves responses of *C. elegans* mutants to a number of DNA damaging agents, this introduction will outline sources of DNA damage relevant to this study and note their pertinent features.

1.1.1.1 Ultraviolet light

Ultraviolet light (UV), particularly UVC light (254 nm wavelength), is historically the most common agent used to experimentally induce DNA damage. Major UV lesions include cyclobutane pyrimidine dimers (CPDs), pyrimidine-pyrimidone (6-4) photoproducts, and DNA-protein cross-links (Friedberg *et al.* 1995).

CPDs involve covalent linkage of adjacent pyrimidines and are extraordinarily stable (Friedberg *et al.* 1995). UV also causes bulky, alkali labile lesions, mainly at cytosines located 3' to pyrimidine nucleosides, known as pyrimidine-pyrimidone (6-4) photoproducts (Friedberg *et al.* 1995). Extraordinarily high doses of UV are able to cause breakage of the polynucleotide chain, but the level of UV irradiation required to induce such damage is too high to be of biological significance (Friedberg *et al.* 1995).

1.1.1.2 Ionizing radiation

Ionizing radiation (IR) induces a wide array of direct and indirect lesions to DNA and is commonly used in conjunction with chemotherapy in cancer treatment. Direct effects derive from the transfer of radiation energy to the DNA while indirect lesions arise from the interaction of DNA with a reactive species generated by radiation elsewhere (Friedberg *et al.* 1995). It is thought that the primary lethal lesion directly generated by IR is a DNA double-strand break (DSB) (Friedberg *et al.* 1995). IR also directly causes DNA single-strand breaks (SSBs) by transferring energy to deoxyribose. Generation of reactive oxygen species as a result of energy transfer to water indirectly causes extensive forms of base damage and additional SSBs (Friedberg *et al.* 1995). Protein-DNA cross-links are also generated and it is thought that IR also catalyzes DNA inter- and intrastrand cross-linking, though whether cross-linking plays significant role in IR pathology remains unknown. It should be highlighted that due to the energy transferred by IR, SSBs and DSBs will very likely possess base damage at their termini and require additional enzymatic processing before becoming suitable substrates for canonical DNA repair pathways (Friedberg *et al.* 1995).

1.1.1.3 *Chemical exposure*

Chemical DNA damaging agents relevant to this study include hydroxyurea (HU), camptothecin, and DNA cross-linking agents. Hydroxyurea inhibits

ribonucleotide reductase, which depletes of the cellular pool of deoxyribonucleoside triphosphates (dNTPs), and at high doses causes replication fork collapse (Lundin *et al.* 2002). As dNTP depletion stalls the polymerase but not the replicative helicase, HU treatment results in processive unwinding of the DNA and generates large tracts of single stranded DNA (ssDNA), approximately 320 base pairs (bp) in length (Sogo *et al.* 2002).

Camptothecin (CPT) is a DNA topoisomerase I (TopI) inhibitor used in the treatment of cancer and is derived from the bark and stem of the *Camptotheca acuminata* tree. TopI functions to relieve torsional constraint in DNA by binding dsDNA, nicking one strand, rotating the free end around the intact strand to dissipate stress, and religating the strand (Stewart *et al.* 1998). Camptothecin creates replication-dependent DSBs by trapping TopI in an intermediate step of this catalytic cycle through a replication runoff mechanism (Strumberg *et al.* 2000). In this model, when a leading strand replisome encounters a CPT-trapped TopI complex, it proceeds to the end, running off the template strand at the site of the ssDNA nick (Strumberg *et al.* 2000). In one study, no DSBs were detected on the lagging strand, suggesting that the replisome either pauses or bypasses the nick (Strumberg *et al.* 2000).

Bifunctional DNA cross-linking agents are chemicals with two reactive groups that can react with the same strand of DNA, to form intrastrand cross-links, or opposing strands of DNA, to form interstrand cross-links (ICLs) (Friedberg *et al.* 1995). ICLs are a notably cytotoxic lesion as they inhibit the cellular processes of replication and transcription; consequently, cross-linking agents are powerful chemotherapeutic agents. Mechlorethamine, or nitrogen mustard (HN2), is a bifunctional alkylating agent that forms ICLs at a relatively low level (approximately 4% of DNA-bound HN2 forms ICLs) (Friedberg *et al.* 1995). However, the ICL is thought to be the primary cytotoxic lesion in the nitrogen mustard class of cross-linking agent, as the ability to form ICLs

correlates very well with cytotoxicity (O'Connor and Kohn 1990; Sunters *et al.* 1992). *cis*-diamminedichloroplatinum (cisplatin, CDDP), another type of cross-linking agent, is activated in aqueous solutions and is able to attack protein, DNA, and RNA (Friedberg *et al.* 1995; Jakupec *et al.* 2003). CDDP forms three types of intrastrand cross-links, as well as ICLs, and the predominant 1,2-intrastrand cross-link (approximately 90% CDDP bound to DNA forms this lesion) is thought to be the primary cytotoxic lesion, though there is evidence that ICLs contribute to cytotoxicity as well (Zwelling *et al.* 1979; Fichtinger-Schepman *et al.* 1985; Pinto and Lippard 1985). Trimethylpsoralen (TMP) is a planar cross-linking agent that initially is only able to bind one strand of DNA to form a monoadduct (Friedberg *et al.* 1995). Treatment with UVA radiation (400-315 nm) activates a second reactive group on the TMP molecule, allowing it to react with the opposite DNA strand to form an ICL (Friedberg *et al.* 1995). A detailed description of repair of ICLs and the relevant intermediates formed will be the subject of section 1.4.

1.1.1.4 Endogenous damage

Of the spontaneous sources of DNA damage previously mentioned, the most relevant to the work described here are reactive oxygen species (ROS). Oxygen free radicals are a by-product of aerobic metabolism and ROS levels have been strongly correlated with both organism metabolism and aging rate (Adelman *et al.* 1988; Marnett and Plastaras 2001; De Bont and van Larebeke 2004). DNA damage can result either from a direct attack by the radicals on DNA bases or deoxyribose, or through oxidation of lipids or proteins to generate molecules that can form adducts on DNA (Marnett and Plastaras 2001). It has been suggested that genomic instability in tumour cells might be driven by an inability to deal with the increased ROS load accompanying their rapid growth rate (Jackson and Loeb 2001).

1.1.2 DNA repair

The reactivity of DNA and unrelenting mutagenic pressure on it is a threat to genomic stability, the loss of which can drive cell death or cancer. Consequently, organisms have evolved a number of mechanisms to repair damage to their DNA. The mechanisms can be classified by their mode of action and the types of lesions they deal with: direct reversal, single strand damage, double strand damage, and lesion bypass. As DNA repair processes are extremely complex and a large number of detailed mechanisms are known, this introduction will briefly summarize the majority of mechanisms while giving a more thorough description of the most relevant pathways.

1.1.2.1 Direct damage reversal

Thymine dimers and alkylated bases can be repaired through direct reversal of the lesion. The enzyme photolyase is able to harness the energy in light (300-500 nm) to catalyze separation of the linked bases (Friedberg *et al.* 1995). Repair of methylated guanine residues involves methyl guanine methyl transferases, which catalyze the removal of the methyl group in an energetically expensive, stoichiometric process (Sedgwick *et al.* 2007). Repair of alkylated adenine and cytosine bases occurs in a mechanistically distinct manner through oxidative demethylation catalyzed by DNA dioxygenases (Sedgwick *et al.* 2007).

1.1.2.2 Single-strand damage repair (BER, MMR, NER)

Repair of single strand damage can proceed through base excision repair (BER), mismatch repair (MMR), or nucleotide excision repair (NER) pathways. BER repairs damage to bases from alkylation, oxidation, hydrolysis, or deamination. Two forms of BER exist: short patch and long patch. Both forms initiate with excision of a damaged

base by a DNA glycosylase (Fortini *et al.* 2003). In short patch BER, in which a single nucleotide is replaced, an incision is made either 5' to the abasic site by an AP endonuclease or 3' to the site by a 3' lyase (Fortini *et al.* 2003). These incisions result in formation of a 5'-abasic sugar phosphate (deoxyribose phosphate; dRP) or a 3'-fragmented deoxyribose, respectively (Memisoglu and Samson 2000). The intermediates are processed by the dRPase activity of DNA polymerase β (Polβ) or a 3'phosphodiesterase, respectively (Fortini *et al.* 2003). Polβ can then fill in the resulting one base pair (bp) gap and the remaining ssDNA break can be sealed by DNA ligase I or III (Memisoglu and Samson 2000). Long patch BER is similar, except that 2-13 nucleotides are replaced. Following AP endonuclease cleavage, the 3' hydroxyl group opposite the dRP residue is extended by either DNA polymerase δ or ε, requiring the replicative β clamp, proliferating cell nuclear antigen (PCNA) (Memisoglu and Samson 2000). This DNA synthesis results in displacement of the strand containing the dRP residue, generating a flap that is the substrate for the FEN1 endonuclease, which cleaves off the flap to leave a SSB that is sealed by DNA ligase (Memisoglu and Samson 2000).

MMR corrects base substitution mismatches and insertion-deletion loop (IDL) mismatches formed as a result of aberrant replication and recombination. MMR is initiated by binding of either the MSH2-MSH6 (MutSα) or MSH2-MSH3 (MutSβ) heterodimer to the mismatch (Kunkel and Erie 2005). The meiosis specific MSH4-MSH5 heterodimer will be discussed in the section on *C. elegans* meiosis (see section 1.5.1). MutSα primarily repairs single base and IDL mismatches, while MutSβ responds to IDL mismatches of up to 16 bp in length (Kunkel and Erie 2005). The MLH1-PMS2 (MutLα) heterodimer plays the most prominent role in MMR with MutLβ and δ complexes playing either unknown or minor roles, respectively (Kunkel and Erie 2005). MMR begins at a pre-existing nick, thought to be between Okazaki

fragments of the lagging strand, following DNA replication (Kunkel and Erie 2005). Replication factor C (RFC) binds to one such nick that is adjacent to the mismatch; this binding can occur either 5' or 3' to the lesion. RFC then loads PCNA at the nick site. RFC, PCNA, and MutSα activate a latent endonuclease activity of MutLα that is biased to the opposite side of the mismatch on the discontinuous strand (Kadyrov *et al.* 2006). MutSα, MutLα and replication protein A (RPA) then interact with ExoI, an exonuclease of 5'-3' polarity, to direct removal of the mismatch, after which DNA synthesis and ligation restore the DNA duplex (Modrich 2006). The endonuclease bias of MutLα is important as it provides a 5' end when the nick is 3' to the mismatch; otherwise, the polarity of ExoI would cause it to travel away from the mismatch when loaded at the nick site.

NER predominantly catalyzes the repair of UV-induced lesions, though it also plays a role in repair of ICLs, which will be outlined in section 1.4. NER repair mechanisms and the substrates it generates are particularly relevant to data presented in Chapter 3; therefore, this repair pathway will be presented in more depth. In budding yeast, genetic analysis of an extensive collection of loci that caused enhanced sensitivity to UV or ionizing radiation placed them into three epistasis groups (Rad3, Rad6, Rad52) thought to mediate distinct responses to DNA damage (Friedberg *et al.* 1995). The Rad3 group mediates the response to UV light and constitutes the NER pathway of repair while the Rad52 group are involved in homologous recombination and will be discussed in depth in section 1.2.1.2. The Rad6 group promotes post-replicative repair and will be briefly discussed in section 1.1.2.4. Mutation in NER factors in humans causes the skin cancer predisposition syndrome Xeroderma pigmentosum (XP), a disorder characterized by extreme sensitivity to sunlight. Mutations in specific NER factors can also cause the developmental disorders Cockayne's syndrome (*CSA* and *CSB* mutations) and trichothiodystrophy (*XPB* and *XPD* mutations) (Friedberg 2001).

As the mechanisms involved in eukaryotic NER were originally elucidated in budding yeast, this process will be the focus, with attention paid to important additional characteristics of mammalian NER, where appropriate.

The first stage of global genome repair, the basic form of NER, involves lesion recognition mediated by Rad4-Rad23 (XPC-hHR23B in humans) and Rad7-16 (no human homolog) heterodimers (Prakash and Prakash 2000). This step is believed to generate helical torsion to drive DNA unwinding and lesion excision. In addition to XPC, human cells also require the Rad14 homolog, XPA, for lesion recognition (Batty and Wood 2000). The heterotrimeric ssDNA binding protein RPA is also involved in recognition of damaged DNA and excision of the lesion (Huang *et al.* 1998; Prakash and Prakash 2000). The remaining NER factors are recruited by TFIIH and Rad14 (Prakash and Prakash 2000). Two helicases, Rad3 (XPD in humans) and Rad25 (XPB in humans) then unwind the DNA by translocating in the 5'-3' and 3'-5' directions, respectively (Sung *et al.* 1996; Evans *et al.* 1997). The ssDNA-dsDNA junctions are incised 5' to the lesion by the Rad1-Rad10 (XPF1-ERCC1 in humans) endonuclease and 3' to the lesion by the Rad2 (XPG in humans) endonuclease (Bardwell *et al.* 1994; Habraken *et al.* 1995; Friedberg 2001). These incisions release a 24-32 base oligonucleotide fragment and the gap is then restored by DNA synthesis, with the remaining nicks sealed by DNA ligase I (Guzder *et al.* 1996; Prakash and Prakash 2000). In human cells, XPA also plays a role in recruiting nucleases and there may be a sequential cutting by the nucleases, with XPG mediating recruitment of XPF to the lesion (Wakasugi and Sancar 1998). In DNA undergoing active transcription a specialized form of NER known as transcription coupled repair occurs. Damage recognition in this instance is mediated by Rad26-Rad28 (CSB-CSA in humans) binding to stalled RNA Pol II (van Gool *et al.* 1994; Bhatia *et al.* 1996). These proteins

catalyze ubiquitination and removal of the stalled polymerase and allow NER factors access to the lesion (Balajee and Bohr 2000; Somesh *et al.* 2005).

1.1.2.3 Double-strand break repair (HRR, NHEJ)

Repair of double stranded lesions proceeds either through the error-prone non-homologous end-joining pathway (NHEJ) or through accurate homologous recombinational repair (HRR). HRR is a critical aspect of this thesis and will be discussed in detail in section 1.2. There is a bias towards repair of DSBs by NHEJ in G1, as the absence of sister chromatids precludes the possibility of HRR (Burma *et al.* 2006). The minimal set of proteins required to perform NHEJ in humans are the Ku70-Ku80 heterodimer, DNA-PKcs, and the XRCC4-Ligase IV complex (Burma *et al.* 2006). DSBs are bound with high affinity by the ring shaped Ku complex that then recruits the serine/threonine kinase DNA-PKcs to the break (Burma *et al.* 2006). In addition to regulatory phosphorylation, DNA-PKcs may play an accessory role in tethering the ends of the DSB together (Burma *et al.* 2006). The DNA-PKcs substrate XRCC4 is recruited along with the tightly bound Ligase IV, which stimulates religation of the break (Burma *et al.* 2006). The XLF protein is thought to facilitate efficient NHEJ by promoting XRCC4-LigIV activity (Burma *et al.* 2006). Any genetic information lost at the break site will not be restored through this repair mechanism, making it error-prone. NHEJ is therefore a less desirable method of DSB repair than HRR, explaining its restriction to G1.

Complex DSBs require additional processing involving factors beyond those described above. Classical processing can involve removal of DNA hairpins by Artemis or the filling of the break end by DNA polymerases to generate an intact end (Weterings and Chen 2008). Alternative processing involves the XLF/Cernunnos protein and is thought to invoke ligation of non-compatible ends. XLF promotes

ligation of a blunt end to a 3' ssDNA overhang, which could provide a substrate for a DNA polymerase to fill in the ssDNA gap (Tsai *et al.* 2007). Ligation of the ssDNA nick left by the polymerase, would complete the repair of non-compatible ends while avoiding break resection (Weterings and Chen 2008).

1.1.2.4 Damage tolerance

The majority of repair pathways outlined here are inherently error-free, with the exception of NHEJ. However, during DNA replication, situations can arise where lesions block progression of the replication fork and accuracy is sacrificed in order to complete replication. Here, the lesions are bypassed through the use of low fidelity polymerases in a process known as translesion synthesis (TLS). There are four Y-family TLS polymerases in mammalian cells (Pols η, ι, κ and Rev1), as well as the B family DNA polymerase, Polζ (comprised of Rev3 and Rev7 subunits) (Lehmann 2006). Polη mutations cause Xeroderma pigmentosum-variant (XP-V), implicating it in repair of UVC-induced lesions. Polη has been shown to replicate past CPD photoproducts, inserting the correct bases (Lehmann 2006). Due to its low processivity, it likely dissociates rapidly after bypassing a CPD (Lehmann 2006). Polη cannot bypass 6-4 photoproducts, but data suggests Rev1 and Polζ play a role in this process (Lehmann 2006).

The specific roles for the TLS polymerases in repair of other lesions are poorly defined, but Rev1, Rev3, and Rev7 were identified as requisite for DNA damaging agent-induced mutagenesis (Lehmann 2006). The Y-family polymerases are nuclear and colocalize with PCNA during S-phase (Lehmann 2006). Upon encountering replication-blocking lesions PCNA is mono-ubiquitinated by the Rad6 E2 ubiquitin conjugating enzyme and the Rad18 ubiquitin ligase (Hoege *et al.* 2002). This mono-

ubiquitination is believed to cause a polymerase switch, substituting the replicative polymerase for a TLS counterpart in an attempt to bypass the lesion.

1.2 Homologous recombinational repair

1.2.1 HRR and DSB repair

A DSB is a lethal event to a cell if left unrepaired. Consequently, cells have evolved mechanisms to ensure faithful repair of the break. As mentioned previously, during the G1 phase of the cell cycle in the absence of a replicated sister chromatid, breaks are preferentially repaired through NHEJ. Since this involves religation of the break without restoring any lost genetic information, it is an inherently error prone process and also has the potential to cause translocations because incorrect termini can be ligated. The alternative to NHEJ is homologous recombinational repair, which uses the intact sister or homologous chromosome as a template to facilitate error-free repair of the DSB.

1.2.1.1 Prokaryotic HRR

The process of homologous recombination was first elucidated in *E. coli* through study of bacterial conjugation. Pioneering work by Clark and Margulies (1965) isolated the first known recombination defective mutant in a screen for bacteria defective in integrating conjugated DNA into their genomes. Since then, a very detailed understanding of prokaryotic HRR has been gained, and mechanistically the process is strikingly similar to eukaryotic HRR. In wild type *E. coli*, the basic genetic requirements for recombination are the RecA protein, the RecBCD enzyme, DNA single-strand binding protein (SSB), DNA polymerase I, DNA gyrase, DNA ligase, and either RecG or the RuvABC enzyme (Kowalczykowski and Eggleston 1994). In the absence of RecBCD, alternative pathways can compensate, such as the RecET or

RecFOR pathways. The role of RecFOR in promoting HRR at non-DSB substrates will be discussed in section 1.2.3.2. The RecBCD pathway generally promotes recombination using linear duplex DNA substrates, usually generated by conjugation, transduction, or transformation. Upon encountering linear dsDNA, the RecBCD complex loads onto an end and translocates exceptionally rapidly (1000 bp/sec) and processively (30,000 bp/binding event) through ATP hydrolysis by its twin helicases of opposite polarity, RecB and RecD (Roman *et al.* 1992; Dillingham *et al.* 2003). The RecBCD complex also possesses nuclease activity and initially degrades the strand terminating with a 3' hydroxyl group (Dixon and Kowalczykowski 1995). Upon encountering an octameric DNA sequence known as Chi (5'-GCTGGTGG-3') the rate of degradation is reduced and the nuclease polarity is switched to degrade the 5' terminating strand (Anderson and Kowalczykowski 1997). Since the helicases still proceed, the switch in polarity results in a single stranded region of DNA terminated at its 3' end by the Chi sequence. Finally, RecBCD stimulates recombination by directly loading the RecA protein onto ssDNA (Anderson and Kowalczykowski 1997). RecA can then oligomerize to form helical filaments that have the remarkable ability to identify and invade homologous sequences through a strand exchange reaction to form what is known as a D-loop (see Figure 1.1D, in following section) (West *et al.* 1981; Cox and Lehman 1982; Kowalczykowski and Eggleston 1994). DNA polymerase I (PolI) is then able to extend the 3' invading end of the D-loop (Kowalczykowski and Eggleston 1994). DNA gyrase (Topoisomerase II) is crucial for relieving torsional constraints, especially when the invaded DNA is covalently closed, as is the case in most prokaryotic genomes (Cassuto 1984; Ennis *et al.* 1987; Kowalczykowski and Eggleston 1994). The RuvAB complex binds to recombination intermediates and promotes branch migration of the invaded DNA while the RuvC homodimer is able to symmetrically cleave four-stranded DNA structures, also known as Holliday junctions

(HJs), on strands of like polarity (Connolly and West 1990; Iwasaki *et al.* 1991; West and Connolly 1992; Bennett *et al.* 1993). The remaining nicks left by HJ resolution are then sealed by DNA ligase (Iwasaki *et al.* 1991; Bennett *et al.* 1993). The branch-migration activity of RuvAB is not essential in a wild type bacterium, because the RecG protein compensates for loss of activity. Although the exact mechanism through which RecG accomplishes this is not completely understood, it is thought to involve binding to junction DNA to catalyze branch migration in the opposite direction to RecA-directed strand exchange (Whitby *et al.* 1993; Whitby *et al.* 1994). This branch migration is predicted to disrupt RecA-mediated pairing and result in dissolution of the D-loop (Lloyd and Sharples 1993; Kuzminov 1999). A model illustrating the common features of prokaryotic and eukaryotic HRR will be presented in section 1.2.1.2.

1.2.1.2 Eukaryotic HRR

In eukaryotes, HRR is an error-free DNA double-strand break repair pathway that uses either an intact sister chromatid or homologous chromosome to repair the break. The other major DNA repair classification to emerge from yeast genetic analysis of radiation sensitive mutants is the Rad52 epistasis group. The Rad52 epistasis group includes Rad50, Rad51, Rad52, Rad54, Rad55, Rad57, Rad59, Mre11 (formerly Rad58), and Xrs2. Of these factors, Rad51, Rad52 and Rad54 are most important for HRR. The key HRR factors and their functions will be introduced first and subsequently four models of HRR, which use different combinations of these factors, will be presented (Szostak DSB repair model, synthesis-dependent strand annealing (SDSA), break-induced replication (BIR), and single strand annealing (SSA)). The mechanism of eukaryotic HRR was first delineated in yeast, which will thus be the focus here, and differences between yeast and mammalian HRR will be noted where appropriate.

The *E. coli* model of HRR outlined previously in section 1.2.1.1 is most similar to the DSB repair model of HRR proposed by Szostak and co-workers (1983). Following resection of the break to generate a 3' ssDNA tail, a recombinase protein is loaded onto this tail, which catalyzes invasion into a stretch of homologous DNA to form a D-loop (Figure 1.1A-D). The 3' end of the invading strand is extended by DNA synthesis and the displaced strand is able to pair with the other end of the DSB in a process called second end capture (Figure 1.1D,E). Ligation of the free ends creates two Holliday junctions that must be resolved to complete recombination (Figure 1.1F).

A common feature of all HRR models is extensive resection of one strand of the DNA to create a 3' tail, very similar to the intermediate produced by RecBCD after encountering a Chi site. The Mre11-Rad50-Xrs2 (MRX) complex is critical for this resection in both mitosis and meiosis, but does not appear to possess the appropriate nuclease activity as its *in vitro* exonuclease activity is of the opposite polarity (Ivanov *et al.* 1994; Tsubouchi and Ogawa 1998). Similar to its *E. coli* counterpart, SbcCD, Mre11 has a hairpin nuclease activity believed to be important for processing the ends of DSBs and promoting HRR at palindromic sequences (Sharples and Leach 1995; Connelly *et al.* 1998; Lobachev *et al.* 2002). The Xrs2 (NBS1 in humans) protein is thought to be involved in targeting the complex to DSBs (Trujillo *et al.* 2003). Rad50 contains two hook domains, flexible zinc-configuring motifs that when free from DNA are typically in an orientation that favours an intracomplex interaction (Moreno-Herrero *et al.* 2005; Wiltzius *et al.* 2005). Binding to DNA leads to a conformational change that favours an intercomplex interaction (Moreno-Herrero *et al.* 2005). Coordinate binding of a Zn^{2+} ion then links two Rad50 molecules in separate complexes, which can

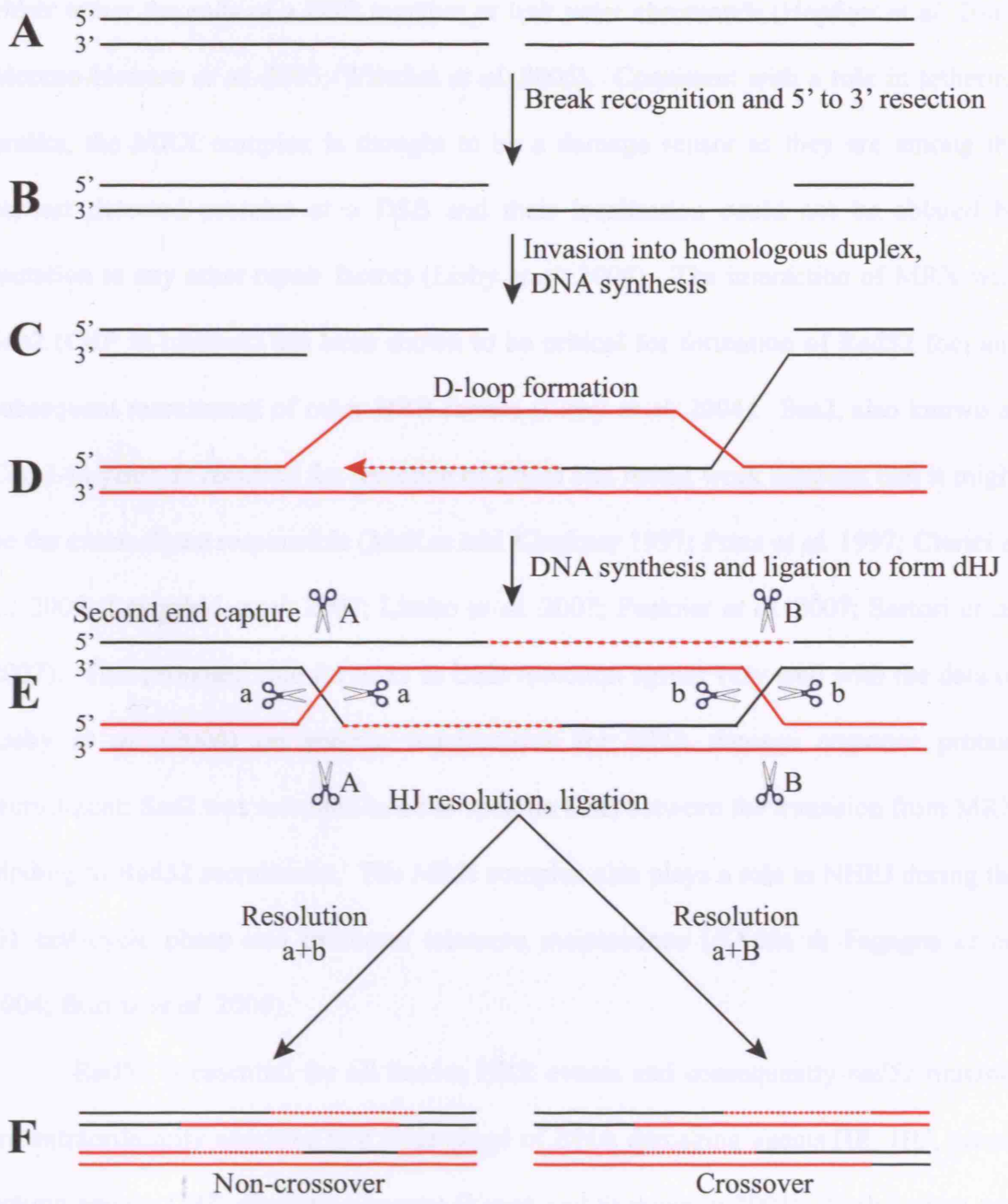

Figure 1.1. DSB repair model. (A,B) Following DSB formation, the ends are recognized and resected by an exonuclease in a 5' to 3' direction resulting in formation of two 3' ssDNA tail. (C) Loading of a recombinase protein catalyzes invasion of one 3' tail into a homologous DNA duplex. (D) DNA synthesis initiated from the 3' hydroxyl group leads to the formation of a D-loop. (E) The subsequent annealing of the D-loop and resected 3' tail from the other end of the DSB is referred to as second-end capture. This provides a 3' end to allow DNA synthesis across the D-loop. Ligation of the newly synthesized ends to the break termini results in formation of a double Holliday junction (dHJ). (F) Symmetrical endonucleolytic cleavage of two strands of the junction resolves the dHJs and depending on the plane of the cuts (a+b or a+B) either a non-crossover or crossover outcome is possible. (Adapted from Krogh and Symington, 2004)

either tether the ends of a DSB together or link sister chromatids (Hopfner *et al.* 2002; Moreno-Herrero *et al.* 2005; Wiltzius *et al.* 2005). Consistent with a role in tethering breaks, the MRX complex is thought to be a damage sensor as they are among the earliest detected proteins at a DSB and their localisation could not be ablated by mutation in any other repair factors (Lisby *et al.* 2004). The interaction of MRX with Sae2 (CtIP in humans) has been shown to be critical for formation of Rad52 foci and subsequent recruitment of other HRR factors (Lisby *et al.* 2004). Sae2, also known as Com1 in yeast, is required for resection of DSBs and recent work suggests that it might be the exonuclease responsible (McKee and Kleckner 1997; Prinz *et al.* 1997; Clerici *et al.* 2005; Lengsfeld *et al.* 2007; Limbo *et al.* 2007; Penkner *et al.* 2007; Sartori *et al.* 2007). This proposed role for Sae2 in DSB resection agrees very well with the data of Lisby *et al.* (2004) on genetic requirements for DNA damage response protein recruitment; Sae2 was recruited to a site specific DSB between the transition from MRX binding to Rad52 recruitment. The MRX complex also plays a role in NHEJ during the G1 cell-cycle phase and promotes telomere maintenance (d'Adda di Fagagna *et al.* 2004; Burma *et al.* 2006).

Rad52 is essential for all known HRR events and consequently *rad52* mutants are extraordinarily sensitive to a wide range of DNA damaging agents (IR, HU, cross-linking agents, CPT, alkylating agents) (Krogh and Symington 2004). Both human and yeast Rad52 form ring shaped oligomers with the ability to promote annealing of ssDNA (Reddy *et al.* 1997; Shinohara *et al.* 1998; Stasiak *et al.* 2000). Rad51 is another key protein as it is required for all modes of HRR with the exception of SSA. Rad51, Rad55, and Rad57 are all homologous to bacterial RecA at the sequence level, but Rad51 is the sole functional homolog, since only Rad51 is able to promote strand exchange and forms similar filaments on ssDNA (Shinohara *et al.* 1992; Ogawa *et al.* 1993; Sung 1994). Rad52 preferentially binds ssDNA, displaces RPA, and loads

Rad51, then stimulates Rad51 strand exchange activity, which results in formation of a D-loop (Sung 1997; New *et al.* 1998; Shinohara and Ogawa 1998; Sugiyama *et al.* 1998; Parsons *et al.* 2000; Song and Sung 2000; Sugawara *et al.* 2003). The polymerization of the Rad51 protein into a filament is regulated by Rad52 and the Rad51 paralogs (Rad55 and Rad57 proteins), while the Rad54 protein is believed to play a key role in remodelling chromatin to facilitate repair (Petukhova *et al.* 1999; Sugawara *et al.* 2003). The preferential substrate for Rad51 is dsDNA with an 3' ssDNA tail, consistent with the critical role for the MRX complex in promoting HRR (Mazin *et al.* 2000).

A major difference between yeast and vertebrate cells is that BRCA2 appears to have assumed many of the roles of yeast Rad52. While vertebrate cells lacking Rad52 are defective in HRR they are not sensitive to DNA damaging agents, which is in sharp contrast to the extreme DNA damage sensitivity and embryonic lethality caused by reduction or loss of BRCA2 function, respectively (Connor *et al.* 1997; Sharan *et al.* 1997; Patel *et al.* 1998; Rijkers *et al.* 1998; Yamaguchi-Iwai *et al.* 1998). Mutations in BRCA2 are responsible for the D1 complementation group of Fanconi anaemia, an autosomal recessive disorder characterized at the cellular level by extreme sensitivity to DNA cross-linking agents, and resulting in congenital abnormalities, progressive bone marrow failure, and cancer predisposition (Howlett *et al.* 2002). Although its physical interaction with Rad51 and DNA damage sensitivity clearly implicates BRCA2 in playing a key role in HRR, its massive size (3418 amino acids) has precluded detailed biochemical analysis (Wong *et al.* 1997; Chen *et al.* 1998). Strikingly, a number of higher metazoan genetic model systems that lack Rad52 have BRCA2 homologs (*C. elegans, D. melanogaster, Ustilago maydis*) (Modesti and Kanaar 2001). *C. elegans* and *Ustilago maydis* are particularly noteworthy as the BRCA2 homologs are significantly shorter than their mammalian counterparts (394 and 1075 residues,

respectively) allowing for detailed structural and mechanistic characterization (Martin *et al.* 2005; Yang *et al.* 2005). Both BRCA2 homologs preferentially bind dsDNA-ssDNA junctions and *Ustilago* Brh2 has been shown to catalyze nucleation of Rad51 onto this substrate (Martin *et al.* 2005; Yang *et al.* 2005). CeBRC-2 is important for transport of RAD-51 into the nucleus, promotes RAD-51 focus formation in mitosis and meiosis, and promotes a RAD-51-independent mode of meiotic DSB repair that is distinct from NHEJ (Martin *et al.* 2005). Further work on CeBRC-2 demonstrated that it could promote single strand annealing similar to Rad52, a likely candidate for the RAD-51-independent repair pathway (Petalcorin *et al.* 2006).

Higher metazoans do not contain Rad55 or Rad57 homologs. Instead, in vertebrate cells, there are five Rad51 paralogs (RAD51B, RAD51C, RAD51D, XRCC2, XRCC3). As this thesis involves characterization of a *C. elegans* Rad51 paralog, the properties of the mammalian paralogs and recently discovered additional yeast Rad51 paralogs will be discussed in detail in section 1.2.2.

As described in section 1.2.1.1, resolution of HJs in *E. coli* involves either the RuvABC or RecG proteins. Although mammalian cells contain factors that symmetrically cleave HJs, fractionation of extracts has failed to identify the responsible protein(s), though the activity is associated with the Rad51 paralogs; resolvase activity is reduced in *RAD51C* and *XRCC3* defective cell lines, and lost when RAD51C is immunodepleted from fractionated extracts (Liu *et al.* 2004). In fission yeast and human cells, the structure specific endonuclease Mus81-Eme1 is able to cleave nicked HJs, but prefers branched substrates by an order of magnitude (Boddy *et al.* 2001; Constantinou *et al.* 2002). Although certain recombinant preparations of budding and fission yeast are able to cleave intact HJs, the symmetrical cleavage activity in human cells does not fractionate with Mus81-Eme1 so the identity of the mammalian resolvase remains unknown (Gaskell *et al.* 2007; West 2008). Alternatively, a complex

consisting of the BLM helicase, Topoisomerase IIIα, and BLAP75 is able to dissolve HJs into non-crossover products similar to the budding yeast homologs (Ira *et al.* 2003; Wu and Hickson 2003; Raynard *et al.* 2006). A comparison of *E. coli, S. cerevisiae,* and human recombination proteins is presented in Table 1.

An alternative to the model presented in Figure 1.1 was devised to explain the low levels of crossing-over that occur during mitotic HRR: synthesis-dependent strand-annealing (SDSA) (Krogh and Symington 2004). In this model, the initial steps of resection, Rad51 loading and invasion of homologous DNA are similar to the DSB repair model (Figure 1.1A-D). Again, the invading strand is extended by DNA synthesis but the Srs2 helicase facilitates displacement of the invading strand, which pairs with the opposite end of the DSB (Figure 1.1D, Figure 1.2A) (Ira *et al.* 2003). A key feature of SDSA is that HJs are not formed in the model. DNA synthesis fills the gap and ligase seals the nicks to finish the repair process, resulting in a non-crossover outcome of repair.

The break-induced replication model was devised to explain non-reciprocal recombination involving hundreds of kilobases of a chromosome (Kraus *et al.* 2001). Again, BIR begins with a resected end that invades a homologous stretch of DNA and is extended by DNA synthesis (Figure 1.1A-D). Synthesis then proceeds extremely processively to the end of the chromosome and is even thought to play a role in telomere maintenance in the absence of telomerase (Figure 1.2B) (Kraus *et al.* 2001). DNA synthesis also occurs on the extruded strand of the D-loop and HJ resolution is required to complete the BIR repair process (Figure 1.2B). Both Rad51-dependent and -independent BIR have been demonstrated to exist in cells, however the Rad51-dependent process is quite difficult to detect owing to the efficiency of gene conversion HRR in budding yeast (Kraus *et al.* 2001). Using a modified diploid with only a short

Table 1. Comparison of Prokaryotic and Eukaryotic HRR factors

HRR stage	Role	*E. coli*	*S. cerevisiae*	*H. sapiens*
Presynapsis	Break recognition	RecBCD	Mre11-Rad50-Xrs2 (MRX)	MRE11-RAD50-NBS1 (MRN)
	Overcoming DNA secondary strucuture	SSB	RPA	RPA
	Break processing	SbcCD	Mre11-Rad50	MRE11-RAD50
	End resection	RecBCD RecQ-RecJ	Sae2	CtIP
	Recombinase loading	RecBCD RecFOR	Rad52 Rad55-Rad57 Shu1-Shu2-Psy3?	BRCA2 RAD51 paralogs? RAD52?
Synapsis	Recombinase	RecA	Rad51	RAD51
	Stabilization of recombinase nucleoprotein filament		Rad54	RAD54
	Chromatin remodelling		Rad54	RAD54
	Rad51 mediators		Rad55-Rad57	RAD51 paralogs?
Post-synapsis	Branch migration	RuvAB RecG	Rad54 Sgs1-Top3-Rmi1?	RAD54 BLM-TOPOIIIα-RMI1
	Holliday junction resolution	RuvC	Sgs1-Top3-Rmi1? Mus81-Eme1	BLM-TOPOIIIα-RMI1 MUS81-EME1 RAD51C-XRCC3 associated protein?

Question marks denote proposed but currently unproven functions of HRR factors.

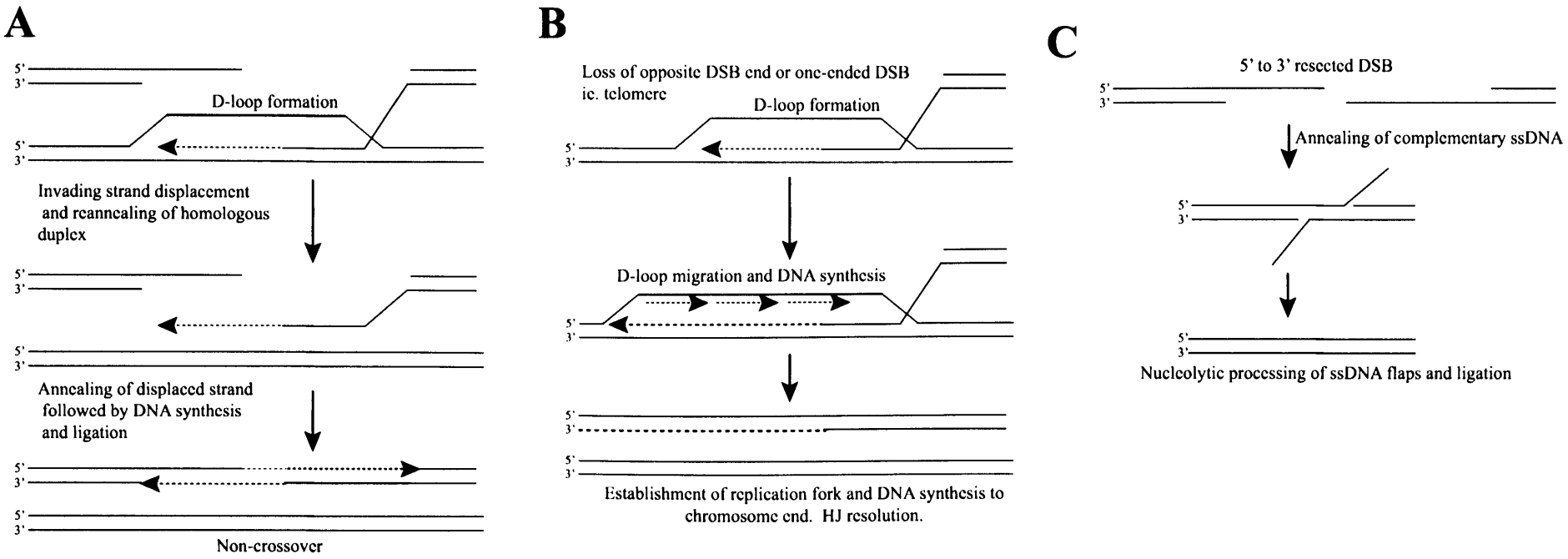

Figure 1.2. Alternative eukaryotic DSB repair models. (A) Synthesis-dependent strand annealing. Following strand invasion and D-loop extension, a helicase displaces the invading strand. The end of the displaced strand anneals to the resected end of the other side of the DSB. DNA synthesis from both free 3' ends followed by ligation completes the repair process, resulting in a non-crossover product. (B) Break-induced replication (BIR). BIR is believed to occur with one-ended DSBs or when the opposite end of the DSB is lost. Following strand invasion and extension, a replisome is established at the invasion site with DNA synthesis also occurring on the extruded DNA of the D-loop. DNA synthesis occurs to the chromosome end and HJ resolution completes the repair process. (C) Single-strand annealing. Following resection, complementary sequences in the ssDNA tails anneal, producing 3' flap structures. Structure-specific endonucleases remove these flaps and ligation restores the duplex. Unlike in the other DSBR models, this process results in a loss of genetic information during the repair process. (Adapted from Krogh and Symington, 2004)

track of homology on the target chromosome that prevents gene conversion, repair was detected after a delay; this break repair involved extensive DNA synthesis (>100 kb) at rates of normal replication (Malkova *et al.* 2005). In the absence of Rad51 or Rad54, Rad52 can promote repair by BIR, potentially by catalyzing strand invasion and the formation of D-loops, an activity that recombinant Rad52, and its metazoan counterparts Brh2, and CeBRC-2 all have been shown to possess (Kagawa *et al.* 2001; Bi *et al.* 2004; Petalcorin *et al.* 2006; Mazloum *et al.* 2007; Mazloum *et al.* 2008).

The final, Rad51-independent model is single strand annealing. SSA only resembles the other models in that its initial step involves break resection (Figure 1.1A,B). Rad52 is able to promote annealing of complementary regions of ssDNA within the resected ends, a process that the Rad59 protein facilitates when the areas of homology are short (Figure 1.2C) (Sugawara and Haber 1992; Ivanov *et al.* 1996; Sugawara *et al.* 2000; Krogh and Symington 2004). The 3' tails created by the annealing reaction are then trimmed by the NER Rad1-Rad10 endonuclease and the resulting nicks are then ligated (Figure 1.2C) (Sugawara *et al.* 1997). This repair mechanism is unique among HRR models as it is error-prone. SSA results in a loss of any genetic information contained between the break termini and the area of microhomology.

1.2.2 Rad51 paralogs

1.2.2.1 Metazoan Rad51 paralogs

In mammalian cells, there are five paralogs of RAD51 (RAD51B, RAD51C, RAD51D, XRCC2, XRCC3), which exhibit 20-30% sequence identity to RAD51 (Thacker 2005). Although they have been demonstrated to be required for HRR, their exact role has not yet been ascertained. They appear to be essential genes, because mutations in *RAD51B*, *RAD51D*, and *XRCC2* in mice cause embryonic lethality

(Pittman *et al.* 1998; Shu *et al.* 1999; Deans *et al.* 2003). Knockout studies in the chicken B cell line, DT40, have demonstrated that mutation in any of the RAD51 paralogs renders cells acutely sensitive to DNA interstrand cross-linking agents, while only mildly sensitive to ionizing radiation (IR) (Takata *et al.* 2001). Furthermore, the same phenotype is observed for RAD51 paralog mutations in Chinese hamster ovary cells (Jones *et al.* 1987; Fuller and Painter 1988; French *et al.* 2002). All of the paralogs influence the formation of IR- or ICL-induced RAD51 foci (Bishop *et al.* 1998; French *et al.* 2002; Godthelp *et al.* 2002).

The paralogs are found in two complexes in cells, a RAD51B-RAD51C-RAD51D-XRCC2 complex (BCDX2) and a RAD51C-XRCC3 complex (CX3) (Masson *et al.* 2001; Masson *et al.* 2001; Miller *et al.* 2002; Wiese *et al.* 2002). Biochemical studies have revealed that a subcomplex of RAD51B and RAD51C can alleviate the inhibitory effect of RPA *in vitro* and promote ATP-independent strand exchange. In addition, the CX3 complex is associated with Holliday junction resolution activity, and the BCDX2 complex preferentially binds Y-shaped DNA and Holliday junctions (Sigurdsson *et al.* 2001; Lio *et al.* 2003; Liu *et al.* 2004; Yokoyama *et al.* 2004). Data showing alleviation of RPA inhibition, strand exchange, and RAD51 focus formation argue that the paralogs play an early role in HRR, possibly as RAD51 co-factors, while preferential binding of Y-shaped DNA and Holliday junction resolution activity associated with the CX3 complex suggest an additional later role in HRR. It has been suggested that the paralogs are general mediators of HRR, but this is inconsistent with their differing sensitivities to IR and DNA cross-linking agents and their DNA binding preferences, both of which suggest a replication specific role.

1.2.2.2 Rad51 paralogs in yeast

Recent work in both *S. cerevisiae* and *S. pombe* has revealed the existence of other Rad51 paralogs, in addition to Rad55 and Rad57. Rlp1 and Rdl1 in *S. pombe* are believed to form a RAD51D-XRCC2-like complex with the two proteins contributing a Walker A and Walker B ATPase motif, respectively (Khasanov *et al.* 2004; Martin *et al.* 2006). Sws1, a novel pro-recombinogenic factor conserved in humans, is also a member of this complex (Martin *et al.* 2006). It has also been suggested that three proteins identified in a genetic screen for *top3* lethality suppressors in *S. cerevisiae*, Shu1, Shu2, and Psy3 form a complex analogous to the Sws1-Rlp1-Rdl1 complex (Shor *et al.* 2005; Martin *et al.* 2006).

1.2.3 HRR and DNA replication

The DNA binding preferences of the Rad51 paralogs and ICL sensitivity suggest a replication-specific role in promoting HRR. Insight into the role of the paralogs might be obtained from previous work in *E. coli* as it provides the most detailed model for the role of HRR in DNA replication. There are two main HRR pathways, both involving RecA, for dealing with replication progression issues in *E. coli*: these are the RecBCD pathway, which responds to replication-dependent DSBs in a similar mechanism as previously described; and the RecFOR pathway, which promotes RecA loading in the absence of a DSB.

1.2.3.1 RecBCD and fork restart

Studies of *E. coli* strains mutant for the DnaB replicative helicase or the PolIII replicative polymerase revealed chromosome linearization in the absence of RecBC, indicating DSB formation at blocked forks (Michel *et al.* 2004). DSBs can be conceivably generated by replication into a nicked strand, endonucleolytic cleavage of a

blocked fork, or fork regression (Figure 1.3A(i-iii), B(iii)). In the former situation, either RecBCD (after encountering a Chi site) or a combination of the RecJ exonuclease and the RecQ helicase would resect the free end to generate a 3' ssDNA tail (Figure 1.3A(iv)) (Kowalczykowski 2000). RecBCD can catalyze loading of RecA protein onto this substrate as in classic DSB repair. Invasion of the RecA filament into the homologous duplex restores the replication fork and the PriA protein can then catalyze reassembly of the replisome, with replication initiated at the 3' end of the invading strand (Figure 1.3A(v)) (Liu and Marians 1999).

In contrast to HRR at DSBs arising during replication, the role of HRR at stalled replication forks is less clear. A stalled replication fork can be regressed spontaneously and non-enzymatically, by positive supercoiling ahead of the fork, or through the actions of the RecA or RecG proteins (Figure 1.3B(i-iv)) (McGlynn *et al.* 2001; Postow *et al.* 2001; Robu *et al.* 2001). The exact role this regressed fork, or "chicken foot" structure, plays in repair is not completely clear, and it has even been suggested to be pathological (Sogo *et al.* 2002). When lesions result in a block to both leading and lagging strand synthesis, fork regression can occur (Figure 1.3Bi,iii). It has been suggested that RecBCD or ExoV can degrade the one-ended DSB that forms following regression to create a substrate more suitable for replication restart (Figure 1.3B(iii,vi)) (Cox 2001). Following lesion removal by pathways such as excision repair, loading of the PriA protein onto the reset fork would then allow for replisome reassembly (Figure 1.3B(vi)) (Cox 2001). When lesions occur on the leading strand, uncoupling of leading and lagging strand synthesis can occur (Figure 1.3B(ii)). Fork regression followed by DNA synthesis on the annealed nascent strands allows for the lesion to be bypassed using the genetic information contained on the nascent lagging strand (Figure 1.3B(iv-v). This substrate is now identical to that formed by regression at a completely blocked replication fork (Figure 1.3B(iii)). If this replication fork was then reversed

Figure 1.3. HRR pathways and DNA replication in *E. coli.* (A) A DSB is generated at a replication fork (iii) following fork intersection with a single-strand gap (i) or through nucleolytic processing of a stalled fork (ii). RecBCD (after encountering a Chi site) or RecQ-RecJ can generate 3' ssDNA tails after loading onto the end of the DSB (iv). RecA is loaded onto the ssDNA and catalyzes invasion into the intact duplex and replication restart can then occur (v). (B) A non-ICL lesion (red square) results in either complete block of the replication fork (i) or block of only leading strand replication (ii). In the case of complete block, the fork regresses (iii). In the case of block of just the leading strand, the newly synthesized strands anneal (iv) and DNA synthesis can occur on the paired nascent strands to extend the regressed fork (v). This synthesis uses the genetic information contained on the newly synthesized lagging strand to replicate past the position where the leading strand was initially blocked and generates an identical structure to that formed in B(iii). This structure is then processed in one of two ways: RecBCD or ExoV degradation (vi) of the one-ended DSB, coupled with lesion removal and replication restart; or RecG reversal of the fork, which allows a newly assembled replisome to recommence replication past the lesion (vii) (Adapted from Cox, 2001; Kowalczykowski, 2000)

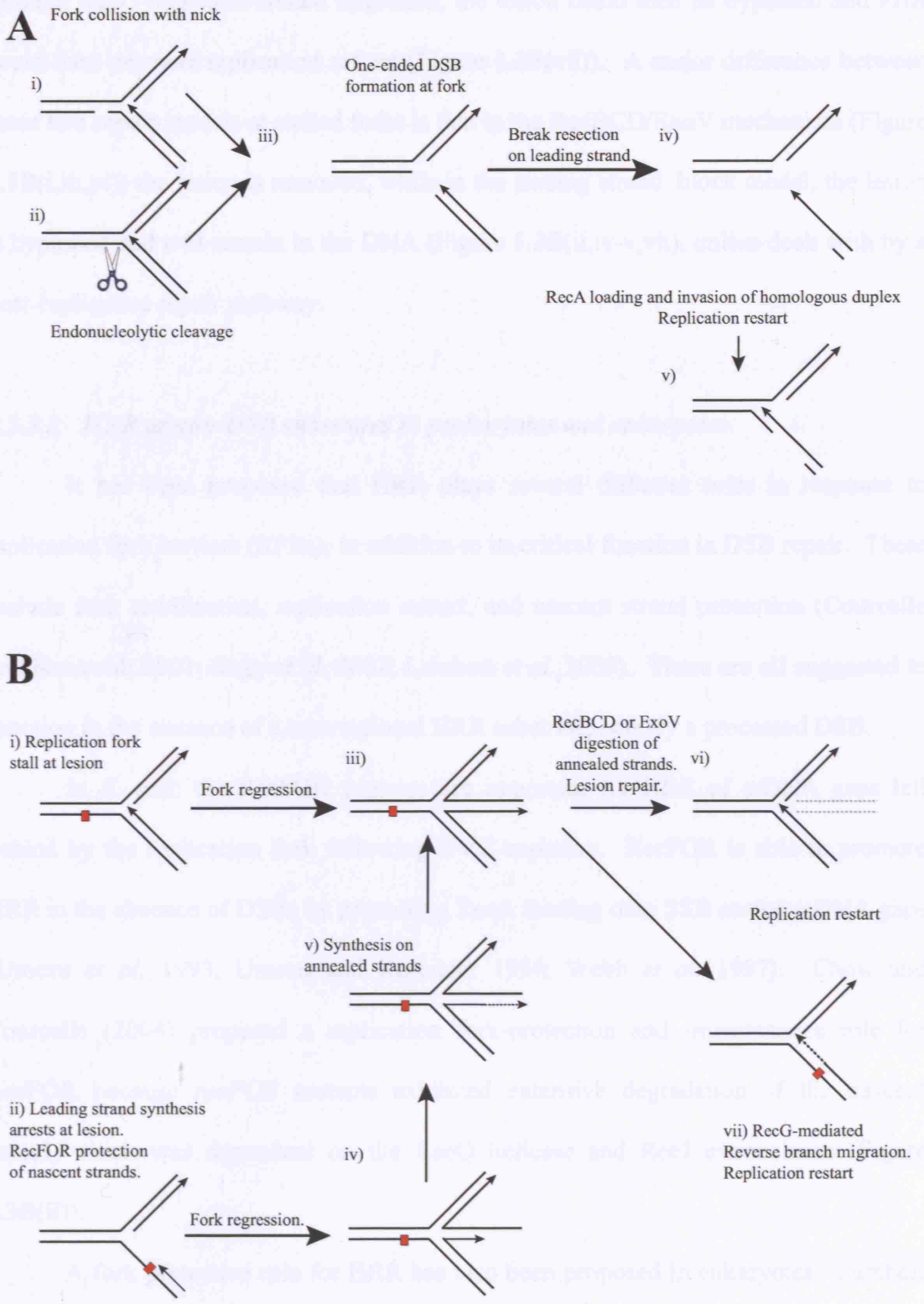

Figure 1.3. HRR pathways and DNA replication in *E. coli*. For figure legend, see preceding page.

through RecG-mediated branch migration, the lesion could then be bypassed and PriA could then promote replication restart (Figure 1.3B(vii)). A major difference between these two repair models at stalled forks is that in the RecBCD/ExoV mechanism (Figure 1.3B(i,iii,vi)) the lesion is removed, while in the leading strand block model, the lesion is bypassed and will remain in the DNA (Figure 1.3B(ii,iv-v,vii), unless dealt with by a post-replicative repair pathway.

1.2.3.2 HRR at non-DSB substrates in prokaryotes and eukaryotes

It has been proposed that HRR plays several different roles in response to replication fork barriers (RFBs), in addition to its critical function in DSB repair. These include fork stabilization, replication restart, and nascent strand protection (Courcelle and Hanawalt 2001; Sogo *et al.* 2002; Lambert *et al.* 2005). These are all suggested to function in the absence of a conventional HRR substrate, namely a processed DSB.

In *E. coli,* the RecFOR proteins are important for HRR of ssDNA gaps left behind by the replication fork following UVC exposure. RecFOR is able to promote HRR in the absence of DSBs by promoting RecA loading onto SSB coated ssDNA gaps (Umezu *et al.* 1993; Umezu and Kolodner 1994; Webb *et al.* 1997). Chow and Courcelle (2004) proposed a replication fork-protection and -maintenance role for RecFOR because *recFOR* mutants exhibited extensive degradation of the nascent strand, which was dependent on the RecQ helicase and RecJ exonuclease (Figure 1.3B(ii)).

A fork protective role for HRR has also been proposed in eukaryotes. Lambert *et al.* (2005) created an inducible, polar RFB in *S. pombe* by making use of the replication termination sequence (*RTS1*), which normally blocks replication forks approaching the *mat* locus from the centromeric direction. They flanked the *ura4* locus with *RTS1* sites, and induced fork stalling by expressing the non-essential genes Swi1 or

Rtf1, which bind to the *RTS1* sequence and create a replication fork block. Interestingly, recombination proteins, but not checkpoint proteins, were required for cell viability in response to the blocked forks. HRR was required for cell viability even when a single RFB was induced. The recruitment of recombination proteins to the stalled fork led to increased levels of recombination that drove gross chromosomal rearrangements such as deletions and translocations. These results presented a paradox in which recruitment of HRR proteins simultaneously resulted in chromosomal aberration and ensured viability of the organism. Thus, Lambert *et al.* suggested an alternative to the proposed role in active repair for HRR at stalled forks, namely a protective one, such as shielding of the nascent DNA strands from exonuclease attack. This is a particularly attractive model, as it would offset the deleterious effects of increased recombination and chromosomal rearrangement at stalled replicons.

1.3 Replication fork barriers (RFBs) and genomic instability

1.3.1 Endogenous RFBs

Work from Lambert *et al.* (2005) clearly showed that artificially blocked replication forks generate a requirement for HRR in cell survival, but that HRR is also recombinogenic and drives chromosomal aberrations, the so called double-edged sword of recombination. A number of endogenously occurring structures present obstacles to replication that a cell must overcome every cell division.

1.3.1.1 DNA secondary structure

G-rich DNA sequences are believed to form replication blocking secondary structures such as G4 quadruplex DNA (Arthanari and Bolton 2001). As will be discussed in section 1.5.3, *C. elegans* mutants for the FANCJ homolog, DOG-1 (deletions of guanine rich DNA), exhibit deletions at runs of greater than 18 consecutive

guanine residues (Cheung *et al.* 2002). Current work in the Boulton lab is trying to ascertain whether G/C-tracts are unstable in FANCJ defective mammalian cells, as these tracts may be a potential source of genomic instability in patients from the J complementation group of Fanconi anaemia. This instability is likely, since it has been demonstrated that the FANCJ helicase is able to promote unwinding of G4 DNA (Brosh 2008).

Fragile sites are another DNA structure-based barrier to replication. Rare fragile sites are caused by trinucleotide repeat expansion and are present in less than 5% of the population (Durkin and Glover 2007). They are susceptible to chromosome breakage during normal DNA replication and lead to hereditary disease; for example, FRAXA (Fragile site on X chromosome-A) is implicated in fragile X syndrome (Durkin and Glover 2007). Common fragile sites are dispersed throughout the genome of all humans and are not normally subject to DSBs during replication (Durkin and Glover 2007). However, when replication is slowed by treatment with either the DNA polymerase inhibitor aphidicolin, or the nucleoside analogs BrdU or 5-azacytidine, breakage can occur. Common fragile sites are less well characterized, with only 13 of 87 having been cloned and characterized (Durkin and Glover 2007). Explanations for the fragility of these sequences include increased DNA flexibility, DNA secondary structure, as well as collision of the replisome with the transcriptional machinery in large genes (Glover *et al.* 2005; Durkin and Glover 2007).

1.3.1.2 Intersection of replication and transcriptional machineries

The best-characterized RFB is a protein-binding sequence that prevents replication fork progression into the 3' end of the ribosomal RNA gene repeats (rDNA) in budding yeast. This binding ensures replication and transcription proceed unidirectionally. The Fob1 protein directly binds to the RFB sequence and inhibits

DNA replication (Kobayashi 2003). Fob1 is also implicated in maintaining copy number of the rDNA repeats through HRR that involves unequal sister chromatid exchange; loss of either Fob1 or the RFB sequence results in reduction in recombination (Kobayashi *et al.* 1998; Kobayashi *et al.* 2001). Using a *fob1* mutant strain with reduced rDNA copy number, collision of the replication and transcriptional machinery was observed, which stimulated recombination (Takeuchi *et al.* 2003). Determination of the genetic requirements for HRR during the intersection of replication and transcription could illuminate the model of DSB repair used.

1.3.1.3 Non-histone DNA-protein complexes

In addition to the transcriptional machinery, other DNA-protein complexes can serve as roadblocks to DNA replication. The Rrm3 helicase functions to clear these protein blocks to replication; in its absence, DSBs frequently form at rDNA, tRNA genes, centromeres, inactive replication origins, and transcriptional silencers, further emphasizing the significance of the impediments encountered by the replication forks during each and every cell cycle (Ivessa *et al.* 2000; Ivessa *et al.* 2002; Ivessa *et al.* 2003).

1.3.2 Genotoxic agents that induce RFBs

A large number of genotoxic agents lead to the formation of RFBs. As mentioned previously, ICLs completely block both replication and transcription by tethering the two strands of a DNA duplex together. Nitrogen mustard and cisplatin can also form intrastrand cross-links, which are bulky lesions that can also interfere with replication. Camptothecin traps topoisomerase I intermediates and leads to either a replication-dependent DSB or a blocked replication fork, depending on the strand on which the TopI enzyme is trapped (Strumberg *et al.* 2000). Bulky lesions are also

formed by the alkylating agents methyl methanesulfonate and ethyl methanesulfonate. Finally, IR-induced damage can result in DNA-protein cross-linking and damaged bases, both of which could lead to fork blocking or stalling.

1.4 Interstrand cross-link (ICL) repair

DNA interstrand cross-linking agents are a clinically important class of DNA damaging agent; cisplatin, mitomycin C, trimethylpsoralen/UVA, and mephalan have been successfully used to treat an array of cancers. Study of these agents is important as it may lead to both improved drugs and understanding of mechanisms of resistance. Since ICLs are complex lesions requiring the interplay of a number of repair pathways, repair of these lesions is poorly understood relative to other types of DNA damage. For the work presented here it is particularly important to differentiate between potential HRR substrates generated during the various enzymatic processes required to bypass this class of lesions during DNA replication. Eukaryotic ICL repair has been characterized in the most detail in *S. cerevisiae*. Therefore, pertinent features of yeast ICL repair will be presented first and then differences and additional factors present in mammalian ICL repair will be highlighted.

1.4.1 Models of ICL repair

1.4.1.1 ICL repair in bacteria and yeast

Like HRR, detailed models of ICL repair were first developed in *E. coli,* based on extensive genetic and biochemical characterization of the repair of cross-links generated by photoactivation of the drug psoralen. The first model, proposed by Cole (1973) and refined over the following decades, involves a combination of NER and HRR proteins, and PolI (Dronkert and Kanaar 2001). In this model, the lesion is recognized and bound by the NER proteins UvrAB, which recruit the UvrC

endonuclease to create nicks to either side of the ICL on one strand (Cole 1973). The exonuclease activity of PolI creates a gap, exposing ssDNA and creating an HRR substrate (Sladek *et al.* 1989). RecA-mediated strand exchange and extension of the invading end by DNA synthesis is followed by HJ formation and resolution, which repairs the gap in an error-free process. The UvrC endonuclease then makes incisions on the other strand to free the ICL from the duplex (Sladek *et al.* 1989). DNA synthesis and ligation complete the repair process.

Subsequent work demonstrated an the existence of alternative error-prone mechanism, in which the TLS polymerase DNA polymerase II synthesizes past the lesion once UvrABC lesion recognition and nicking of the DNA has occurred (Berardini *et al.* 1999). After TLS DNA synthesis, the lesion is excised from the other strand and the repair process is completed as in the error-free mechanism (Dronkert and Kanaar 2001). The error-free mechanism would account for the sensitivity of *recFOR* mutants to ICLs. However, *recBCD* mutants are also sensitive to ICLs, implying the formation of a DSB at some point in the process (Zdraveski *et al.* 2000). For example, when a replication fork collides with the ICL, as is predicted to occur in eukaryotic ICL repair. It is not clear whether RecFOR functions only in non-replicating ICL repair, or if it plays an additional role in fork protection, as has been described at UVC lesions (Chow and Courcelle 2004).

Although not as biochemically well-defined as the *E. coli* model, ICL repair in *S. cerevisiae* provides the clearest picture of the repair process in eukaryotes. Like *E. coli,* NER, HRR and TLS play prominent roles and epistasis analysis has revealed that these represent three genetically distinct repair pathways (Grossmann *et al.* 2001). These three epistasis groups suggest that error-free and error-prone ICL repair pathways exist in eukaryotes, as they do in *E. coli.* The observation that DNA extracted from NER-defective cells could not be denatured, but HRR-defective and wild type cell DNA

could, suggested that NER was important to unhook the lesion while HRR functioned post-incision (Miller *et al.* 1982; Meniel *et al.* 1995). Consistent with a post-incision role, intact chromosomes following ICL treatment are difficult to recover in HRR mutants, suggesting the failure to repair DNA damage (Jachymczyk *et al.* 1981; McHugh *et al.* 2000). HRR was shown to be required for ICL repair in exponentially growing cells but not stationary phase cells (Jachymczyk *et al.* 1981; McHugh *et al.* 2000). NHEJ is not thought to play a role in ICL repair, even in the absence of HRR in G1 cells (McHugh *et al.* 2000).

DSB formation was identified as a repair intermediate in yeast ICL repair through density gradient centrifugation analysis performed by Jachymczyk *et al.* (1981). The Rad3 epistasis group, which is required for NER, and Rad1 in particular, was initially identified as being responsible for incisions leading to the DSB (Jachymczyk *et al.* 1981; Magana-Schwencke *et al.* 1982). This finding is controversial, for McHugh *et al.* (2000) failed to abolish DSB formation in any NER mutant and also found *mlh1* (a MMR endonuclease), *rad27* (flap endonuclease), *mre11,* and BER to be dispensable for DSB formation. Thus, whether DSBs are formed topologically due to torsional stress as the replication fork advances towards the ICL or through an active, enzymatic process remains unknown.

The current model for yeast S-phase ICL repair is similar to the *E. coli* model, with slight differences (Dronkert and Kanaar 2001). After replication fork arrest at the ICL, a DSB is induced and then resected to generate an HRR substrate. NER proteins excise the ICL on one strand and HRR proteins, the second epistasis group, mediate error free repair through replication restart and bypass of the lesion (similar to Figure 1,3A(iii,iv)). NER proteins excise the ICL from the DNA, then the gap is filled by DNA synthesis, and ligation completes the repair process.

The third epistasis group in ICL repair, the Rad6 pathway (TLS), is believed to play a key function in G1 in the absence of a sister chromatid, in constrast to the Rad52 epistasis group (HRR) (McHugh *et al.* 2000). Mutants for Rev3, which with Rev7 forms the TLS polymerase Polζ, are sensitive to HN2 in stationary phase but not in exponentially growing cells (McHugh *et al.* 2000). This suggests that like in DSB repair, error-prone pathways play a predominant role in the absence of a homologous sister chromatid template. Polζ interacts with the Y-family TLS polymerase, Rev1, which was shown to display an indistinguishable phenotype from Polζ with respect to repair of HN2-induced lesions (Sarkar *et al.* 2006). This is in contrast to Polη, which is dispensable for ICL repair, suggesting its predominant function is in replicating past UV-induced CPDs (Sarkar *et al.* 2006). The current model for ICL repair in G1 involves NER-dependent incisions flanking the ICL to free it from one strand (Sarkar *et al.* 2006). The major replicative polymerase, Polδ, commences gap repair, as occurs during normal NER, but becomes stalled at the oligonucleotide attached to the HN2 adduct. The stalled polymerase triggers the mono-ubiquitination of PCNA, leading to a switch from Polδ to one of the TLS polymerases, Polζ or Rev1.

There is a role for the Pso2 protein in ICL repair downstream of the incisions, but it is as yet undefined. Also known as Snm1, it is a 5' exonuclease epistatic to the Rad3 (NER) pathway in repair of ICLs (Henriques and Moustacchi 1981; Li *et al.* 2005). Interestingly, the MutS MMR complexes Msh2-Msh3 and Msh2-Msh6, along with ExoI, play a role that is redundant to Pso2 in repair of ICLs during S-phase (Barber *et al.* 2005). Pso2 is not involved in classic MMR and, curiously, downstream MMR factors such as MLH1 do not display an additive sensitivity when combined with *pso2* whereas the upstream MutS components do (Barber *et al.* 2005). Loss of Pso2-MutS/ExoI activity impairs repair of the DSB generated at the ICL and also hampers

HRR at inverted repeats, suggesting a more general role in repair of endogenous RFBs (Barber *et al.* 2005).

1.4.1.2 ICL repair in mammals

Mammalian ICL repair is most relevant to this study, but remains poorly characterized relative to yeast. HRR, NER, TLS, Pso2/Snm1, and MMR are involved, but differences exist, such as the involvement of the Fanconi anaemia (FA) group of proteins, which are specific to metazoans (Dronkert and Kanaar 2001). Other major differences include a specific role for the Rad51 paralogs in ICL repair, different genetic requirements for DSB formation at the ICL and a more pronounced role for the XPF-ERCC1 endonuclease relative to other NER proteins. Many current models of mammalian ICL repair exist, though none are definitive. Most of these models derive from the yeast models described in the previous section and although more factors are involved in the repair process, the predicted enzymatic steps are very similar: fork arrest at the ICL, DSB generation, excision of the ICL, lesion bypass by HRR, gap filling by replicative or TLS polymerases, and replication restart (for details see Figure 1.4). A combination of models is presented, based on current models proposed by Laura Niedernhofer (2006) and Weidong Wang (2007), to illustrate a potential ICL repair pathway as well as to call attention to potential DNA substrates generated in the repair process (Figure 1.4).

FA is a multigenic autosomal recessive cancer predisposition syndrome characterized at the cellular level by hypersensitivity to DNA cross-linking agents with a concomitant mild sensitivity to IR. To date the mutations responsible for 13 complementation groups (A, B, C, D1/BRCA2, D2, E, F, G, I, J/BRIP1, L, M and N/PALB2 have been identified (Wang 2007). Eight of these proteins (FANCA, B, C, E, F, G, L and M) are found in a large complex referred to as the FA core complex

Figure 1.4. Proposed mammalian ICL repair model. (A) A fork stalled at an ICL is stabilized by the FA core (FANCA, B, C, E, F, G, L and M) and BLM complexes (BLM helicase, TopoIIIα, RMI1, and RPA). The FA core complex catalyzes mono-ubiquitination of the FANCD2-FANCI heterodimer, which then becomes localized to the site of the ICL. (B) The Mus81-Eme1 endonuclease cleaves the replication fork, creating a DSB. (C) The XPF-1-ERCC1 endonuclease cleaves the same strand of DNA on the opposite (5') side of the ICL, freeing the lesion from one strand. (D) The FA proteins recruit a TLS polymerase (Rev1 or Polζ) that fills in the gap created by the endonucleolytic incisions. (E) The DSB is resected in preparation for HRR, and NER endonucleases incise the DNA strand that the adduct remains covalently bound to. (F) The oligonucleotide bound to the ICL is removed, leaving a ssDNA gap. BRCA2 and PALB2 catalyze loading of RAD51 onto the resected break. (G) After the ssDNA gap is filled by DNA synthesis and ligation, RAD51 catalyzes invasion of the repaired duplex. DNA synthesis results in formation of a D-loop. (H) After resolution of the Holliday junction, potentially by BLM-TopoIIIα, the replication fork is restored and replication recommences. (Adapted from Niedernhofer *et al.*, 2005 and Wang, 2007)

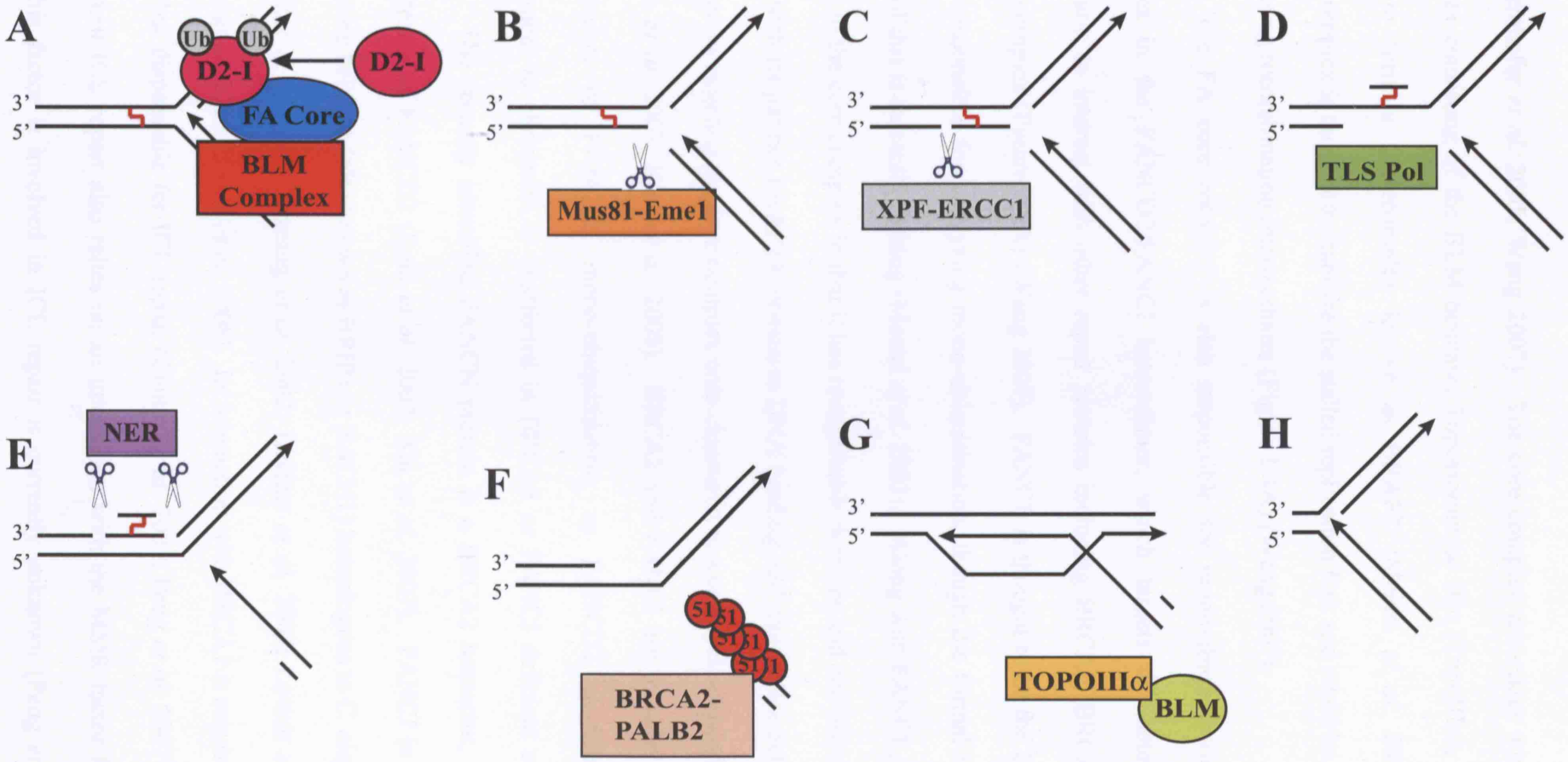

Figure 1.4. Speculative mammalian ICL repair model. For figure legend, see preceding page.

(Niedernhofer *et al.* 2005; Wang 2007). The core complex associates with a second complex consisting of the BLM helicase, Topoisomerase IIIα (TopoIIIα), RMI1, and RPA to form a supercomplex known as BRAFT (Meetei *et al.* 2003). This supercomplex is thought to stabilize the stalled replication fork and could be involved in processing recombination intermediates (Figure 1.4A) (Wang 2007).

The FA core complex is also responsible for mono-ubiquitination of both proteins in the FANCD2/FANCI heterodimer, which targets the heterodimer to chromatin to interact with other repair proteins including BRCA1, BRCA2 and the MRN complex (Figure 1.4A) (Wang 2007). FANCL is thought to be the E3 ubiquitin ligase responsible for catalyzing mono-ubiquitination, though the formal biochemical proof of this is currently lacking (Meetei *et al.* 2003).. Along with FANCL, FANCM is unique in the core complex in that it has recognizable domains and activities; FANCM, along with its partner FAAP24, possesses DNA binding and translocase activity and is involved in targeting the core complex onto chromatin in a cell cycle-dependent manner (Ciccia *et al.* 2007; Kim *et al.* 2008). BRCA2 and FANCJ are thought to function downstream of FANCD2 mono-ubiquitination, as FANCD2 modification and recruitment to chromatin is unaffected in BRCA2 or FANCJ deficient cells (Wang 2007). The recently identified FANCN protein is a BRCA2 interactor, also acting downstream of FANCD2 (Reid *et al.* 2007; Xia *et al.* 2007). FANCJ is a BRCA1-interacting helicase (also known as BRIP1 or BACH1) homologous to *C. elegans* DOG-1 (Cantor *et al.* 2001; Cheung *et al.* 2002; Levitus *et al.* 2005; Levran *et al.* 2005; Litman *et al.* 2005; Youds *et al.* 2008). Its interaction with BRCA1 is required for DSB repair but dispensable for ICL repair (Cantor *et al.* 2001; Peng *et al.* 2007). FANCJ-dependent ICL repair also relies on an interaction with the MMR factor MutLα, but how this factor is involved in ICL repair is currently unknown (Peng *et al.* 2007). Interestingly, the MMR factor MulLβ has also been implicated in ICL repair in the

damage recognition and uncoupling stage (Zhang *et al.* 2002). The exact function of the FA network in ICL repair is currently unknown, but suggested roles have included direct enzymatic processing, promotion of TLS, and activation of a cell cycle checkpoint (Figure 1.4D) (Niedzwiedz *et al.* 2004; Kennedy and D'Andrea 2005).

As already discussed in section 1.2.2, mutations in any of the mammalian Rad51 paralogs cause cellular hypersensitivity to DNA cross-linking agents but only a mild sensitivity to IR. Their roles in ICL repair are not yet defined and will be discussed in Chapter 3. To date, the *S. cerevisiae* Rad51 paralogs Shu2 and Psy3 have not been tested for ICL sensitivity. Given the more advanced model of budding yeast ICL repair, it would be illuminating to test these mutants for ICL sensitivity to determine what step(s) in repair they promote.

DSB formation in mammalian ICL repair has been suggested to be result from replication fork collapse, breakage due to torsional stress or an active enzymatic process. Recent evidence suggests that it is the latter, since both XPF and Mus81 have been implicated in DSB formation at ICLs (Figure 1.4B) (Hanada *et al.* 2006; Mogi and Oh 2006). Of the data demonstrating involvement of the two enzymes, that implicating Mus81 is much more convincing; physical breakage was directly measured using pulsed-field gel electrophoresis after treatment with both CDDP and mitomycin C (MMC). Additionally, two separate studies found that DSBs still form in ERCC1 (XPF heterodimeric partner) defective cells after MMC treatment, and in fact that the breaks seem to persist (Niedernhofer *et al.* 2004; Hanada *et al.* 2006). Persisting DSBs suggest a repair defect as opposed to a DSB induction defect. Although the study by Mogi and Oh (2006) claiming that XPF is required for DSB formation at ICLs used an array of ICL-inducing agents (the psoralen derivative HMT, angelicin, and MMC), a major issue is that phosphorylation of the variant histone H2AX (γ-H2AX) was relied on to detect DSBs (Mogi and Oh 2006). H2AX phosphorylation as a DSB marker is particularly

problematic as phosphorylation also occurs following UV damage and is therefore not strictly induced by DSBs (Marti *et al.* 2006).

Although it does not appear that XPF-ERCC1 are generating the DSB at ICLs in mammalian cells, these proteins have evolved an expanded role in ICL repair as mutants are hypersensitive to DNA cross-linking agents, while other NER mutants are only mildly sensitive (Figure 1.4E) (De Silva *et al.* 2002). This contrast was surprising, as other NER factors, such as XPG, are required to excise a CDDP-adduct from DNA but mutant cell lines were not particularly sensitive, possibly reflecting an expanded role for XPF-ERCC1 in mammalian HRR (De Silva *et al.* 2002). In addition to its role in SSA, XPF-ERCC1 has also been shown to be required for efficient gene conversion and SDSA (Al-Minawi *et al.* 2008).

1.5 *C. elegans* as a DNA repair model

Increasingly, *C. elegans* is being used as a model to study repair at both DSBs and RFBs. Not only are all the major metazoan DNA repair pathways conserved in *C. elegans*, but viable mutants are available, including genes involved in BER, NER, TLS, MMR, Fanconi anaemia, HRR, and NHEJ. In addition to the obvious genetic strengths of *C. elegans*, the germ line is useful for analysis of cell cycle checkpoints, apoptosis and chromosome stability. It is a particularly elegant tool for dissecting DNA repair pathways, as it is both temporally and spatially polarized, with cells first progressing through mitosis before passing through meiotic prophase I (Figure 1.5). The restriction of SPO-11 induced DSBs to a specific region of the meiotic compartment allows for distinction between factors required for repair of meiotic DSBs and factors required for the repair of replication-induced DSBs. In addition, techniques such as purification of

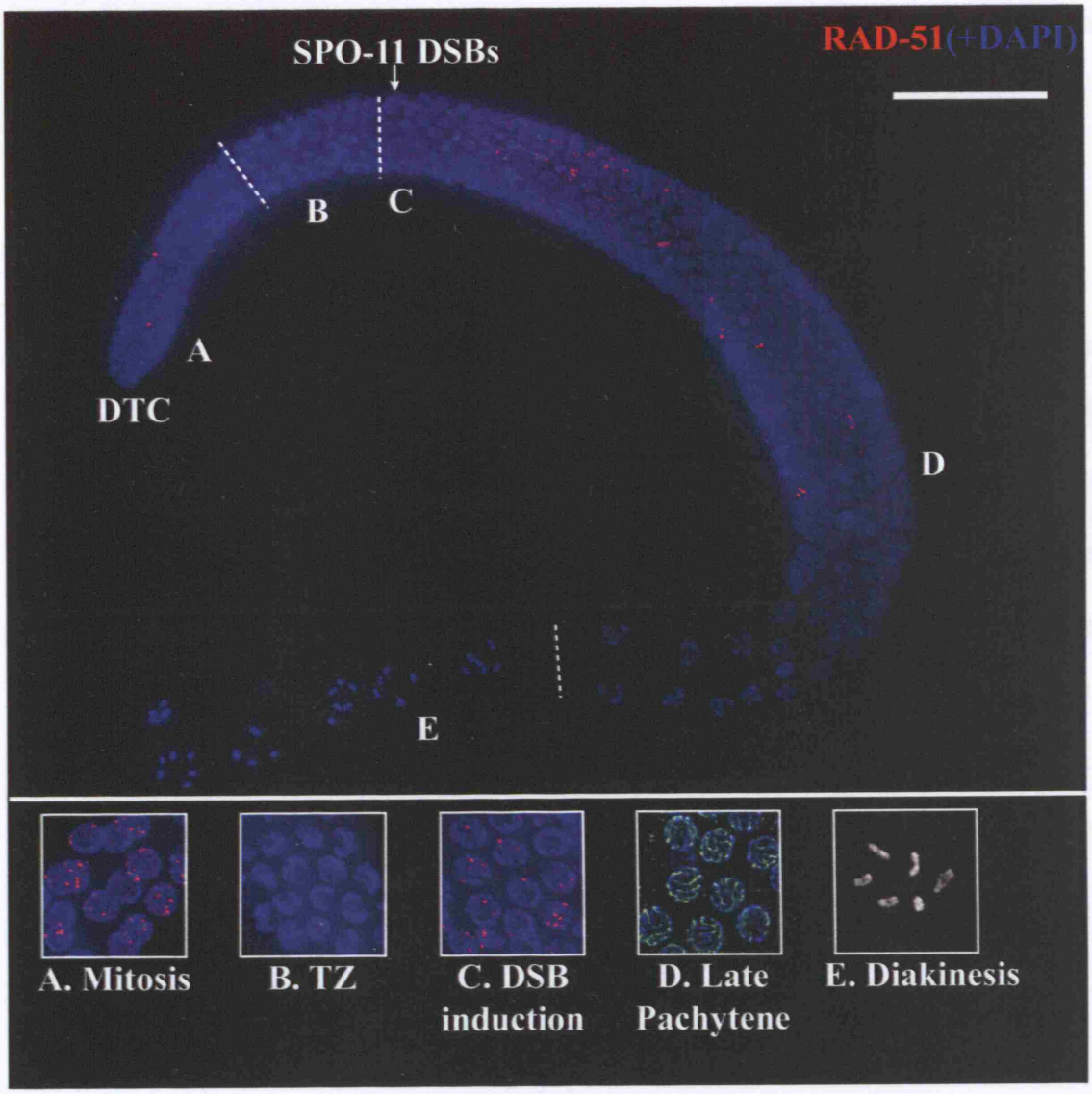

Figure 1.5. Features of the *C. elegans* germ line. Nematodes contain two polarized, U-shaped gonads. Shown is a representative, composite image of a RAD-51 (red) stained germ line counterstained with DAPI (blue) to show DNA. A distal tip cell (DTC) generates a population of proliferative mitotic cells (A). As the cells move away from the DTC they enter the transition zone (TZ) where pairing of homologous chromosomes is initiated (B). Nuclei in the TZ have a characteristic crescent shape. Nuclei then enter meiosis where the SPO-11 protein induces DSBs to initiate meiotic recombination (C). The homologous chromosomes synapse and are held together by the synaptonemal complex in pachytene (D; SYP-1 protein staining, green). This allows RAD-51 to catalyze HRR repair, using the homolog as a template. In diakinesis, the end of meiotic prophase I, the promotion of a single crossover outcome of DSB repair results in a linkage (chiasmata) between homologs (E). This yields six bivalents, consisting of paired homologous chromosomes. Experimentally, the mitotic zone is used to examine damage-induced cell cycle arrest, chromosome integrity, and localization of DNA repair factors (A; damage-induced RAD-51 foci shown). RAD-51 staining of meiotic nuclei throughout meiosis (from C-E) is utilized to follow initiation and completion of DSB repair. Apoptosis of damaged nuclei occurs at the germ line bend, in pachytene (D) and assembly and disassembly of the synaptonemal complex can also be monitored during meiosis (C-E). Chiasma formation can be assessed at diakinesis to examine crossover generation while chromosome integrity is often a reflection of repair of both mitotic and meiotic DNA damage (E). Scale bars, 40 µm. (Adapted from Garcia-Muse and Boulton, 2007)

TAP tagged proteins and improved targeted genetic engineering have recently been developed for the nematode (Polanowska *et al.* 2006; Robert and Bessereau 2007).

1.5.1 Meiotic HRR

The temporal and spatial polarization of the *C. elegans* germ line, in combination with well developed immunofluorescence techniques and both forward and reverse genetics, make the nematode a powerful model in which to study the process of meiosis. *C. elegans* hermaphrodites possess two X chromosomes (XX) while males are XO, arising from non-disjunction of the X chromosome, which is a rare event occurring in 0.1-0.2% of hermaphrodite self-progeny (Hodgkin *et al.* 1979). Mutations that impair meiotic chromosome segregation frequently have a high incidence of males (Him) phenotype and increased embryonic lethality, reflecting X chromosome and general autosome segregation difficulties, respectively (Garcia-Muse and Boulton 2007).

A stem cell at the distal tip of the germ line provides a pool of mitotic cells that enter what is referred to as the transition zone (TZ) as they move towards the proximal end of the germ line (Figure 1.5A,B). Here the HIM-17, PROM-1, and SUN-1 proteins initiate the transition from mitosis to meiosis (Bessler *et al.* 2007; Jantsch *et al.* 2007; Penkner *et al.* 2007). The zinc-finger proteins HIM-8, ZIM-1, ZIM-2, and ZIM-3 then promote homologous pairing, which allows for formation of the synaptonemal complex (SC), a proteinaceous structure that maintains the homologs in close proximity to facilitate meiotic recombination (Figure 1.5D) (Page and Hawley 2004; Phillips *et al.* 2005; Phillips and Dernburg 2006). In *C. elegans,* the SC is comprised of the central elements SYP-1 and SYP-2 and the axial elements HIM-3, HTP-1, HTP-2, and HTP-3 (Zetka *et al.* 1999; Couteau *et al.* 2004; Couteau and Zetka 2005; MacQueen *et al.* 2005; Martinez-Perez and Villeneuve 2005). In early pachytene, the evolutionarily

conserved SPO-11 protein introduces DSBs that are then repaired through HRR (Figure 1.5C) (Dernburg *et al.* 1998). Unlike the situation in mammals and yeast, DSB induction and SC formation are independent of one another, similar to the situation in *Drosophila*, allowing for analysis of DSB repair in the absence of homolog pairing (Garcia-Muse and Boulton 2007). SPO-11 dependent DSB formation requires processing by MRE-11, RAD-50, and COM-1, which as described in section 1.2.1.2 also occurs at mitotic DSBs (Chin and Villeneuve 2001; Hayashi *et al.* 2007; Penkner *et al.* 2007). CeBRC-2 loads RAD-51 onto the resected break to catalyze HR repair of the DSB. A crossover (CO; chiasmata) between homologous chromosomes must be generated by HRR in order for meiotic chromosome segregation to occur properly. If this crossover is prevented either through loss of the SC or SPO-11-induced DSBs, then 12 univalent chromosomes will be observed at the end of meiotic prophase I (diakinesis), instead of the six bivalents (homologs linked by chiasmata) seen in wild type animals (Figure 1.5E). Mutations in the MutS homologs *msh-4* (originally known as *him-14)* or *msh-5* lead to high embryonic lethality and dramatically increases the incidence of males, even in the presence of an intact SC and SPO-11 DSBs (Zalevsky *et al.* 1999; Kelly *et al.* 2000; Colaiacovo *et al.* 2003). The MSH-4-MSH-5 heterodimer, in a poorly defined manner, is critical to promote COs once RAD-51 mediated strand invasion has occurred. Additionally, a number of mitotic HRR factors such as the *C. elegans* BRCA1, BARD1, XPF, and BLM (HIM-6) homologs have weak to moderate meiotic phenotypes, but their specific role in meiosis is currently unclear (Hodgkin *et al.* 1979; Boulton *et al.* 2004; Wicky *et al.* 2004; O'Neil 2008).

1.5.2 Mitotic HRR

In contrast to meiotic DSB repair, much less work has been done to characterize mitotic DSB repair in *C. elegans.* In addition to being essential for meiotic

recombination, RAD-51 and CeBRC-2 are also essential for DSB repair in the mitotic compartment (Martin *et al.* 2005). Further work from the Boulton lab has demonstrated that *brc-1* (*C. elegans* BRCA1) and *brd-1* (*C. elegans* BARD1) knockdown causes embryonic sensitivity to IR and a massive increase in apoptotic corpses following gamma irradiation (Boulton *et al.* 2004). HIM-6 was demonstrated to be involved in repair of IR-induced DSBs, but not UVC-induced lesions, and also plays a role in RFB repair, as will be discussed in the following section (Kim *et al.* 2005).

1.5.3 RFB repair

As previously discussed in section 1.2.3, HRR has been implicated in stability of impeded replication forks as well as repair of conventional DSBs. The mitotic compartment of the germ line is increasingly being used to study repair at impeded forks arising from treatment with drugs such as DNA cross-linking agents as well as more physiologically relevant endogenous lesions.

C. elegans provides a very strong model to study ICL repair as it contains homologs of mammalian repair factors that yeast lack (BRCA1/BARD1, Fanconi anaemia proteins, BRCA2/FANCD1). Although *C. elegans* does not contain obvious homologs of the FA core complex, it does contain some established homologs as well as candidates for the known downstream FA effector proteins. FCD-2 (*C. elegans* FANCD2) is involved in repair of ICL-induced lesions, but not IR-lesions, as mutants were only sensitive to cross-linking agents and FCD-2 foci formed after replication stress but not following irradiation (Collis *et al.* 2006). Like its human homolog, FCD-2 is ubiquitinated after DNA damage and interacted with a putative E3 ubiquitin ligase in a yeast two-hybrid screen, suggesting *C. elegans* also has a functional analog of FANCL (Collis *et al.* 2006). A FANCJ homolog, DOG-1, is also specifically involved in repair of RFBs. *dog-1* mutants are sensitive to ICL-inducing agents but not IR or

UVC, and *dog-1* is epistatic to *fcd-2,* but not *brc-1,* with respect to repair of ICLs (Youds *et al.* 2008). This is a key result that demonstrates the presence of at least two genetically distinct ICL-repair pathways in *C. elegans.* The observation that RAD-51 and FCD-2 focus formation following replication stress is unaffected in *dog-1* mutants indicates that DOG-1 is operating downstream of or parallel to these two factors in ICL repair (Youds *et al.* 2008). A FANCM candidate, D2005.5, was recently implicated in repair of both IR and camptothecin induced lesions (Nakamura *et al.* 2007). However, this study only used RNAi and study of the available null mutant will be important to solidify these findings. Work from the Boulton and Rose groups has identified a DOG-1 related helicase, SPAR-1, as playing an anti-recombinase role functionally similar to *S. cerevisiae* Srs2 (Barber *et al.* 2008). Like *dog-1* and *fcd-2* mutants, loss of *spar-1* causes hypersensitivity to fork blocking lesions, but not to IR or UVC damage (Barber *et al.* 2008). Now that a large number of RFB repair genes in *C. elegans* have been identified and characterized, the field is poised to assess the interplay between these factors with respect to ICL repair.

DOG-1 was also implicated in the prevention of deletions at polyG/C tracts in the *C. elegans* genome and is believed to prevent fork stalling by removing secondary structures formed by the G/C tracts (Cheung *et al.* 2002). Recent work has demonstrated that the HRR proteins RAD-51, BRD-1, HIM-6 and XPF-1 as well as the TLS polymerases POL eta and POL kappa contribute to polyG/C tract stability in the absence of DOG-1 (Youds *et al.* 2006). HIM-6, along with TOP-3 (*C. elegans* Topoisomerase III), is also required for prevention of mitotic catastrophe in response to endogenously arising RFBs (Kim *et al.* 2002; Wicky *et al.* 2004). The mitotic fragmentation observed in *him-6; top-3(RNAi)* animals is suppressed by *rad-51* mutations, indicating that HRR intermediates arising at endogenously generated lesions are being processed by HIM-6 and TOP-3 (Wicky *et al.* 2004). The S-phase checkpoint

proteins ATL-1 (*C. elegans* ATR) and CLK-2 are also required for prevention of mitotic catastrophe at endogenously arising lesions (Garcia-Muse and Boulton 2005).

1.6 The Biological question

Although the vertebrate Rad51 paralog proteins are thought to be general mediators of HRR, their specific sensitivity to DNA cross-linking agents and mild sensitivity to IR suggests that they play a specialized role in repair. Their specific role has been elusive due to difficulties in performing genetic analysis in vertebrate cell lines (chicken DT40 cells being the exception), and the early embryonic lethality caused by their loss. The fact that only a single Rad51 paralog, RFS-1, appeared to be present in *C. elegans* afforded the possibility of exploiting nematode genetics and cytology to gain insight into the function of the mammalian Rad51 paralogs in HRR.

1.6.1 RFS-1 plays a specific role at impeded replication forks

After obtaining a predicted loss-of-function mutation in *rfs-1*, a detailed characterization of its response to DNA damaging agents was initiated. Unexpectedly, RFS-1 was dispensable for RAD-51 recruitment to meiotic and ionizing radiation (IR)-induced DSBs and following replication fork collapse, yet was essential for RAD-51 recruitment to RFBs formed by DNA cross-linking agents and other replication blocking lesions. Loss of RFS-1 led to an increase in apoptosis and chromosomal aberrations, specifically following treatment with RFB-inducing agents. Deletion of *rfs-1* suppressed the accumulation of toxic HRR intermediates in *him-6*; *top-3(RNAi)* mutants and accelerated deletion formation at presumed endogenous RFBs formed by polyG/C tracts in the absence of DOG-1. This suggested that RFS-1 is not a general mediator of HRR dependent DSB repair, but acts specifically to promote HRR at RFBs. These data demonstrated that HRR substrates generated at conventional DSBs or

following replication fork collapse are therefore intrinsically different from those produced during normal repair of blocked replication forks.

1.6.2 A novel RFS-1 interacting protein, RIP-1, also specifically responds to RFBs

A genome-wide yeast two-hybrid screen was performed in an effort to identify interactors that could provide insight into the role of RFS-1 at RFBs. The interaction between RFS-1 and RIP-1 (RFS-1 interacting protein) was found multiple times using either RFS-1 or RIP-1 as bait. Although RIP-1 lacks any obvious homologs outside the genus *Caenorhabditis,* RIP-1 phenocopies RFS-1 with respect to specific promotion of HRR at RFBs. Mapping of the interaction domains of RFS-1 with each of RAD-51 and RIP-1 revealed different binding sites, suggesting the possibility that RIP-1 and RAD-51 can simultaneously interact with RFS-1. Possible roles for RIP-1 in HRR are discussed in Chapter 4.

1.6.3 RFS-1 and oxidative stress

A major issue yet to be resolved in the FA field is the nature of the endogenous lesion(s) to which the FA proteins respond. Endogenous ICLs arising from oxidation products have been suggested to be the natural substrate for FA protein recognition. In an effort to see if oxidative stress leads to replication blocking lesions, the effect of loss of *daf-16,* a transcription factor that promotes the expression of a large number of stress response genes, on the phenotype of *rfs-1* mutant animals was examined. These results will be discussed more in Chapter 5.1.

1.6.4 RFS-1 and meiosis

rfs-1 mutants display a very similar Him phenotype to *brc-1* mutants without significant embryonic lethality, indicating a non-essential meiotic role. The loss of RFS-1 also suppressed the massive accumulation of recombination intermediates in *mus-81; him-9/xpf-1* mutant animals. Surprisingly the source of these recombination intermediates appeared to be meiotic in origin as opposed to mitotic. Possible roles for RFS-1 in meiosis will be discussed in Chapter 5.2.

2 Chapter 2: Materials and Method

2.1 *C. elegans* stocks and genetics

2.1.1 General *C. elegans* culturing

2.1.1.1 Culture conditions

C. elegans strains were cultured and maintained as described previously (Brenner 1974). Liquid culturing was performed in M9 medium (95.8 g/L Na_2HPO_4, 3.0 g/L KH_2PO_4, 0.5 g/L NaCl, 1.0 g/L NH_4Cl) or S-medium. S-medium was prepared by taking one litre of sterile S-basal medium (5.85 g NaCl, 1 g K_2HPO_4, 6 g KH_2PO_4, 1 ml of 5 mg/ml cholesterol (in ethanol)) and adding the following sterile solutions: 10 ml 1 M potassium citrate (pH 6), 3 ml 1 M $CaCl_2$, 3 ml 1 M $MgSO_4$, and 10 ml trace metals solution. Trace metals solution is comprised of 1.86 g/L disodium EDTA, 0.69 g/L $FeSO_4$•7 H_2O, 0.2 g/L $MnCl_2$•4 H_2O, 0.29 g/L $ZnSO_4$ •7 H_2O, and 0.025 g/L $CuSO_4$•5 H_2O.

2.1.1.2 Staging and sexing of animals

Fourth stage larvae (L4) were staged by selecting animals with a white crescent in the centre of the abdomen. Young adults were obtained by aging L4s for 24 hours and later by visual examination of size. Gravid adults were identified on the basis of size and the presence of a large number of eggs in the germ line. Males were distinguished by their

characteristic fan shaped tail, thinner and smaller body, and particular movements, such as doubling back upon themselves.

2.1.1.3 C. elegans strains used

All strains utilized in this study are listed in Table 2.

2.1.2 DNA damage sensitivity assays

Camptothecin, cisplatin, and nitrogen mustard sensitivity assays were performed by incubating the animals in S-medium containing the desired agent. Ionizing and UVC irradiation was carried out on OP50 seeded MYOB six-well plates and plates were incubated O/N for 22 hours at 20^{0}C. Specific details about solution preparation (CPT, CDDP, HN2) or irradiation (IR, UVC) for each agent are provided in subsequent paragraphs. Sensitivity assays to liquid agents were performed by placing worms in 2 ml total volume of S-basal+drug+concentrated HB101 bacteria (50 μl). Worms were protected from light and put on a slow shaker (approximately 100 revolutions per minute; rpm) at room temperature (RT) for 19 hours. Animals were then washed in phosphate buffered saline (PBS; 137 mM NaCl, 2.7 mM KCl, 4.3 mM Na_2HPO_4, 1.47 mM KH_2PO_4) then transferred to an OP50 seeded MYOB six-well plate and left for two to three hours to recover on solid food for optimal egg laying. For all agents tested, at 22 hours post-treatment, individual worms were picked to single OP50 seeded wells of a 24-well MYOB plate. Twelve worms/strain/dose were scored. The plates were incubated for four hours at 20°C, and then at 26 hours post-treatment the parental worms were removed. The eggs were counted and the plate was then incubated for two days at 20°C. The eggs that failed to

Table 2. ***C. elegans*** **strains**

Strain	Genotype	Source	Use
DW101	*atl-1(tm853) V*	S. Mitani-NBRP	Role of RFS-1 in promoting RAD-51 loading at collapsed forks
DW102	*brc-1(tm1145) III*	S. Mitani-NBRP	Positive control for sensitivity and increased apoptosis following DNA damage
DW104	*brc-2(tm1086) III/hT2[bli-4(e937) let-?(q782) qIs48] I;III*	S. Mitani-NBRP	Negative control for meiotic and damage induced RAD-51 foci
SP506	*clk-2/rad-5(mn159) III*	CGC	Cell cycle arrest control
GR1307	*daf-16(mgDf50) I*	CGC	Endogenous RFB work
	daf-16(mgDf50) I; him-6(ok412) IV	M. Grabowski and H. Tissenbaum	Endogenous RFB work
CF1038	*daf-16(mu86) I*	CGC	Endogenous RFB work
	daf-16(mu86) I; him-6(ok412) IV	M. Grabowski and H. Tissenbaum	Endogenous RFB work
DW110	*daf-16(mu86) I; rfs-1(ok1372) III*	This study	Endogenous RFB work
DW111	*daf-16(mu86) I; rfs-1(ok1372) III; him-6(ok412) IV*	This study	Endogenous RFB work
VC13	*dog-1(gk10) I*	A. Rose	RFS-1 and polyG/C tract stability
	dog-1(gk10) I; dpy-13(e184) rad-51(lg8701)IV	J. Youds and A. Rose	RFS-1 and polyG/C tract stability
DW106	*dog-1(gk10) I; rfs-1(ok1372) III*	This study	RFS-1 and polyG/C tract stability
TG9	*dpy-13(e184) rad-51(lg8701) IV/nT1[let-?(m435)] IV;V*	T. Gartner	Negative control for meiotic and damage induced RAD-51 foci
CB1416	*eDf25 III*	J. Yanowitz	Demonstrating loss of RFS-1 is responsible for observed phenotypes
VC193	*him-6(ok412) IV*	CGC	Mitotic catastrophe suppression

Table 2. continued

Strain	Genotype	Source	Use
CB1487	*him-9/xpf-1(e1487) II*	CGC	HRR substrate generation
AV115	*msh-5(me23) IV/nT1[unc-?(n754) let-?] IV;V*	CGC	RFS-1 and meiotic repair pathways
DW107	*mus-81(tm1937) I*	Mitani/This study	HRR substrate generation
DW116	*mus-81(tm1937) I; him-9/xpf-1(e1487)/mIn[gfp] II*	This study	HRR substrate generation
DW119	*mus-81(tm1937) I; him-9/xpf-1(e1487)/mIn[gfp] II; spo-11(ok79) IV/+*	This study	Source of RAD-51 accumulation in *mus-81; xpf-1* double mutants
DW117	*mus-81(tm1937) I; him-9/xpf-1(e1487)/mIn II; rfs-1(ok1372) III*	This study	HRR substrate generation
DW105	*rfs-1(ok1372) III*	OMRF KO Consortium/This study	All experiments
DW108	*rfs-1(ok1372) III; atl-1(tm853) V*	This study	Role of RFS-1 in promoting RAD-51 loading at collapsed forks
DW109	*rfs-1(ok1372) III; him-6(ok412)IV*	This study	Mitotic catastrophe suppression; endogenous RFB work
DW115	*rfs-1(ok1372) III; msh-5(me23) IV/nT1[unc-?(n754) let-? qIs50] IV;V*	This study	RFS-1 and meiotic repair pathways
DW120	*rfs-1(ok1372) III; syp-2(ok307) V/nT1[unc-?(n754) let-?(m435)] IV;V*	This study	RFS-1 and meiotic repair pathways
DW112	*rfs-1(ok1372)III/eDF25 III*	This study	Demonstrating loss of RFS-1 is responsible for observed phenotypes

Table 2. continued

Strain	Genotype	Source	Use
DW113	*rip-1(tm2948) III*	S. Mitani-NBRP/This study	Genetic characterization of RFS-1 interacting protein
AV157	*spo-11(ok79) IV/nT1[unc-?(n754) let-?] IV;V*	CGC	Source of RAD-51 accumulation in *mus-81; him-9/xpf-1* mutants
AV307	*syp-1(me17) V/nT1[unc-?(n754) let-? qIs50] IV;V*	CGC	RFS-1 and meiotic repair pathways
AV276	*syp-2(ok307) V/nT1[unc-?(n754) let-?(m435)] IV;V*	CGC	RFS-1 and meiotic repair pathways
N2 (ancestral)	Wild type	CGC	Wild type control
RB864	*xpa-1(ok698) I*	CGC	HRR substrate generation
DW114	*xpa-1(ok698) I; rfs-1(ok1372) III*	This study	UV sensitivity analysis

CGC-*Caenorhabditis* genetics centre
NBRP-National Bioresource project, headed by Shohei Mitani
OMRF-*C. elegans* gene knockout consortium, Oklahoma Medical Research Foundation lab, headed by Robert Barstead

hatch (dead eggs) were counted and % embryonic survival was calculated by the formula: 100% x (1-(number of dead eggs/total number of eggs))

Camptothecin (CPT; Sigma) stock solutions were made at 10 mg/ml in dimethyl sulfoxide (DMSO; v/v in M9). Gentle heating was applied to get the CPT into solution. Camptothecin working solutions were as follows:

Dilution of original 10 mg/ml stock	Final Concentration[1]	µl of diluted CPT stock	µl DMSO	µl M9
—	0 nM	0	30	570
1:1000	50 nM	10.72	19.28	570
1:1000	100 nM	21.44	8.56	570
1:10	500 nM	1.072	28.93	570
1:10	1000 nM	2.144	27.85	570

[1]Final concentration, takes into account the 1:10 dilution performed by adding 200 µl of DMSO or camptothecin:DMSO solution in M9 to 2 ml of worm-bacteria mix in six-well plates.

Nitrogen mustard (HN2, mechlorethamine; Sigma) stock solutions were made at 80 mM (15.4 mg/ml) in dH_2O, which was then diluted in dH_2O to a 20 mM working stock. This 20 mM stock was then diluted in S-basal medium to make 50 µM, 100 µM, and 150 µM solutions of HN2. All stocks were made in the fume hood, and all waste solutions and equipment that contacted the mustard was decontaminated in concentrated sodium hydroxide.

1.8 mM cisplatin (CDDP; Sigma) stock solutions (5.4 mg/10 ml) were made in dH_2O. CDDP is quite insoluble, so solutions were rotated for two to three hours at room

temperature, protected from light. This stock was then diluted in S-basal to make 90 μM, 180 μM, and 270 μM solutions

A UVC dosimeter was used to determine the dose rate of a 254 nm germicidal UVC lamp. This rate was used to calculate exposure times (1 $mW/cm^2/sec$=10 $J/m^2/sec$) for 25, 75 and 125 J/m^2. The ionizing radiation dose was calculated using the dose rate (in seconds/Gy; based on the calibration value of the 137 Cs source and provided with the irradiator) and worms were exposed to 25, 50, 75, or 125 Gy.

2.1.3 Scoring apoptosis

The apoptosis quantitation in Chapter 3 was performed as described previously (Boulton *et al.* 2002). Briefly, young adult animals were mounted in 20 μl of 10 mM levamisole on a 4% agarose pad (w/v in dH_2O) 24 hours post-treatment with the indicated genotoxic stress. The animals were then examined using DIC microscopy. Apoptotic corpses were identified as flat, round, highly refractile disks, usually located at the bend in the germ line.

For subsequent assays, and to detect corpses which are not visible using DIC microscopy, apoptosis was determined using the vital dye SYTO12 (Molecular Probes), as described previously (Gumienny *et al.* 1999; Youds *et al.* 2006). The 5 mM stock solution of SYTO12 (Invitrogen) was diluted 1:150 into M9 to create a 33 μM solution. The worms were incubated three hours in 50 μl of 33 μM SYTO12 solution in a 200 μl PCR tube at 20°C protected from light. Worms were washed one to three times in 3 ml of PBS in a six-well plate. Worms were then plated on a seeded six-well MYOB plate and incubated one hour in the dark at RT to purge the SYTO12 stained bacteria from their gut. Worms were

then mounted in 10 mM levamisole on a 4% agarose pad and scored using an excitation wavelength of 488 nm on an Axioskop2 microscope (Zeiss).

2.1.4 Cell cycle arrest assay

Hydroxyurea (HU) treatment was performed as described previously (Ahmed *et al.* 2001). Briefly, L4 larvae were transferred to MYOB plates containing 40 mM HU for 16 hours prior to analysis, unless otherwise indicated. Animals were washed in 2 ml of PBS, and then transferred in 20 µl of PBS to a well made using an Immun-Edge pen (Vector) on a poly-L-lysine coated 22x40 mm glass slide. Animals were anesthetized using 5 µl of 10 mM levamisole and germ lines were extruded by nicking the animals at the anus or at the posterior bulb of the pharynx using a 22-gauge needle. Germ lines were fully extruded out of the animals, fixed using 2% paraformaldehyde for 10 minutes, and then permeabilized for five minutes in PBS+0.1% Triton X-100. After three washes with 50 µl PBS, the samples were mounted in Vectashield containing 1 µg/ml of 4',6'-diamidino-2-phenylindole (DAPI). Germ lines were visualized using Deltavision microscopy as described in 2.5.1. For quantitation of mitotic cell cycle arrest, the germ lines were optically bisected through the longitudinal axis and the number of cells from the distal tip to the start of the pachytene region was counted. This correlates to a distance of approximately 70 µm and volume of 54,000 μm^2 in most animals.

2.1.5 RNA interference

2.1.5.1 dsRNA generation and injection

Oligonucleotides containing T7 RNA polymerase promoter sequences (top-3 RNAi-F and top-3 RNAi-R; Table 8, appendix) were used to amplify the *top-3* cDNA sequence (for PCR conditions see section 2.2.1). The template pGEM-T-Easy-*top-3* was a gift from Dr. Toni Gartner. A MEGAscript T7 *in vitro* transcription kit (Ambion) was used to generate dsRNA from the T7 tagged *top-3* cDNA PCR product according to manufacturer's instructions. dsRNA purified using an RNeasy kit (Qiagen) was then injected into animals as previously described (Fire *et al.* 1998).

2.1.5.2 RNAi by feeding

RNAi by feeding was performed as previously described (Fire *et al.* 1998; Boulton *et al.* 2002). Briefly, genes to be targeted by RNAi were Gateway cloned into pL4440-Dest, a vector carrying tandem T7 promoters flanking the cDNA insert. The constructs were transferred into HT115(DE3) bacteria and plated onto LB plates containing ampicillin (Amp, 50 μg/ml). For bacterial strain, antibiotic, and transformation information, see section 2.3. For each experiment, a fresh lawn of bacteria carrying the RNAi construct was used. The lawns were resuspended in 200 μl of LB broth, and 50 μl of this suspension was used to seed six-well MYOB+Amp plates containing 6 mM isopropyl β-D-1-thiogalactopyranoside (IPTG). The plates were dried, and then two P0 worms of the desired genotype were placed in each well and incubated at 15°C for 72 hours. Three F1 progeny were transferred to RNAi plates as above, and allowed to lay eggs for 24 hours.

The F2 progeny were then analyzed for desired phenotypes. For each experiment a negative (L4440 vector control) and positive (*rpa-1* RNAi) control were included.

2.1.6 *C. elegans* neutral comet assay

The neutral comet assay was attempted on dissected germ lines and isolated primary cells. Germ lines were dissected by nicking the pharyngeal bulb or anus with a 27 gauge needle and the germ lines from adult worms either mock treated or irradiated with 120Gy were extruded onto a poly-L-lysine coated Comet slide (Trevigen). The comet assay was performed as described previously, with modifications listed below (Wojewodzka *et al.* 2002). Sixty µl of 0.5 % low melting agarose (in PBS) was added to cover the germ lines. The nuclei were lysed for one hour at 4°C in lysis solution (2.5 M NaCl, 100 mM ethylenediaminetetraacetic acid (EDTA), 10 mM Tris Base, 1% sodium lauryl sarcosinate, 1% Triton X-100, 10% dimethyl sulfoxide, pH 9.5). The slides were washed three times in electrophoresis buffer (100 mM Tris, 300 mM sodium acetate, pH 8.3) then equilibrated for 60 minutes at 4°C, for one hour. The slides were then electrophoresed for 60 minutes at 4°C at 14 V and 120 mA. Following electrophoresis, the slides were washed three times, for five minutes each time, in a buffer to reduce background staining (300 mM NaOH, 1 mM EDTA). Then three washes, for five minutes each wash, were performed with neutralizing buffer (0.4 M Tris, pH 7.4). The slides were then incubated in 70% ethanol for 10 minutes and then air dried for one hour. To visualize DNA, slides were stained with 20 µl of 1 µM DAPI under a coverslip in a dark humid chamber. The slides were examined using the 63X objective of a DeltaVision microscope (Applied Precision). *C. elegans* primary cell culture was performed as previously described (Christensen *et al.* 2002; Strange *et al.* 2007). Six microlitres of isolated cells, either untreated, or exposed to 75 Gy

of ionizing radiation, were embedded in 60 µl of low melting point agarose (0.5% in PBS) and added on top of a Comet slide that had been previously coated with a bottom layer of 1.5% agarose in PBS (Trevigen). The comet assay was then performed as described above.

2.2 Molecular biological techniques

2.2.1 PCR

PCR reactions for cloning and genotyping were performed as described below. A table listing all oligonucleotides used in this study for PCR and sequencing is provided in Table 8, in the appendix.

2.2.1.1 PCR for cloning

PCR reactions for cloning purposes were carried out with KOD DNA polymerase (Novagen) using the EL PCR program. References to the EL program throughout this work include a number, which refers to extension time in minutes (i.e. EL1=1min extension). PCR reactions were set up as follows:

29 µl dH_2O

5 µl 10X buffer

5 µl dNTPs (stock, 2 mM each)

2 µl $MgSO_4$ (stock, 25 mM)

1 µl template DNA

1 µl 5' primer (stock, 5µM)

1 µl 3' primer (stock, 5µM)

1 µl DMSO

1 µl KOD hot start polymerase

EL PCR program

a) 94°C denaturation: 3 minutes

b) 94°C denaturation: 1 minute

c) 56°C annealing: 90 seconds

d) 68°C extension: 1 minute/kilobase pair (kb)

repeat b-d 34 times

e) 68°C final extension: 6 minutes

2.2.1.2 PCR for C. elegans genotyping

For genotyping, with the exception of *him-9/xpf-1(e1487),* nested PCR was performed. Worms were lysed in 5 µl of worm lysis buffer (50 mM KCl, 10 mM Tris pH 8.3, 2.5 mM $MgCl_2$, 0.45% NP-40 (IGEPAL), 0.45% Tween-20, 1 mg/ml proteinase K added immediately prior to use) then frozen on dry ice for ten minutes. The lysate was incubated at 65°C for 60 minutes, then the proteinase K was inactivated by a 10 minute treatment at 95°C. Next, 0.5 µl of this lysate was used as template in a 10 µl external PCR reaction (1X PCR buffer (Sigma), 0.5µM primers, 0.2 mM of each dNTP, 0.5 µl Taq DNA polymerase (5 U/µl)). For the internal PCR, reaction 0.2 µl of the external reaction was used as template in a 10 µl reaction. For most genotyping PCR reactions, the KO-FCD-2 program was used as shown below:

KO-FCD-2 program

a) 94°C denaturation: 2 minutes

b) 94 °C denaturation: 30 seconds

c) 55 °C annealing: 30 seconds

d) 72 °C extension: 2 minutes 30 seconds/kb

repeat b-d 34 times

e) 72 °C final extension: 3 minutes

For *him-9/xpf-1(e1487)* genotyping, worms were lysed in a 10 µl reaction as described above. A single round of triplex PCR was performed using 5 µl of the lysate in a 25 µl reaction volume using the following PCR and cycling conditions:

11 µl dH_2O

2.5 µl dNTP

2.5 µl 10X buffer

1 µl Taq (5U)

1 µl of each primer (NON 50+53+87; stock 5 µM)

HIM-9/XPF program

a) 94°C denaturation: 2 minutes

b) 94 °C denaturation: 30 seconds

c) 58 °C annealing: 30 seconds

d) 72 °C extension: 90 seconds

repeat b-d 42 times

e) 72 °C final extension: 3 minutes

2.2.1.3 PCR to monitor polyG/C tract stability

The stability of the polyG/C tract in the *vab-1* locus was monitored by PCR, as previously described (Youds *et al.* 2006). Briefly, nested PCR reactions (detailed in section 2.2.1.2) were performed on single young adults of the desired genotypes. Animals were scored as positive when one or more deletion bands, in addition to the wild type PCR product, were observed. The oligonucleotides used (vab-1 E1, E2, I1 and I2) are detailed in Table 8 in the appendix. External and internal PCR reactions were performed using the following cycling conditions:

vab-1 external PCR program

a) 94°C denaturation: four minutes

b) 94 °C denaturation: 30 seconds

c) 58 °C annealing: 30 seconds

d) 72 °C extension: 90 seconds

repeat b-d 33 times

e) 72 °C final extension: 10 minutes

vab-1 internal PCR program

a) 94°C denaturation: four minutes

b) 94 °C denaturation: 30 seconds

c) 62 °C annealing: 30 seconds

d) 72 °C extension: 60 seconds

repeat b-d 33 times

e) 72 °C final extension: 10 minutes

2.2.2 DNA sequencing

Sequencing was performed using the Big Dye Terminator kit. Reactions were cleaned using a DyeEx 2.0 spin kit (Qiagen) and capillary sequencing was performed by the staff at the LIF equipment park. The following reaction parameters were used:

Sequencing Reaction

15 µl DNA/water

0.67 µl primer (5µM stock)

3.75 µl buffer

0.5 µl Big Dye Mix 3.1

For double stranded plasmid templates, 150-200 ng was used. For sequencing PCR products, the following amount of template was used: 100-200 bp, 1-3 ng; 200-500 bp, 3-10 ng; 500-1000 bp, 5-20 ng; 1000-2000 bp, 10-40 ng; >2000 bp, 20-50 ng.

Sequencing program

a) 94°C denaturation: 1 minute

b) 94 °C denaturation: 10 seconds

c) 53 °C annealing: 10 seconds

d) 60 °C extension: 4 minutes

repeat b-d 25 times

e) 60 °C final extension: 2 minutes

2.2.3 Gateway recombinational cloning

Cloning using the Gateway system (Invitrogen) was performed according to the manufacturer's instructions.

2.3 Bacterial strains and plasmids

Bacterial strains were cultured in LB broth (Luria-Bertani; 10 g/L tryptone, 5 g/L yeast extract, 10 g/L NaCl, pH 7.5) or on LB plates (LB broth+15 g/L agarose) with appropriate antibiotics. For growth in liquid and on agarose plates, antibiotics were used at the following concentrations: ampicillin (Amp)-100 μg/ml; chloramphenicol (Cam)-34 μg/ml; kanamycin (Kan)-50μg/ml; streptomycin (Strep)-50 μg/ml; and tetracycline (Tet) 12.5 μg/ml. The bacterial strains used are listed in Table 4, while the plasmids used in this study are found in Table 4. Competent cell generation and transformation was performed using the KCM method as previously described (Walhout *et al.* 2000)

2.4 Immunofluorescence

Gravid hermaphrodites were washed in 2 ml PBS then transferred to 20 μl PBS in a well created using an ImmunEdge pen (Vector Laboratories, Burlington, CA) on a poly-L-lysine coated slide (slides were washed with 70% ethanol then subsequently given two coats of 100% poly-L-lysine with air drying between the coats). Twenty microlitres of 10 mM levamisole was added and germ lines were then extruded through cutting the pharyngeal bulb and anus of the animal with a fine-gauge (27 G) needle. The levamisole was subsequently replaced with 2% paraformaldehyde (PFA) in PBS for 10 minutes. The

Table 3. Bacterial strains used in this study.

Strain	Resistance	Use
DB3.1	-	Propagating Gateway entry and destination vectors before insert is introduced
DH5 α	-	General plasmid propagation
HT115(DE3)	-	RNAi by feeding
Rosetta Blue (DE3)	Tet, Cam	Bacterial protein expression. Carries tRNAs for codons rarely found in prokaryotes.
BL21(DE3)	-	Bacterial protein expression.
HB101	Strep	Worm culture
OP50	-	Worm culture

Table 4. Plasmids used

Plasmid	Resistance	Source	Use
CMV-FLAG-dest	Amp	S. Boulton	Expression control, vector generation
CMV-FLAG-dest-brc-2	Amp	S. Boulton	Protein expression in 293T cells; pull-down experiments
CMV-FLAG-dest-C49C3.10	Amp	S. Boulton	
CMV-FLAG-dest-R01H10.5	Amp	S. Boulton	"
CMV-FLAG-dest-rad-51	Amp	S. Boulton	"
CMV-GST-dest		S. Boulton	"
CMV-GST-dest-rfs-1	Amp	This study	"
L4440	Amp	A. Fire	RNAi feeding control
p221	Kn	Invitrogen	Entry vector
p221-C49C3.10	Kn	MRC	C49C3.10 entry vector
p221-R01H10.5	Kn	MRC	RO1H10.5 entry vector
p221-rfs-1	Kn	MRC	*rfs-1* entry vector
p221-stp	Kn	This study	Generating expression vector controls
pAD	Amp	S. Boulton	Yeast two-hybrid
pAD-brc-2 (1-114)	Amp	S. Boulton	Yeast two-hybrid
pAD-brc-2 (FL)	Amp	S. Boulton	Yeast two-hybrid
pAD-C30A5.3	Amp	This study	Yeast two-hybrid
pAD-C49C3.10	Amp	This study	Yeast two-hybrid
pAD-R01H10.5	Amp	This study	Yeast two-hybrid
pAD-rfs-1	Amp	S. Boulton	Yeast two-hybrid
pDB	Amp	S. Boulton	Yeast two-hybrid
pDB-brc-1 (1-114)	Amp	S. Boulton	Yeast two-hybrid
pDB-brc-2 (FL)	Amp	S. Boulton	Yeast two-hybrid
pDB-C30A5.3	Amp	This study	Yeast two-hybrid
pDB-C49C3.10	Amp	This study	Yeast two-hybrid
pDB-R01H10.5	Amp	This study	Yeast two-hybrid
pDB-rfs-1	Amp	S. Boulton	Yeast two-hybrid
pDEST-GST			Destination vector
pDEST-GST-R01H10.5	Amp	This study	Bacterial protein expression
pDEST-GST-rfs-1	Amp	This study	Bacterial protein expression
pDEST-his			Destination vector
pDEST-his-rfs-1	Amp	This study	Bacterial protein expression
pDEST-MAL			Destination vector
pDEST-MAL-R01H10.5	Amp	This study	Bacterial protein expression

Table 4. continued

Plasmid	Resistance	Source	Use
pDEST-MAL-rfs-1	Amp	This study	Bacterial protein expression
pGEM-T-Easy-top-3 cDNA	Amp	T. Gartner	RNAi by feeding, positive control
pL440-rpa-1	Amp	S. Boulton	RNAi by feeding
pL4440-R01H10.5	Amp	This study	RNAi by feeding
pL4440-rfs-1	Amp	This study	RNAi by feeding
pMAL-stp	Amp	This study	Protein expression in bacteria
pREX-GFP	Amp	S. Collis	Transfection control
pSMT3	Kn	C. Lima	Protein expression in bacteria
pSMT3-R01H10.5	Kn	This study	Protein expression in bacteria

PFA was then removed and the germ lines were permeabilized in TBST-Tx: Tris-buffered saline (TBS; 150 mM NaCl, 10 mM Tris-HCl, pH 7.5) containing 0.5% bovine serum albumin (BSA) and 0.1% Triton X-100 for five minutes. Three washes of five minutes with TBSB (TBS+0.5% BSA) were performed, and then germ lines were blocked with TBSB at RT for 30 minutes. Primary antibodies were diluted in TBSB and 25 µl per well was incubated in a humid chamber O/N at 4°C. Primary antibodies were reused for multiple experiments by removing the diluted antibody after the incubation, adding 1/100 volume 1% sodium azide, and storing at 4°C. After the primary antibody incubation, germ lines were washed three times with TBSB for 30 minutes each time. They were then incubated with secondary antibodies diluted in TBSB for two hours at RT in a dark humid chamber. The germ lines were washed three times in TBSB for 30 minutes before being mounted on coverslips with Vectashield containing 1 µg/ml of DAPI. To assay chromosomal abnormalities, adult animals were dissected and fixed as described above twenty-four hours after treatment with 75 Gy IR or 180 µM CDDP. The slides were then mounted on coverslips with Vectashield containing DAPI. The dilutions of antibodies used are provided in Table 5.

2.5 Microscopy

2.5.1 DeltaVision microscopy

DeltaVision microscopy was used to examine germ lines using either 40x or 63x, 1.4 NA Planapochromat lenses on an Olympus inverted microscope (IX71), and images were captured using SoftWorx computer software (Applied Precision). Three dimensional data sets were computationally deconvolved, and regions of interest were then projected into

Table 5. Antibodies for immunofluorescence

Antibody	Raised in	Dilution	Source
anti-guinea pig-FITC	goat	1/5000	Sigma
anti-rabbit-Cy3	sheep	1/10 000	Sigma
anti-ATL-1	rabbit	1/1000 (HU treatment)	Boulton lab
anti-ATL-1	rabbit	1/200 or 1/500 (IR treatment)	Boulton lab
anti-BRC-2 (32)	rabbit	1/2000	Boulton lab
anti-BRD-1	rabbit	1/500	Boulton lab
anti-HIM-3	rabbit	1/500	Anne Villeneuve
anti-HIM-8	guinea pig	1/200	Abby Dernburg
anti-MRE-11 (62)	rabbit	1/2000	This study
anti-RAD-51 (16)	rabbit	1/200	Toni Gartner
anti-RPA-1	rabbit	1/500	Toni Gartner
anti-SYP-1	guinea pig	1/200	Anne Villeneuve

one dimension. Merged colour images were recorded using GIMP software and single colour images were created using Adobe Photoshop.

2.6 Biochemical techniques

2.6.1 Protein expression

2.6.1.1 Protein expression using E. coli

A single colony was picked into 5 ml of LB broth containing appropriate antibiotics and shaken O/N at 37°C. The following day this culture was diluted to an OD of 0.1 in fresh LB and appropriate antibiotics were added. For pilot experiments, a final volume of 10ml was used; for scaled up expression, 1 L cultures were used. Cultures were grown shaking at 30°C until the OD reached 0.6. At this point, a 1 ml uninduced sample was taken, the bacteria were pelleted by centrifugation at 16,000xg for one minute, and the supernatant (S/N) was removed. The pellet was resuspended in 50 µl of lysis buffer (Invitrogen) containing 5% β-mercaptoethanol (BME) and lysed by boiling for five minutes. A freshly made 100 mM isopropyl-beta-D-thiogalactopyranoside (IPTG) stock was diluted 1:100 into the culture to induce protein expression and the culture was grown shaking at 30°C for a further four hours. At this point, a 1 ml induced sample was taken and prepared similarly to the uninduced sample, except the pellet was resuspended in 100 µl of lysis buffer to account for culture growth. To generate soluble protein the culture was pelleted and resuspended in appropriate column buffer containing Complete Protease Inhibitor-EDTA (Roche) (see section 2.6.3). For 10 ml cultures, the pellet was resuspended in 1 ml of buffer and sonicated on ice (3x30 seconds at 10% amplitude). The lysate was centrifuged at 16,000xg for 30 minutes at 4°C and a 100 µl soluble fraction was taken. This

fraction was boiled with lysis buffer as described above. For 1 L cultures, the bacteria were pelleted by centrifugation at 4000xg for 15 minutes at 4°C and the pellet was resuspended in 50 ml of column buffer+protease inhibitor. The bacteria were lysed by three passages through a Stansted cell disruptor and the lysate was split into two fractions, placed in thick walled tubes and spun at 30 000xg for 30 minutes at 4°C in a Beckman Ti-70 rotor. A 100 µl soluble fraction was taken, as described above.

2.6.2 Protein analysis

2.6.2.1 SDS-PAGE

Protein samples were denatured by boiling for five minutes in NuPAGE 1X LDS sample buffer (Invitrogen)+5% BME. Samples were run on NuPAGE 4-12% Bis-Tris gels (Invitrogen) in NuPAGE MOPS SDS running buffer (Invitrogen) at 200 V for 50 minutes. SeeBlue Plus2 (Invitrogen) prestained standard was used as a molecular weight marker. When protein needed to be visualized, the gels were stained with Coomassie blue solution (0.025% Coomassie Brilliant blue R 250, 40% methanol, 7% acetic acid) at RT for one hour to O/N. The gels were then washed in destain solution (10% acetic acid, 10% methanol) for one to two hours, or until the background staining was removed from the gel.

2.6.2.2 Immuno-blotting

Immuno-blotting was performed using a semi dry transfer method. Gels to be transferred were equilibrated by soaking in semi dry transfer buffer (25 mM Tris, 192 mM glycine, 0.1% SDS, 20% methanol) for five minutes. Nitrocellulose membranes, cut the same size as the polyacrylamide gel, were activated by soaking in methanol for two

minutes, and then rinsed in semi dry transfer buffer. Three pieces of filter paper also cut the same size as the gel were soaked in semi dry transfer buffer, then placed on the bottom plate of a Trans-Blot SD semi-dry electrophoretic transfer cell (Bio-Rad). The nitrocellulose was placed on the filter paper, and then the gel was placed on top of the nitrocellulose membrane. Three more gel-sized filter paper pieces soaked in transfer buffer were placed on top of the gel and any air bubbles were removed by rolling a pipette over the top of the stack. The top plate was then set in place and a current of 0.15 mA/gel was applied for 40-50 minutes. A maximum of four gels could be simultaneously run in the apparatus. The membrane was blocked in TBST-M (TBS, 0.1% Tween-20, 5% skim milk w/v) for 30 minutes, and then incubated with an appropriate dilution of primary in TBST-M O/N at 4°C (Table 6). The following day, the membrane was washed five times, for ten minutes each wash, in TBST (TBS, 0.1% Tween-20). The blot was then incubated for one hour at RT with an appropriate dilution of horseradish peroxidase (HRP)-conjugated secondary antibody in TBST-M (Table 6). Again, the blot was washed five times for 10 minutes per wash in TBST. Kodak BioMax light films were exposed to blots treated with ECL Western blotting detection reagent (Amersham) according to manufacturer's instructions. When either weak or undetectable signal was observed, the blots were developed as described above using Visualizer Western blot detection kit (Millipore) according to manufacturer's instructions.

2.6.2.3 Immunoprecipitation from 293T cells

293T cells were maintained according to standard tissue culture practice (Picot 2005). For transfection experiments, each 10 cm plate was seeded with approximately 500,000 cells. When plates reached 60-70% confluence, cells were transfected with 2 μg of

Table 6. Antibodies for immuno-blotting

Antibody	Raised in	Dilution	Source
anti-guinea pig-HRP	goat	1/5000	Dako
anti-mouse-HRP	sheep	1/2000	Dako
anti-rabbit-HRP	sheep	1/2000	Dako
anti-BRC-2 C E2 (29)	rabbit	1/250	Boulton lab
anti-FLAG	mouse	1/2000	Sigma
anti-Glutathione-S-Transferase (GST)	mouse	1/2000	Sigma
anti-6xHis	mouse	1/3000	GE Healthcare
anti-Maltose Binding Protein (MBP)	rabbit	1/2000	NewEngland Biolabs
anti-R01H10.5 N-term (35)	guinea pig	1/2000	This study
anti-R01H10.5 N-term (36)	guinea pig	1/2000	This study
anti-RAD-51 (16)	rabbit	1/500	Toni Gartner
anti-RFS-1 C-term (34)	guinea pig	1/2000	This study
anti-RFS-1 C-term (41)	rabbit	1/2000	This study
anti-RFS-1 N-term (32)	guinea pig	1/2000	This study

each construct using Lipofectamine and Plus reagent (Invitrogen) according to manufacturer's instructions. Four micrograms of a GFP expressing control plasmid was also transfected to monitor transfection efficiency. Forty-eight hours post-transfection, cells were washed three times with ice cold PBS. One millilitre of cell lysis buffer (50 mM Tris, pH 8.0, 200 mM NaCl, 1% Triton X-100, 1 mM dithiothreitol (DTT), 1 mM EDTA, 50 U benzonase (Novagen), 1 tablet Complete EDTA-free protease inhibitor (Roche)/50 ml, 1X phosphatase inhibitor (Sigma)) was added per plate and the cells were scraped into the buffer, then transferred into a 1.5 ml Eppendorf tube. The cells were placed on ice then lysed by sonication (2x10 seconds at 20% amplitude). The lysates were then spun at 15,000xg for 10 minutes at 4°C. The S/N was collected and a 50 µl sample was taken as "input". Glutathione beads (Clontech) were then prepared as follows: 40 µl x the number of samples of bead slurry was transferred to an Eppendorf tube and spun at 10,600xg for 5 seconds to pellet the beads (40 µl bead slurry is approximately 10 µl bed volume). The S/N was removed and 200 µl of wash buffer (lysis buffer without benzonase) per sample was added. The bead mixture was then split into "x" tubes (where "x"=number of samples), centrifuged and aspirated again. This was repeated two times with fresh wash buffer. After the final wash the S/Ns were aspirated and the cell lysates were added to the beads and incubated O/N at 4°C. The following day, the bead-lysate mixture was spun at 15,000xg for five seconds at 4°C. The S/Ns were collected and a 50 µl unbound sample was removed. The samples were then washed three times by rotating with 500 µl of fresh wash buffer at 4°C for thirty minutes per wash. At the end of each wash the beads were pelleted, the S/N aspirated, and 500 µl of fresh buffer was applied. After the final wash was removed, the bound fraction was eluted by adding 20 µl of NuPAGE 2X LDS sample buffer (Invitrogen) and boiling for five minutes. The samples were stored at -80°C prior to

analysis. Before loading onto an SDS-polyacrylamide gel, the bound fraction was re-centrifuged to pellet the beads. SDS-PAGE and immuno-blotting were performed as described in 2.6.2.1 and 2.6.2.2. For analysis 12.5 µl (approximately 1% of the total) input and 7µl of bound samples were run.

2.6.3 Protein purification

2.6.3.1 MBP tagged protein affinity purification

Fifty millilitre cultures of MBP and MBP-RIP-1 expressing Rosetta Blue bacteria were grown as described in 2.6.1.1, with the exception that 0.2% glucose was added to the medium. Glucose is crucial because it represses expression of the bacterial amylase gene. If amylase is present it will breakdown the maltose on the beads and the protein will fail to bind to the resin.

To prepare the beads, two millilitres of bead-ethanol slurry was transferred to a 50 ml Falcon tube (this corresponds to about 1 ml packed beads). The tube was filled with 25 ml of column buffer (20 mM Tris-HCl, 200 mM NaCl, 1 mM EDTA, pH 7.4) to wash the beads. The beads were centrifuged at 698xg for five minutes. The S/N was removed, discarded, and the wash was repeated three times. The wash was removed and the clarified extract was added to the beads and incubated rotating at 4 °C for two hours. The extract was removed (a 100 µl unbound sample was taken and boiled in lysis buffer for SDS-PAGE analysis) and the beads were washed three times, for 30 minutes each wash, at 4°C. A 100 µl sample of each wash was taken as previously described. The final wash was removed and the protein was eluted with 2 ml of elution buffer (column buffer+10 mM maltose). A 100 µl sample of the eluate was taken and electrophoresed on an SDS-PAGE

gel along with lysate, soluble fraction, washes, and unbound fractions (10 µl of each fraction). The approximate amount of protein in the sample was determined from the A280 value using a NanoDrop.

To regenerate beads, they were washed as follows:

Water: three column volumes,

0.1% SDS: three column volumes

Water: one column volume

Column buffer: three column volumes

The resin was reused up to five times.

2.6.4 Peptide array analysis

Mapping of RAD-51 and RIP-1 binding to the C-terminal half of RFS-1 was analyzed by peptide array as previously described (Thorslund *et al.* 2007). Peptide arrays were generated by the CRUK peptide synthesis service. Briefly, the membrane was activated by soaking in methanol for two minutes, washed in TBST (TBS+0.1% Tween-20), and then blocked for five minutes at RT in TBST-M. Twenty microlitres of purified RAD-51 (220 µg) in 20 ml of TBST-M was added and incubated O/N with the array at 4°C. A parallel control where no RAD-51 was added was also performed. The following day, the TBST-M was removed and replaced with 5 ml of TBST-M with anti-RAD-51 antisera (1:1000) and incubated for one hour at RT. The incubation was carried out on a parafilm sheet in a sealed container to minimize the amount of antibody required. The arrays were washed three times for five minutes each with TBST, then incubated with 20 ml of anti-rabbit-HRP conjugated secondary antisera (1:2000) for one hour at RT. Three 15 minute

washes with TBST were performed, then Visualizer ECL substrate (Millipore) was added and the blot was developed. After developing, the membranes were Ponceau stained (Sigma) for 30 minutes to one hour, and then destained in successive washes of 5% acetic acid (v/v in dH2O) until peptide spots were visible.

For mapping of RIP-1 binding, the same protocol was followed as described above with two exceptions: firstly, 500 µl of partially purified (see 2.6.3.1) MBP-RIP-1 or MBP control (115 and 55 µg, respectively) was added to 20 ml of TBST-M and incubated O/N at 4°C; secondly, the arrays were incubated in 25 ml of anti-MBP antisera (1:2000).

2.6.4.1 Peptide array stripping

To regenerate peptide arrays for reuse the arrays were treated as follows: first, two 30 minute washes with 50 mM Tris-HCl pH 8.00, 10% SDS, 10 mM BME (added immediately before use) at were performed at 55°C. The arrays were then rinsed with five 100 ml washes of PBS. Next, the arrays were subjected to two 30 minute washes in 50% ethanol, 10% acetic acid, again at 55°C. After five more 100 ml washes in PBS, the arrays were twice soaked in 100 ml of ethanol, then removed and air-dried. The dried arrays were kept in sealed plastic bags at -20°C

2.7 Antibody generation

2.7.1.1 Generation of anti-MRE-11 antibody

To generate an anti-MRE-11 antibody, a C-terminal synthetic peptide (CKVV-STRQIDSDGFEIINDSP) was generated by the Peptide Synthesis Laboratory, Cancer Research UK. Rabbits were immunized (Harlan Sera Labs, Loughborough, UK) with 1 mg

of the peptide coupled to activated keyhole limpet hemocyanin (Pierce, Rockford, Ill.). Antibodies were affinity purified as described previously, dialyzed O/N against 20 mM Tris-acetate pH 8.0, 0.2 M potassium acetate, 10% glycerol, 1 mM EDTA, and 0.5 mM DTT (Martin et al., 2005). The purified antibodies were then tested in N2 (Wt) and *mre-11(ok179)* animals either untreated or post-treatment with 150 Gy of ionizing radiation, 180 μM cisplatin, or 200 μM nitrogen mustard.

2.7.1.2 Generation of anti-RFS-1 antibodies

To generate RFS-1 antibodies, synthetic N-terminal (CDPSENVFKYETA-YDLLVRL) and C-terminal (CKGEQDDGMNRIEFKIGDRG) peptides were generated by the Peptide Synthesis Laboratory, Cancer Research UK. Antibodies were produced and purified as described in 2.7.1.1. The antibodies were tested in immuno-blotting using bacterial lysates containing overexpressed 6xHis-RFS-1, GST-RFS-1, and MBP-RFS-1 fusions. The purified antibodies were also tested for use in immunofluorescence in N2 (Wt) and *rfs-1(ok1372)* worms either untreated or post-treatment with 150 Gy of ionizing radiation or 180 μM cisplatin.

2.7.1.3 Generation of anti-RIP-1 antibodies

To generate RIP-1 antibodies, synthetic N-terminal (CSPKIDDHLFAKAIRW-ADQN) and C-terminal (CNVDDGRAVVVIDLR) peptides were generated by the Peptide Synthesis Laboratory, Cancer Research UK. Antibodies were produced and purified as described in 2.7.1.1. The antibodies were tested in immuno-blotting using bacterial lysates containing overexpressed SUMO-6xHis-RIP-1, GST-RIP-1, and MBP-RIP-1 fusions. The purified antibodies were also tested for use in immunofluorescence in N2 (Wt) and *rip-*

1(tm2948) worms either untreated or post-treatment with 150 Gy of ionizing radiation or 180 μM cisplatin.

2.8 Yeast two-hybrid (Y2H) assays

2.8.1 Yeast transformation

S. cerevisiae strain MaV103 was patched onto a YEPD plate (10 g/L BactoYeast, 20g/L BactoPeptone, 20 g/L dextrose, 20 g/L agar for plates) and incubated O/N at 30°C. The yeast were resuspended in 50 ml of YEPD liquid medium to obtain an OD600 of 0.1. The culture was shaken at 225 rpm at 30°C until the OD600 reached between 0.4 and 0.5 (approximately five hours). At this point, salmon sperm DNA (5 μl/transformation reaction) was boiled for five minutes and then left to chill on ice. The cells were harvested by centrifugation at 1800 rpm (141xg) at RT for five minutes. The S/N was discarded and the yeast were resuspended by gentle shaking in 5ml of sterile water. The yeast were pelleted again as described above, the S/N was discarded, and the yeast were resuspended in 1 ml of TE/LiAc solution (10 mM Tris-HCl pH 8.0, 1 mM EDTA, and 0.1 M lithium acetate (LiAc), made freshly the day of the experiment from 100X TE and 1 M LiAc stocks). The solution was transferred to a 1.5 ml Eppendorf and the yeast were pelleted by centrifugation at (400xg) at RT for five minutes. The S/N was aspirated and the yeast were resuspended in a volume of TE/LiAc corresponding to the final OD600. (eg. for an OD600 of 0.5, the yeast would be resuspended in 0.5 ml) One microlitre of either RIP-1-DB or RFS-1-DB plasmid minipreps was added to 5 μl of chilled salmon sperm DNA. This was mixed with 50 μl of the TE/LiAc-yeast suspension. Next, 300 μl of TE/LiAc/PEG (TE/LiAc solution prepared with 44% w/v polyethylene glycol (PEG) 3350, again prepared

fresh the day of the experiment) was added to the yeast-DNA mixture and gently mixed. This solution was incubated at 30°C for 30 minutes, then heat shocked at 42°C for exactly 15 minutes. A five second pulse in a microfuge pelleted the yeast, the S/N was aspirated, and the pellet was resuspended in 300 µl of sterile water. This mixture was then plated on synthetic complete dropout medium lacking leucine (SC-Leu) and incubated for two days at 30°C. SC-Leu was made from a SC-Leu,-Trp,-His,-Ura precursor stock (1.3 g/L amino acid powder [lacking leucine (Leu), tryptophan (Trp) histidine (His), uracil (Ura)], 1.7 g/L yeast nitrogen base, 5 g/L ammonium sulfate, pH 5.9 added to autoclaved agarose to achieve a final concentration of 20 g/L agarose). For each approximately 500 ml aliquot of SC-Leu,-Trp,-His,-Ura, 50 ml of 20% glucose was added prior to pouring plates after the media cooled to 55°C. Depending on the desired constitution of the media, 2 ml of 10 mg/ml stocks of His, Trp, or Ura were also added to the medium prior to plate pouring.

2.8.2 Genome wide yeast two-hybrid screening

Genome wide Y2H screening was performed using a MaV103 yeast strain carrying either RFS-1 or RIP-1 fused to the Gal4p DNA binding domain (DB). Both the DB containing strains and the Y2H screening transformations were performed as described in section 2.8.1. The DB bait strains were transformed with the AD-Orfeome cDNA library; in which 58% of the known *C. elegans* open reading frames are fused to the Gal4p activation domain (AD) (Reboul *et al.* 2003). This procedure yielded six transformation reactions per strain. To determine the degree of library coverage, three microlitres of one transformation reaction was diluted 1:100 into sterile water and plated on a SC-Leu,-Trp plate using sterile glass beads. The remainder of the transformation reactions were plated

on selective SC-Leu,-Trp,-His containing 20 mM 3-aminotriazole (3AT) using sterile glass beads. Yeast were grown for two days at 30°C. To calculate library coverage, the number of colonies on the SC-Leu,-Trp plate was multiplied by 100 (the dilution factor), then by six (the number of transformation reactions). Interactions allowed for growth on the histidine analog 3AT.

To confirm positive interactions, 3AT growth was retested and β-galactosidase activity was assessed. Candidates were patched onto YEPD plates and grown O/N at 30°C. This plate was photographed to confirm that the strains had no intrinsic growth defect. They were then replica plated, first onto SC-Leu,-Trp,-His+3AT plates, and then onto YEPD plates onto which a nitrocellulose filter had been placed. The SC-Leu-Trp-His+3AT plate was blotted with velvet until no colonies were visible. These plates were then incubated for two days at 30°C and subsequently photographed. The yeast on the nitrocellulose filter were allowed to grow overnight at 30°C, or until colonies were clearly visible. Two Whatman filter papers were placed in an empty 15 cm Petri plate and soaked in 4 ml Z-buffer (16.1 g/L $Na_2HPO_4 \cdot 7H_2O$, 5.5 g/L $NaH_2PO_4 \cdot H_2O$, 0.75 g/L KCl, 0.246 g/L $MgSO_4 \cdot 7H_2O$) with 11 µl BME and 100 µl 4% 5-bromo-4-chloro-3-indolyl-beta-D-galacto-pyranoside (X-Gal) in dimethylformamide. All air bubbles were removed. The nitrocellulose filter containing the yeast was then removed from the YEPD plate and immersed in approximately 200 ml of liquid nitrogen for 10 seconds. The filter was removed and thawed at RT, then placed immediately, yeast side up, on the soaked Whatman filters, with care made to avoid air bubbles. The lid was placed on the Petri dish and the dish was incubated at 37°C. The reaction was checked at regular intervals and, where appropriate, photographed.

The identity of the interactors was determined by yeast colony PCR followed by sequencing. Interactors were grown freshly on YEPD plates O/N at 30°C. A volume of

yeast cells approximately the size of a match head was resuspended in 10 µl of 20 mM NaOH (made freshly from 1 M stock) and microwaved for 30 seconds. Three microlitres of lysate was used as template in a 50 µl PCR reaction (as described in 2.2.1.1) using AD and Term primers (Table 8 in appendix) and the EL3 cycling program. Resulting PCR products were size fractionated on a 1% agarose gel, excised, gel purified, and sequenced as described in 2.2.2.

2.8.3 Small scale interaction matrices

To test for pairwise interactions between C30A5.3, an N-terminal fragment of CeBRC-2 (amino acids 1-114), full-length CeBRC-2, RAD-51, RFS-1, C49C3.10, and R01H10.5, small scale matrices were made. DB fusions of the above proteins, as well as a control only containing DB, were transformed into MaV103 as described in 2.8.1. Each of these seven DB strains was transformed with AD fusions of the same proteins, as well as an AD-only control, and plated on SC-Leu-Trp, yielding 49 strains. Each strain was patched onto a YEPD plate in a 7x7 grid, grown O/N at 30°C and then photographed. The matrix was then replica plated, first onto SC-Leu,-Trp,-His+3AT plates and then onto YEPD plates onto which a nitrocellulose filter had been placed. Interactions were tested for by growth on 3AT and β-galactosidase expression, as described in section 2.8.2.

3 Chapter 3: RFS-1 plays a specific role in promoting homologous recombination at impeded replication forks

3.1 Phenotypic analysis of *rfs-1(ok1372)*

3.1.1 RFS-1 appears to be the single *C. elegans* RAD-51 paralog

C30A5.2 was originally identified as a yeast two-hybrid interacting partner of RAD-51 in a screen to identify novel DNA damage response proteins (Boulton *et al.* 2002). PSI-BLAST sequence homology searches with C30A5.2 revealed a RAD51/DMC1/RADA like domain present in all Rad51 paralog proteins, and given this homology, and smaller size relative to RAD-51, the protein was named RFS-1 (Rad fifty-one short-1) (Boulton *et al.* 2002). Subsequent studies not only confirmed the RAD-51 interaction, but also found that RFS-1 interacted with the N-terminal domain of CeBRC-2 (Martin *et al.* 2005). Phylogenetic analysis suggests RFS-1 is most closely-related to the RAD51D group of the RAD51 family (Figure 3.1), and sequence alignments demonstrate conservation of the Walker A and B ATPase motif (Figure 3.2). No other obvious Rad51 paralog proteins based on sequence are evident in the *C. elegans* genome, although the presence of highly divergent paralogs cannot be ruled out.

3.1.2 Description of *ok1372* allele of *rfs-1*

To examine the contribution of RFS-1 to HRR-mediated repair processes, the allele *rfs-1(ok1372)* was characterized. This allele was generated by the *C. elegans* Gene Knockout Consortium, an organization which uses a high throughput PCR-based screening strategy to isolate deletion mutants from TMP/UVA mutagenized populations of nematodes. The *ok1372* deletion partially removes exon one and eliminates the

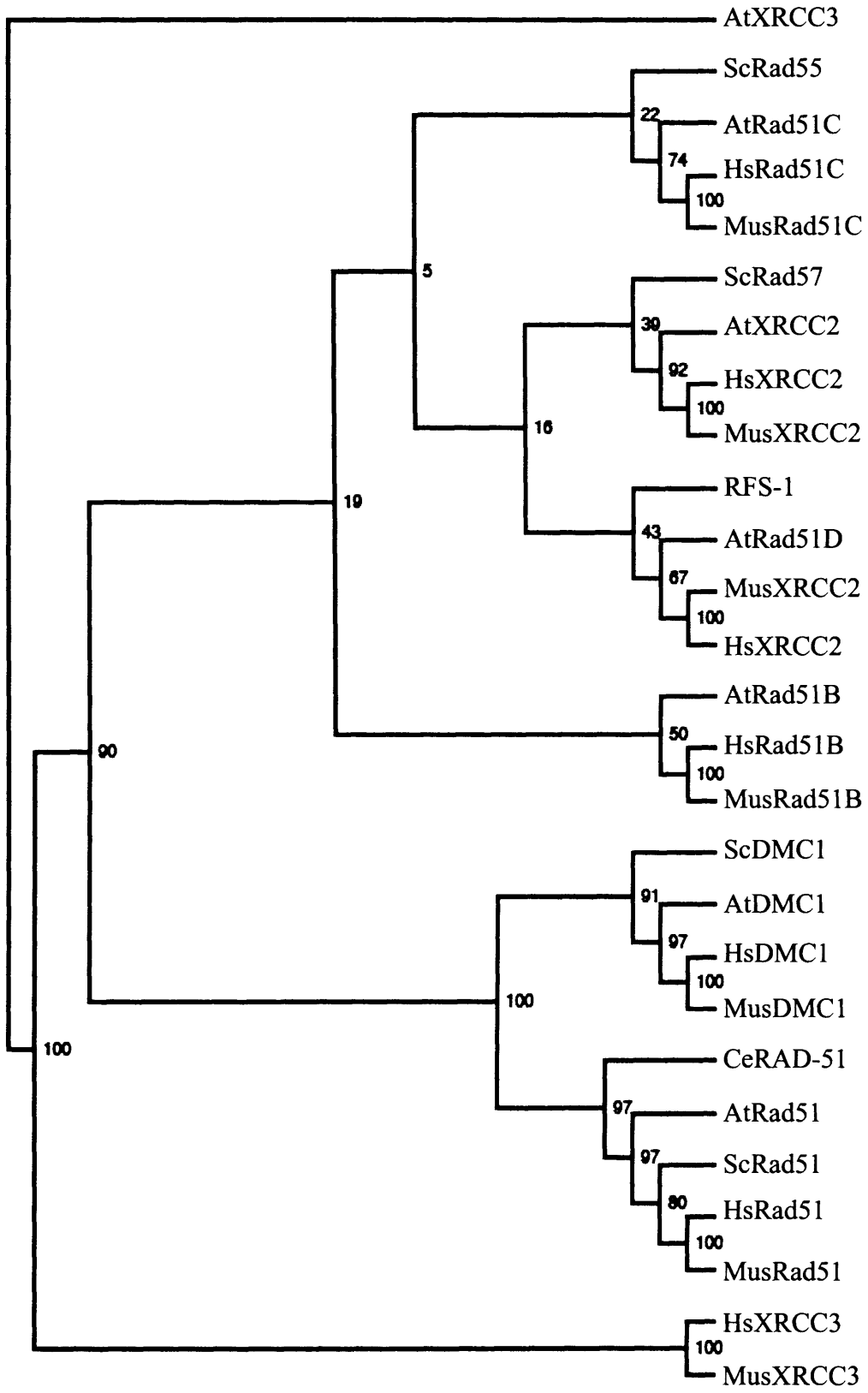

Figure 3.1. Cladogram of the RAD-51 protein family. Protein sequences were obtained from GenBank. Phylogenetic analysis of the RAD-51 family of proteins from *S. cerevisiae* (Sc), *C. elegans* (Ce), *A. thaliana* (At), *M. musculus* (Mm), and *H. sapiens* (Hs) was performed using Phylip 3.65. Values for 100 bootstrap replicates are shown.

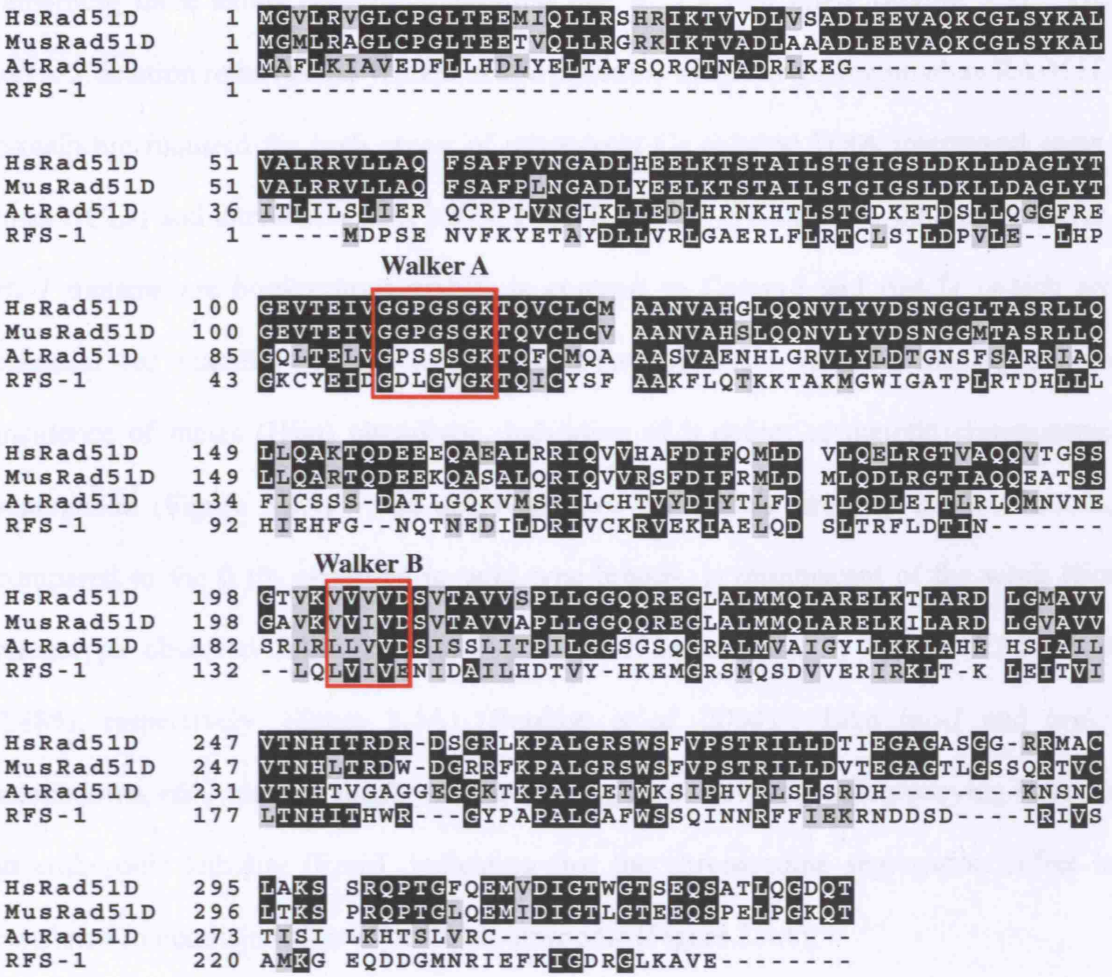

Figure 3.2. Alignment of RFS-1 with human (Hs), mouse (Mus), and Arabidopsis (At) RAD51D proteins. Alignments were performed using ClustalW 1.83. The Walker A and B ATP binding motifs are indicated by red boxes. White letters on black background indicates conserved residues, black letters on grey background specifies semi-conserved residues, and black lettering on a white background represents non-conserved residues.

remaining three exons entirely, suggesting that it is a null allele (Figure 3.3). The *ok1372* deletion removes the Walker A and B boxes, which in the mammalian RAD51D protein are required for both repair of mitomycin C- induced DNA interstrand cross-links (ICLs) and interaction with XRCC2 and RAD51C (Wiese *et al.* 2006). However, *rfs-1* mutants are homozygous viable, in contrast to *Cebrc-2* and *rad-51,* which are essential for viability (Figure 3.4A). Interestingly, *rfs-1* mutants display a high incidence of males (Him) phenotype, indicative of a defect in meiotic chromosome segregation (Figure 3.4A). The observation of 2.2% male progeny in *rfs-1* broods, compared to the 0.1% observed in wild type broods, is reminiscent of the weak Him phenotype observed following *brc-1* and *brd-1* knockdown by RNAi (2.54% and 2.88%, respectively; Figure 3.4A) (Boulton *et al.* 2004). Like *brc-1* and *brd-1* knockdown, *rfs-1* mutants display a Him phenotype without any accompanying increase in embryonic lethality (Emb), indicating that the chromosome segregation defect is restricted to nondisjunction of the X chromosome (Figure 3.4A).

3.1.3 RFS-1 is dispensable for repair of meiotic DNA double-strand breaks

To further examine the role of *rfs*-1 in meiosis, a detailed cytological examination of the germ line was performed. The *C. elegans* germ line is polarized in a distal-to-proximal manner with respect to proliferation and meiotic prophase I. The distal portion of the germ line comprises a zone of mitotic proliferation, which is the only actively dividing cell population in the adult animal. Mitotic cells then enter the leptotene phase of meiotic prophase I, where homologous chromosomes align, synapse, and are held together along their entire length by the synaptonemal complex (SC). Meiotic recombination is initiated by the action of SPO-11, which induces the formation of DSBs that can be followed by the appearance of RAD-51 foci (Dernburg *et al.* 1998; Alpi *et al.* 2003; Colaiacovo *et al.* 2003; Martin *et al.* 2005). The

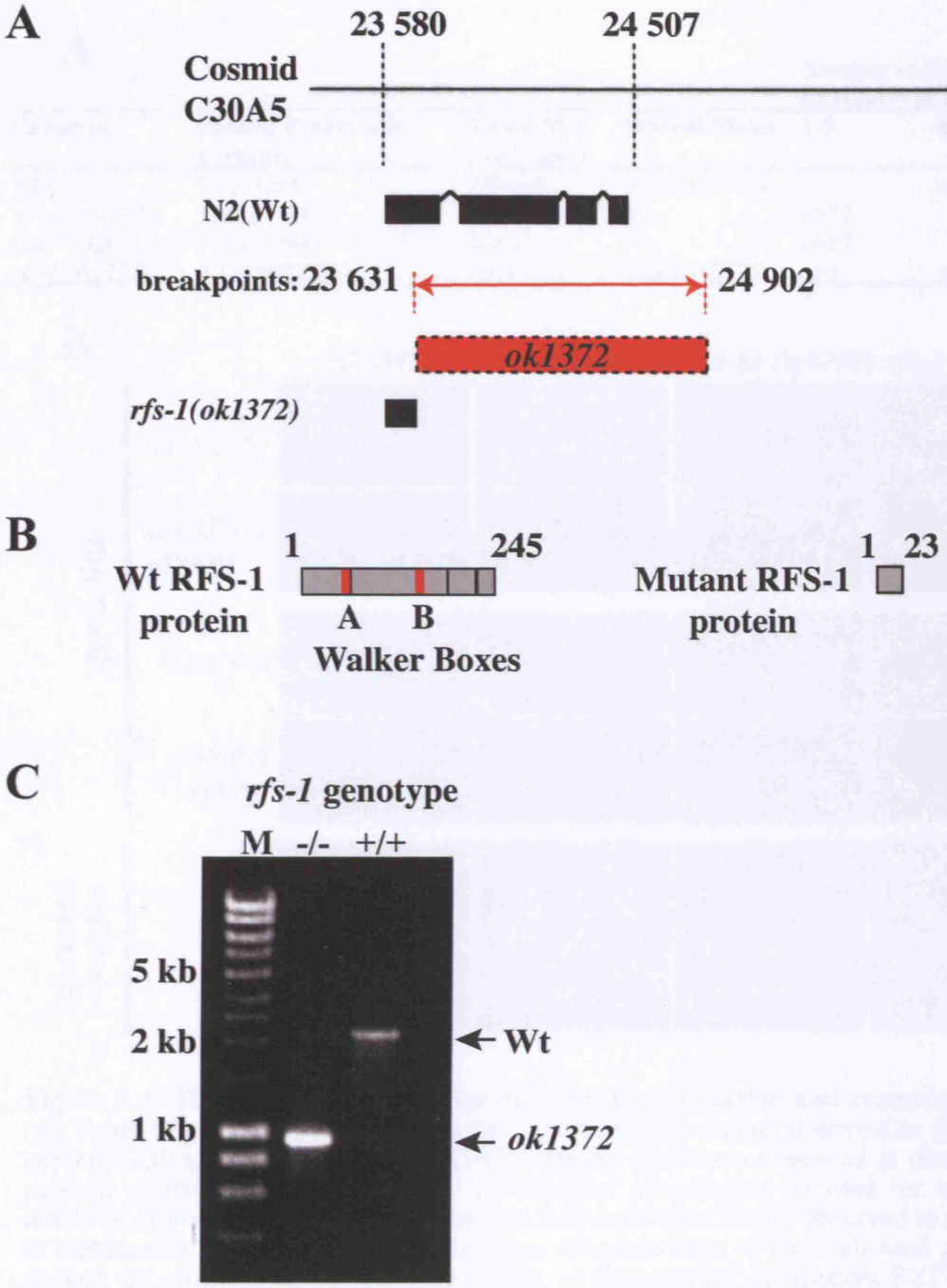

Figure 3.3. *rfs-1* gene, deletion, and protein domain architecture. (A) The numbers indicate nucleotide position in cosmid C30A5, which contains the genomic sequence that includes *rfs-1*. This sequence was used to determine the deletion breakpoints. The gene structure of *rfs-1* (C30A5.2) is shown, along with the location of the *ok1372* deletion (red box), which is a 1271 bp deletion in the *rfs-1* gene that removes half of exon 1 and the entirety of exons 2, 3, and 4. (B) The predicted protein structure for wild type (245 residue protein) and mutant RFS-1 protein (23 aa). The conserved Walker A and B ATPase domains (red boxes) are indicated. (C) Nested PCR, using primers flanking the *rfs-1* gene, from a single wild type N2 animal (+/+) or single *rfs-1(ok1372)* mutant (-/-) showing the 1271 bp *ok1372* deletion. The primers are predicted to amplify a 2226 bp product in wild type (Wt) animals and a 1025 bp product in *rfs-1(ok1372)* mutants. A DNA size marker (M) is included on the gel; fragment sizes are indicated in kilobase pairs.

A

Genotype	Percent Embryonic Lethality	Brood Size (±std. dev.)	Percent Males	Number of DAPI stained structures at diakinesis: 1-5	6
N2 (wt)	0 (n=3064)	255±31	0.10 (n=3064)		n=84
brc-2(tm1086)	100 (n=376)	52±31	n/a	n=57	
rad-51(lg08701)	100 (n=568)	34±32	n/a	n=67	
rfs-1(ok1372)	0.13 (n=2276)	207±73	2.20 (n=2276)	n=1	n=80

B

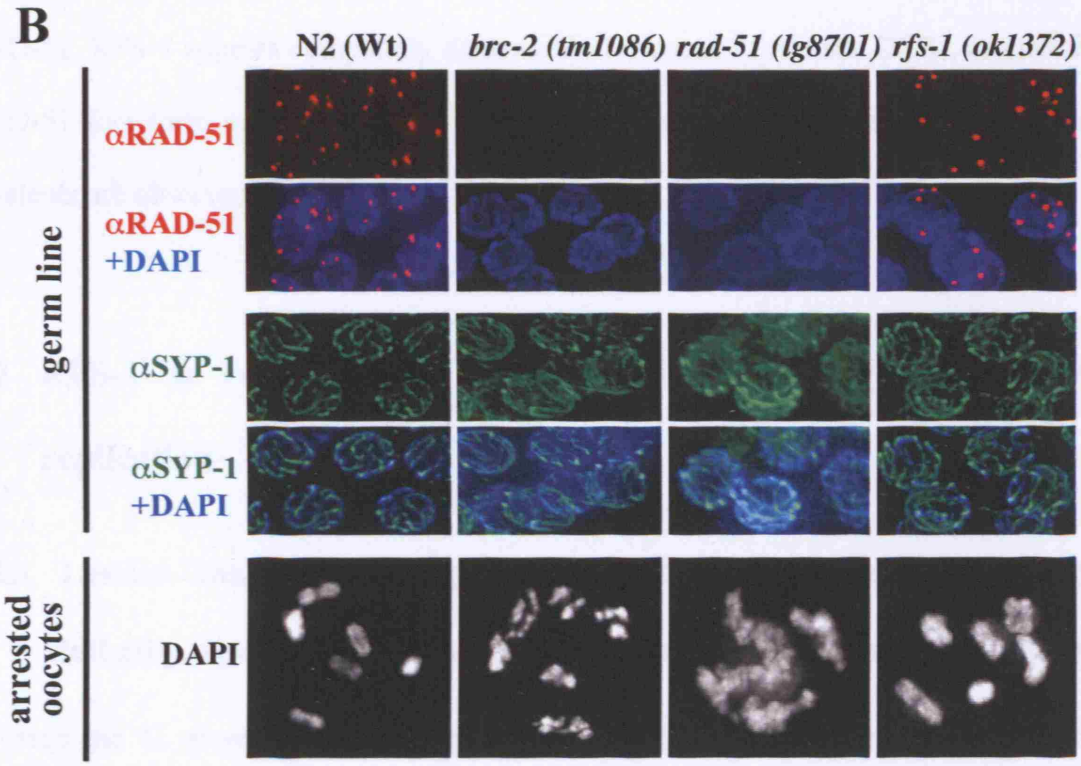

Figure 3.4. RFS-1 is dispensable for meiotic recombination and crossing over. (A) Table of percent embryonic lethality, brood size (± standard deviation (std. dev)), percent males, and the number of DAPI-stained structures observed at diakinesis in animals of the indicated genotypes (n=numbers of embryos counted for embryonic lethality, animals scored for percent males, and number of nuclei observed in each class at diakinesis). (B) Representative images of germ lines of the indicated genotypes stained for either RAD-51 (red, top panel), or the core SC component SYP-1 (green, middle panel). DNA is counterstained with DAPI (blue, top and middle panels). Representative images of DAPI-stained single oocyte nuclei of the indicated genotypes arrested at diakinesis (grey, bottom panel).

completion of meiosis I results in six bivalents, pairs of homologs held together by a chiasmata, the result of successful crossing over. Like in *Cebrc-2* and *rad-51* mutants, the synaptonemal complex is unperturbed in *rfs-1* mutants, as indicated by intact germ line immunostaining against a core component of the SC, SYP-1 (Figure 3.4B) (MacQueen *et al.* 2002; Martin *et al.* 2005). However, in contrast to CeBRC-2 and RAD-51, RFS-1 appears completely dispensable for repair of meiotic DSBs, as meiotic RAD-51 foci form in *rfs-1* mutants and the normal complement of six DAPI stained bivalents are observed at diakinesis (Figure 3.4B).

3.2 RFS-1 is required for repair of lesions that impede DNA replication

3.2.1 Lesions that impede replication forks cause increased progeny lethality, apoptosis, and chromosomal fragmentation in *rfs-1* mutants.

Because the *C. elegans* BRCA1 homolog *(brc-1)* is also dispensable for crossover formation in meiosis but is crucial for repair of IR-induced DSBs (Boulton *et al.* 2004), the *rfs-1* mutant was assayed for enhanced sensitivity to IR. Whilst irradiated *brc-1(tm1145)* mutants have extensive embryonic lethality at the relatively low dose (for *C. elegans)* of 50 Gy irradiation, *rfs-1(ok1372)* mutants are only moderately sensitive to IR (Figure 3.5A). As DT40 cells mutant for any of the Rad51 paralogs are also mildly sensitive to IR, but are acutely sensitive to ICLs, *rfs-1* mutants were tested for sensitivity to the cross-linking agents cisplatin (CDDP) and nitrogen mustard (HN2) (Takata *et al.* 2001). Both *brc-1(tm1145)* and *rfs-1(ok1372)* mutations significantly compromised progeny survival relative to wild type animals (Figure 3.5B,C). Next, the sensitivity of *rfs-1* mutants to camptothecin (CPT) was assessed; CPT is a topoisomerase I poison that inhibits the enzyme and prevents its release from DNA,

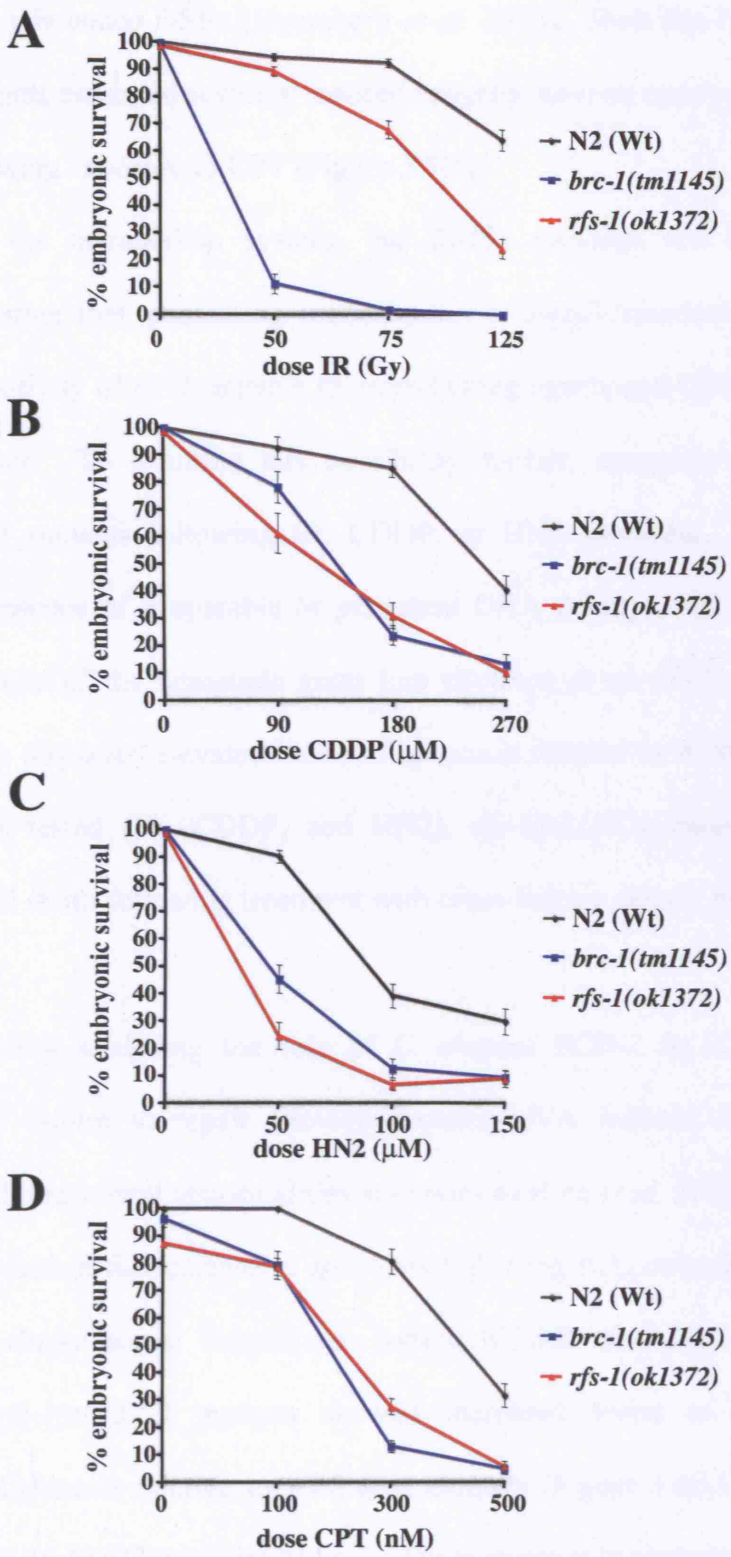

Figure 3.5. Lesions that impede replication forks cause increased progeny lethality in *rfs-1* mutants. (A-D) Percentage progeny survival in animals of the indicated genotypes treated with the indicated doses of ionizing radiation (IR; A), cisplatin (CDDP; B), nitrogen mustard (HN2; C), and camptothecin (CPT; D). Error bars indicate S.E.M. from at least 24 adult worms over two independent experiments.

creating capped single ended DSBs (Strumberg *et al.* 2000). Both *brc-1(tm1145)* and *rfs-1(ok1372)* mutants exhibited severely reduced progeny survival rates relative to wild type animals following exposure to CPT (Figure 3.5D).

Since, in the mammalian system, the Rad51 paralogs are implicated in promoting HRR rather than possessing a checkpoint or signal-transduction role, it is likely that the sensitivity of *rfs-1* mutants to cross-linking agents and CPT is a result of compromised repair. To examine this possibility further, apoptotic corpses were quantified in *rfs-1* mutants following IR, CDDP, or HN2 treatment. Apoptosis is induced by the presence of irreparable or persistent DNA damage, and can be easily observed in the bend of the nematode germ line (Boulton *et al.* 2002). While *brc-1(tm1145)* animals displayed elevated levels of apoptosis relative to Wild type animals for all treatments tested (IR, CDDP, and HN2), *rfs-1(ok1372)* mutants displayed increased germ cell death following treatment with cross-linking agents, but not with IR (Figure 3.6A).

Previous work analyzing the role of *C. elegans* FCD-2 in ICL repair had demonstrated that failure to repair trimethylpsoralen-UVA induced ICLs in *fcd-2* mutants leads to chromosomal abnormalities at diakinesis (Lee *et al.* 2007). Therefore, it was examined whether the increase in apoptosis following ICL-induced damage was accompanied by chromosomal aberrations. Indeed, CDDP treatment of both *brc-1(tm1145)* and *rfs-1(ok1372)* mutants showed increased levels of chromosomal abnormalities at diakinesis relative to wild type animals (Figure 3.6B,C). However, while irradiated *rfs-1(ok1372)* mutants had a moderate increase in abnormalities relative to wild type animals after IR-treatment, virtually all chromosomes at diakinesis examined in irradiated *brc-1(tm1145)* mutants were aberrant (Figure 3.6B,C). Interestingly, both ICL- and CPT-derived lesions impede replication forks, ultimately causing fork stalling. Together these data emphasize a severe defect in repairing DNA

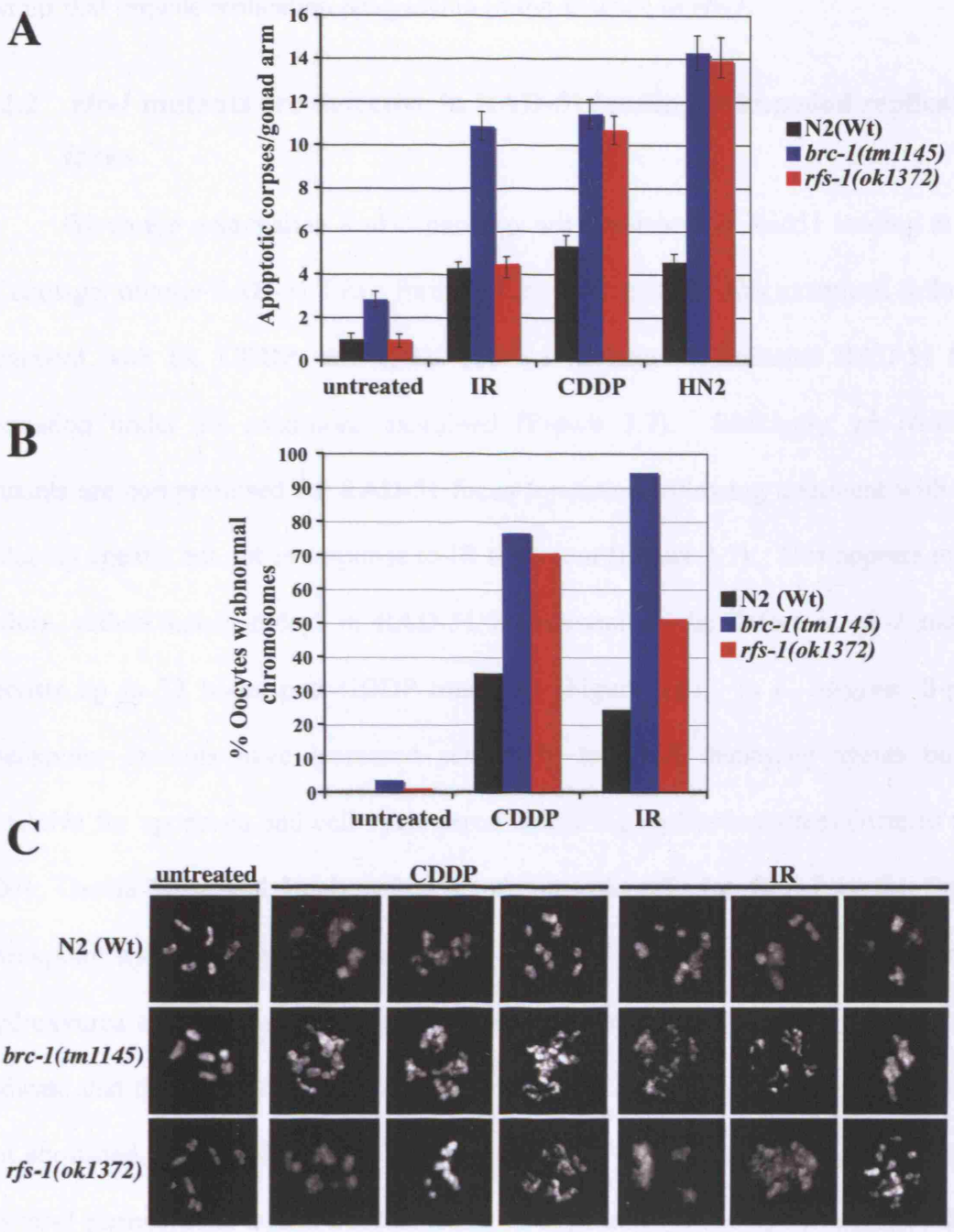

Figure 3.6. Replication blocking lesions cause increased apoptosis and chromosomal aberrations in *rfs-1* mutants. (A) Number of apoptotic corpses scored by DIC microscopy in animals of the indicated genotypes either untreated or 24 hours post-treatment with 75 Gy IR, 180 µM CDDP, or 150 µM HN2. Error bars indicate S.E.M. from at least 20 adult animals. (J. Ward and S.J. Boulton) (B) Percentage of examined chromosomes at the diakinesis stage of meiosis I with abnormalities. Young adult animals were dissected either untreated or 24 hours post-treatment with 75 Gy IR or 180 µM CDDP and DNA was observed by counterstaining with DAPI. At least 50 oocyte nuclei at diakinesis were scored for chromosomal abnormalities (e.g. alteration in bivalent number or fragmentation) per strain for each condition. (C) Representative images of aberrant chromosomes, stained with DAPI (grey), at diakinesis following treatment with ionizing radiation or cisplatin. Young adult animals were dissected and fixed either untreated or 24 hours post-treatment with 75 Gy IR or 180 µM CDDP.

lesions that impede replication progression in the absence of *rfs-1*.

3.2.2 *rfs-1* mutants are defective in RAD-51 loading at impeded replication forks

Given the mammalian Rad51 paralogs are implicated in Rad51 loading at sites of damage, mitotic RAD-51 focus formation in *rfs-1* mutants was examined following treatment with IR, CDDP, and HN2. *Cebrc-2* mutations eliminated RAD-51 focus formation under all conditions examined (Figure 3.7). Strikingly, *rfs-1(ok1372)* mutants are compromised for RAD-51 focus formation following treatment with ICL-inducing agents, but not in response to IR treatment (Figure 3.7). This appears to be a failure, rather than a delay, in RAD-51 recruitment as the defect in *rfs-1* mutants persists up to 32 hours post-CDDP treatment (Figure 3.8). In *C. elegans,* S-phase checkpoint mutants have increased sensitivity to DNA damaging agents but are defective for apoptosis and cell cycle arrest following replication stress (Ahmed *et al.* 2001; Garcia-Muse and Boulton 2005). A possible role for RFS-1 in the S-phase checkpoint was tested by examining cell cycle arrest following nucleotide depletion by hydroxyurea treatment. The reduction in number and enlargement of mitotic nuclei indicate that the checkpoint is intact (Figure 3.9). The fact that apoptosis is elevated, not abolished, combined with the observation of an HU-induced arrest, indicates that the *rfs-1* phenotype is due to a repair issue, as opposed to a checkpoint defect. Thus it seems likely that the sensitivity, elevated apoptosis and chromosome abnormalities observed in the absence of *rfs-1* following treatment with CDDP and HN2 result from a failure to load RAD-51 specifically at lesions that block DNA replication, but not at conventional DSBs.

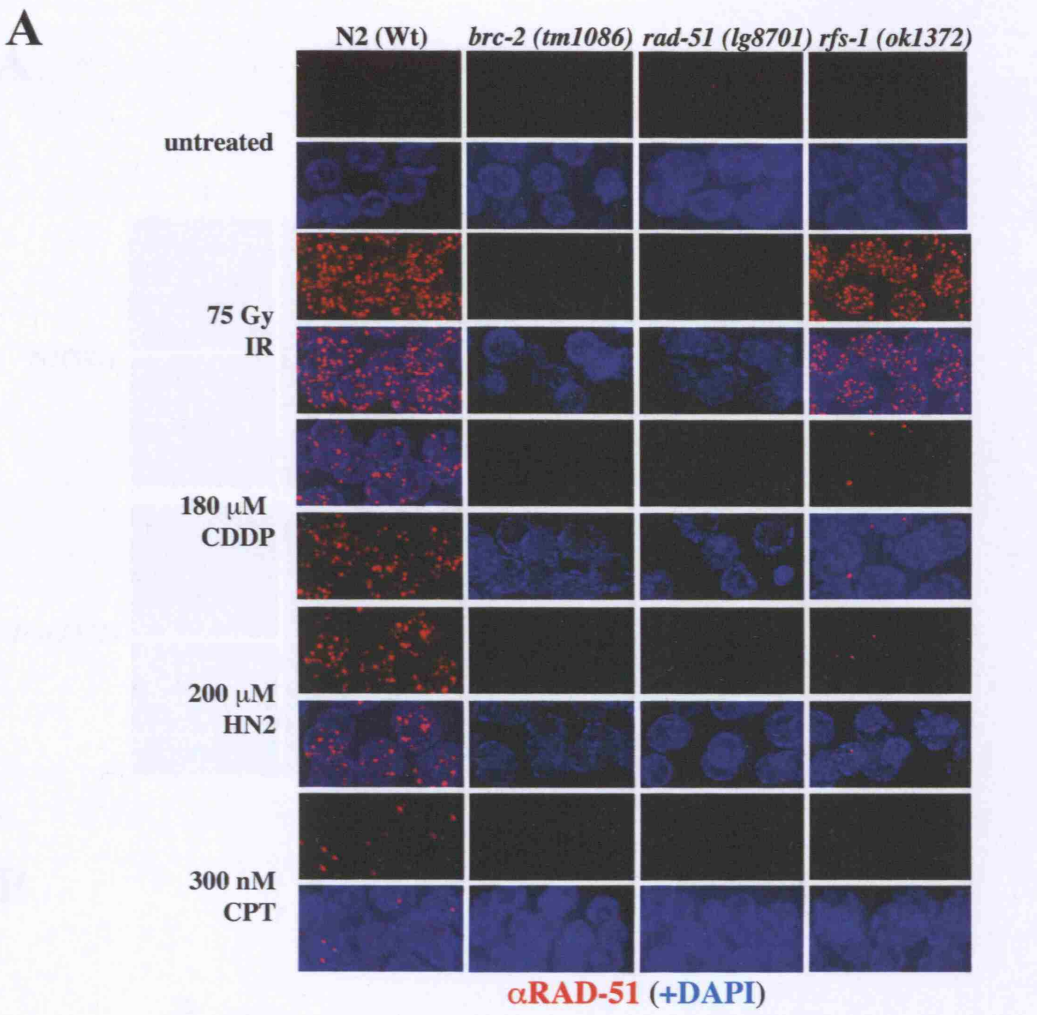

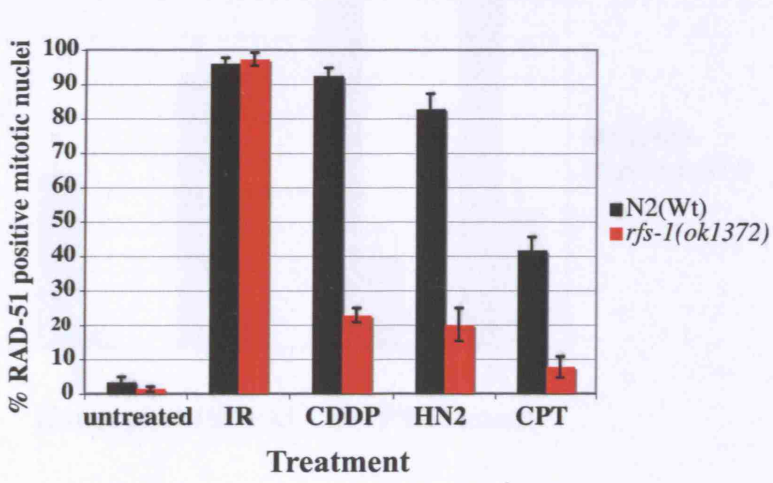

Figure 3.7. RFS-1 mutants are defective for RAD-51 focus formation specifically following replication blocking damage. (A) Representative images of RAD-51 staining (red) in fixed mitotic nuclei of the indicated genotypes either untreated, 4 hours post-treatment with 75 Gy IR, 18 hours post-treatment with 180 μM CDDP, 16 hours post-treatment with 200 μM HN2, or seven hours post-treatment with 300 nM CPT. DNA was observed by counterstaining with DAPI (blue). (B) Quantification of RAD-51 positive N2 (Wt) and *rfs-1(ok1372)* mitotic nuclei as treated in (A). Error bars indicate S.E.M. from 20 mitotic nuclei from 10-15 worms of each genotype from two independent experiments.

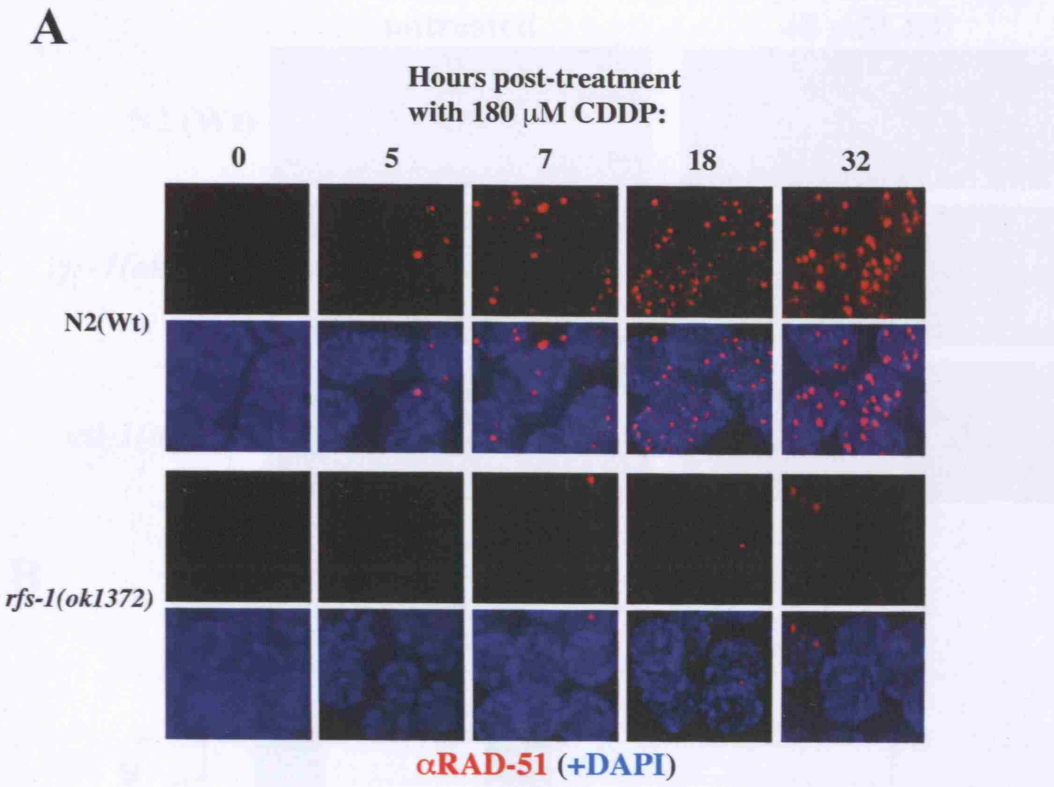

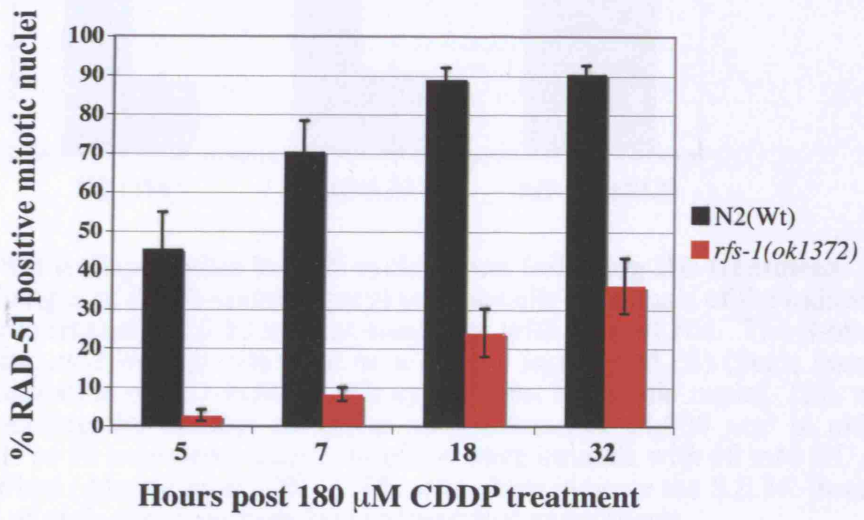

Figure 3.8. CDDP-induced RAD-51 focus formation is defective, not delayed in *rfs-1* mutants. (A) Representative images of RAD-51 staining (red) in fixed mitotic nuclei of the indicated genotypes animals either untreated or 5, 7, 18, and 32 hours post-treatment with 180 μM CDDP. DNA was observed by counterstaining with DAPI (blue). (B) Quantitation of RAD-51 positive mitotic nuclei of the indicated genotypes as treated in (A). Error bars indicate S.E.M. from 20 mitotic nuclei from 10-15 worms of each genotype from two independent experiments.

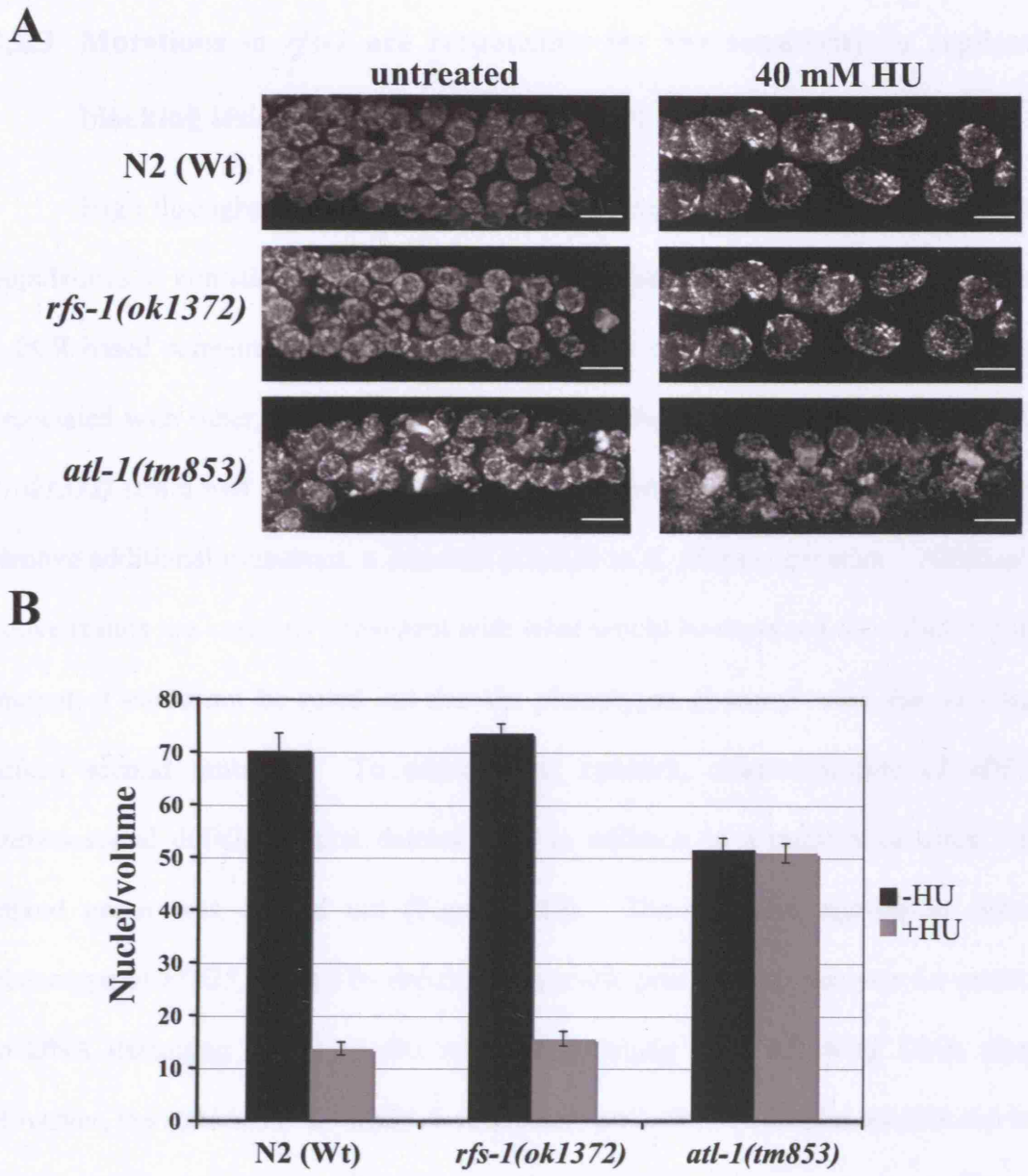

Figure 3.9. RFS-1 is dispensable for cell cycle arrest following HU treatment. (A) Representative images of DAPI-stained (grey) mitotic cells in animals of the indicated genotypes either untreated or 16 hours post-treatment with 40 mM HU. The S-phase checkpoint mutant *atl-1(tm853)* was used as a control in (A) and (B) (Scale bars=5 μm). (B) Quantification of HU-induced cell cycle arrest in mitotic nuclei. This was determined by scoring the number of nuclei in a volume of 54,000 μm^3 in either untreated animals or 16 hours post-treatment of L4 stage animals with 40 mM HU, as previously described (Ahmed *et al.*, 2001). The error bars indicate the S.E.M. from at least 10 animals of each genotype from two independent experiments.

3.2.3 Mutations in *rfs-1* are responsible for the sensitivity to replication blocking lesions and a defect in RAD-51 loading at these lesions

High throughput mutant generation in *C. elegans* currently relies on exposing populations of animals to high doses of a mutagen and isolating deletion alleles through a PCR-based screening strategy. Due to the high mutagen doses, mutants are often associated with other chromosomal aberrations in the background. Therefore, the *rfs-1(ok1372)* strain was extensively backcrossed against the wild type strain (six times) to remove additional mutations, a standard practice in *C. elegans* genetics. Although the above results are certainly consistent with what would be expected for a Rad51 paralog mutant, it could not be ruled out that the phenotypes observed were due to a tightly linked second mutation. To address this concern, characterization of *eDf25*, a chromosomal deficiency that deletes *rfs-1* in addition to a number of other closely linked genes was carried out (Figure 3.10). The recessive egg-laying defective phenotype of *eDf25,* caused by deletion of *unc-86,* precluded its analysis for sensitivity to DNA damaging agents as this relies on hatching rates following DNA damage. However, the *rfs-1(ok1372)/eDf25* transheterozygote, showed similar sensitivities to IR, CDDP, HN2, and CPT as *rfs-1(ok1372)* homozygotes (Figure 3.11A). Additionally, like *rfs-1(ok1372)* mutants, both *eDf25* and *rfs-1(ok1372)/eDf25* transheterozygotes are compromised for RAD-51 focus formation following treatment with ICL-inducing agents, whereas IR-induced RAD-51 foci are unaffected (Figure 3.11B). Finally, an independent laboratory has demonstrated that the Him phenotype observed in *eDf25* (originally isolated as *him-15* in a screen for increased males) is due to the loss of *rfs-1* (Hodgkin *et al.* 1979; Yanowitz 2008). Together these results convincingly indicate that the deletion of *rfs-1* is responsible for all of the phenotypes observed.

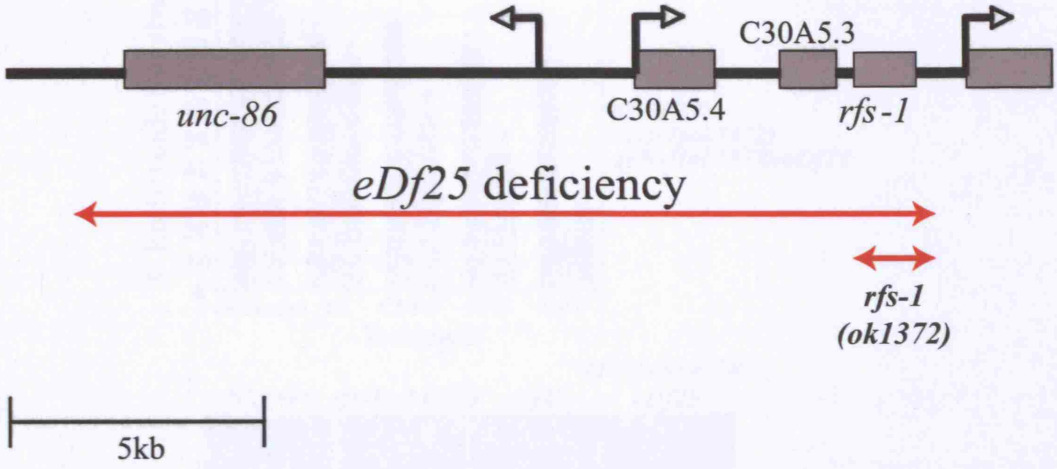

Figure 3.10. *eDf25* is a deficiency that deletes the entire coding region of *rfs-1*. *eDf25*, originally known as *him-15,* is a deficiency that deletes the entire coding region of *rfs-1*, as well as *unc-86* and C30A5.4 (Hodgkin *et al.*, 1979; Yanowitz, 2007). Red bars indicate the region deleted in each strain. Figure courtesy of J. Yanowitz.

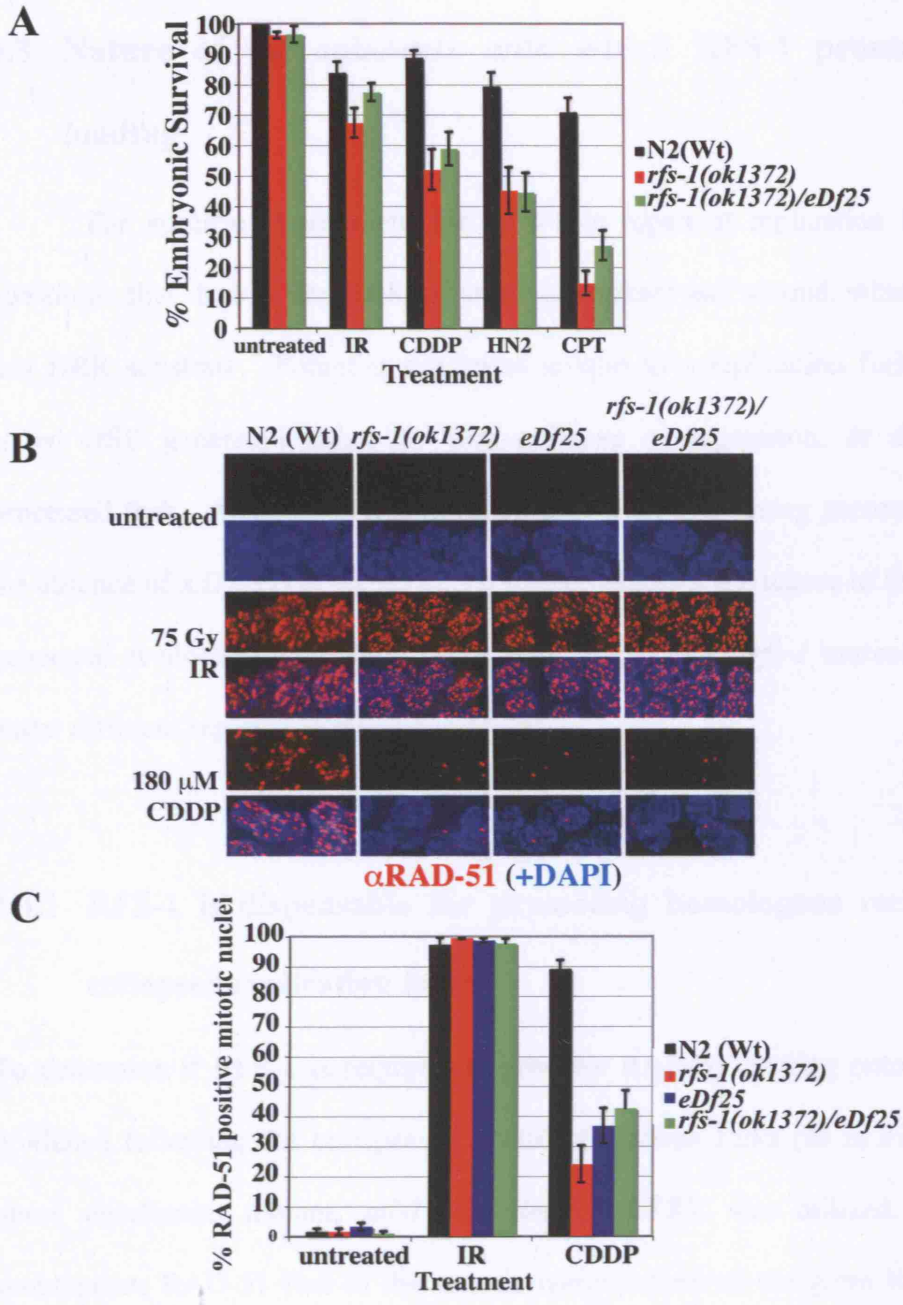

Figure 3.11. *rfs-1(ok1372)/eDf25* transheterozygotes display a similar phenotypes to *rfs-1(ok1372)* homozygotes. (A) Percentage progeny survival of N2 (Wt), *rfs-1(ok1372),* and *rfs-1(ok1372/)eDf25* transheterozygote animals treated with 75 Gy of ionizing radiation (IR), 180 μM cisplatin (CDDP), 50 μM nitrogen mustard (HN2), and 300 nM camptothecin (CPT). Error bars indicate S.E.M. from at least 24 adult worms over two independent experiments. (B) Representative images of RAD-51 staining (red) in fixed mitotic nuclei of the indicated genotypes either untreated, four hours post-treatment with 75 Gy IR or 18 hours post-treatment with 180 μM CDDP. DNA is counterstained with DAPI (blue). (C) Quantitation of RAD-51 positive mitotic nuclei in the indicated genotypes, as treated in (B). Error bars indicate S.E.M. from 20 mitotic nuclei from 10-15 worms of each genotype from two independent experiments.

3.3 Nature of the substrate onto which RFS-1 promotes RAD-51 loading

The specific requirement for RFS-1 in repair at replication forks raises two questions: first, how is the HRR substrate generated; and second, what is the nature of this HRR substrate. Potential substrates unique to a replication fork include a one-ended DSB generated either by fork collapse or regression, or an enzymatically processed fork. Alternatively, it is possible that HRR is being promoted at ssDNA in the absence of a DSB (Figure 3.12). To further examine the nature of the HRR substrate generated at blocked replication forks, the phenotypes of *rfs-1* mutants was examined under different replication stress conditions.

3.3.1 RFS-1 is dispensable for promoting homologous recombination at collapsed replication forks.

To determine if RFS-1 is required to promote RAD-51 loading onto free DNA ends produced following the collapse of stalled replication forks (as in Fig 3.12B), the S-phase checkpoint mutant, *atl-1 (C. elegans* ATR), was utilized. *atl-1* exhibits spontaneous RAD-51 foci in the mitotic compartment of the germ line as a result of replication fork collapse (Garcia-Muse and Boulton 2005). Surprisingly, *rfs-1; atl-1* double mutants display similar levels of spontaneous RAD-51 foci to those observed in *atl-1* single mutants, indicating that RFS-1 is dispensable for promoting HRR at collapsed replication forks (Figure 3.13A,C). It is known that stalled replication forks frequently collapse to generate DSBs when treated with high doses of hydroxyurea, an agent that inhibits ribonucleotide reductase (Lundin *et al.* 2002). While *Cebrc-2* and *rad-51* mutations eliminate HU-induced RAD-51 foci, surprisingly, *rfs-1* mutants resemble wild type animals with respect to RAD-51 focus formation (Figure 3.13B,C).

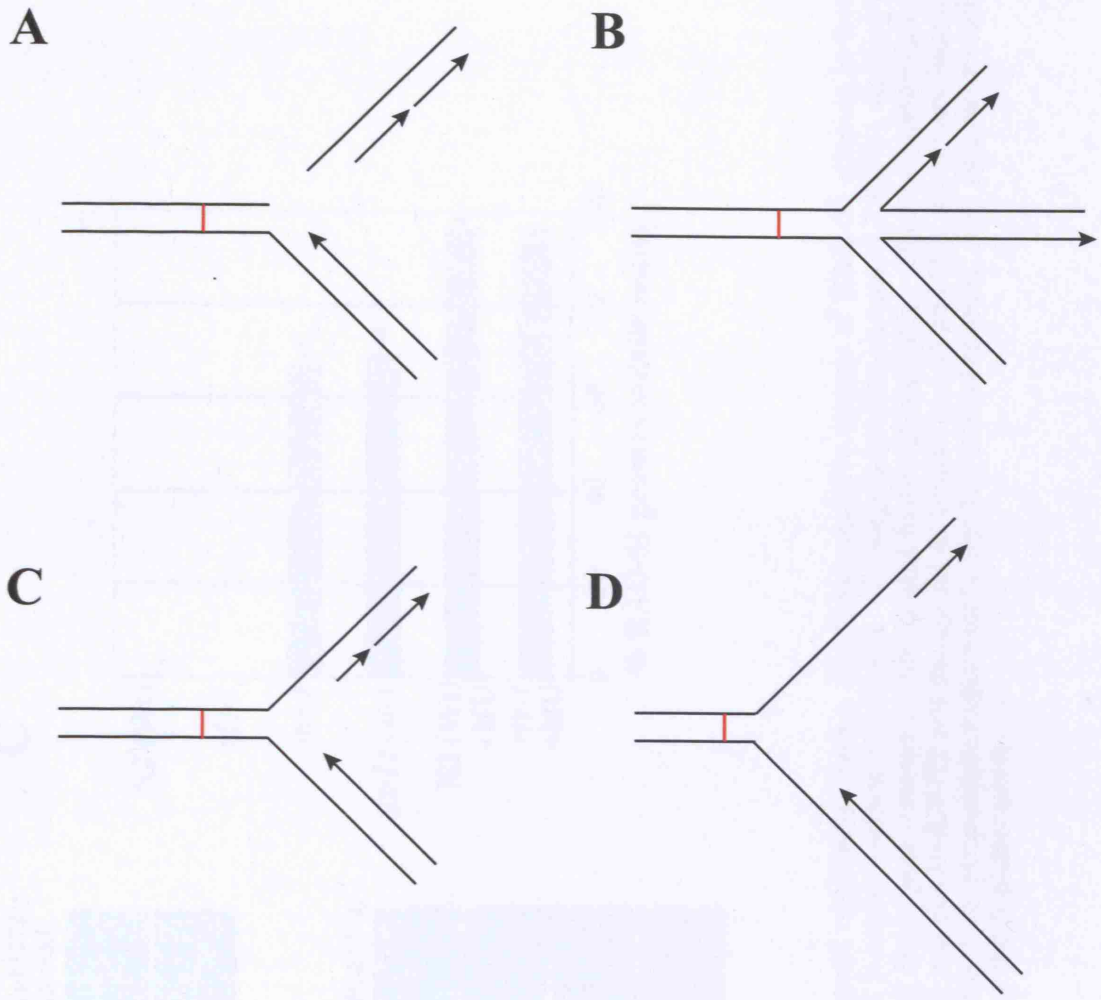

Figure 3.12. Potential HRR substrates generated at fork blocking lesions. The fork-blocking lesion is indicated in this figure by a red bar to the left of the stalled replication fork. (A) Nucleolytic incision of an ICL will generate a one-ended DSB as well as a short tract of ssDNA on the uncut strand. Camptothecin treatment also generates this substrate. (B) Fork regression through annealing of the nascent synthesized strands to generate a "chicken foot" structure. This four-way junction resembles a Holliday junction and also creates a single ended DSB. (C) An arrested fork can generate short stretches of ssDNA at the site of the stall. (D) Fork processing, such as unwinding or nucleolytic degradation can create a conventional HRR substrate (dsDNA:replication protein A coated ssDNA junction).

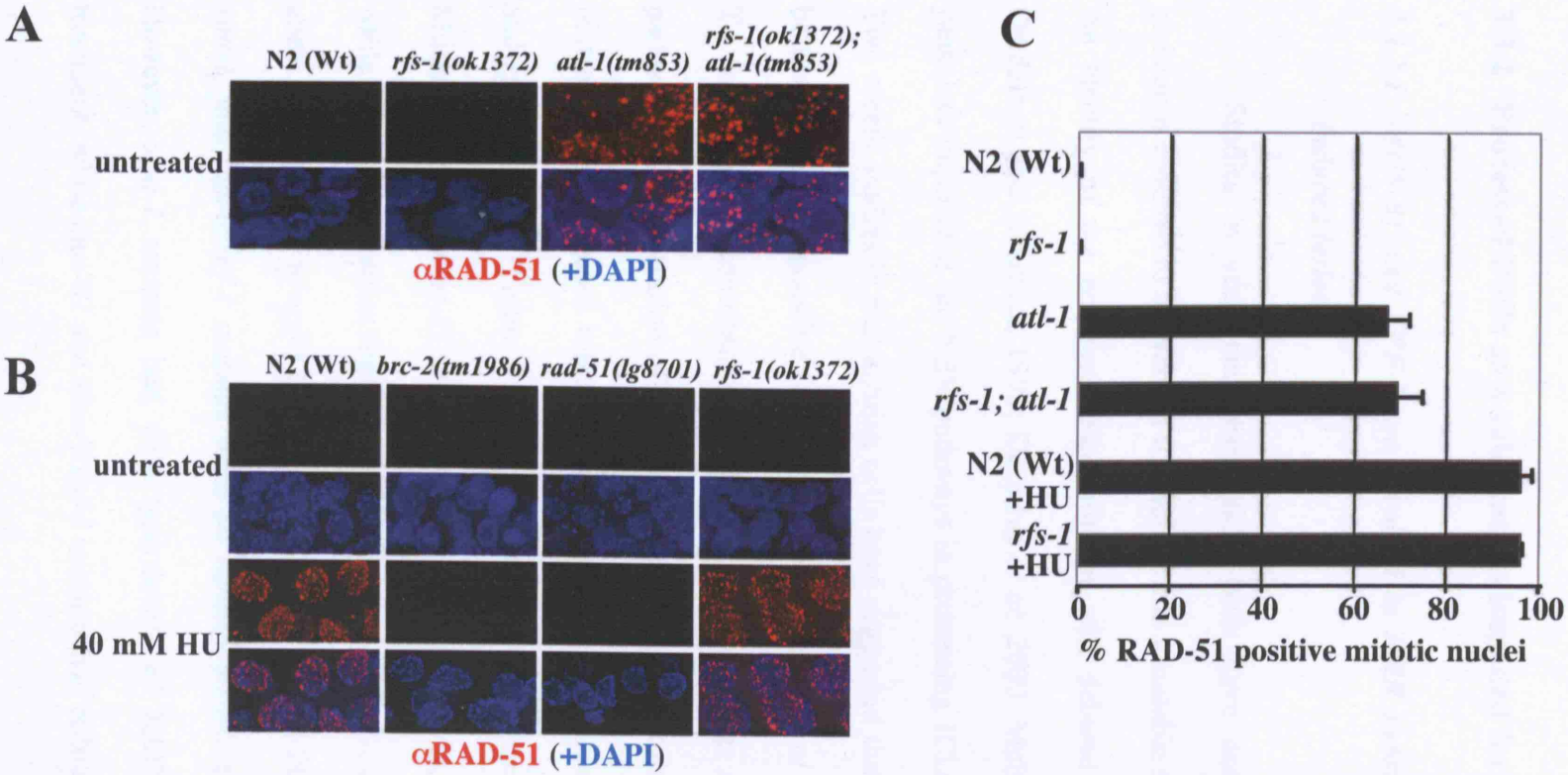

Figure 3.13. RFS-1 is not required for RAD-51 loading at collapsed replication forks. (A) Representative images of RAD-51 staining in fixed mitotic nuclei in untreated animals of the indicated genotypes. DNA is counterstained with DAPI. (B) Representative images of RAD-51 staining in fixed mitotic nuclei of the indicated genotypes either untreated or 16 hours post-treatment with 40 mM hydroxyurea (HU). DNA is counterstained with DAPI (blue). (C) Quantification of RAD-51 positive N2 (Wt) and *rfs-1(ok1372)* mitotic nuclei as treated in (A) and (B). Error bars indicate S.E.M. from 20 mitotic nuclei from 10-15 worms of each genotype from two independent experiments. For HU treated animals, only 10 mitotic nuclei were scored due to the reduction in mitotic nuclei number induced by the S-phase arrest.

The specific HRR defects in *rfs-1* mutants imply that inherent differences exist between HRR at collapsed forks versus impeded forks.

3.3.2 Processed DSBs as a substrate at impeded forks

3.3.2.1 MUS-81 and XPF-1 are involved in HRR substrate generation at CDDP-induced lesions.

Studies in yeast and mammalian cells have demonstrated that nucleolytic incision is required to convert an ICL lesion into a suitable substrate for HRR; however, the identity of the nuclease responsible is still debated (Jachymczyk *et al.* 1981; Dardalhon and Averbeck 1995; De Silva *et al.* 2000; McHugh *et al.* 2000). Work in yeast has implicated the NER pathways in processing ICLs (Jachymczyk *et al.* 1981). Two recent studies in mammalian cells have suggested that either Mus81 or XPF may be the nuclease responsible for ICL incision (Hanada *et al.* 2006; Mogi and Oh 2006). To determine the contributions of Mus81 and homologs of components of the NER pathway in the generation of an HRR substrate at ICL lesions in *C. elegans,* nematode mutants for these genes were obtained, including *mus-81(tm1937)*, *him-9/xpf-1(e1487)* and *xpa-1 (ok698)* (Figure 3.14) (Park *et al.* 2002; Denver *et al.* 2006; O'Neil 2008). Mutations in both *mus-81* and *xpa-1* were large deletions, and are likely null alleles, while *him-9* is a complex rearrangement affecting the *xpf-1* gene and is also likely a null allele, with respect to *xpf-1* (Denver *et al.* 2006; O'Neil 2008). Surprisingly, *mus-81, xpa-1,* and *him-9/xpf-1* mutants were all acutely sensitive to CDDP (Figure 3.15A). However, *xpa-1* mutants had wild type levels of RAD-51 foci following CDDP treatment, while *mus-81* and *him-9/xpf-1* mutants had reduced, but not abolished levels

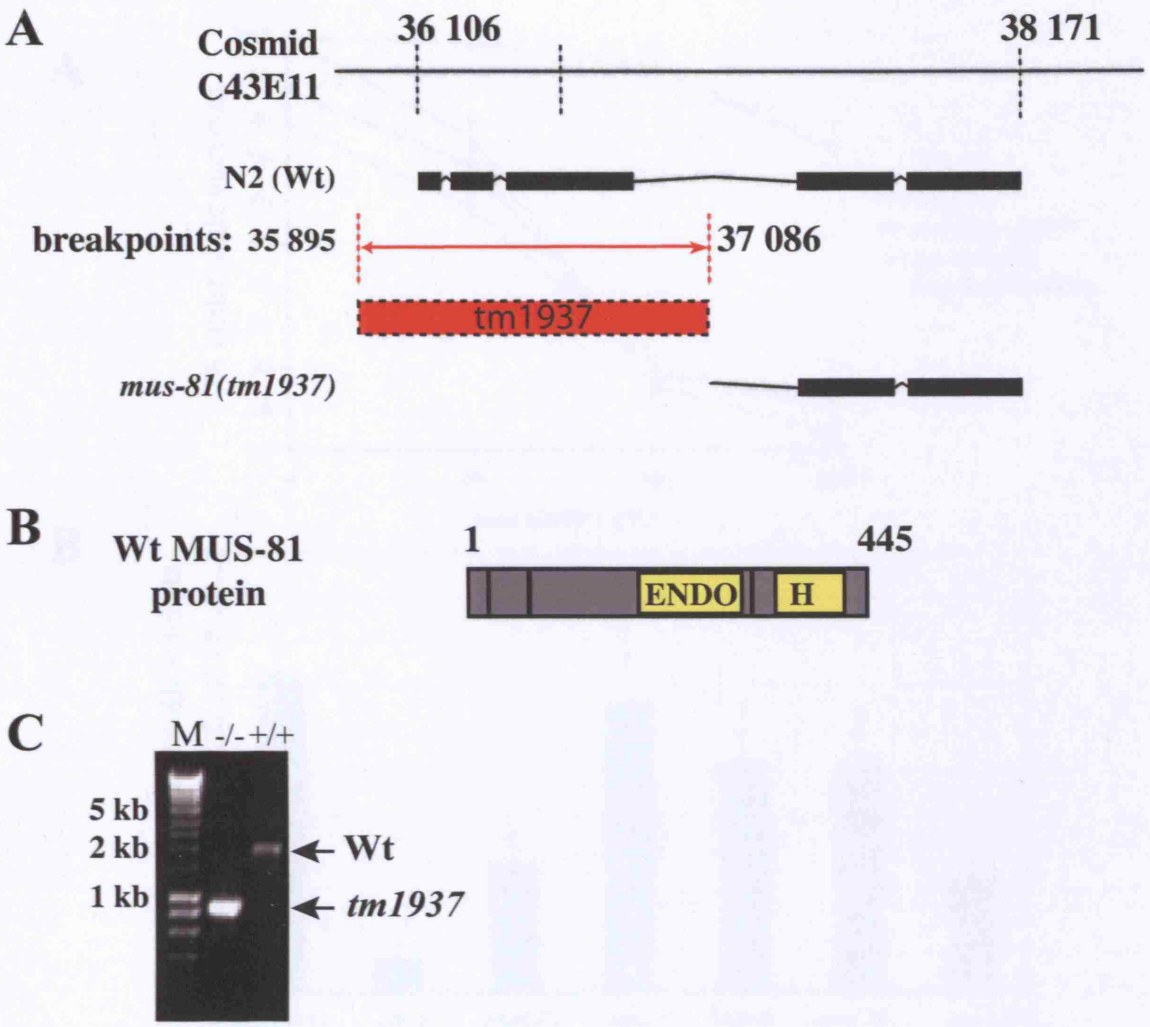

Figure 3.14. *mus-81* gene, deletion, and protein domain architecture. (A) The numbers indicate nucleotide position in cosmid C43E11, which contains the genomic sequence that includes *mus-81*. This sequence was used to determine the deletion breakpoints. The gene structure of *mus-81* (C43E11.2) is shown, along with the position of the *tm1937* allele. *tm1937* is a 1192 bp deletion (red box) in the *mus-81* gene that removes the first two exons and 210 bases of sequence upstream of the translation start site, and is predicted to eliminate expression. (B) The predicted MUS-81 protein structure is shown for wild-type N2 (Wt) (445 residue protein). The conserved endonuclease (ENDO) and helix-hairpin-helix (H) (yellow boxes) are indicated. (C) Nested PCR, using primers flanking the *mus-81* gene, from a single wild type animal (+/+) or single *mus-81(tm1937)* mutant (-/-) showing the 1192 bp deletion. The primers are predicted to amplify a 2070 bp product in wild type (Wt) animals and a 878 bp product in *mus-81(tm1937)* mutants. A DNA size marker (M) is included on the gel; fragment sizes are indicated in kilobase pairs.

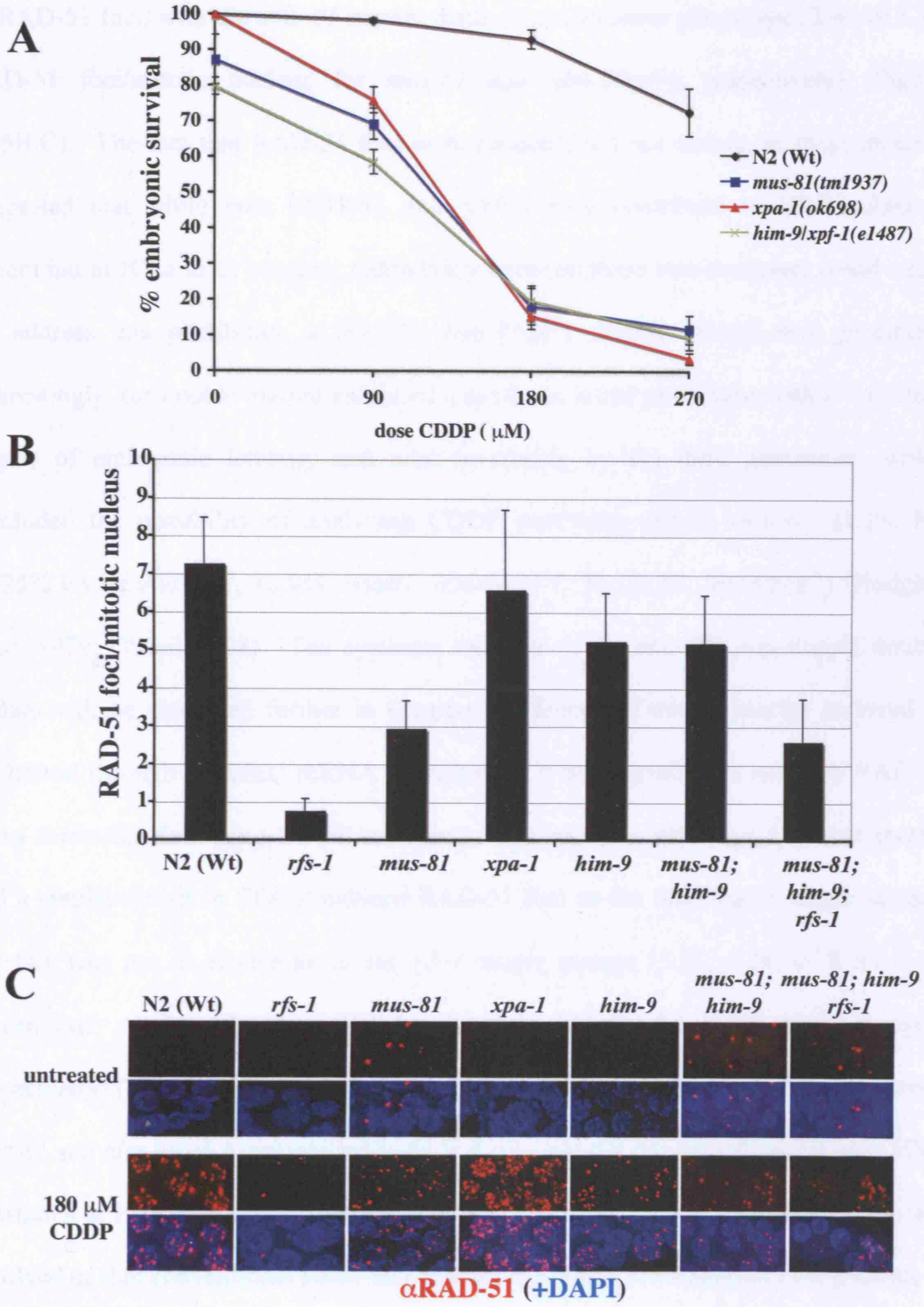

Figure 3.15. MUS-81 and XPF-1 both are involved in HRR substrate generation at CDDP-induced lesions. (A) Percentage progeny survival in animals of the indicated genotypes following treatment with the specified doses of CDDP. Error bars indicate S.E.M. from at least 24 adult worms over two independent experiments. (B) Quantification of the number of RAD-51 foci per mitotic nucleus in animals of the indicated genotype dissected 18 hours post-treatment with 180 μM CDDP. Error bars indicate S.E.M. from at least 10 nuclei from 20-35 animals of each genotype from three independent experiments. (C) Representative images of RAD-51 staining (red) in fixed mitotic nuclei either untreated, or 18 hours post-treatment with 180 μM CDDP. DNA is counterstained with DAPI (blue).

of RAD-51 foci, with the *mus-81* mutant displaying a stronger phenotype (2.94 vs 5.24 RAD-51 foci/mitotic nucleus for *mus-81* and *him-9/xpf-1*, respectively) (Figure 3.15B,C). The fact that RAD-51 foci were reduced, but not absent, in these mutants suggested that while both MUS-81 and XPF-1 may contribute to HRR substrate generation at ICLs in *C. elegans*, redundancy between these two nucleases could exist. To address this possibility, a *mus-81; him-9/xpf-1* double mutant was generated. Interestingly, the double mutant exhibited a synthetic lethal phenotype with a very high degree of embryonic lethality and total inviability by the third generation, which precluded the possibility of analyzing CDDP sensitivity (Emb: *mus-81*: 21.1% F1, 59.25% F3; *him-9/xpf-1*, 15.9%; *mus81; him-9/xpf-1,* 74.2% F1, 99.54% F3) (Hodgkin *et al.* 1979; O'Neil 2008). The synthetic lethality of the *mus-81; him-9/xpf-1* double mutant will be discussed further in Chapter 5. Since the double mutant survived to adulthood through maternal mRNA contribution it was possible to examine RAD-51 focus formation following CDDP treatment. The *mus-81; him-9/xpf-1* double mutant had a similar defect in CDDP-induced RAD-51 foci as the *him-9/xpf-1* single mutant, but this was not as severe as in the *rfs-1* single mutant (5.21, 5.24, 0.78 RAD-51 foci/mitotic nucleus in *mus-81; him-9/xpf-1, him-9/xpf-1*, and *rfs-1* animals, respectively) (Figure 3.15B,C). The similar defect in RAD-51 focus formation between *mus-81* and *him-9/xpf-1* mutants indicates that they are not redundantly generating HRR substrates at ICL lesions in *C. elegans*. It is likely that either additional nucleases are involved or that conventional HRR substrate generation is not a requisite for a subset of RAD-51 loading. Interestingly, addition of an *rfs-1* allele to the *mus-81; him-9/xpf-1* background further reduced the number or RAD-51 foci but, again, failed to phenocopy *rfs-1* single mutants. This observation that *mus-81; xpf-1/him-9; rfs-1* triple mutants have more CDDP-induced RAD-51 foci than *rfs-1* single mutants suggests that the

absence of MUS-81 and XPF-1 increases the amount of RFS-1-independent HRR substrates generated at an ICL lesion.

3.3.2.2 DSB generation in rfs-1 mutants following CDDP treatment

An important question is whether the defect in RAD-51 loading at replication blocking lesions reflects a direct role for RFS-1 in RAD-51 loading or an indirect role via conventional HRR substrate generation. One potential method of addressing this issue would be to determine whether DSBs are generated in *rfs-1* mutants following treatment with DNA cross-linking agents. However, detecting DSBs proved difficult to determine due to the limitations of *C. elegans.* In yeast, DSBs that form following ICL treatment are commonly detected through pulsed-field gel electrophoresis (PFGE). As *C. elegans* adults are post mitotic and the only cells dividing are in the germ line, it appeared too difficult to detect DSBs in such a small percentage of cells (approximately 4%). In mammalian cells, the single cell gel electrophoresis or comet assay is another method used to directly detect DSBs (Olive *et al.* 1990). This method relies on the faster migration of small fragments of DNA generated by DSBs through an agarose gel following cell lysis. The number of DSBs in a cell is correlated with the percentage of DNA in the fast migrating fraction and the sizes of fragments are correlated to the distance the DNA migrates. The initial attempts at developing the comet assay involved dissecting out germ lines, embedding them in agar, then lysing and subjecting them to an electric current. Unfortunately, as the germ line is a syncytium, it was impossible to resolve signals from individual nuclei. Although no *C. elegans* cell lines exist, primary embryonic cell culture techniques do (Christensen *et al.* 2002; Strange *et al.* 2007). Adult worms were treated with 150 Gy of ionizing radiation, a dose expected to create a large number of DSBs per nucleus, then embryonic cells were isolated. These cells were then subjected to the comet assay; they rapidly differentiated by the end of the

assay, and most of the cells observed were reminiscent of neurons, with large, branching projections and consistent with previous reports (Christensen *et al.* 2002). No difference between irradiated and unirradiated cells was observed; therefore, the efforts to develop the comet assay in *C. elegans* were discontinued. Terminal deoxynucleotidyl transferase-mediated dUTP-biotin nick end labelling (TUNEL) was another potential approach for directly detecting DSBs in CDDP treated mitotic cells. A problem with TUNEL is that it labels all DNA ends, both double-stranded and single-stranded, and in replicating DNA will label the ends produced at the replication fork. No difference in staining between untreated, irradiated, and CDDP-treated wild type mitotic nuclei was detected and therefore this approach was also abandoned. In mammalian and yeast cells, DSBs are also identified through the use of markers, such as phosphorylation of the variant histone, H2AX (γH2AX) (Rogakou *et al.* 1998). The phosphorylation site in H2AX is not obviously conserved in *C. elegans* so antibodies were raised against another protein involved in the initial steps of DSB processing, MRE-11 (Figure 1.1D). Characterization demonstrated constitutive meiotic staining and damage induced mitotic staining (Figure 3.16B-D) (Goodyer *et al.* 2008). Interestingly, MRE-11 foci form in response to IR and ICLs in *Cebrc-2*, *rad-51*, and *rfs-1* mutants, potentially indicating that DSBs are still forming at ICLs in the absence of RFS-1 (Figure 3.16C). However, further characterization of the MRE-11 antibody revealed that foci also form in response to UVC treatment, which causes replication stress without DSB formation (Figure 3.16D). Thus, in *C. elegans*, MRE-11 responds to both DSBs and replication stress and therefore cannot be used to analyze HRR substrate generation at ICLs.

Figure 3.16. MRE-11 responds to both DSBs and replicative stress. (A) Western blot analyses using extracts derived from 50 adult hermaphrodites of the indicated genotype probed with αMRE-11 antibody. A single MRE-11 isoform of 81.5 kDa is predicted in *C. elegans*. Wild type levels of MRE-11 are detected in *spo-11* mutants, but no protein is detectable in *mre-11* deletion mutants and decreased levels are detected in *rad-50* mutants. The faster migrating band on the Western Blot of approximately 66 kDa is non-specific. (B) Representative images of MRE-11 staining (grey) in fixed meiotic mid-pachytene nuclei of the indicated genotypes. DNA is counterstained with DAPI (grey). Scale bars, 2 μm. (C) Representative images of MRE-11 staining (red) in fixed mitotic nuclei of the indicated genotypes either untreated, two hours post-treatment with 75 Gy IR, 18 hours post-treatment with 180 μM CDDP, or 16 hours post-treatment with 200 μM HN2. DNA is counterstained with DAPI (blue). (D) Representative images of MRE-11 staining (red) in fixed N2 (Wt) mitotic nuclei either untreated, 2 hours post treatment with 200 J/m^2 UVC, or 16 hours post-treatment with 200 μM HN2. DNA is counterstained with DAPI (blue). Figures A and B were provided by M. Zetka (Goodyer *et al.* 2008).

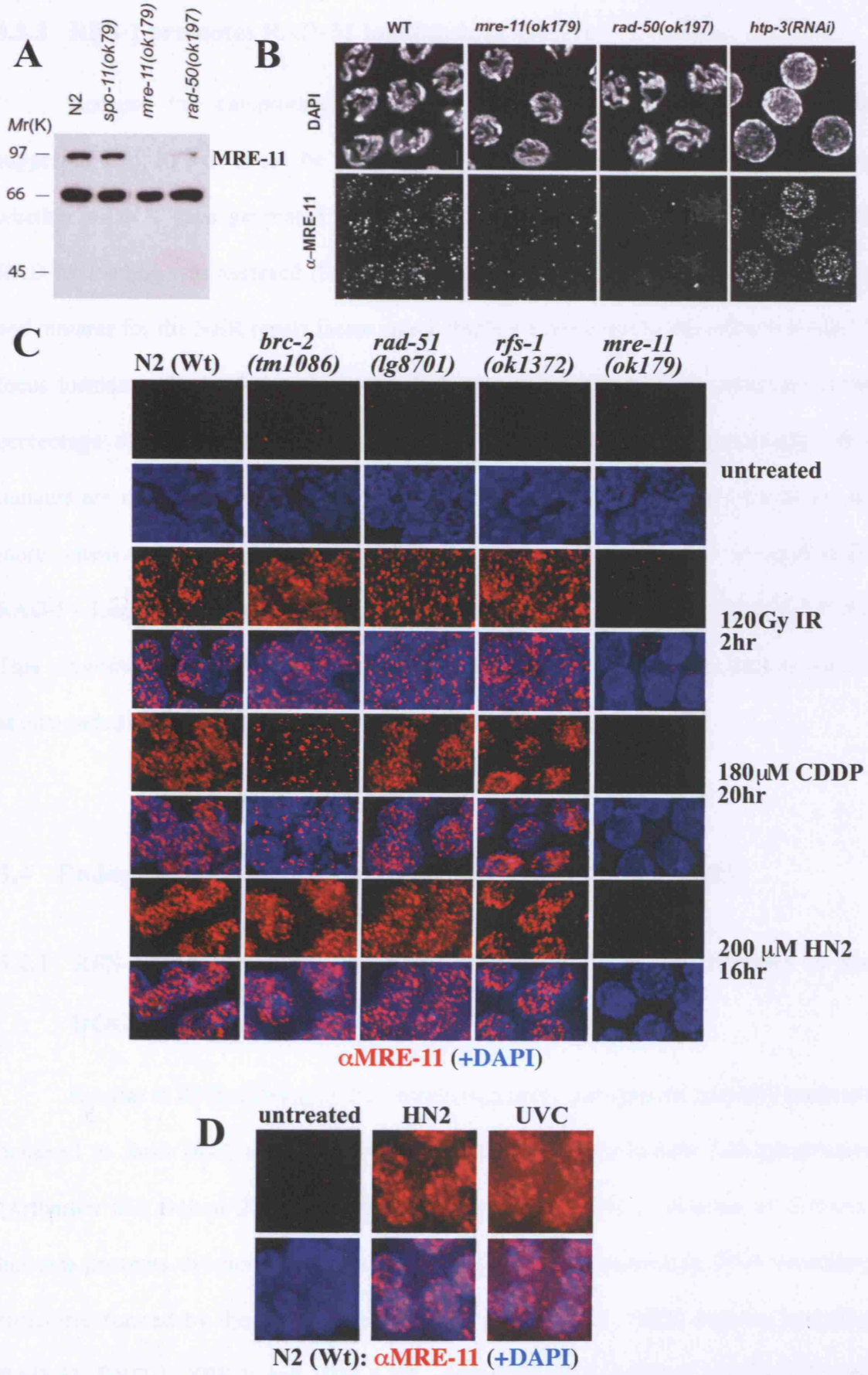

Figure 3.16. MRE-11 responds to both DSBs and replicative stress. For figure legend, see preceding page.

3.3.3 RFS-1 promotes RAD-51 loading onto ssDNA

Because the camptothecin sensitivity and RAD-51 focus formation data suggested that RFS-1 could be promoting RAD-51 loading at single-ended DSBs, whether ssDNA gaps generated by UVC are also a substrate for RFS-1-dependent RAD-51 loading was assessed (Strumberg *et al.* 2000). While both wild type animals and mutants for the NER repair factor *xpa-1* displayed extensive UVC-induced RAD-51 focus formation, both *rfs-1* and *xpa-1; rfs-1* mutants exhibited severe reduction in the percentage of RAD-51 positive mitotic cells (Figure 3.17B,C). Interestingly, *rfs-1* mutants are not particularly sensitive to UVC and *xpa-1; rfs-1* double mutants are no more sensitive than *xpa-1* single mutants, suggesting that while RFS-1 is required for RAD-51 loading at UVC induced lesions, it is not critical for repair (Figure 3.17A). This suggests that RFS-1 is able to promote RAD-51 loading at ssDNA gaps as well as at one-ended DSBs.

3.4 Endogenous substrates at which RFS-1 promotes HRR

3.4.1 RFS-1 is required for polyG/C tract stability in the absence of the DOG-1 helicase

Similar to RFBs formed by ICL-inducing agents, endogenous polyG/C tracts are believed to form DNA secondary structures that hinder replication fork progression (Arthanari and Bolton 2001). Data suggests that the DOG-1 (deletion of G-tracts) helicase prevents deletion formation at polyG/C tracts by unwinding DNA secondary structures formed by these sequences (Cheung *et al.* 2002). HRR proteins including RAD-51, BRD-1, XPF-1, and HIM-6 (*C. elegans* BLM) have been implicated in the maintenance of poly G/C tract integrity in the absence of DOG-1 (Youds *et al.* 2006).

Figure 3.17. RFS-1 is required for RAD-51 loading at UVC-induced lesions, but not for repair. (A) Percentage progeny survival of animals of the indicated genotype treated with the indicated doses of UVC. Error bars indicate standard error of the mean (S.E.M.) from at least 24 adult worms over two independent experiments. (B) Representative images of RAD-51 staining (red) in fixed mitotic nuclei either untreated or two hours post-treatment with 200 J/m^2 UVC. DNA is counterstained with DAPI (blue). (C) Quantification of RAD-51 positive mitotic nuclei as treated in (A). Error bars indicate S.E.M. from 20 mitotic nuclei from 10-15 worms of each genotype from two independent experiments.

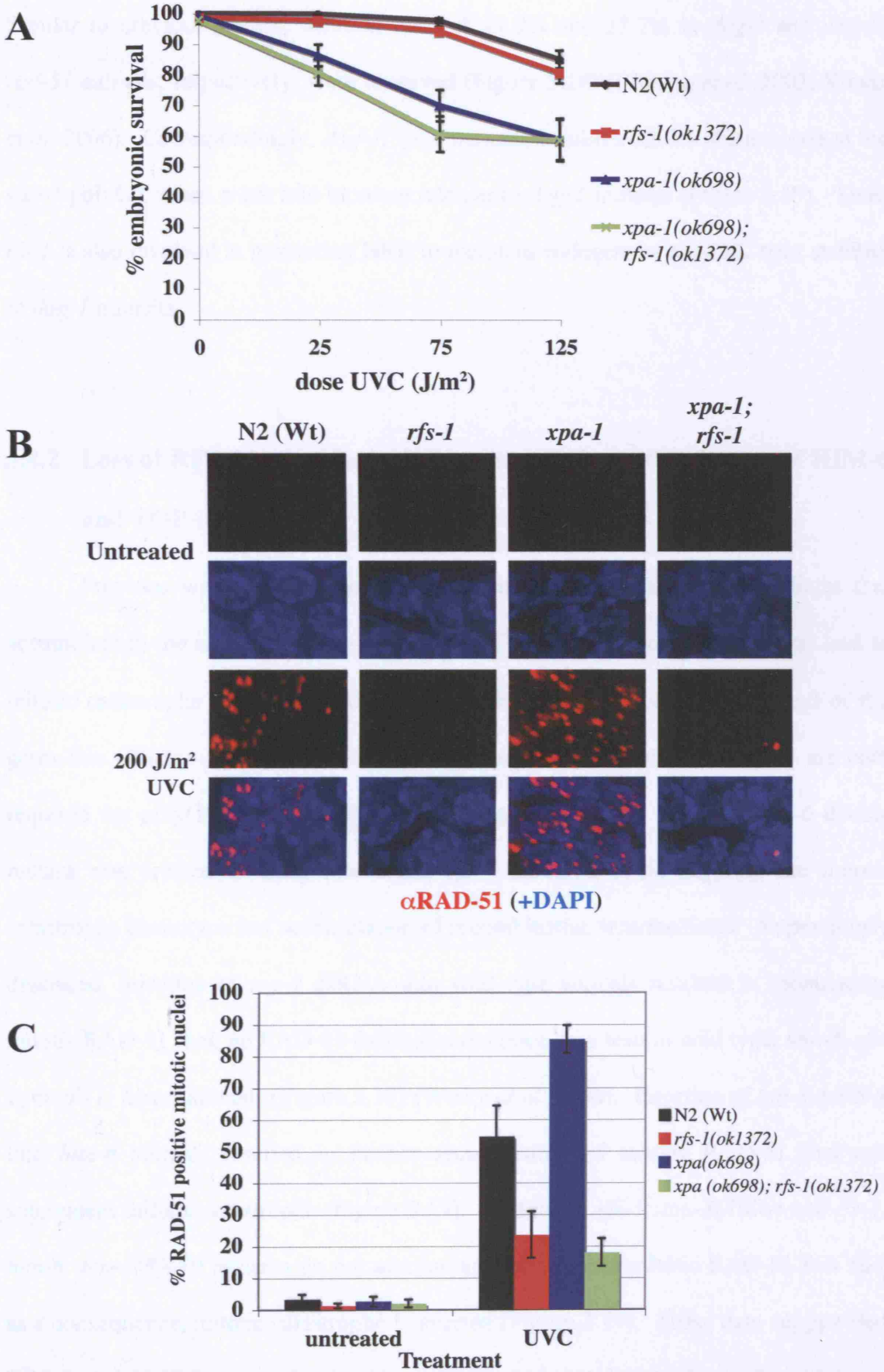

Figure 3.17. RFS-1 is required for RAD-51 loading at UVC-induced lesions, but not for repair. For figure legend, see preceding page.

Similar to previous studies, deletion rates of 11.2% and 37.7% in *dog-1* and *dog-1; rad-51* animals, respectively, were observed (Figure 3.18) (Cheung *et al.* 2002; Youds *et al.* 2006). Correspondingly, *dog-1; rfs-1* mutants exhibit a 32.4% deletion rate at the *vab-1* polyG/C tract, a 2.9 fold increase relative to *dog-1* mutants (Figure 3.18). Thus, *rfs-1* is also involved in promoting HRR to maintain endogenous polyG/C tract stability in *dog-1* mutants.

3.4.2 Loss of RFS-1 suppresses mitotic catastrophe in the absence of HIM-6 and TOP-3

Previous work has demonstrated that toxic recombination intermediates that accumulate in the absence of *him-6* and *top-3* (*C. elegans* Topoisomerase IIIα) lead to mitotic catastrophe and spontaneous RAD-51 foci in the mitotic compartment of the germ line (Wicky *et al.* 2004). Given the observation that *him-6* and *rfs-1* are both required for polyG/C tract stability in the absence of *dog-1,* an *rfs-1; him-6* double mutant was created to determine if the *rfs-1* mutation could suppress the mitotic catastrophe phenotype and accumulation of recombination intermediates. As previously described, injection of *top-3* dsRNA into wild type animals resulted in spontaneous mitotic RAD-51 foci; no RAD-51 focus accumulation was seen in wild type, *him-6*, *rfs-1*, or *rfs-1; him-6* animals (Figure 3.19) (Wicky *et al.* 2004). Injection of *top-3* dsRNA into *him-6* animals resulted in further accumulation of mitotic RAD-51 foci and subsequent mitotic catastrophe (Figure 3.19). Strikingly, *rfs-1; top-3(RNAi)* and *rfs-1; him-6; top-3(RNAi)* mutants do not accumulate spontaneous mitotic RAD-51 foci and, as a consequence, mitotic catastrophe is averted (Figure 3.19). These data suggest that TOP-3 and HIM-6 act predominantly on recombination intermediates formed in an RFS-1 dependent manner at impeded replication forks.

A

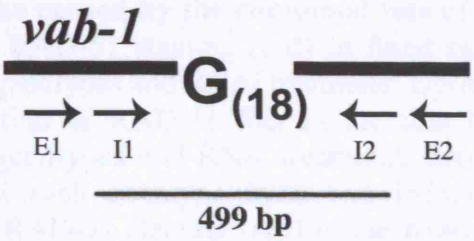

B

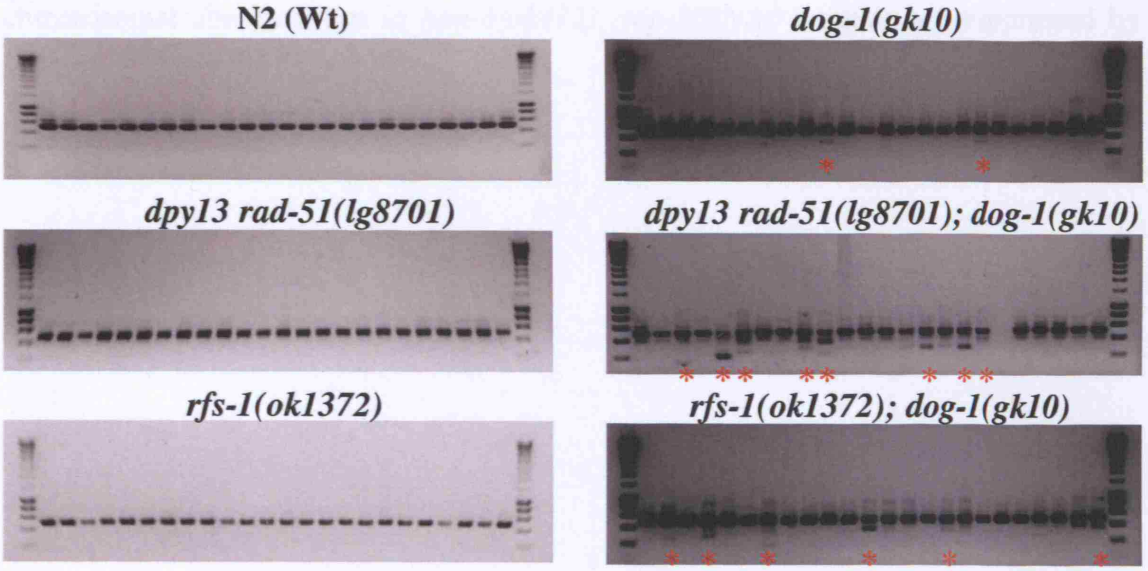

C

Deletion rate in the *vab-1* poly G/C tract

Genotype	Animals assayed	% animals with deletions	P-value in t-test with *dog-1*	Fold increase relative to *dog-1*
N2	95	0		
dog-1	428	11.2		1.0
dpy-13 rad-51	94	0		
dog-1; dpy-13 rad-51	69	37.7	0.00085	3.4
rfs-1	96	0		
dog-1; rfs-1	333	32.4	0.00045	2.9

Figure 3.18. RFS-1 is required for stability of polyG/C tracts in the absence of DOG-1. (A) Schematic representation of the polyG/C tract in the *vab-1* locus showing the relative positions of the nested PCR primers and expected internal product size in wild type animals. (B) Representative nested PCR reactions performed on single animals of the indicated genotypes. Red stars indicate lanes containing deletions. (C) Table of deletion rate in the *vab-1* polyG/C tract. The percentage of animals with deletions is the number of individual animals that showed one or more deletions in the *vab-1* locus polyG/C tract (as determined by PCR) divided by the total number of animals assayed.

Figure 3.19. *rfs-1* mutants suppress RAD-51 focus formation and mitotic catastrophe caused by the combined loss of HIM-6 and TOP-3. (A) Representative images of RAD-51 staining (red) in fixed mitotic nuclei in untreated animals of the indicated genotypes and RNAi treatment. DNA is counterstained with DAPI (blue). (B) Quantification of RAD-51 foci in the first twenty mitotic nuclei in animals of the specified genotypes and RNA treatment. Error bars indicate S.E.M. from at least 22 animals of each genotype from two independent experiments. (C) Representative images of RAD-51 staining (red) in the fixed mitotic zone in animals of the indicated genotype and RNAi treatment. DNA is counterstained with DAPI (blue). The severe chromosomal abnormalities in *him-6(ok412); top-3(RNAi)* animals are suppressed by *rfs-1(ok1372)*. Scale bars, 5 μm.

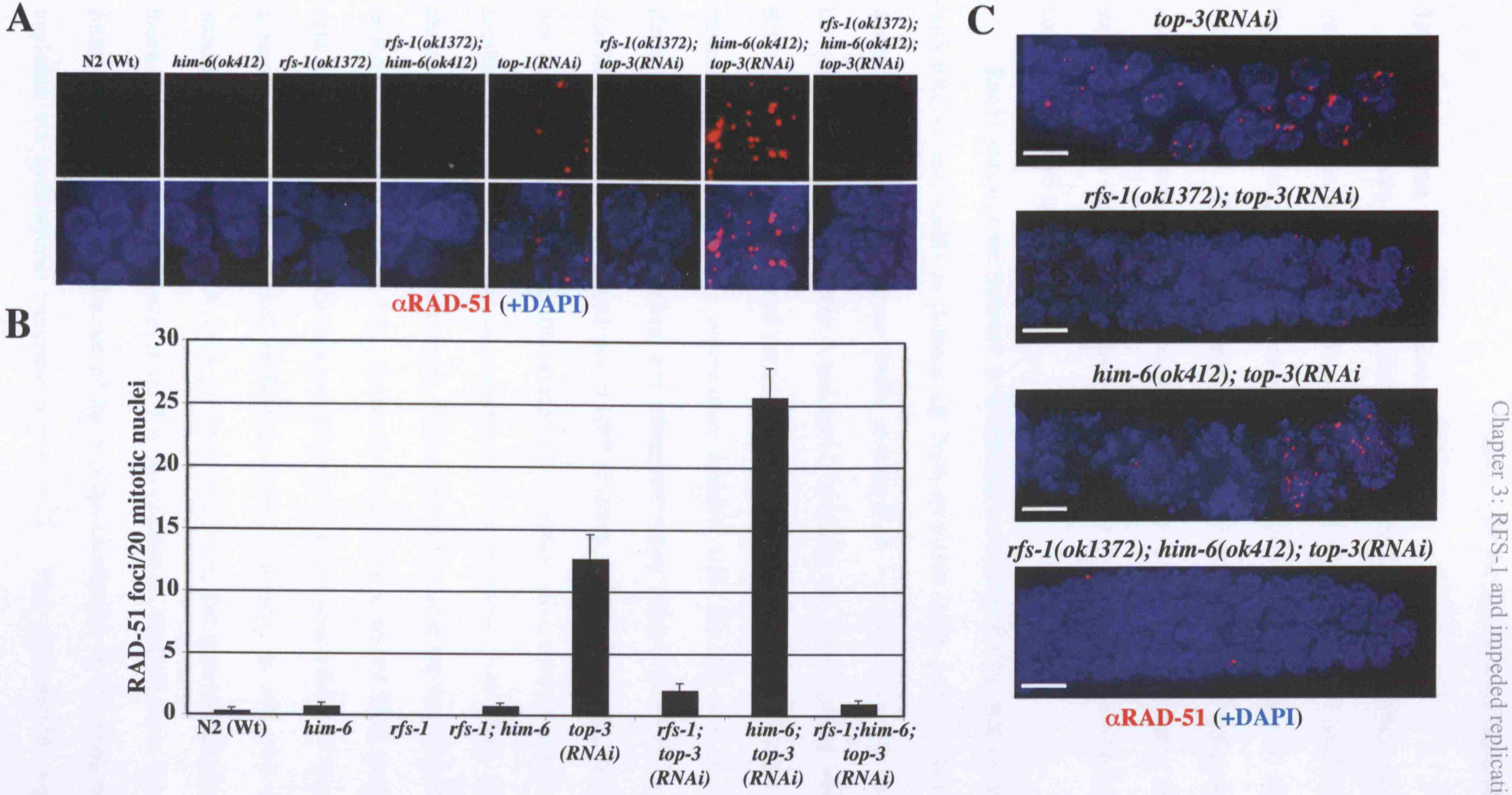

Figure 3.19. ***rfs-1*** **mutants suppress RAD-51 focus formation and mitotic catastrophe caused by the combined loss of HIM-6 and TOP-3.** For figure legend, see preceding page.

3.4.3 Discussion and Conclusions

DNA lesions encountered during replication are a major threat to genome integrity. It is known that HRR plays a critical role in maintenance of genome stability through its participation in regeneration of active replication forks at replication blocking lesions. The work described here has revealed unexpected differences in the nature of HRR substrates at impeded replication forks versus conventional DSBs that support the idea that repair of blocked replication forks does not proceed through a conventional DSB intermediate.

Rad51 paralogs are believed to be general mediators of HRR that act in concert with BRCA2 and Rad51 to promote all HRR-mediated repair events. However, the analysis of the single *C. elegans* Rad51 paralog (RFS-1) suggests that this may not be the case. In contrast to *Cebrc-2* and *rad-51* mutants, *rfs-1* mutants are viable, load RAD-51 onto SPO-11 induced meiotic DSBs and complete meiotic recombination as normal (Figure 3.4). This observation coupled with the fact that *rfs-1* is also dispensable for RAD-51 loading and subsequent repair of IR-induced DSBs suggests that RFS-1 is not a general mediator of HRR (Figures 3.5, 3.6, 3.7). Although RFS-1 is not critical for meiotic and IR-induced DSB repair, *rfs-1* mutants are profoundly sensitive to agents that impact on replication fork progression (Figure 3.5). Strikingly, the underlying cause of the sensitivity of *rfs-1* mutants to these agents is a severe defect in RAD-51 loading (Figure 3.7). Rather than acting as a general HRR mediator, the data suggest that RFS-1 performs a specialized role in promoting RAD-51 loading onto a substrate unique to blocked replication forks. Initially, an attractive candidate substrate was the free DNA ends produced following the processing/collapse of a blocked replication fork. However, *rfs-1* is dispensable for RAD-51 focus formation at forks that collapse in the absence of the S-phase checkpoint or following nucleotide depletion via hydroxyurea treatment (Figure 3.13). This dispensability argues that

collapsed forks resemble conventional DSBs similar to those formed by SPO-11 in meiosis or following IR-treatment. The defect in RAD-51 focus formation at both CPT and UVC-induced lesions suggest that the substrate(s) specific to impeded replication forks could be a one-ended DSB and/or a ssDNA gap (Strumberg *et al.* 2000).

An important issue raised by these findings is how HRR substrates are generated at blocked forks. Current models of ICL repair predict that nucleolytic processing of an ICL lesion generates a DSB that is processed into a substrate for HRR, which leads to subsequent repair of the lesion (Dronkert and Kanaar 2001; Niedernhofer *et al.* 2005). In yeast, the NER proteins have been implicated in generation of the HRR substrate, while in mammalian cells both Mus81 and XPF have been implicated in substrate generation (Jachymczyk *et al.* 1981; Hanada *et al.* 2006; Mogi and Oh 2006). The data presented here show that *C. elegans xpa-1* mutants are wild type for RAD-51 focus formation after CDDP treatment indicating that the NER pathway is not generally involved in generation of HRR substrates at ICLs in *C. elegans* (Figure 3.15). However, while both *mus-81* and *him-9/xpf-1* mutants have reduced RAD-51 foci following CDDP treatment, they fail to phenocopy *rfs-1* mutants, indicating that neither is solely responsible for generating an HRR substrate at ICL lesions (Figure 3.15). The reduction, but not complete attenuation, of RAD-51 foci at ICL lesions could suggest that functional redundancy exists between MUS-81 and XPF-1 with respect to HRR substrate generation. However, the similar reduction of RAD-51 foci in the double mutant relative to the *him-9/xpf-1* single mutant demonstrates that this is not the case. One possibility is that redundancy exists between MUS-81 and XPF-1 with other unidentified endonucleases. Further genetic analysis of RAD-51 focus formation at ICL lesions in mutant combinations between *mus-81, him-9/xpf-1,* and other endonuclease mutants could address this (eg. XPG-1, APE-1, FEN-1). Although unlikely, an alternative possibility is that RFS-1 could be involved in the generation of a DSB at an

ICL during S-phase. This would make ICL processing unique in *C. elegans* in relation to other eukaryotes. An explanation favoured by this author is that the difference in CDDP-induced RAD-51 foci in *rfs-1* and *mus-81; him-9/xpf* mutants reflects RAD-51 loading at a non-conventional HRR substrate. In this model, a subset of RAD-51 foci are generated at a conventional DSB formed through incision by MUS-81/XPF-1 at an ICL, while the remainder of foci occur at an alternative substrate such as a one-ended DSB formed by fork regression or ssDNA exposed by the impeded fork. Interestingly, a *mus-81; him-9/xpf-1; rfs-1* triple mutant had reduced RAD-51 foci following CDDP treatment, but again failed to phenocopy *rfs-1* single mutants. This suggests that in the absence of MUS-81/XPF-1 processing at an ICL, an RFS-1-independent HRR substrate is generated. Presumably a fork would remain stalled at an ICL in the absence of incision and this could potentially lead to fork collapse, which as demonstrated by data in this chapter, is an RFS-1-independent substrate.

Detection of mitotic DSBs has proved to be quite difficult in *C. elegans* as only 3-5% of the cells in the adult animal are actively dividing, making assays such as pulsed field gel electrophoresis extremely difficult. PFGE might be worth attempting because, although only 3-5% of cells are dividing, the replicating percentage of cells might be higher. A recent paper reported that animal size is determined by ploidy of the hypodermis, which is also a syncytium, through a process known as endoreduplication (Lozano *et al.* 2006). Hydroxyurea treatment resulted in smaller animals due to ploidy reduction in the hypodermal syncytium. The combined number of cells dividing in the germ line and hypodermis might allow for the detection of replication-dependent DSBs. Measurement of DSBs using the comet assay was hampered by the fact that the germ line is a syncytium, which prevented resolution of individual nuclei. Endoreduplication will not alleviate the issues encountered with the comet assay. Primary embryonic cell culture does not seem like a viable alternative for generating cells for the comet assay,

possibly due to rapid differentiation. This assertion is confirmed by the failure to detect DSBs after treatment with a large dose of IR. Development of a comet assay in *C. elegans* will likely have to wait until the creation of a *C. elegans* immortal cell line, if this is indeed possible. There was hope that an MRE-11 antibody, which could be used as a marker for early HRR events, would allow for detection of DSB formation at ICLs. Unfortunately, similar to the situation in human cells, MRE-11 forms foci at both DSBs and in response to replication stress (Figure 3.16) (Robison *et al.* 2004). Since replication stress will be generated at an ICL regardless of DSB formation, the MRE-11 antibody was not useful for analyzing HRR substrate generation at ICLs, though it has proven to be a very valuable tool in analyzing meiotic DSB generation (Goodyer *et al.* 2008).

PolyG/C tracts are believed to form secondary DNA structures that hinder replication fork progression and are predicted to be removed by the action of a specialized helicase, DOG-1 (Cheung *et al.* 2002). A recent study has shown that in the absence of DOG-1, HRR proteins are required to prevent polyG/C tract instability and deletion (Youds *et al.* 2006). The fact that RFS-1 is also required for stability of polyG/C tracts in *dog-1* mutants suggests that these sequences can indeed form endogenous replication blocking lesions that represent a source of spontaneous DNA damage in S-phase (Figure 3.18). Interestingly, HIM-6 (*C. elegans* BLM helicase) is also required for polyG/C tract stability in *dog-1* mutants. Combined depletion of HIM-6 and TOP-3 leads to spontaneous RAD-51 foci and mitotic catastrophe analogous to that observed in S-phase checkpoint mutants (Wicky *et al.* 2004; Garcia-Muse and Boulton 2005). The *him-6; top-3(RNAi)* phenotype is believed to be caused by the accumulation of toxic recombination intermediates as *rad-51* mutations can suppress these phenotypes; similarly, *rad51, rad54, rad55,* and *rad57* mutations suppress the *top3* growth defect in *S. cerevisiae* (Wicky *et al.* 2004; Shor *et al.* 2005). The ability of

rfs-1 to suppress the *him-6; top-3(RNAi)* phenotype is similar to the ability of mutations in the *S. cerevisiae* Rad51 paralogs *shu1, shu2* and *psy3* to suppress *top-3* lethality (Figure 3.19) (Shor *et al.* 2005). In contrast to the inability of *rfs-1* to suppress spontaneous RAD-51 focus formation at collapsed replication forks in *atl-1* mutants (*C. elegans* ATR), the *rfs-1* mutation suppresses both RAD-51 focus formation and mitotic catastrophe in *him-6; top-3(RNAi)* animals (Figure 3.13, Figure 3.19). These data argue that HIM-6 and TOP-3 are predominantly acting on RFS-1-dependent recombination intermediates formed by naturally occurring RFBs. Interestingly, it has been proposed that Sgs1/Top3 and Mus81/Eme1 function in *S. cerevisiae* to prevent accumulation of toxic recombination intermediates at ssDNA exposed by stalled replication forks as opposed to at DSBs (Fabre *et al.* 2002). This would be consistent with the observed dependence on RFS-1 for RAD-51 focus formation at UV-induced ssDNA gaps (Figure 3.17). Recently, it has been demonstrated that the *S. cerevisiae* Rad51 paralogs are able to channel replication slowing lesions induced by methyl methanesulphonate (MMS) into HRR intermediates that are acted on by the Sgs1-Top3-Rmi1 complex (Mankouri *et al.* 2007). Further studies of the role of RFS-1 in unperturbed mitosis should illuminate the nature of the endogenous replication blocking lesions that RFS-1, HIM-6, and TOP-3 respond to *in vivo*.

Although RFS-1 is clearly dispensable for RAD-51 loading at IR-induced lesions and mutants are not as sensitive to IR as *brc-1* mutants, it must be noted that *rfs-1* mutants do still exhibit a significant sensitivity to IR. There are two possible explanations for the sensitivity of *rfs-1* mutants despite apparently correct loading of RAD-51 in response to IR. One possibility is that the IR-sensitivity is due to non-DSB lesions that block DNA replication, such as DNA-protein cross-linking. Sensitivity of *rfs-1* to agents that induce DNA-protein cross-linking, such as arsenite, would support this notion (Ramirez *et al.* 2000). Alternatively, the early steps of homologous

recombinational repair, including RAD-51 loading at IR-lesions, could be unaffected in the absence of RFS-1 and the sensitivity might reflect an additional role for RFS-1 in the later stages of HRR. This later role would be consistent with the involvement of the RAD51C-XRCC3 paralogs in the resolution of HRR intermediates. Interestingly *Rad51C* hypomorphic mice are infertile due to sexually dimorphic defects in meiotic recombination (Kuznetsov *et al.* 2007). Spermatocytes from these mice undergo an early developmental arrest in meiotic prophase I which was suggested to be due a defect in the early steps of meiotic recombination (Kuznetsov *et al.* 2007). In contrast, oocytes progress to metaphase II but severe defects such as chromosome fragmentation, aneuploidy, and sister chromatid separation are observed at this stage (Kuznetsov *et al.* 2007). These defects were postulated to arise from a defect in resolution of Holliday junctions. To determine whether RFS-1 plays both early and late roles in *C. elegans* HRR it will be important to assay purified RFS-1 for biochemical activities such as HJ binding, branch migration and/or resolution.

A specialized role for RFS-1 in promoting early HRR steps at blocked replication forks rather than conventional DSBs could be unique to *C. elegans*, but this is unlikely. Rad51 paralog knockouts in DT40 cells, while acutely sensitive to DNA cross-linking agents, are only mildly sensitive to IR (Takata *et al.* 2001). Furthermore, Rad51 paralog mutants in Chinese hamster ovary cells are also extremely sensitive to DNA cross-linking agents and only mildly sensitive to IR (Jones *et al.* 1987; Fuller and Painter 1988; French *et al.* 2002). It was surprising that IR-induced RAD-51 foci formed in *rfs-1* mutants, given the role of the vertebrate Rad51 paralogs in promoting RAD-51 loading at both IR and ICL-induced lesions and in repair at I-*Sce*I induced DSBs (Figure 3.7) (Bishop *et al.* 1998; Johnson *et al.* 1999; Pierce *et al.* 1999; Takata *et al.* 2001; French *et al.* 2002; Godthelp *et al.* 2002). However, if Rad51 paralogs were general mediators of HRR, one would predict that paralog deficient cells should

phenocopy Rad51 knockout cell lines, which are inviable (Sonoda *et al.* 1998). This proposed general role in mediating HRR is clearly not the case as paralog deficient cell lines are viable. The failure to phenocopy *rad51* mutant cells does not appear to be due to functional redundancy between the paralogs, for DT40 lines that are mutant for two components of the same complex (*rad51B/rad51d*), or for one member in each of the complexes (*rad51d/xrcc3*) are viable and have mild sensitivities to IR that are comparable to single mutants (Yonetani *et al.* 2005). It is possible that the decreased Rad51 recruitment to IR-induced lesions in vertebrate cells reflects a defect in loading Rad51 at replication blocking lesions caused by the high doses of IR (8-12 Gy) used in these studies. Consistent with this hypothesis, at doses of 1-3 Gy in Xrcc3 defective CHO cells, the defect in Rad51 loading is much less pronounced (Bishop *et al.* 1998). Interestingly, while RAD51 and RAD51C levels are highly enriched in S-G2 cell cycle phases at sequences adjacent to an induced I-*Sce*I DSB in human cells (10.2 and 7.5-fold, respectively), RAD51D, XRCC2, and XRCC3 levels are only enriched 1.62-, 1.56-, and 1.65-fold, respectively (Rodrigue *et al.* 2006). The presence of RAD51C at DSBs could reflect the postulated late role for RAD51C in DSB repair in mammalian cells (Liu *et al.* 2004).

Competitive binding studies found that the human BCDX2 complex preferentially binds to branched DNA structures such as Y-shaped DNA and synthetic Holliday junctions that resemble structures believed to form at blocked replication forks (Yokoyama *et al.* 2004). The preferential binding of BCDX2 to branched DNA over ssDNA, dsDNA, 3' and 5' tailed duplexes and nicked DNA is consistent with the proposed replication-specific role for RFS-1 and its vertebrate counterparts (Yokoyama *et al.* 2004; Rodrigue *et al.* 2006). RFS-1 could be involved in targeting RAD-51 and CeBRC-2 to impeded forks or could bind and stabilize impeded forks to facilitate HRR substrate generation. Unfortunately, the CeBRC-2 antibody has been inconsistent and

thus definitive results have not been obtained regarding whether CeBRC-2 foci still form at ICL lesions in *rfs-1* mutants. An alternative possibility is that RFS-1 could promote RAD-51 loading at impeded forks in order to protect the newly synthesized nascent strands from nucleolytic degradation. A strand-protective function is consistent with the proposed role for the RecFOR proteins in *E. coli* in loading RecA onto ssDNA at exposed replication forks to prevent degradation by the RecJ nuclease (Umezu *et al.* 1993; Umezu and Kolodner 1994; Chow and Courcelle 2004). RAD51 loading for the protection of nascent strands rather than active repair has also been proposed to occur at an inducible RFB in *S. pombe,* as HRR leads to gross chromosomal rearrangements at impeded forks (Lambert *et al.* 2005). It was proposed that RAD51 loading could promote fork protection/stabilization until specialized helicases/nucleases removed the blocking lesion. It is therefore possible that the role of RFS-1 in promoting HRR at impeded forks may be one of stabilization rather than active participation in repair.

In summary, study of the single *C. elegans* Rad51 paralog has revealed that HRR substrates generated at impeded replication forks are intrinsically different from substrates generated following replication fork collapse or at conventional DSBs. The data detailed here would suggest that RFS-1 plays a specialized role in promoting RAD-51 loading onto ssDNA gaps generated at stalled replications forks and/or one-ended DSBs, potentially formed following replication fork regression. It is likely that further study will allow refinement of the role of the Rad51 paralogs in HRR and give insight into the nature and function of the HRR substrate generated during the normal repair of impeded replication forks.

4 Chapter 4: Characterization of R01H10.5, a novel RFS-1 interacting protein

4.1 Identification of R01H10.5 as an interacting partner of RFS-1

4.1.1 Y2H screening for RFS-1 interacting proteins

In an effort to gain insight into the role of RFS-1 in promoting HRR at impeded replication forks, a yeast two-hybrid screen (Y2H) was performed to identify interacting proteins. An RFS-1-DB fusion was used as bait to screen the normalized AD-Orfeome library, which contains 11,984 of the predicted 20,800 *C. elegans* ORFs, for interacting partners of RFS-1 (Reboul *et al.* 2003). The primary screen used 20 mM 3-aminotriazole (3AT), which positively selects for expression of a *GAL1:HIS3* reporter. Interactors were verified by retesting on 20 mM 3AT, and by analyzing expression of a *GAL1:lacZ* reporter through conversion of the chromogenic substrate X-Gal into a blue precipitate. A total of approximately 50,000 transformants were screened giving 4.2-fold library coverage. Six interacting candidates were isolated, and of these six, four reproducibly tested positive for 3AT resistance and LacZ expression: RAD-51, R01H10.5 (isolated twice), and C49C3.10. RAD-51 and R01H10.5, an uncharacterized ORF, were previously identified as RFS-1-interactors in a high throughput Y2H analysis of the *C. elegans* DNA damage response, while C49C3.10 (*C. elegans* Jun-N-terminal kinase) is a novel RFS-1 interacting candidate (Figure 4.1A) (Boulton *et al.* 2002). These three candidates were then tested for interaction with novel and previously identified RFS-1 interactors in a small scale matrix assay. Included in this assay were CeBRC-2 (both an N-terminal fragment (amino acids 1-114) and full length), RAD-51, RFS-1, and C30A5.3, the gene upstream of *rfs-1* that is predicted to be in an operon with *rfs-1* (Figure 4.1B) (Martin *et al.* 2005). As previously described,

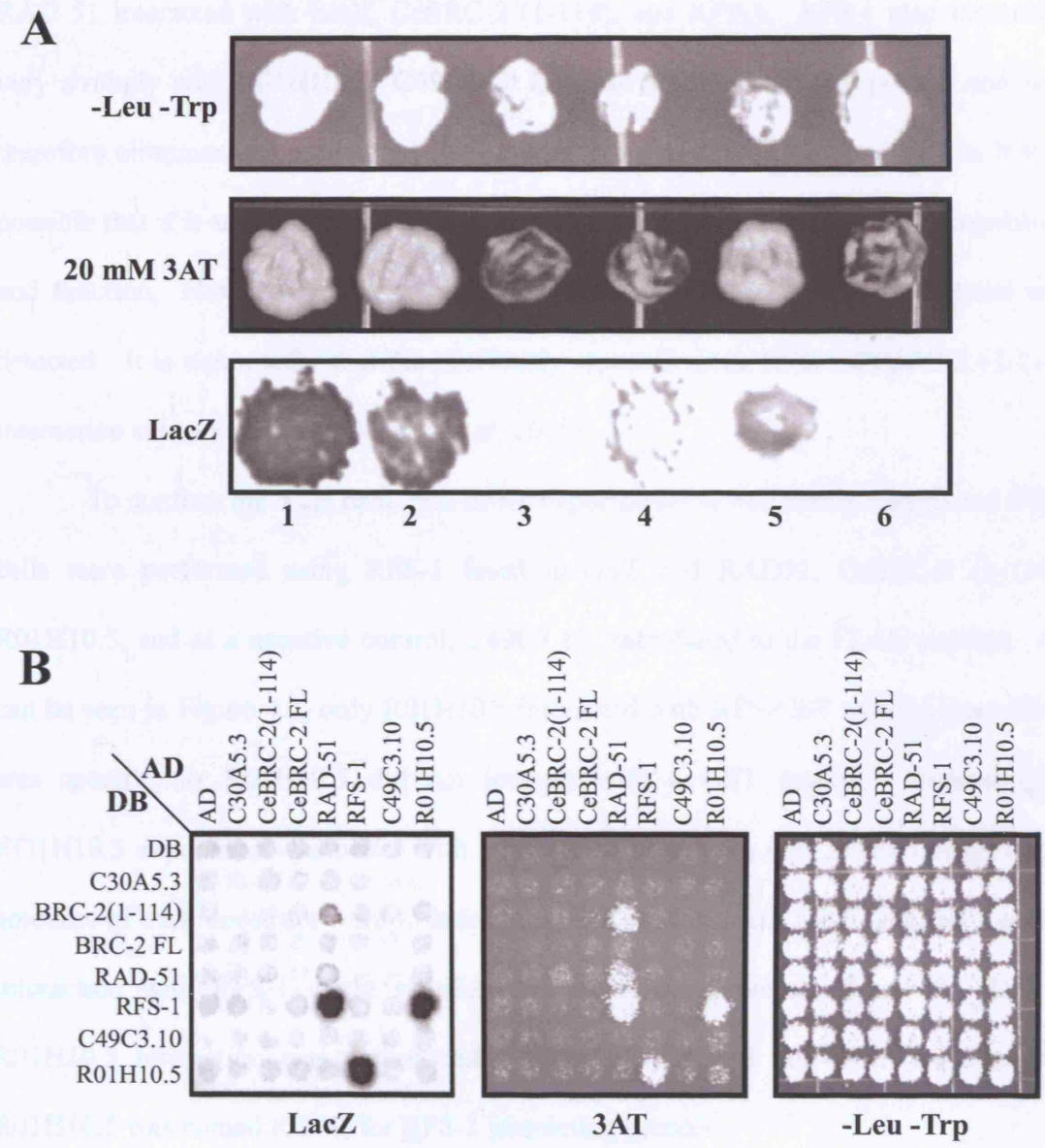

Figure 4.1. Yeast two-hybrid identification of RFS-1 interactors. (A) Confirmation of six RFS-1-interacting candidates, isolated by genome wide yeast two-hybrid (Y2H) screening, by growth on 20 mM 3AT and by LacZ expression. Growth on permissive –Leu –Trp plates is provided as a control. The interacting candidates contained the following AD-fusions: 1: RAD-51; 2 and 5: R01H10.5; 3: W02F12.2; 4: C49C3.10; and 6: C13G3.1. Only RAD-51, R01H10.5, and C49C3.10 retested positively. (B) Small scale matrix to test Y2H interactions between novel and previously identified RFS-1 interactors. All pairwise permutations of the AD and DB fusions of C30A5.3, an N-terminal fragment of CeBRC-2 (1-114), full length CeBRC-2 (FL), RAD-51, RFS-1, C49C3.10, and R01H10.5, as well as AD and DB controls were tested for growth on 20 mM 3AT and LacZ expression. Growth on permissive –Leu –Trp plates is provided as a control.

RAD-51 interacted with itself, CeBRC-2 (1-114), and RFS-1. RFS-1 also interacted very strongly with R01H10.5. C49C3.10 failed to interact with any protein and was therefore eliminated as a potential RFS-1-interactor. C30A5.3 was included as it was possible that if it and RFS-1 were in an operon, there might be similarities in regulation and function. However, no interaction between C30A5.3 and any other proteins was detected. It is noteworthy that the previously reported weak RFS-1-CeBRC-2 (1-114) interaction was not repeated (Martin *et al.* 2005).

To confirm the Y2H data, pull-down experiments in transiently transfected 293T cells were performed using RFS-1 fused to GST and RAD51, CeBRC-2 (1-114), R01H10.5, and as a negative control, C49C3.10, each fused to the FLAG peptide. As can be seen in Figure 4.2, only R01H10.5 interacted with RFS-GST and the interaction was specific, as R01H10.5 did not interact with a GST control. Interestingly, RO1H10.5 expression was better with RFS-1-GST than with GST, even though equal amounts of each construct were transfected. This enhancement might suggest that the interaction with RFS-1 could stabilize the R01H10.5 protein. Since the RFS-1-R01H10.5 interaction was demonstrated in both Y2H and pull-down experiments, R01H10.5 was named RIP-1, for RFS-1 interacting protein.

4.1.2 Reciprocal yeast two-hybrid screening to identify RIP-1 interacting proteins

Sequence analysis of RIP-1 failed to yield any obvious homologs. To address the possibility that it could be a highly divergent Rad51 paralog, phylogenetic analysis was performed on RIP-1, the Rad51 family of proteins, and Sws1, a recently identified paralog interactor in yeast (Martin *et al.* 2006). The *Caenorhabditis* RIP-1 proteins were outliers in this analysis and appear to be true orphan proteins (Figure 4.3). Therefore, to gain insight into the potential biological role of RIP-1, a Y2H screen was

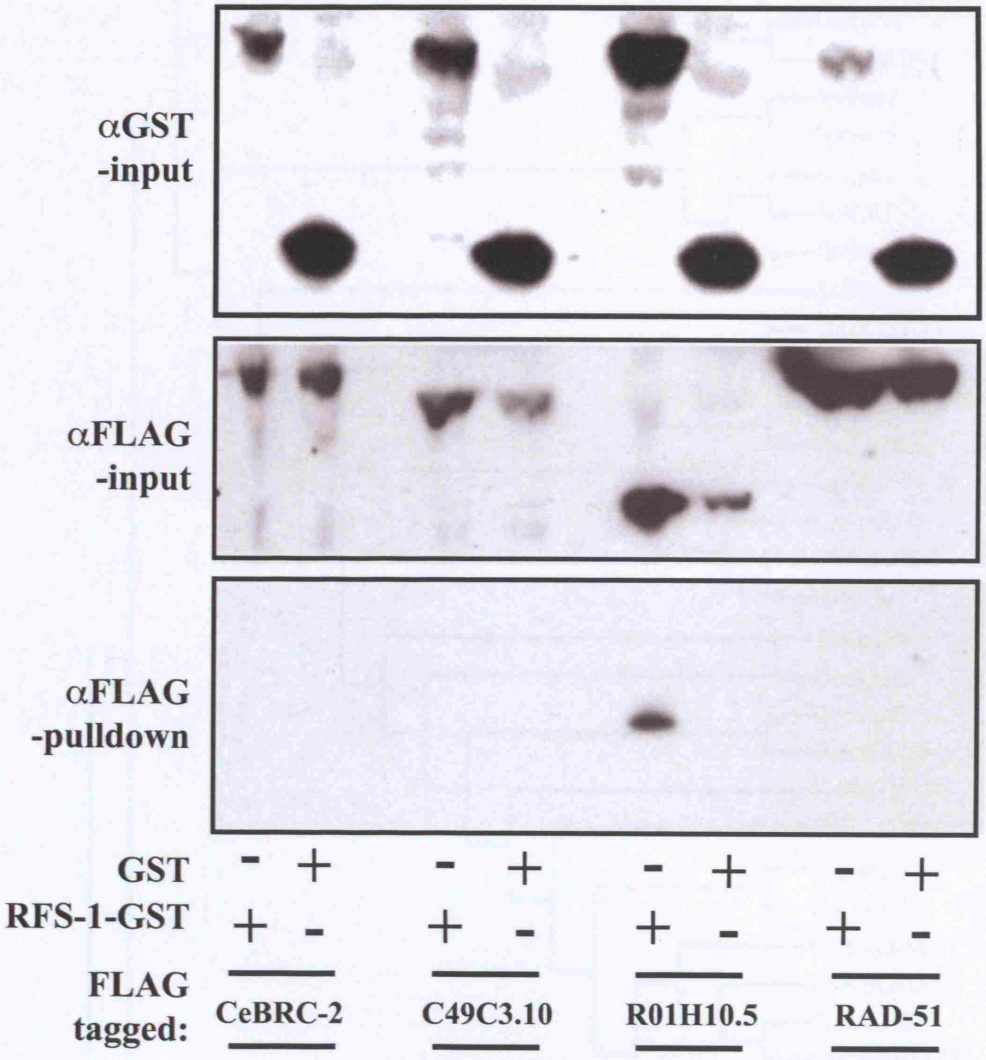

Figure 4.2. Verification of RFS-1-RIP-1 interaction by GST pull-down. 293T cells were cotransfected with either RFS-1-GST or GST and FLAG epitope tagged CeBRC-2, C49C3.10, R01H0.5, or RAD-51 constructs. Cell lysates were incubated with glutathione beads and the pulled-down proteins were run on an SDS-polyacrylamide gel and immuno-blotted with αFLAG antisera. One percent of the input was also run and immuno-blotted with either αGST or αFLAG antisera.

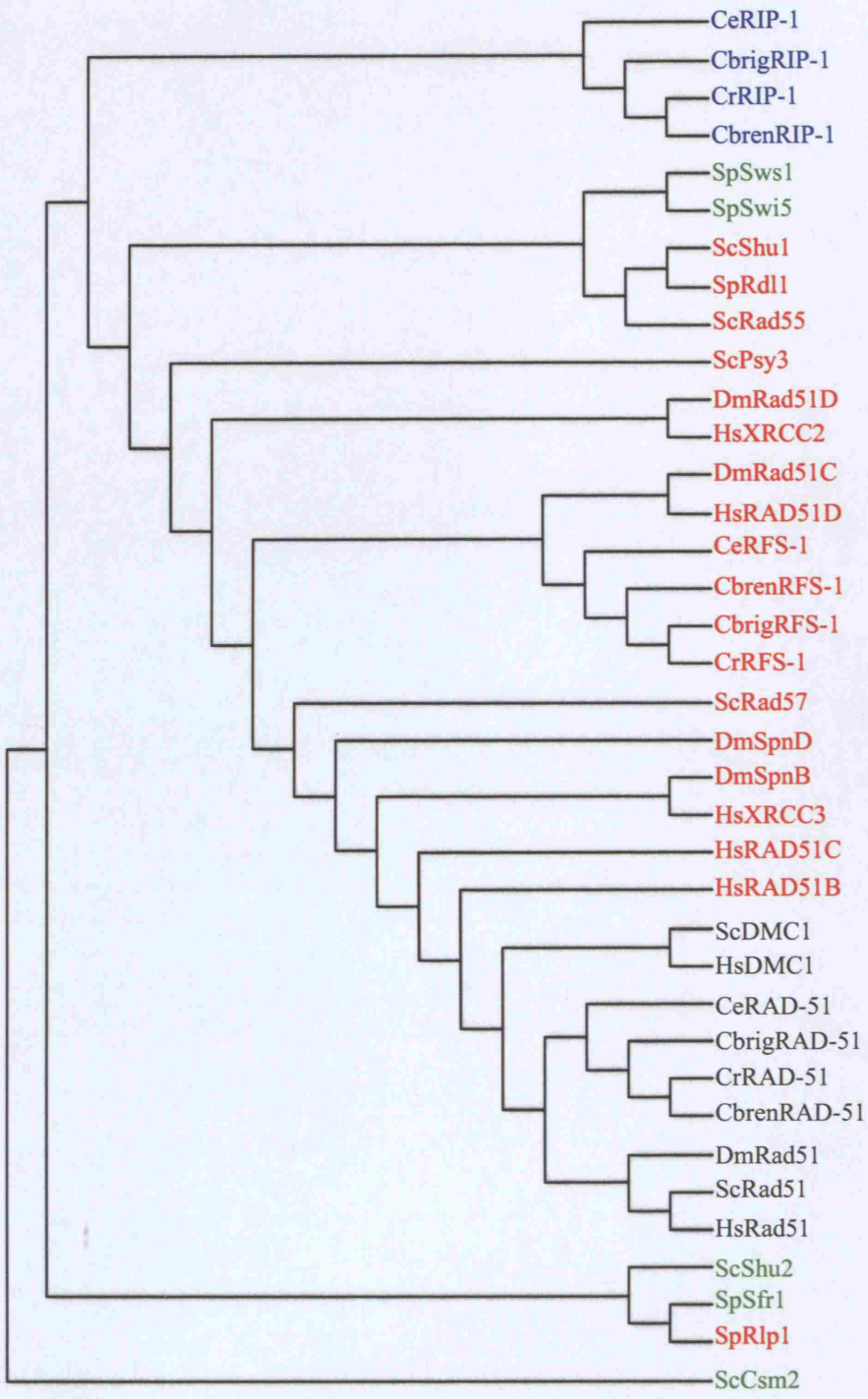

Figure 4.3. RIP-1 is a true phylogenetic orphan protein. Phylogenetic analysis of RIP-1 (blue), DMC1 and Rad51 (black), Rad51 paralogs (red), and Rad51 mediator/paralog associated proteins (green) from *C. elegans* (Ce), *C. briggsae* (Cbrig), *C. brennari* (Cbren), and *C. remmanei* (Cr), *D. melanogaster* (Dm), humans (Hs), *S.* cerevisiae (Sc), and S. *pombe* (Sp). The tree was generated by aligning and calculating neighbour joining distance with ClustalX 2.0, and then visualizing the data with NJPlot. This figure is courtesy of Mike Mitchell, CRUK Bioinformatics and Biostatistics service.

performed using RIP-1-DB as bait against the AD-Orfeome library. Approximately 150,000 transformants were screened as described in 4.1.1, giving 12.5-fold library coverage. Strikingly, all seven confirmed interacting ORFs were RFS-1. In all, the RFS-1-RIP-1 interaction was found a total nine times in two different screens, demonstrating an extremely robust interaction.

4.2 Biological role of RIP-1

4.2.1 Phenotypic analysis of *rip-1(tm2948)*

Given the number of times the RFS-1-RIP-1 interaction was isolated by Y2H screening and the subsequent confirmation of the interaction by GST pull-downs, it was highly likely that RIP-1 would impact on RFS-1 function. To analyze the interplay between these factors, a deletion mutant, *rip-1(tm2948),* which is lacking the central two exons, was obtained (Figure 4.4). This allele was isolated by the National Bioresource Project for the Nematode, another organization that performs high throughput, PCR-based screening for deletions in TMP/UVA-mutagenized nematode genomes. The *tm2948* deletion generates a frameshift in the predicted mutant protein, altering the fourth exon and creating a premature stop codon. Like *rfs-1* mutants, *rip-1* mutants are dispensable for both SC formation and HRR repair of meiotic DSBs as evidenced by SYP-1 and RAD-51 staining and the presence of six bivalents at diakinesis (Figure 4.5A). Also like *rfs-1* mutants, the *rip-1* mutant displayed a weak Him phenotype without a significant degree of embryonic lethality, indicative of a role in meiotic recombination at some level, and had a slightly smaller brood size than wild type animals, similar to the *rfs-1* brood sizes reported in Chapter 3 (Figure 4.5B). Interestingly, the brood size of an *rfs-1* strain that had been growing in the lab for several months was significantly smaller than the initial brood size of the freshly

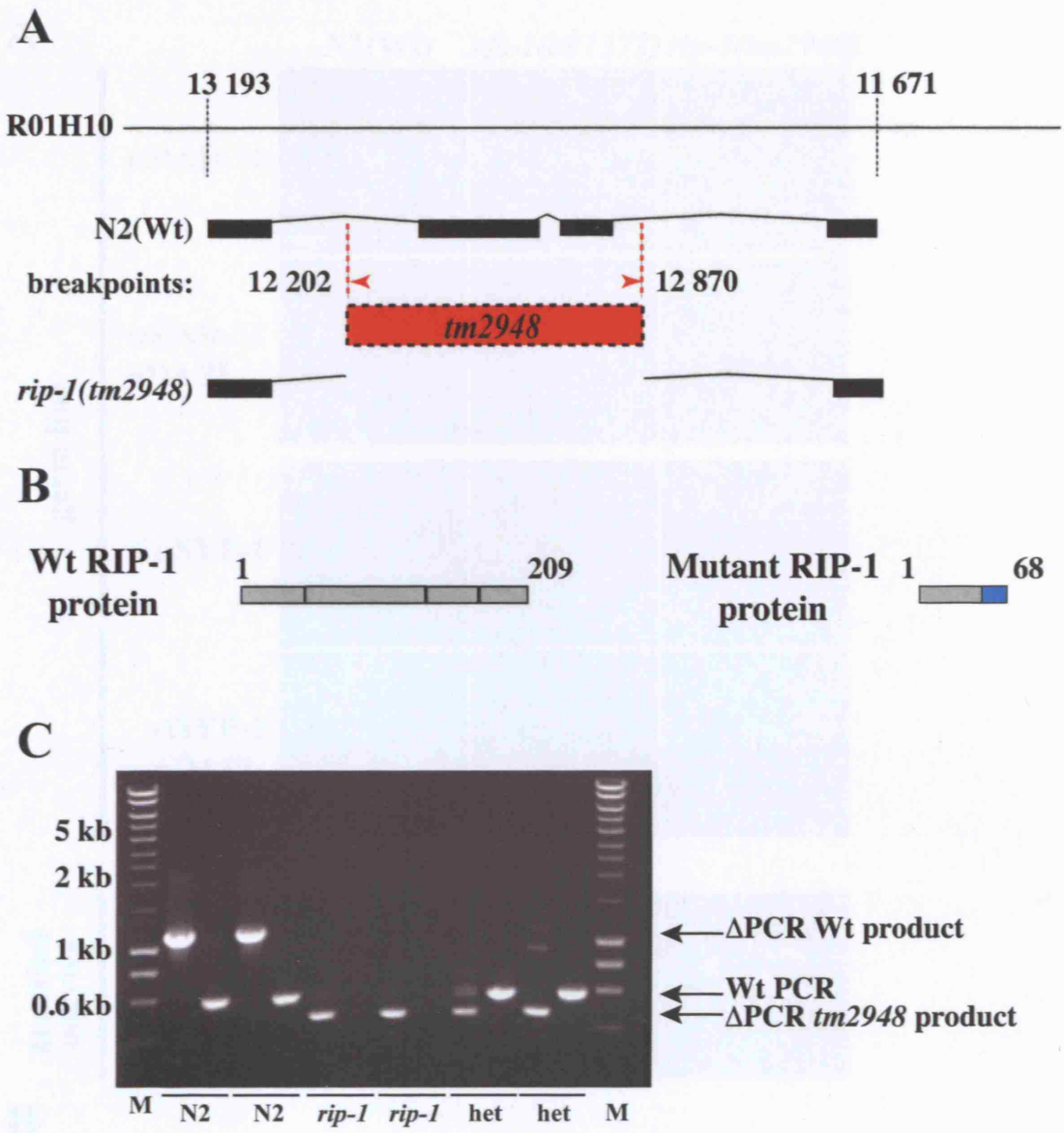

Figure 4.4. Schematic of *rip-1* deletion. (A) The numbers indicate nucleotide position in cosmid R01H10, which contains the genomic sequence that includes *rip-1*. This sequence was used to determine the deletion breakpoints. The gene structure of *rip-1* (R01H10.5) is shown, along with the position of the *tm2948* allele. *tm2948* is a 668 bp deletion (red box) in the *rip-1* gene that removes exons 2 and 3. (B) The RIP-1 predicted protein structure in wild type animals (209 aa) and RIP-1 mutants (68 aa). The blue box indicates the altered reading frame and premature stop codon generated by the deletion. (C) *rip-1* genotyping PCR. Nested PCR, using primers flanking the *rip-1* gene, from a two wild type N2 animals, two *rip-1(tm2948)* mutants, and two *rip-1(tm2948)/+* heterozygotes (het). The primers are predicted to amplify a 1146 bp region in wild type animals and 478 bp product in *rip-1(tm2948)* mutants (ΔPCR-Wt and *tm2948* products). A nested primer set with the right oligonucleotides recognizing sequence within the deleted area were used to detect the presence of wild type *rip-1* (Wt PCR) to differentiate *rip-1(tm2948)* homo- and heterozygote animals. This primer set is predicted to amplify a 594 bp region in wild type animals and yield no product in *rip-1(tm2948)* animals. A DNA size marker (M) is included on the gel; fragment sizes are indicated in kilobase pairs.

A

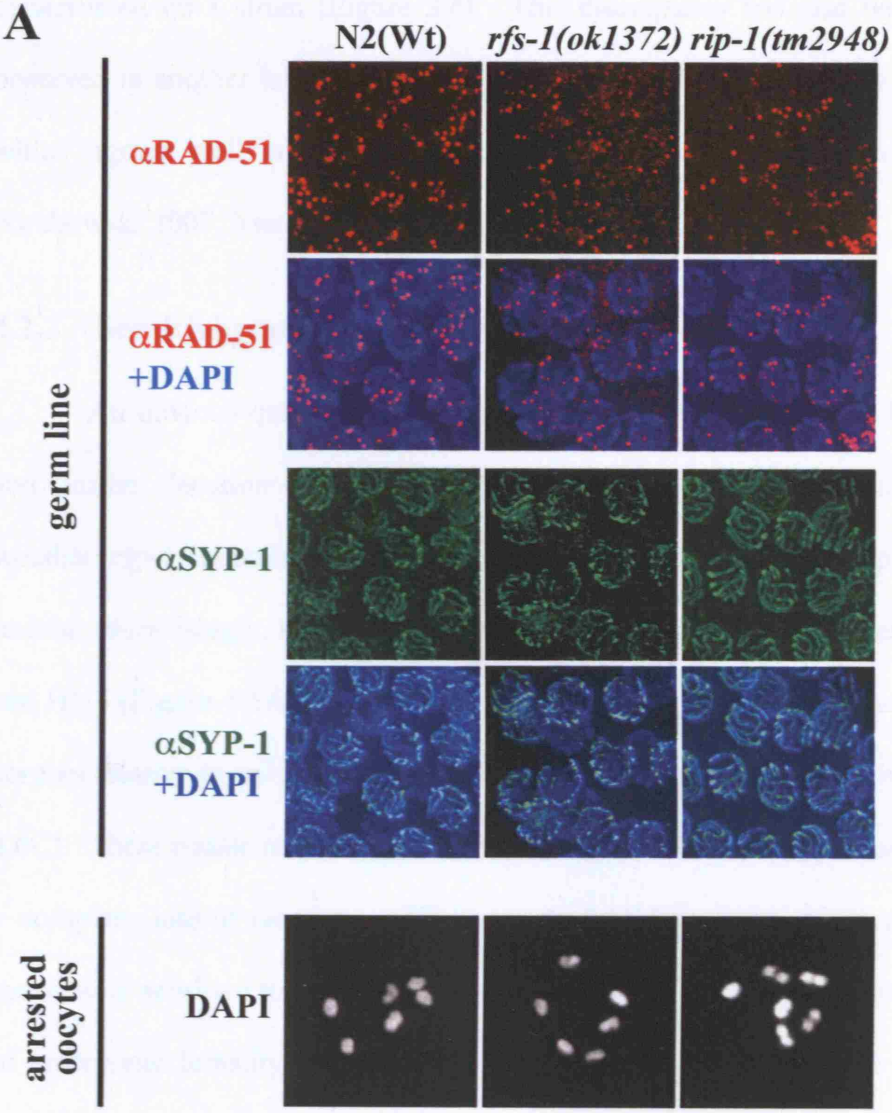

B

Genotype	Brood Size (±std. dev.)	%Embryonic Lethality	% Males
N2(Wt)	257.2 ±20.3	0.63 (n=471)	0 (n=1286)
rfs-1(ok1372)	116.83±87.4	4.74 (n=506)	2.71 (n=701)
rip-1(tm2948)	194±40.4	1.48 (n=1723)	1.00 (n=2328)
*rfs-1(ok1372)**	206.9 ±73.1	0.13(n=2276)	2.20 (n=2276)

*Data from Chapter 3

Figure 4.5. RIP-1 is dispensable for meiotic recombination and crossing over. (A) Representative images of germ lines of the indicated genotypes stained against either RAD-51 (red) or the core SC component, SYP-1 (green). DNA is counterstained with DAPI (blue). Representative images of single oocyte nuclei of the indicated genotypes arrested at diakinesis, counterstained with DAPI (grey, bottom panel). (B) Table of embryonic lethality, brood size (±std. dev), percent males (n=numbers of embryos counted for embryonic lethality and animals scored for percent males).

backcrossed *rfs-1* strain (Figure 3.4). This discrepancy has also been independently observed in another lab and indicates a progressive loss of fecundity of *rfs-1* mutants, which agrees well with a 4% spontaneous mutation rate observed in the strain (Grabowski 2007; Yanowitz 2008).

4.2.2 Sensitivity to DNA damaging agents

An obvious question, given the physical interaction between RFS-1 and RIP-1 and similar elevation of male progeny in nematodes mutant for these proteins, was whether *rip-1* mutants would also be specifically sensitive to replication blocking lesions. Surprisingly, *rip-1* mutants appeared to be only moderately sensitive to both IR and HN2 (Figure 4.6A,B). However, they displayed an increased number of apoptotic corpses relative to wild-type animals following treatment with HN2, but not IR (Figure 4.6C). These results might suggest that the *tm2948* allele is a hypomorph as opposed to a complete loss-of-function. When exposed to low doses, *rip-1* mutants are only moderately sensitive to replication blocking agents, while at high doses they have levels of embryonic lethality and increased apoptosis that are comparable to *rfs-1* mutants (Figure 4.6).

4.2.2.1 RAD-51 focus formation following treatment with DNA damaging agents

The increased sensitivity, apoptosis, and chromosome fragmentation of *rfs-1* mutants in response to replication blocking lesions was very likely due to a failure to load RAD-51. Given the moderate sensitivity and increased apoptosis of *rip-1* mutants following HN2 treatment, the question of whether RAD-51 focus formation was similarly perturbed in the absence of RIP-1 was addressed. Again, a very similar situation emerged to that detailed in Chapter 3. *rip-1* mutants were severely

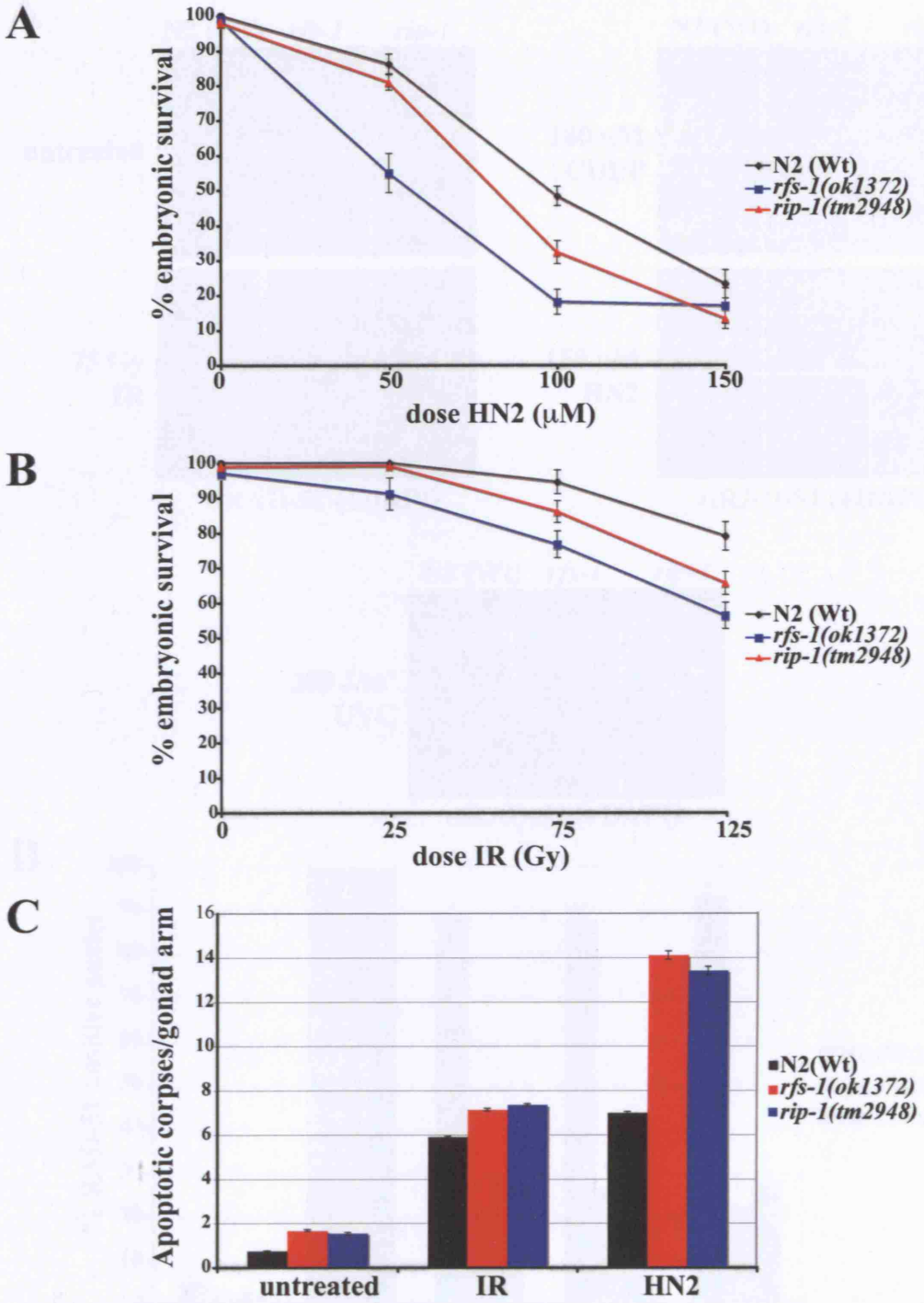

Figure 4.6. *rip-1* mutants are moderately sensitive to IR and HN2 but only exhibit increased apoptosis in response to HN2. (A,B) Percentage progeny survival of animals of the indicated genotypes treated with the noted doses of nitrogen mustard (HN2; A) and ionizing radiation (IR; B). Error bars indicate S.E.M. from at least 24 adult worms over two independent experiments. (C) Number of apoptotic corpses scored by SYTO12 staining in gonads from animals of the indicated genotype either untreated, or 24 hours post-treatment with 75 Gy IR, or 150 μM HN2. Error bars indicate S.E.M. from at least 28 adult animals scored in two independent experiments.

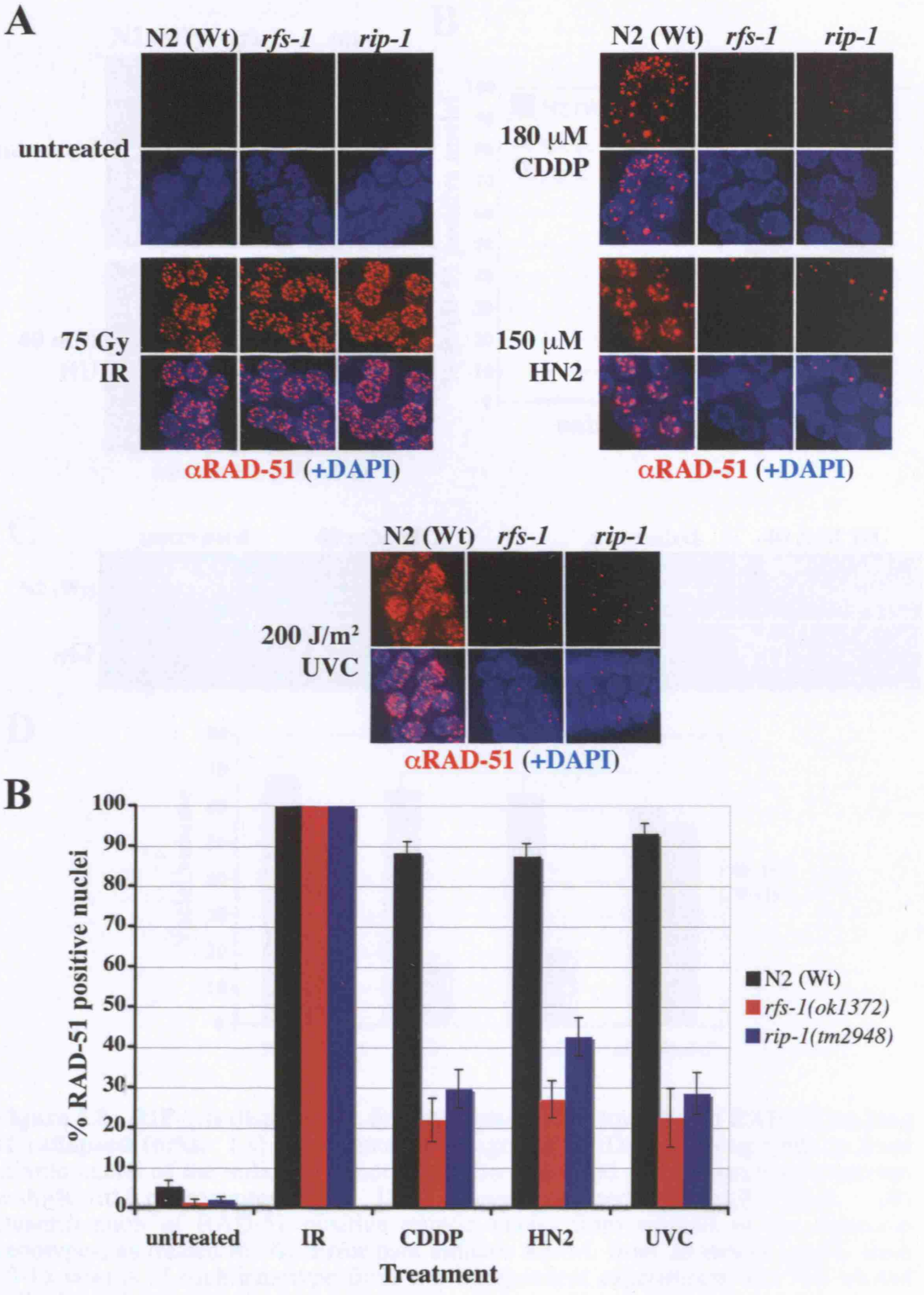

Figure 4.7. RIP-1 mutants are also defective for RAD-51 focus formation specifically following replication blocking damage. (A) Representative images of RAD-51 staining (red) in fixed mitotic nuclei of the indicated genotype either untreated, four hours post treatment with 75 Gy IR, 18 hours post-treatment with 180 μM CDDP, 16 hours post-treatment with 200 μM HN2, or two hours post-treatment with 200 J/m² UVC. DNA is counterstained with DAPI (blue). (B) Quantification of RAD-51 positive mitotic nuclei of the indicated genotypes, as treated in (A). Error bars indicate S.E.M. from 20 mitotic nuclei from 10-25 worms of each genotype from two independent experiments.

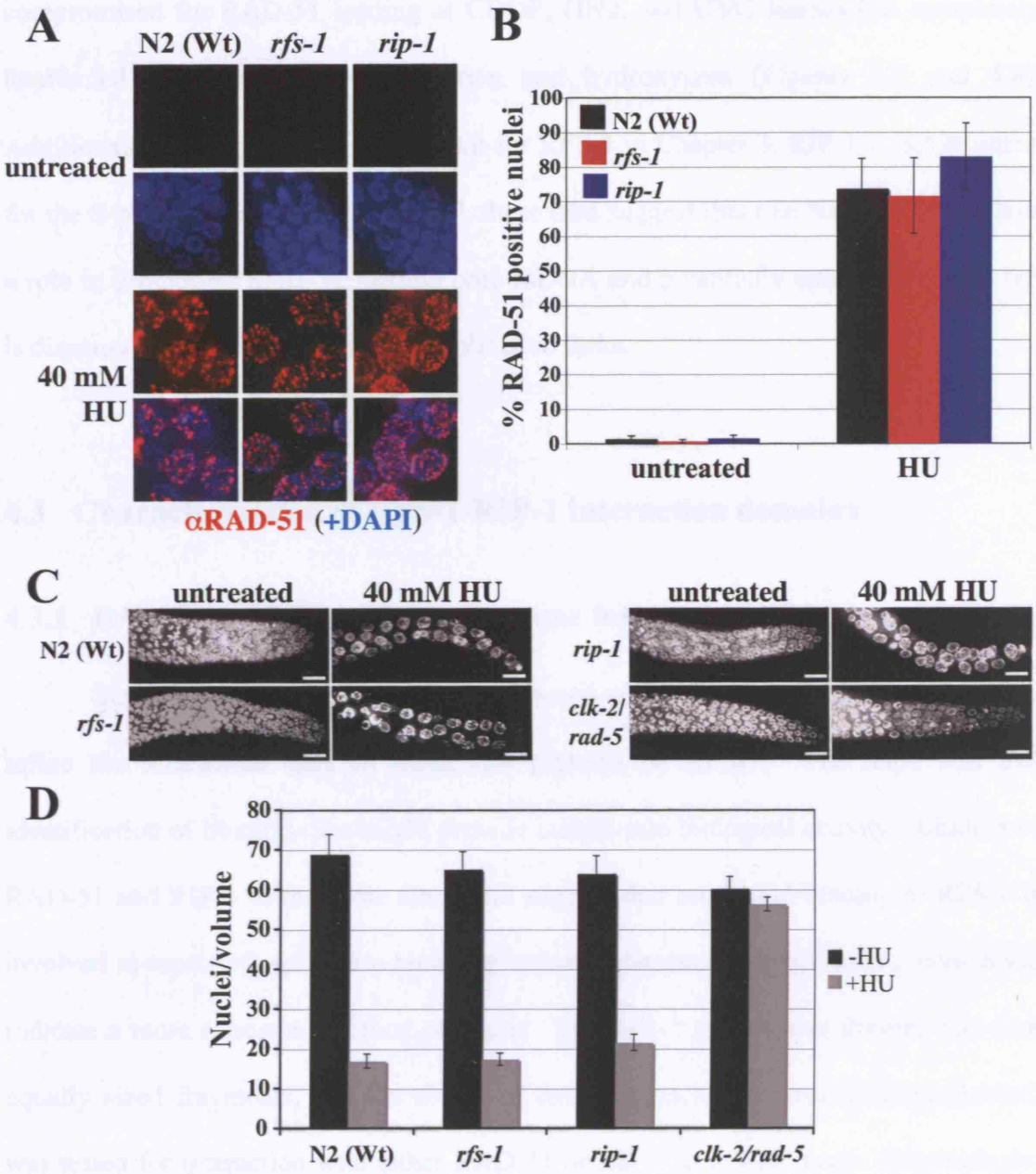

Figure 4.8. RIP-1 is dispensable for the S-phase checkpoint and RAD-51 loading at collapsed forks. (A) Representative images of RAD-51 staining (red) in fixed mitotic nuclei of the indicated genotypes either untreated or 16 hours post-treatment with 40 mM hydroxyurea (HU). DNA is counterstained with DAPI (blue). (B) Quantification of RAD-51 positive mitotic nuclei from animals of the indicated genotypes, as treated in (A). Error bars indicate S.E.M. from 20 mitotic nuclei from 10-15 worms of each genotype from two independent experiments. For HU treated animals, only 10 mitotic nuclei were scored due to the reduction in mitotic nuclei number induced by the S-phase arrest. (C) Representative images of DAPI-stained (grey) mitotic nuclei in animals of the indicated genotypes either untreated or 16 hours post-treatment with 40 mM HU. The S-phase checkpoint mutant *clk-2/rad-5(mn159)* was used as a control in (C) and (D). (Scale bars=10 μm) (D) Quantification of HU-induced cell cycle arrest in mitotic nuclei of the indicated genotypes. Degree of arrest was determined by scoring the number of nuclei in a volume of 54 000 μm^3 16 hours after treatment of L4 stage animals with 40 mM HU, as previously described (Ahmed *et al.*, 2001). The error bars indicate the S.E.M. from at least 10 animals of each genotype from two independent experiments.

compromised for RAD-51 loading at CDDP, HN2, and UVC lesions but completely unaffected in response to γ–irradiation and hydroxyurea (Figures 4.7 and 4.8). Additionally, similar to what was shown for RFS-1 in Chapter 3, RIP-1 is not required for the S-phase checkpoint. Combined, these data suggest that like RFS-1, RIP-1 plays a role in promoting RAD-51 loading onto ssDNA and potentially one-ended DSBs but is dispensable for HRR at collapsed replication forks.

4.3 Characterization of RFS-1-RIP-1 interaction domains

4.3.1 RAD-51 and RIP-1 bind to the same fragment of RFS-1

Since both RAD-51 and RIP-1 interacted with RFS-1, attempts were made to refine the interaction sites of these two proteins on RFS-1. The hope was that identification of binding sites might provide insight into biological activity. Binding of RAD-51 and RIP-1 to the same site could suggest that sequential binding to RFS-1 is involved in repair of replication blocking lesions, whereas differing binding sites could indicate a more concerted method of repair. The RFS-1 protein was divided into four equally sized fragments, and the ability of these fragments, or combinations thereof, was tested for interaction with either RAD-51 or RIP-1 in a Y2H assay. Interestingly, fragment three, which contains the Walker B ATPase motif, was able to interact with both RAD-51 and RIP-1 (Figure 4.9). Fragment four was also able to interact with RIP-1, very weakly (Figure 4.9). Only full length RFS-1 and RFS-1 fragment three strongly interacted with RIP-1 or RAD-51 in the Y2H assay. The observation that other combinations containing fragment three (eg. fragments 2+3, 3+4, etc.) failed to yield positive reactions might reflect alterations to secondary structure that block the interaction. RIP-1 was similarly divided into four fragments, which were then tested for interaction with RFS-1 in a Y2H assay. Unfortunately, only full length RIP-1 interacted

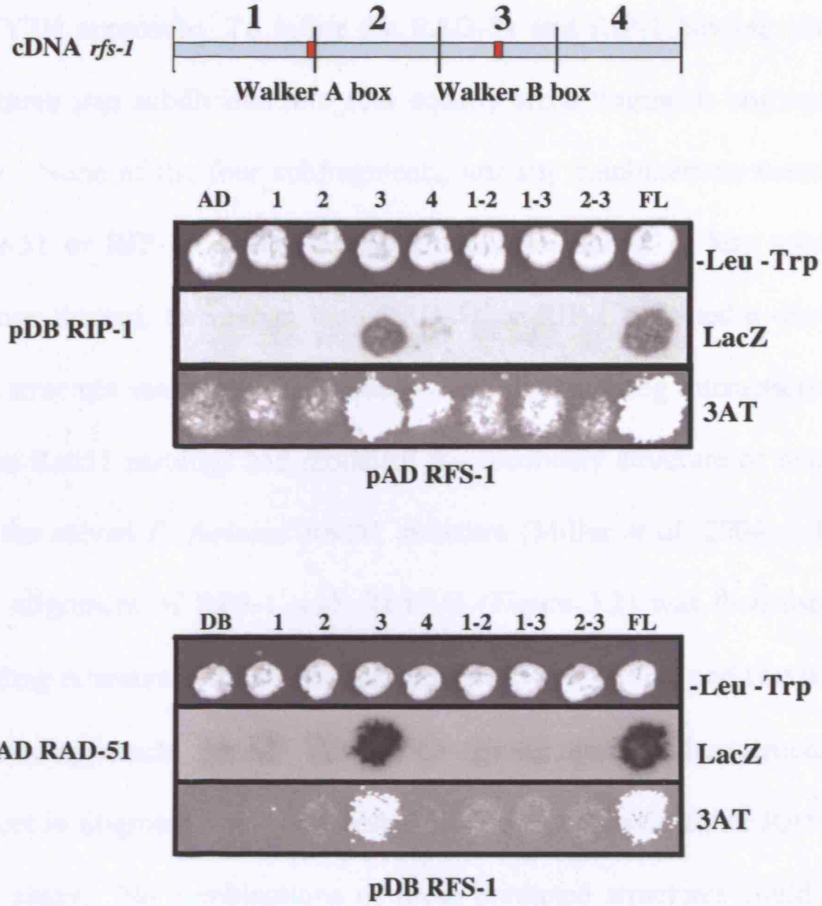

Figure 4.9. Mapping of RAD-51 and RIP-1 binding to RFS-1 by Y2H fragment analysis. The *rfs-1* cDNA was divided into four evenly sized fragments and the ability of each fragment, as well as combinations of the fragments, to interact with RAD-51 or RIP-1 was examined. Both LacZ expression and growth on 20 mM 3AT were used to identify positive interactions. Growth on permissive –Leu –Trp plates is provided as a control.

with RFS-1. Therefore, RFS-1 binding sites on RIP-1 could not be similarly dissected using the Y2H approach. To refine the RAD-51 and RIP-1 binding sites on RFS-1, fragment three was subdivided into four equally sized fragments and again tested for interaction. None of the four subfragments, nor any combinations thereof, interacted with RAD-51 or RIP-1. It was possible that the inability of any subfragments, or combinations thereof, to interact with RAD-51 or RIP-1 reflected a disruption to the secondary structure mediating the binding. A study analyzing interactions between the mammalian Rad51 paralogs had modelled the secondary structure of murine Rad51D, based on the solved *P. furiosus* Rad51 structure (Miller *et al.* 2004). The sequence homology alignment of RFS-1 with Rad51D (Figure 3.2) was then used to identify corresponding domains in RFS-1, which included two α-helices and two β-barrels. In a more targeted approach, cloned fragments containing the secondary structures predicted to be present in fragment three were tested for interaction with either RAD-51 or RIP-1 in a Y2H assay. No combinations of these predicted structures could interact with RAD-51 or RIP-1. It can be inferred that it is likely that all of fragment three is needed to mediate the Y2H interaction between RFS-1 and RAD-51/RIP-1.

4.3.2 Peptide array analysis of RAD-51 and RIP-1 binding to RFS-1

Due to the technical limitations encountered in mapping of the binding sites by Y2H, peptide array technology was utilized to further refine the interaction sites. A potential issue with the Y2H approach is that fusions to small fragments might result in occluded binding due to the large sizes of the DB and AD domains. Peptide arrays circumvent this issue, since peptides of a particular size are covalently linked to a membrane, and therefore are accessible for binding. Additionally, since the protein is divided into a series of overlapping peptides, problems intrinsic to Y2H analysis, such as disruption of key interaction sites when dividing a protein of interest into fragments,

are avoided. The peptide array approach has recently been successful in mapping the interaction between BRCA2 and DMC1, the human meiotic recombinase (Thorslund *et al.* 2007). A peptide array was generated, using 30mer peptides, covering the C-terminal 125 amino acids of RFS-1. Each successive position on the array was shifted by one residue relative to its neighbours, meaning that each peptide spot had 29 residues in common with the adjacent positions. This array was then used to test whether any RFS-1 C-terminal 30mer was able to bind recombinant RAD-51. Remarkably, a single peptide was able to interact with RAD-51 (Figure 4.10A). At the centre of this peptide was the Walker B motif, which in human RAD51D is critical for mediating resistance to mitomycin C and interaction with RAD51C and XRCC2 (Figure 4.10A,C) (Wiese *et al.* 2006). The fact that the interaction is lost by shifting one residue in either direction could suggest one of two possibilities: either RAD-51 has a large, specific binding site; or that regions peripheral to the binding site contain disruptive secondary structure. Repeating the experiment with maltose binding protein (MBP) tagged RIP-1 demonstrated that two separate RFS-1 peptides specifically interact with RIP-1. Strikingly, the first site lies adjacent to the Walker B box, while the second is near the C-terminus of the protein. The RIP-1 binding is specific, since an MBP control failed to bind to the peptides (Figure 4.10B,C). The peptide array results agree very well with the Y2H domain mapping, because RAD-51 and RIP-1 both interacted with peptides located in domain three, with RIP-1 also interacting with a peptide in domain four.

The identification of specific RAD-51 and RIP-1 interacting sequences in RFS-1 afforded the opportunity to identify key residues through a mutagenized peptide array approach. Peptide arrays were generated in which each residue in the 30mer peptide was sequentially mutated to each of the 20 amino acids in a 20x30 matrix. Using this approach, key residues, whose alteration completely abrogated RIP-1 binding, were

Figure 4.10. Peptide array fine mapping of RAD-51 and RIP-1 binding sites on RFS-1. An array consisting of 30mer peptides that correspond to the C-terminal 125 amino acids of the RFS-1 protein was created to fine map the RAD-51 and RIP-1 interaction sites. Each successive spot on the array represents a single-residue "shift" along the protein, requiring 96 spots for full coverage of the region. (A) The array was probed with recombinant RAD-51 and analyzed by immuno-blotting. The membrane was subsequently Ponceau stained to visualize position of the peptides within the array. A control where no RAD-51 was added was also performed (mock). The RAD-51 binding peptide is indicated by a blue box. (B) An array was probed with recombinant MBP-RIP-1 and analyzed by immuno-blotting. The membrane was subsequently Ponceau stained to visualize peptide positions. A control where MBP alone was added was also performed (mock). The RIP-1 interacting peptides are indicated by blue boxes. (C) Sequences of RAD-51 and RIP-1 interacting peptides, and their locations within the RFS-1 protein. The Walker B box sequence in the peptide is indicated by red.

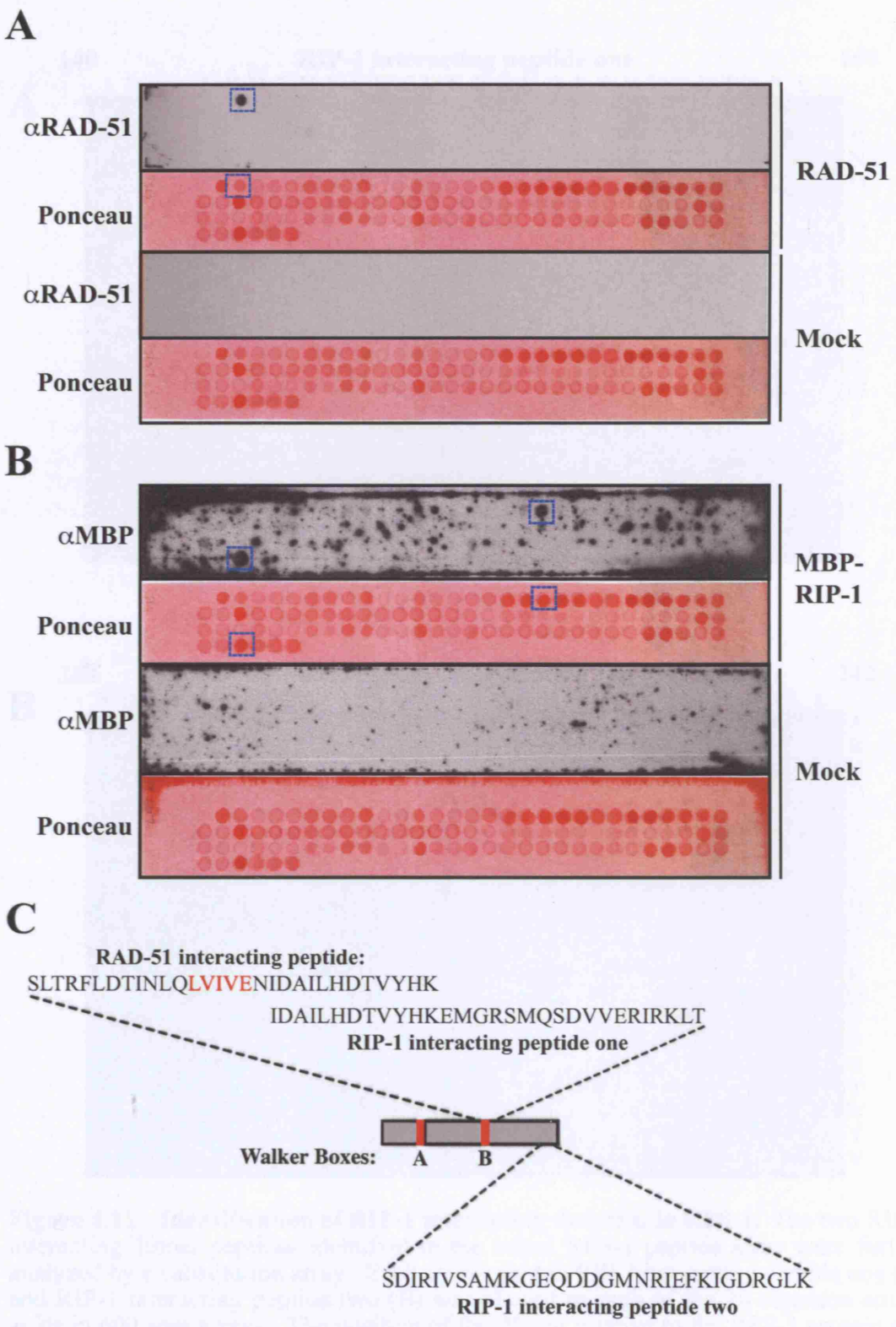

Figure 4.10. Peptide array fine mapping of RAD-51 and RIP-1 binding sites on RFS-1. For figure legend, see preceding page.

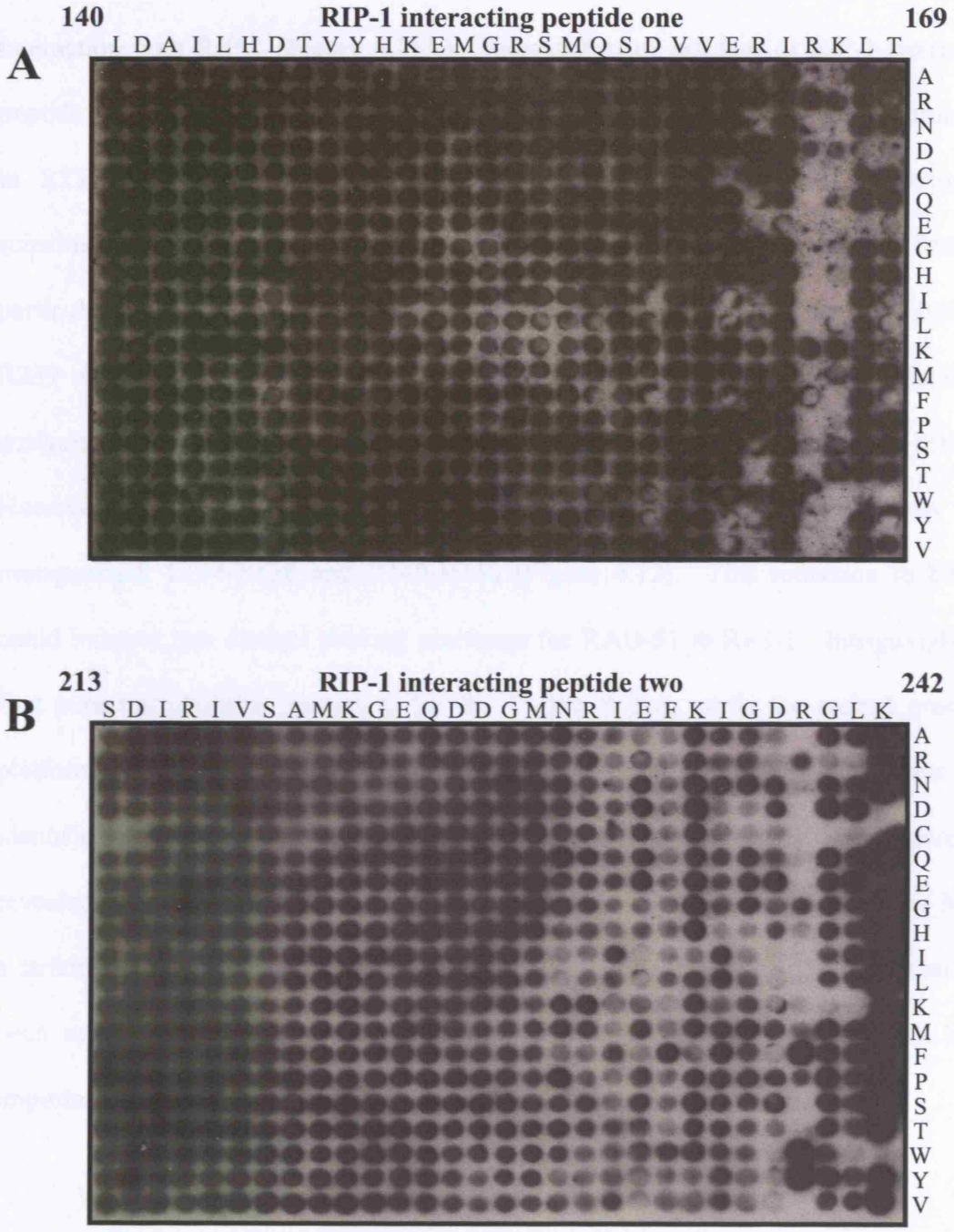

Figure 4.11. Identification of RIP-1 interacting domains in RFS-1. The two RIP-1 interacting 30mer peptides identified in the initial RFS-1 peptide array were further analyzed by a substitution array. Each amino acid in RIP-1 interacting peptide one (A) and RIP-1 interacting peptide two (B) was altered to each of the 20 common amino acids in 600 spot arrays. The position of the 30mer relative to the RFS-1 protein and the sequences of the original peptides are given at the top of each array, while the identity of the substituted residue is on the right side of each array.

sensitive to change at residues R166 and K167, with most alterations abrogating interaction with RIP-1 (Figure 4.11A). Substitution of residues in RIP-1-intertacting peptide two between R231 and D238 reduced binding to various degrees, but mutations in R239 had very pronounced effects on binding (Figure 4.11B). Almost all substitutions reduced or prevented RIP-1 binding (Figure 4.11B). However, particularly striking was the increase in RIP-1 binding that accompanied substitution of R239 with any of the aromatic amino acids (W, Y, F) (Figure 4.11B). Mutational analysis of the RAD-51-interacting peptide failed to isolate any essential residues. However, reduced binding by RAD-51 was observed when two regions were mutagenized: L134-E138 and Y149-H150 (Figure 4.12). This reduction in binding could indicate two distinct binding platforms for RAD-51 to RFS-1. Intriguingly, the first potential platform appears to be the Walker B box, while the second predicted platform lies downstream of this motif. The peptide and mutagenic arrays have identified key interaction sites in RFS-1 for both RAD-51 and RIP-1 and have also revealed point mutations that specifically disrupt each interaction. In the case of RIP-1, a striking gain-of-function point mutation in the second RIP-1 interacting domain has been uncovered. Extension of these studies both *in vitro* and *in vivo* will be an important future direction for this work.

4.4 Preliminary purification of RFS-1 and RIP-1

Cytological, biochemical and structural analysis of RFS-1 and RIP-1 could provide powerful mechanistic insight into the roles of these proteins at impeded replication forks. This is especially important for RIP-1, given its lack of identifiable homologs or domains. To this end, development of antibodies that recognize RFS-1 and RIP-1, and purification of these proteins would greatly further this work.

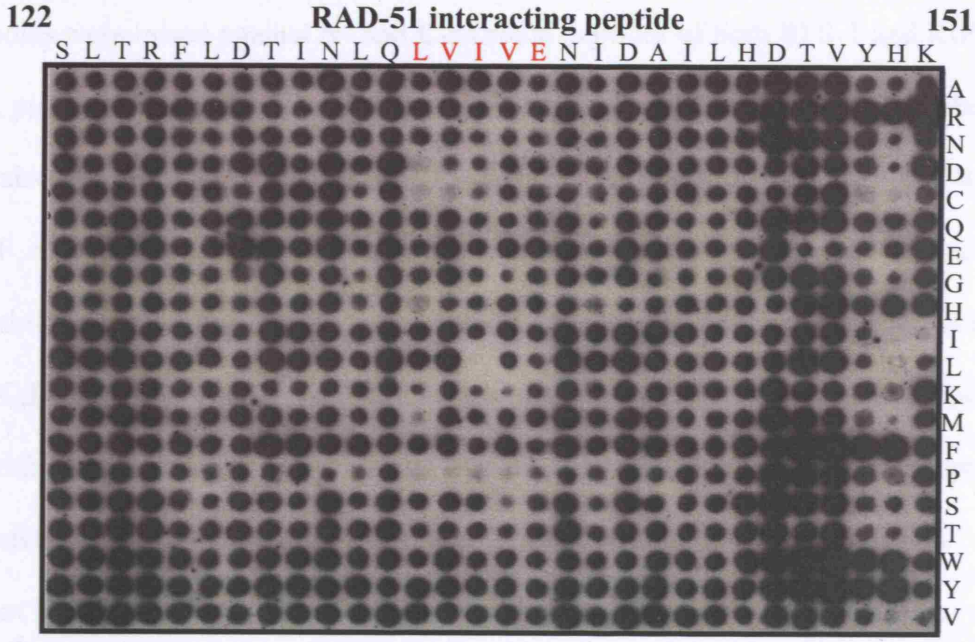

Figure 4.12. Substitution analysis of RAD-51 binding to RFS-1. The RAD-51 interacting peptide identified by peptide array analysis of RFS-1 was subjected to substitution analysis. Each amino acid in the peptide was altered to each of the 20 common amino acids in a 600 spot array. The position of the 30mer relative to the RFS-1 protein and the sequence of the original peptide are given at the top of each array, while the identity of the substituted residue is on the right side of each array. The position of the Walker B ATPase motif is indicated in red.

Given the utility of antibodies as a reagent for studying protein interactions and cellular localization, attempts were made to develop these tools for RFS-1 and RIP-1. Antibodies were raised against N- and C-terminal peptides of both RFS-1 and RIP-1 in guinea pigs; using the same RFS-1 N- and C-terminal peptides, additional antibodies were raised in rabbits. Recombinant RFS-1 and RIP-1 were produced (Figure 4.13A and E,F, respectively), and following affinity purification, the antibodies were tested for their ability to recognize the recombinant proteins in immuno-blotting (Figure 4.13B,C,D,G,H). For RFS-1, an antibody raised against a C-terminal peptide in rabbits, and antibodies raised in guinea pigs against both N- and C-terminal peptides, successfully recognize recombinant protein (Figure 4.13and C,D, respectively). Two different polyclonal antibodies raised against a C-terminal RIP-1 peptide were successful in recognizing recombinant RIP-1 (Figure 4.13G,H). Although these antibodies are clearly recognizing recombinant RIP-1 and RFS-1, they fail to detect the proteins in worm extracts, suggesting that the proteins are expressed at low levels. All of these antibodies have failed in immunofluorescence so far; they either fail to react regardless of the conditions, or inappropriate staining is observed, even in *rfs-1* and *rip-1* mutants. The development of robust antibodies will be important for future cytological study of RFS-1 and RIP-1.

Purification of RFS-1 and RIP-1 for biochemical analysis is important in order to further refine the roles of these proteins at impeded replication forks. Using Gateway recombination site flanked *rip-1* and *rfs-1* cDNA containing vectors, a series of protein expression vectors were created containing RIP-1 and RFS-1 fused to a series of N-terminal tags (6xHis, GST, MBP). *rip-1* was also cloned into a vector containing an N-terminal 6xHis-SUMO tag using conventional methods. These recombinant forms of RFS-1 and RIP-1 were initially used to test for specificity of antibodies raised against

Figure 4.13. Development of RFS-1 and RIP-1 antibodies. All protein gels and immuno-blots contain a molecular weight marker (M); estimated protein sizes are indicated in kiloDaltons (kDa). (A) Coomassie stained gel of pilot RFS-1 expression. Uninduced (U), induced (I), and soluble (S) fractions are shown for N-terminal fusions of 6xHis, GST, and MBP to RFS-1. The predicted molecular weights of the fusion proteins are approximately 30 kDa, 55 kDa, and 68 kDa, respectively. (B) Immuno-blot of an uninduced control, and induced samples of bacteria expressing RFS-1 containing His, GST, and MBP N-terminal fusions probed with a polyclonal anti-RFS-1 antibody raised against a C-terminal peptide of RFS-1 in rabbits. (C and D). Immuno-blots of an uninduced control, and induced samples of bacteria expressing RFS-1 containing GST, Gbl (~34 kDa fusion protein) and MBP N-terminal fusions were probed with two different polyclonal anti-RFS-1 antibodies. The antibodies were raised against either an N-terminal peptide (C), or a C-terminal peptide (D) of RFS-1 in guinea pigs. (E and F) Coomassie stained gels of RIP-1 expressing cells. Uninduced (U), induced (I), and soluble (S) fractions are shown for N-terminal fusions of 6xHis-SUMO (E), GST, and MBP (F) to RIP-1. The predicted molecular weights of the fusion proteins are approximately 36.9 kDa, 50.6 kDa, and 63.6 kDa, respectively. (G and H) An uninduced control and induced samples of bacteria expressing RIP-1 containing 6xHis-SUMO, GST, and MBP N-terminal fusions was probed with two different polyclonal α-RIP-1 antibodies. Each of the two separate antibodies was raised against an N-terminal peptide of RFS-1 in guinea pigs. Antibodies raised against a C-terminal peptide failed to recognize the same recombinant proteins.

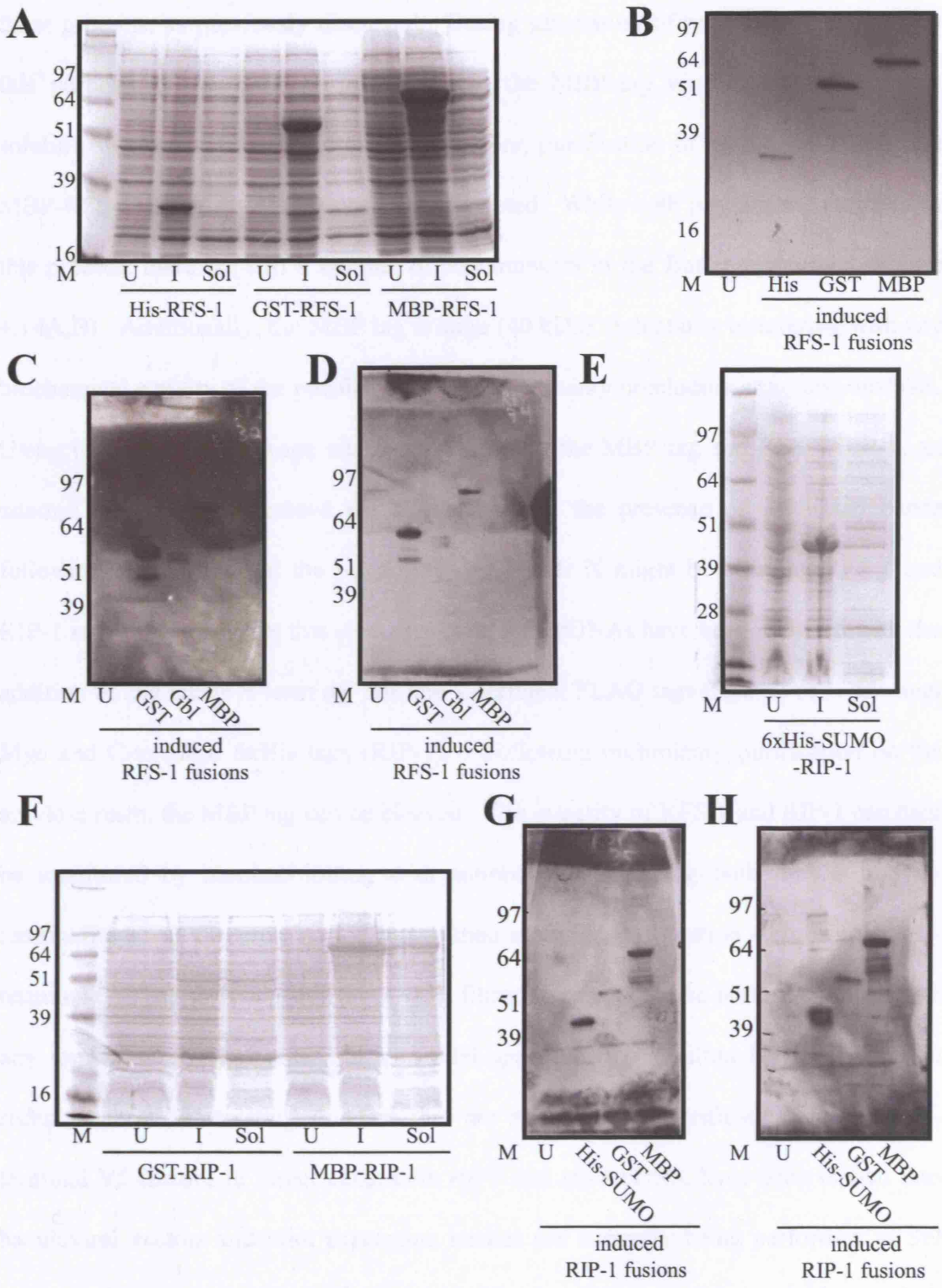

Figure 4.13. Development of RFS-1 and RIP-1 antibodies. For figure legend, see preceding page.

these proteins, as previously discussed. During generation of recombinant protein for this purpose, it was consistently noted that the MBP tag was notably effective at solublilizing both RFS-1 and RIP-1. Therefore, purification of both MBP-RIP-1 and MBP-RFS-1, using amylose resins, was attempted. While both proteins are enriched in this process, there are still a number of contaminants in the final preparations (Figure 4.14A,B). Additionally, the MBP tag is large (40 kDa), potentially interfering with any biochemical activity of the purified protein, and certainly precluding structural analysis. Using the Factor X cleavage site located between the MBP tag and RFS-1/RIP-1, an attempt was made to remove the tag. However, the presence of additional bands following cleavage raised the possibility that Factor X might be cleaving RFS-1 and RIP-1 as well. To address this cleavage issue, both cDNAs have been recloned with the addition of and either N-terminal HA and C-terminal FLAG tags (RFS-1) or N-terminal Myc and C-terminal 6xHis tags (RIP-1). Following preliminary purification on the amylose resin, the MBP tag can be cleaved. The integrity of RFS-1 and RIP-1 can then be monitored by immunoblotting with antibodies recognizing both the N- and C-terminal tags. If the proteins are intact, then a second purification step using the C-terminal tags can then be carried out. Gel filtration could then be performed to remove any remaining contaminants. In a parallel approach, the Boulton lab has had great recent success in isolating proteins that are refractory to purification by using N-terminal V5-fusions in insect cells; both *rip-1* and *rfs-1* cDNA have been cloned into baculoviral vectors and pilot expression studies are currently being performed in Sf9 cells. Preliminary expression data suggests that it will be possible to obtain purified, soluble RFS-1 and RIP-1, a key development for future study of these proteins.

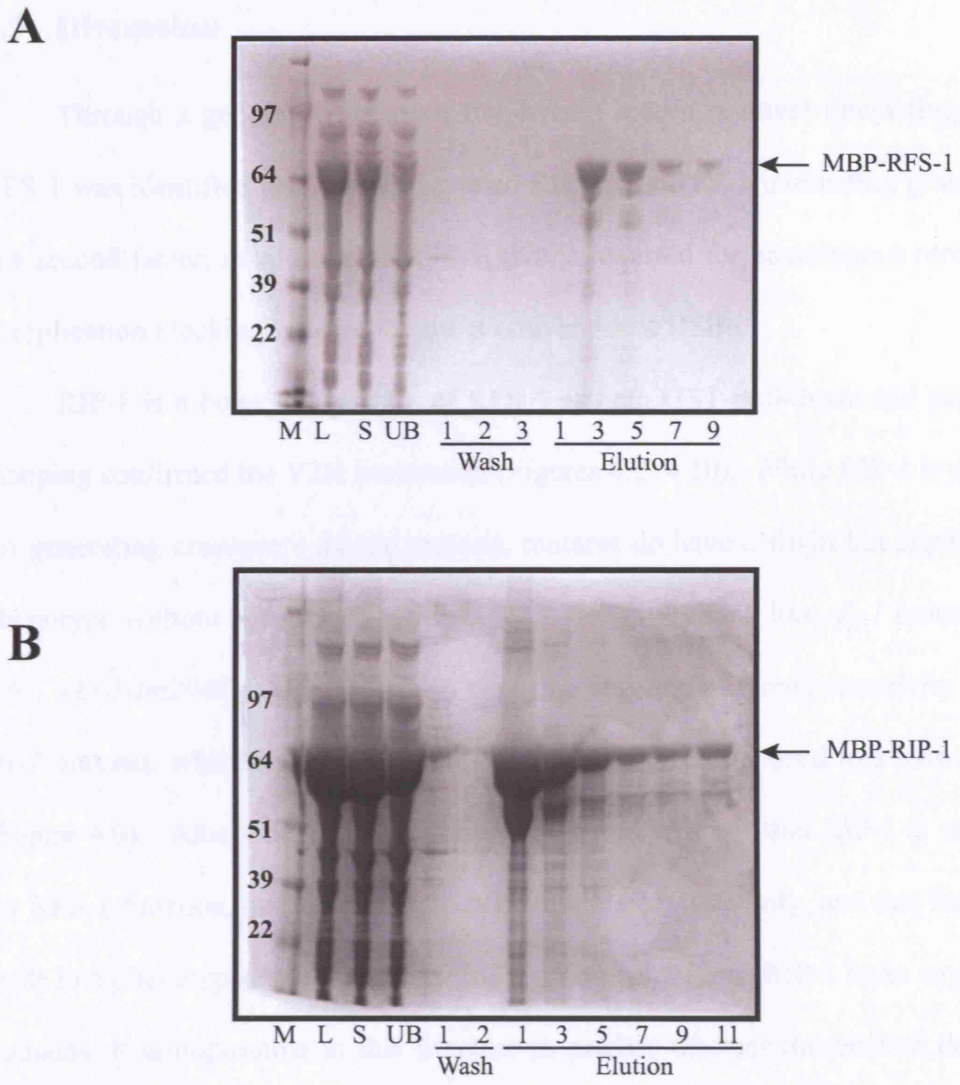

Figure 4.14. Preliminary partial purification of RFS-1 and RIP-1. Coomassie stained gels carrying the various steps of purification. Both protein gels contain a molecular weight marker (M) indicating estimated protein sizes in kiloDaltons (kDa). MBP-RFS-1 and MBP-RIP-1 predicted molecular weights are 68 and 63.6 kDa, respectively. (A) A one litre culture of *E. coli* expressing MBP-RFS-1 was lysed (L) and insoluble debris was cleared to make a soluble fraction (S). This fraction was bound to 5 ml of amylose beads overnight and the unbound fraction (UB) was collected. The beads were extensively washed and then eluted in 1 ml fractions using 20 mM maltose. (B) RIP-MBP was purified as in (A); one fewer wash and two additional elution fractions were taken.

4.5 Discussion

Through a genome wide yeast two-hybrid screen, a novel interacting partner of RFS-1 was identified and has been named RIP-1, for RFS-1 interacting protein. RIP-1 is a second factor, in addition to RFS-1, that is required for homologous recombination at replication blocking lesions but not at conventional DSBs.

RIP-1 is a *bona fide* partner of RFS-1 as both GST-pull-down and peptide array mapping confirmed the Y2H interaction (Figures 4.2, 4.10). While RIP-1 is dispensable for generating crossovers during meiosis, mutants do have a slight but significant Him phenotype without accompanying embryonic lethality, much like *rfs-1* mutants (Figure 4.5). *rip-1(tm2948)* does not exhibit the same severe embryonic sensitivity to HN2 as *rfs-1* mutants, which might suggest it is a hypomorph as opposed to a loss-of-function (Figure 4.6). Alternatively, this discrepancy could indicate that RIP-1 is not essential for RFS-1 function, but rather regulates or modulates its activity, and that loss of RIP-1 leads to a phenotype expected of an *rfs-1* hypomorph. Since RIP-1 lacks any detectable domains, it is impossible at this juncture to predict whether the *tm2948* deletion is a hypomorphic or amorphic, or even a dominant negative allele. Analysis of a *rip-1(tm2948)*/+ heterozygote would determine whether the phenotype observed is dominant negative. Either RNAi knockdown or generation of other alleles of *rip-1* might permit discrimination between *rip-1* hypomorphic and loss-of-function phenotypes. Given the observations that RIP-1 physically interacts with RFS-1 and that *tm2948* is a large deletion with similar phenotypes to the *rfs-1(ok1372)* allele, it is likely that the *tm2948* deletion results in a loss, as opposed to gain, of function.

Whatever the allele class of *tm2948*, a strong phenotype is only observed upon exposure to high doses of agents that cause replication blocking lesions, presumably because this requires more RFS-1 activity. Consistent with this hypothesis, *rip-1(tm2948)* animals phenocopy *rfs-1* mutants with respect to elevated apoptosis relative

to wild type animals in response to HN2 but not IR. Further, both *rfs-1* and *rip-1* mutations attenuate RAD-foci following treatment with CDDP, HN2, and UVC but not IR. Like RFS-1, RIP-1 is dispensable for the S-phase checkpoint and for RAD-51 loading at forks collapsed by hydroxyurea. Cumulatively, these data suggest that RIP-1 is also somehow positively regulating or promoting HRR at impeded replication forks, but not DSBs *per se*.

Considering the physical interaction with RFS-1 and the similarity in phenotypes between *rip-1* and *rfs-1* mutants, it is almost certain that the phenotypes described in this chapter are attributable to the deletion in *rip-1*. However, although extremely unlikely, a tightly linked second-site mutation could theoretically be responsible. To address this, a transgene rescue or verification of the phenotypes with either RNAi or another allele must be performed. Transgene rescue is extremely difficult in the *C. elegans* germ line due to silencing. RNAi by feeding *E. coli* expressing *rip-1* dsRNA has so far failed to yield a phenotype, though it is possible that direct injection of dsRNA into the germ line will meet with some success. Transgene-mediated co-suppression, a technique by which stable transgenes result in functional silencing of loci through a mechanism that overlaps with but is distinct from RNAi, is another method that could be used to generate a *rip-1* loss of function animal (Dernburg *et al.* 2000). As *rip-1* is predicted to be the second gene in an operon, the *rip-1* cDNA was fused to the ubiquitously expressed *dpy-30* promoter and this construct can now be injected to generate stable co-suppression lines (Hsu *et al.* 1995; Dernburg *et al.* 2000). Previous work has demonstrated that co-suppression by a P*dpy-30-him-14* cDNA fusion is as effective as co-suppression induced by the *him-14* cDNA containing its native promoter (Dernburg *et al.* 2000). Even if *rip-1* is indeed in an operon, off target effects should not be generated through co-suppression, because RNAi knockdown of one gene in a bicistronic operon was shown to have no effect on the expression of the second gene

(Montgomery *et al.* 1998). Relying on the knockout consortiums to generate mutants is a lottery, as evidenced by the early acquisition of the *rfs-1* allele and very late isolation of the *rip-1* allele in this project. To circumvent this dependence, the Boulton lab has very recently turned to TILLING (Targeting Induced Local Lesions in Genomes) in an attempt to generate mutants (Till *et al.* 2003). TILLING uses EMS mutagenesis to induce point mutations throughout the genome, followed by PCR amplification of target loci with fluorescently tagged PCR primers. An endonuclease that specifically cleaves mismatches is added and mutations are detected as PCR products of shorter sizes. This approach has been very successful in generating *C. elegans* mutants, where as described in a recent publication, missense or nonsense mutants were obtained in each of ten different genes; for eight of these no prior alleles existed (Gilchrist *et al.* 2006). There is a high probability that this technique will be able to isolate further mutations in *rip-1*, which will complement the data generated using the *tm2948* allele.

Although the preliminary results regarding RIP-1 are exciting, the *rip-1* allele was obtained quite late in the project. Consequently, much subsequent work is required to characterize it and refine the role played by its interaction with RFS-1 in promoting HRR at blocked forks. The fact that RIP-1 and RFS-1 physically interact, and that they exhibit similar mutant phenotypes, strongly suggest that the two proteins are working in concert to promote RAD-51 loading at blocked forks. However, this assertion needs to be formally proven. To this end an *rfs-1 rip-1* double mutant has been generated, which is viable. Future work will involve confirming that there is no additive apoptosis or embryonic sensitivity to DNA damaging agents in the *rfs-1 rip-1* double mutant relative to the single mutants. Further characterization of *rip-1* requires assays of the mutant's sensitivities to CDDP and CPT, analysis of apoptosis after CDDP and CPT, and examination of chromosome fragmentation following HN2 and CPT. A role for RIP-1

in maintenance of poly-G/C tracts in a *dog-1* mutant background is likely and will be explored.

Efforts to generate RFS-1 and RIP-1 antibodies have met with only moderate success. While they were able to recognize recombinant protein, they failed in detecting protein in whole animal extracts and in the germ line by immunofluorescence (Figure 4.13). Antibodies capable of detecting RFS-1 and RIP-1 by immuno-fluorescence could be useful in the analysis of the genetics of focus formation at ICL lesions. It would be of great interest to see if RFS-1 and RIP-1 are able to form foci in the absence of each other or if one is obligate for targeting the other to an impeded fork. Based on analysis of Rad51 paralogs in other systems, it is likely that RFS-1 will be expressed at very low levels. To date, only telomere associated RAD51D, meiotic RAD51C and XRCC3, and IR-induced XRCC3 foci have been reported (Forget *et al.* 2004; Tarsounas *et al.* 2004; Liu *et al.* 2007). It is possible that the RFS-1 and RIP-1 antibodies could be used in combination with a biotin-streptavidin amplification kit to raise the signal to the threshold of detection for immunofluorescence.

The peptide array analysis of RFS-1 interaction with RAD-51 and RIP-1 provided some potentially very interesting insight into the interplay between these three proteins during HRR at an RFB. The fact that RAD-51 and RIP-1 interact with separate and distinct regions of RFS-1 presents the possibility that RIP-1 and RAD-51 are able to interact with RFS-1 simultaneously as opposed to sequentially (Figure 4.10). Gel filtration experiments and RIP-1 and RAD-51 pull-down assays involving all three proteins will address whether the proteins form a single complex. Using a similar approach to that taken by Thorslund *et al.* (2007) critical residues in RFS-1 for mediating the interaction with RIP-1, and to a lesser extent with RAD-51, were identified (Figures 4.11, 4.12). Binding was extremely sensitive to substitution of two key residues in RIP-1 interacting peptide one (R166 K167), but tolerated alterations to

the rest of the peptide (Figure 4.11). Although binding to RIP-1 interacting peptide two was more sensitive to alterations in residues R231- D238, mutation of a key residue (R239) had a much more pronounced effect on binding (Figure 4.11). Substitution at this position either reduced or prevented binding, with a very striking exception. Mutation of R239 to any of the aromatic amino acids actually increased affinity for RIP-1 (Figure 4.11). Unlike with RIP-1-interacting peptides, RAD-51 binding did not seem hypersensitive to any one particular mutation; there was no loss of interaction that was as severe as what was seen in the R166, K167, and R239 mutations of the RIP-1 interacting peptides. Rather, mutations in either the Walker B (L134 to E138) box or a site downstream (Y149-H150) reduced binding, but did not prevent it (Figure 4.12). This result could suggest that there are two interaction sites for RAD-51 within the peptide. A double substitution peptide array, with L134 and H150 both sequentially mutated to all 20 amino acids in all 400 permutations, will be ordered. If two binding sites exist for RAD-51 in RFS-1, then the double substitution array should identify multiple RAD-51 binding-deficient alleles of RFS-1.

The information obtained from the peptide arrays will now be used in several ways. First, site-directed mutagenesis of the RFS-1 protein will be performed. The loss of interaction between RFS-1 and each of RAD-51 and RIP-1 can then be confirmed through yeast two-hybrid analysis and through pull down experiments. The ability of biotinylated wild type and mutant peptides to pull down recombinant RAD-51 and RIP-1 will also be examined. Second, the appropriate peptides can be used in a dominant-negative peptide injection experiment, similar to that of Martin *et al.* (2005). Apoptosis and RAD-51 focus formation following ICL damage can then be assayed in the injected animals to determine the biological consequences of blocking RFS-1 interaction with either RAD-51 or RIP-1. Interaction deficient peptides can be injected as controls for these experiments.

Finally, progress has been made in purification of RFS-1 and RIP-1 proteins using MBP tags, which in turn can be used in the development of functional biochemical assays (Figure 4.14). There are still a number of contaminating proteins, but this is being addressed in two ways. First, additional N- and C-terminal tags, such as HA and FLAG (for RFS-1) and Myc and 6xHis (for RIP-1), are being introduced, which should allow for tandem affinity purification. Second, the bulky MBP tag will be proteolytically cleaved from the RFS-1 and RIP-1. Immuno-blotting against both N - and C-terminal tags will be used to confirm that RFS-1 and RIP-1 were not cleaved during removal of the MBP tag. Since RFS-1 and RIP-1 seem to interact so strongly, their stabilities might be enhanced if the proteins are coexpressed. A series of Gateway compatible expression vectors containing a wide array of cleavable tags (GST, MBP, Trx, Gbl, NusA, DsbA) have been obtained for this purpose. Together, these strategies should yield large amounts of pure protein with minimal additional residues. If pure RFS-1 and RIP-1 can be obtained, then ATPase activity, DNA substrate preference, and the effect of these proteins on RAD-51 mediated strand exchange can be examined, as can their abilities to resolve Holliday junctions. RFS-1 mutants defective for interaction with RAD-51 and RIP-1 generated based on the mutagenized peptide arrays can also be used as controls in the above experiments. It will be extremely interesting to examine the effect of an R239W mutation in RFS-1, which should bind RIP-1 with greater affinity that the wild type RFS-1. Whether this will improve the performance of RFS-1 in biochemical assays or function as a dominant negative remains to be determined.

Further work is required to address the role of RIP-1 in HRR at replication blocking lesions. Given the lack of any detectable domains or homologs outside the genus *Caenorhabditis*, there are not any obvious roles for RIP-1, but a number of possibilities do exist. RIP-1 could be either a highly divergent paralog of RAD-51 or a homolog of Swsl. Swsl is a recently identified interactor of the *S. pombe* Rad51

paralogs that is also a positive modulator of homologous recombination (Martin *et al.* 2006). Bioinformatic analysis of RIP-1 has failed to find similarity between it and any of the Rad51 paralogs or Swsl homologs (Figure 4.3). All Rad51 paralogs identified to date have, minimally, a Walker A or B box, while Swsl possesses a zinc-finger domain, all of which are lacking in RIP-1. This observation, combined with the identification of RIP-1 as a phylogenetic outlier, mean it is improbable that RIP-1 is a divergent version of these proteins (Figure 4.3). In Chapter 3, a number of similarities between RFS-1 and the RecFOR recombination proteins of *E. coli* were outlined. Although secondary structure prediction has failed to identify any similarity between RIP-1 and RecFOR, it is possible that RFS-1-RIP-1 is a RecFOR analog in *C. elegans.* If amounts in the order of one to ten milligrams of RFS-1 and RIP-1 can be purified, then it would be feasible to attempt to crystallize the proteins and solve the structure using X-ray diffraction. As RIP-1 is a small protein (23.6 kDa), it might be amenable to nuclear magnetic resonance (NMR) structural analysis as a complementary approach. A structural approach is likely to be fruitful as it could provide insight into the biological function that might not be obtained from sequence analysis or structural analysis.

Intriguingly, one possible role for RIP-1 could be in regulation of calcium levels at sites of HRR. A previous high throughput Y2H interaction mapping study identified TNC-2 as a RIP-1 interactor. TNC-2 is a protein with moderate similarity to human Calmodulin-1, but has so far only been implicated in regulation of pharyngeal muscle and ovarian contraction in *C. elegans* (Ono and Ono 2004). Studies of both the *C. elegans* and human Rad51 proteins have demonstrated that strand exchange activity is stimulated by calcium (Bugreev and Mazin 2004; Petalcorin *et al.* 2006). If RIP-1 does target TNC-2 to regulate calcium levels at sites of repair, it would likely do so specifically at RFBs as opposed to conventional DSBs, raising the question as to the purpose of differential calcium regulation at blocked forks as opposed to DSBs.

Building on the earlier discussion of potential roles for RFS-1 at impeded forks (Chapter 3), a very interesting possibility is that RAD-51 loading serves to protect nascent strand ends from degradation rather than to facilitate active repair. Prevention of strand exchange activity at sites of replication fork blockage could be accomplished by local control of calcium availability. Although certainly intriguing, this model is completely speculative at current. A major concern is that TNC-2 was supposedly present in the AD-Orfeome library and was not identified in the RIP-1 interaction screen despite 12.5-fold genome coverage and the identification of RFS-1 seven times. It will be important to confirm the interaction between RIP-1 and TNC-2 in small scale Y2H assays and determine whether these proteins interact through pull-down assays. If a potential interaction between RIP-1 and TNC-2 is real, then it would be extremely interesting to add RIP-1 and TNC-2 to a strand exchange reaction and see if activity would be inhibited. Unfortunately, mutant alleles of *tnc-2* do not currently exist, but it might be possible to perform dsRNA injection or generate mutants by TILLING and address whether RAD-51 focus formation or DNA repair is altered at ICL lesions.

In summary, a genome wide Y2H screen has identified a novel interacting partner of RFS-1 that is also required for RAD-51 loading at impeded replication forks, likely through either a ssDNA or a one-ended DSB substrate. Further biochemical characterization of RIP-1 and RFS-1 will illuminate the function of these two proteins in promoting HRR at impeded forks and give further insight into the differences in substrates generated at RFBs versus impeded forks.

5 Chapter 5: Work in progress

5.1 RFS-1 and oxidative stress

The lesions to which RFS-1 and RIP-1 were shown to respond in Chapters 3 and 4 are caused by either chemicals (CDDP, HN2, CPT) or specific genetic backgrounds (*dog-1* and *him-6; top-3(RNAi)*). A major question arising from these findings regards the nature of endogenously arising lesions to which RFS-1, and by extension, the mammalian Rad51 paralogs, responds. It is very clear that the mammalian Rad51 paralogs play an important role *in vivo* in dealing with endogenous lesions, given the early embryonic lethality of Rad51B, Rad51D, and XRCC2 knockout mice (Pittman *et al.* 1998; Shu *et al.* 1999; Deans *et al.* 2003). Interestingly, one possible class of lesion requiring RFS-1-mediated repair is lipid peroxidation products such as glyoxal or malondialdehyde, which have been shown to cross-link DNA (Kasai *et al.* 1998; Niedernhofer *et al.* 2003). Cells defective in the FA/BRCA pathway have recently been demonstrated to be sensitive to plasma levels of the oxidation product formaldehyde, which produces DNA-protein cross-links, another replication blocking lesion (Ridpath *et al.* 2007). Strikingly, Niedernhofer *et al.* (2006) demonstrated in mice that chronic DNA damage, loss of XPF or ERCC1, caloric restriction, and aging all caused reduced growth hormone/insulin-like growth factor 1 (IGF1) signalling and similar gene expression profiles (Niedernhofer *et al.* 2006). These similar expression profiles suggested an interesting intersection of RFB repair and the conserved IGF1 response. The powerful genetics, emerging RFB repair field, and the recent explosion in information regarding aging and stress resistance in *C. elegans* make the nematode an ideal model in which to explore this connection. Therefore, the possibility of a relationship between IGF1 and RFBs that is the inverse of that demonstrated by

Niedernhofer *et al.* (2006) showed was explored: can reduced IGF1 signalling drive the formation of replication blocking lesions?

5.1.1 *daf-16* mutations increase mutation rates in *clk-2* and *him-6* mutants, but not in *rfs-1* mutants

The conserved insulin signalling pathway has been shown to regulate aging and stress resistance in *C. elegans.* A signalling cascade involving the insulin/IGF-1 receptor DAF-2, the phosphoinositide 3-kinase (PI3K) AGE-1 (p110 catalytic subunit homolog), PDK-1 (3-phosphoinositide-dependent kinase 1 ortholog), and AKT-1/AKT-2 (Akt/PKB homologs) result in the phosphorylation of DAF-16 (FOXO1A homolog), causing it to be excluded from the nucleus (Kenyon 2005). DAF-16 is a transcription factor that increases expression of a host of stress response genes, including anti-microbial proteins, catalases, superoxide dismutases and heat shock factors (Murphy *et al.* 2003). Thus, *daf-2* mutants are long-lived due to increased DAF-16 activity in the nucleus and, conversely, *daf-16* mutants have increased sensitivity to a variety of insults. To address whether a general increase in oxidative stress could drive ICL formation, a *daf-16; rfs-1* double mutant was generated for genetic and cytological characterization.

The proposed potential interplay between *rfs-1* and *daf-16* mutants was very complementary to data provided by Melissa Grabowski and Heidi Tissenbaum. While exploring the mechanism underlying the accelerated aging phenotype observed in RecQ helicase mutants, they had observed that while mutants for any of *daf-16, him-6,* or the S-phase checkpoint gene, *clk-2*, had a mild spontaneous mutator phenotype (approximately 4%), *daf-16; clk-2* and *daf-16; him-6* double mutants had dramatic

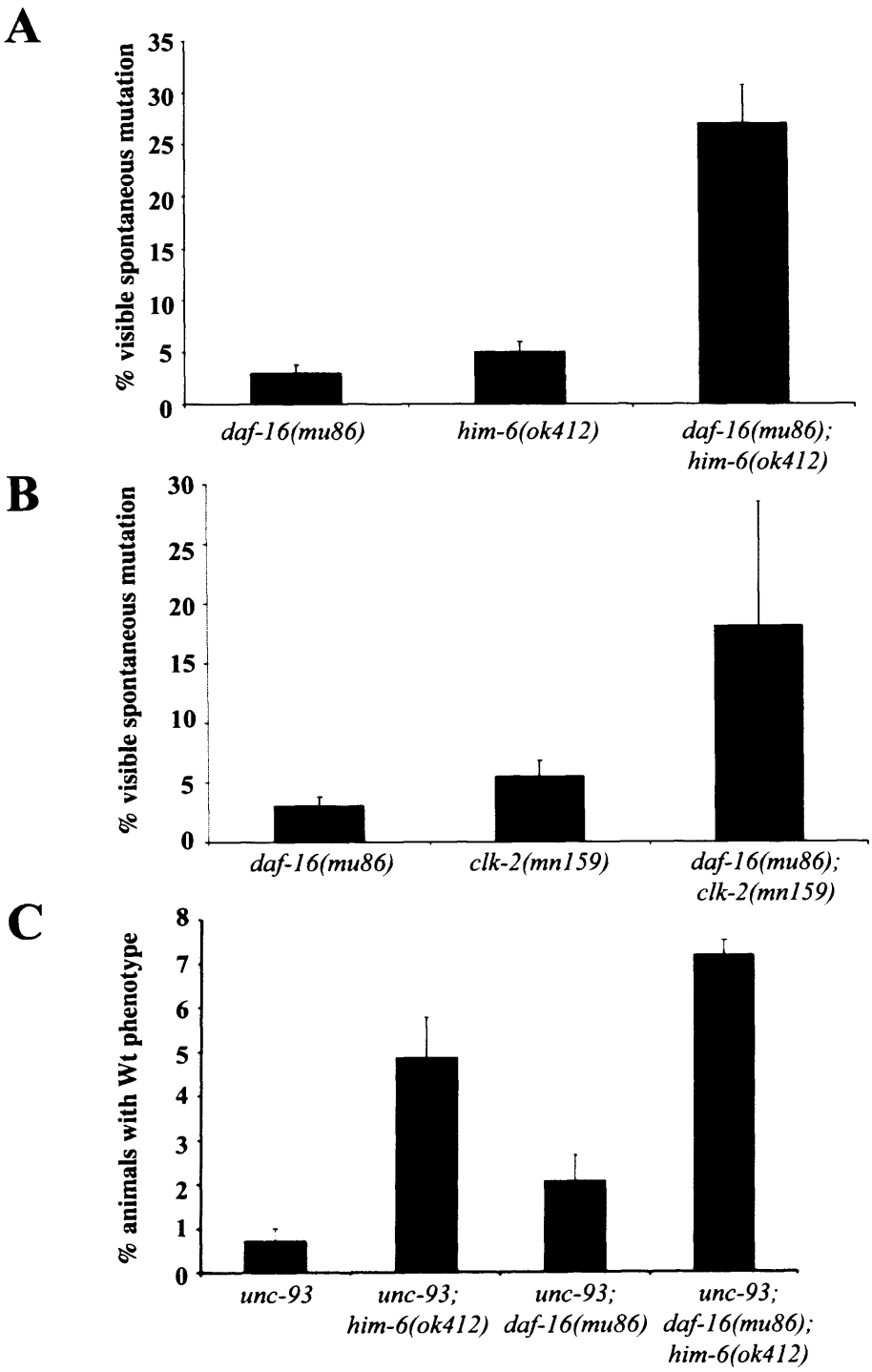

Figure 5.1. Effects of *clk-2*, *daf-16*, and *him-6* mutations on spontaneous mutation rates. (A and B) Spontaneous mutations in the indicated genotypes were quantified by scoring animals for spontaneously arising, visible mutations (alterations to animal movement and body morphology). Wild type animals exhibited no spontaneous mutations. (C) Spontaneous mutation rates in the indicated genotypes was monitored by reversion of *unc-93(e1500)* mutants to a wild type pattern of movement. Courtesy of M. Grabowski.

increase in mutations (Figure 5.1). To confirm the spontaneous mutator phenotype they performed an *unc-93(e1500)* reversion assay. The well-characterized *unc-93(e1500)* allele causes a dominant negative uncoordinated (Unc) phenotype. The susceptibility of any given genotype to DNA mutation can then be inferred by the spontaneous loss of this allele, as visualized by reversion to a wild type movement pattern (Greenwald and Horvitz 1980; Greenwald and Horvitz 1982; De Stasio *et al.* 1997). Both *him-6* and *daf-16* had increased incidence of reversion of *unc-93(e1500);* again, the double mutant had an additive phenotype, though not as strong as the spontaneous reversion result (Figure 5.1). Given the interaction between *rfs-1* and *him-6* previously shown in this work (Figure 3.19), a collaboration was initiated to examine the interplay between *rfs-1, him-6*, and *daf-16* in repair and lifespan. Interestingly, Melissa has now shown that while the *rfs-1* mutant has an approximately four percent spontaneous mutation rate, that the *daf-16; rfs-1* double mutant has no increase in mutation rate over the single mutants. The lack of an additive effect on mutation rate suggests the surprising possibility that RFS-1 and DAF-16 function in the same pathway to suppress or repair spontaneous mutations. Melissa is now measuring the spontaneous mutation rates of *rfs-1*; *him-6* double mutants and *daf-16; rfs-1*; *him-6* triple mutants to confirm this; if RFS-1 and DAF-16 function in a common pathway, one would predict that these mutants will display a similar increase in spontaneous mutation rate as the *daf-16; him-6* double mutant. Loss of *daf-16* does not affect either the brood size or embryonic lethality of *him-6* or *rfs-1* mutants (Table 7). As mentioned in Chapter 4, the *rfs-1* brood size decreases over time, possibly due to accumulation of mutations. The *daf-16; rfs-1* brood size resembles that of a freshly outcrossed *rfs-1* mutant. Strikingly, there was a very strong synthetic lethality (SL) observed between *rfs-1* and *him-6* (Table 7). It will be very interesting to determine whether this SL is accompanied by an increased spontaneous mutation rate in the surviving progeny.

Table 7. Brood size analysis of *daf-16*, *him-6*, and *rfs-1* single, double, and triple mutants.

Genotype	Viable progeny (±std. dev)	Percent Embryonic lethality
N2(Wt)	257.2±20.3	0.63 (n=471)
rfs-1(ok1372)	116.83±87.4	4.74 (n=506)
*rfs-1(ok1372)**	206.9±73.1	0.13 (n=2276)
*daf-16(mu86)***	246	0
*him-6(ok412)***	70	44.2
*daf-16(mu86); him-6(ok412)***	78	36.9
daf-16(mu86); rfs-1(ok1372)	194.0±84.4	1.44 (n=2362)
rfs-1(ok1372); him-6(ok412)	17.4±14.4	85.95 (n=1488)
daf-16(mu86); rfs-1(ok1372); him-6(ok412)	58.5±26.6	71.5 (n=2470)

Data from:
* Chapter 3
** M. Grabowski
Std. dev. (viable progeny) and "n" (number of embryos scored; percent embryonic lethality) values not available for M. Grabowski data.

5.1.2 *daf-16* mutations do not cause increased apoptosis or mitotic RAD-51 foci in *him-6* or *rfs-1* mutants

There are a number of ways that DAF-16 and RFS-1 could be functioning that can be tested experimentally. If loss of *daf-16* is driving ICL formation and the increased mutation rate in *daf-16; him-6* and *daf-16; clk-2* double mutants is due to faulty ICL repair, then an increase in spontaneous mitotic RAD-51 foci could result. If there is, indeed, an increase in mitotic RAD-51 foci, then based on the results in Chapter 3, loss of *rfs-1* should suppress these RAD-51 foci. Disappointingly, in two separate *daf-16* mutants (*mu86* and *mgDf50*) there were no discernable effects on spontaneous RAD-51 focus formation (Figure 5.2). However, it is possible that only a few ICLs would occur and these would be below the threshold of detection. Therefore, whether *daf-16* mutations affect apoptosis was examined. There is a reported role for DAF-16 in promoting apoptosis in tumourous germ lines, so it is possible that the spontaneous mutation rate was being driven by a failure to clear damaged cells (Pinkston *et al.* 2006). However, the loss of *daf-16* failed to suppress the elevated levels of apoptosis in *him-6, rfs-1,* or *rfs-1; him-6* genetic backgrounds. Thus, the spontaneous mutation rate is not due to a failure to execute the apoptotic programme (Figure 5.2B). If *rfs-1* and *daf-16* do function in the same pathway, it is possible that *daf-16* mutants would also be sensitive to replication blocking lesions. The spontaneous mutation rates in *daf-16* and *daf-16; him-6* animals might reflect defects in repair at endogenously arising RFBs. However, preliminary results suggest that *daf-16* mutants are not sensitive to HN2. Although this experiment as yet needs be repeated with the double and triple mutants, this result is consistent with a recent report that *daf-16* mutants are insensitive to UVC and the alkylating agent methane methylsulfonate, which also causes fork-blocking lesions (Kim *et al.* 2007).

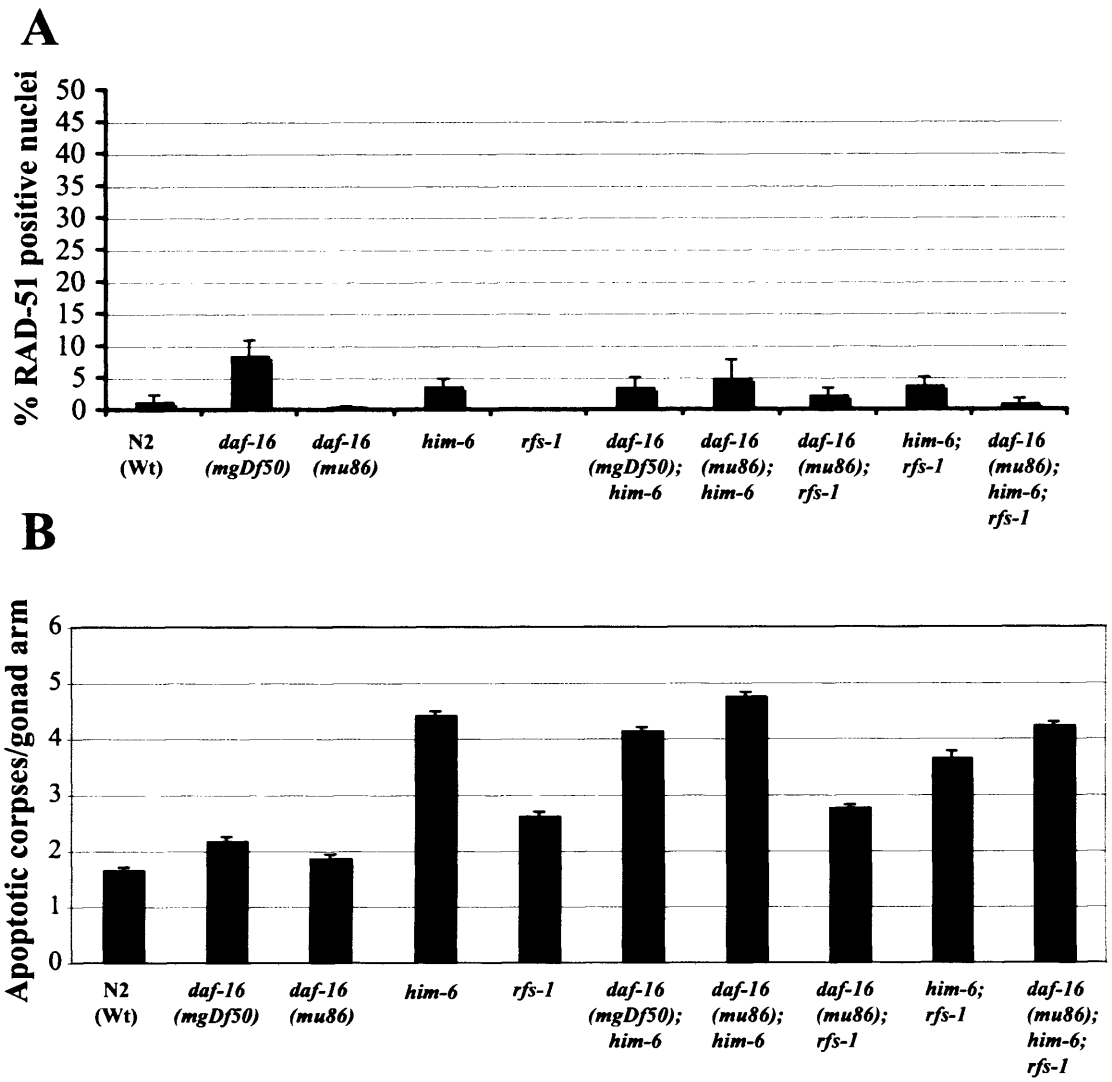

Figure 5.2. RAD-51 foci and apoptosis in *daf-16, him-6, rfs-1* single, double, and triple mutants. (A) RAD-51 positive nuclei were quantitated in mitotic nuclei from animals of the indicated genotypes. Error bars indicate S.E.M. from 20 mitotic nuclei from 7-15 worms of each genotype from two independent experiments. (B) Number of apoptotic corpses per gonad arm, scored by SYTO12 staining in animals of the indicated genotype. Error bars indicate S.E.M. from at least 33 adult animals from two independent experiments.

5.1.3 Conclusions

It is very clear that loss of DAF-16 activity impacts upon spontaneous mutation rate and that this effect is exacerbated by *him-6* and *clk-2* mutation (Figure 5.1). However, the nature of the damage driving the increased spontaneous mutation rate and where it occurs in the animal is currently unclear. Work described here has refined the role for DAF-16 to a few possibilities. The increase in spontaneous mutation rate seen in *daf-16; clk-2* double mutants relative to single mutants suggests that DAF-16 somehow impacts upon DNA replication (Ahmed *et al.* 2001; Garcia-Muse and Boulton 2005; Collis *et al.* 2007). Loss of *daf-16* does not lead to spontaneous RAD-51 foci, nor does it suppress the incidence of apoptosis. These results strongly suggest that DAF-16 does not play a role in protecting the germ line from DNA damage. Since oxidative stress could also generate single strand nicks in DNA, experiments will be performed to address this possibility. In conjunction with Dr. Julie Martin, an antibody that detects poly-ADP-ribosylation of proteins, a frequent modification that occurs in response to ssDNA nicks, is being optimized for use in immunofluorescence. This antibody would allow detection of ssDNA nicks resulting from increased oxidative damage in *daf-16* germ lines. The failure of *daf-16* mutants to exhibit any embryonic sensitivity tc UVC, HN2, or MMS, further indicated no effect on DNA repair in the germ line (Figure 5.2) (Kim *et al.* 2007).

These results were particularly surprising, given Cynthia Kenyon's recent work demonstrating that DAF-16 promotes apoptosis in tumourous *gld-1* mutant animals (Pinkston *et al.* 2006). GLD-1 is a translational repressor that controls the expression of a number of mRNAs in the germ line; mutants enter meiosis properly, but instead of progressing through meiosis, *gld-1* mutants exit from the pachytene stage and return to a mitotically proliferative state, filling the animal with mitotic cells (Francis *et al.* 1995). This work demonstrated that DAF-16 not only promotes apoptosis in

hyperproliferative *gld-1* mitotic nuclei, but it also promotes apoptosis in gamma-irradiated nematode germ lines. However, as presented here, *daf-16* mutants were not sensitive to replication blocking drugs and did not affect apoptosis in *him-6*. Its role in promoting apoptosis in hyperproliferating *gld-1* nuclei is likely in response to replication stress, so it is therefore unlikely to act in a specific response to DSBs. If its ability to suppress apoptosis is DSB specific, then DAF-16 would also promote apoptosis in response to collapsed forks in the *gld-1* mutant. It will be important to determine if loss of *daf-16* prevents apoptosis in response to replication blocking lesions caused by HN2, CPT, or UVC. Importantly, the IR-induced apoptosis and embryonic survival phenotypes of *daf-16* mutants should be re-examined to confirm the studies by Pinkston *et al.* (2006). If DAF-16 does indeed promote apoptosis in response to IR-induced lesions, then abrogation of damage-induced apoptosis in *daf-16* mutants should result in profound embryonic sensitivity to IR. Indeed, severe embryonic sensitivity has been observed in irradiated *cep-1* (p53 homolog) mutants, which are defective for DNA damage induced apoptosis (Derry *et al.* 2001).

None of the evidence presented in this chapter has convincingly implicated DAF-16 in preventing DNA damage in the germ line. A very real possibility is that elevated mutagenesis observed in *daf-16* mutants is occurring not in the germ line, but during the embryonic divisions. These possibilities could be distinguished by determining whether the spontaneous mutations are heritable; the lack of heritability would indicate that the mutations are occurring outside of the germ line. It would also be interesting to examine the nature of the various *unc-93* suppressor mutations that arose in *daf-16, him-6,* and *daf-16; him-6* animals and to determine whether the different genetic backgrounds drive different sorts of reversions. A bias towards a particular type of mutations (deletion, insertion, frameshift, transition, transversion) could give insight into the (repair) processes DAF-16 affects. Such an investigation

could be complemented with Marcel Tijsterman's mutator reporter, which contains a heat-shock promoter-driven, out of frame LacZ gene (Tijsterman *et al.* 2002). Frameshift mutations result in expression of LacZ, and, given the nematode's defined lineage, the time and location at which the mutation occurred can be inferred by the identities of the LacZ-positive cells.

Finally, a very interesting and unexpected result was the *rfs-1; him-6* synthetic lethality. It seems to be unrelated to the results of the previously described epistasis experiment involving *rfs-1* and *daf-16,* since *daf-16; him-6* double mutants resembled *him-6* animals with respect to embryonic lethality and brood size. The first issue to be addressed is whether the synthetic lethality is due to mitotic or meiotic problems. There is no evidence of fragmentation, chromosomal aberrations, or increased RAD-51 staining in the mitotic compartment of *rfs-1; him-6* animals (Figures 3.19, 5.2) and results will be presented in section 5.2 that suggest this lethality is a meiotic issue. Given the emerging overlap between IGF1 signalling and repair of replication blocking lesions, the potential functioning of DAF-16 and RFS-1 in a common pathway is of great interest and should be explored in the future.

5.2 RFS-1 and meiosis

5.2.1 Him phenotype

The majority of the work detailed thus far has centred on the roles of RFS-1 and RIP-1 in repair of replication blocking lesions in mitosis. However, equally intriguing is their increase in male progeny, indicative of increased chromosome non-disjunction, but without any accompanying embryonic lethality. This phenotype is in stark contrast to meiotic factors such as *spo-11* (99.4% Emb, 50% males in viable progeny), *syp-1* (95% Emb, 38% males in viable progeny), and *him-6* (54% Emb, 12% males in viable

progeny) (Dernburg *et al.* 1998; MacQueen *et al.* 2002; Wicky *et al.* 2004). The fact that *brc-1, brd-1,* and *him-9/xpf-1* animals also have very low levels of embryonic lethality, are dispensable for crossover (CO) formation, and have a similar Him phenotype to *rfs-1* and *rip-1* mutants was very striking; these phenotypes suggest that these factors play a non-essential role in meiotic HRR, in addition to their roles in mitotic DNA repair (Hodgkin *et al.* 1979; Boulton *et al.* 2004).

5.2.2 Meiotic DSB repair through intersister HRR

The specific non-essential role that RFS-1 plays in meiosis is currently unclear. Given the similar increases in apoptosis and embryonic sensitivity following treatment with cross-linking agents in *brc-1* and *rfs-1* mutants, it was therefore interesting to examine whether RFS-1 played a similar meiotic role to that recently demonstrated for BRC-1. Capitalizing on the independence of synaptonemal complex generation and meiotic DSB induction in *C. elegans*, Adamo *et al.* (2008) have shown that BRC-1 functions specifically in an intersister pathway of meiotic DSB repair (Dernburg *et al.* 1998). Once a SPO-11 break is generated during meiosis, the MSH-4/HIM-14-MSH-5 heterodimer promotes interhomolog crossovers and a barrier to intersister HRR ensures a chiasma is generated between homologous chromosomes (Dernburg *et al.* 1998; Zalevsky *et al.* 1999; Kelly *et al.* 2000). The barrier is then lifted during pachytene to ensure that remaining DSBs are repaired before completion of meiotic prophase (Bishop and Zickler 2004). *brc-1* mutants have an increase in meiotic RAD-51 foci in late pachytene, at a time when most meiotic DSBs have been resolved (Adamo *et al.* 2008). *brc-1; syp-2* double mutants lack the synaptonemal complex and this consequently prevents homolog alignment; these double mutants display an increase in DAPI stained bodies and in fragmented, unstructured chromatin, reminiscent of *rad-51* and *Cebrc-2* mutant diakineses (Alpi *et al.* 2003; Martin *et al.* 2005; Adamo *et al.* 2008). This result

is suggestive of a role for BRC-1 in repair through the sister chromatid, as fragmentation indicates failure to repair meiotic DSBs when the homolog is not available as a repair template. Critically, double mutants for *brc-1* and *msh-5,* in which the homologs are in close proximity but the crossover cannot be formed, also exhibited an increase in DAPI stained bodies at diakinesis, indicating chromosome fragmentation as a result of failure to repair DSBs through the sister chromatid. Interestingly, the previously observed elevation in apoptotic corpses in *brc-1* mutants was suppressed by a *spo-11* mutation, indicating that the phenotype was due to aberrant repair of meiotic, as opposed to mitotic, DSBs (Boulton *et al.* 2004; Adamo *et al.* 2008). To determine whether RFS-1 also played a role in repair through the sister chromatid, *rfs-1; msh-5* and *rfs-1; syp-2* double mutants were generated to test whether fragmentation at diakinesis, similar to that seen in the analogous *brc-1* double mutants, occurs. *rfs-1; msh-5* double mutants were very similar to *msh-5* single mutants and while *rfs-1; syp-2* did exhibit a slight increase in unstructured chromatin bodies relative to *syp-2* mutants, the increase was 18% lower than the *brc-1;syp-2* double mutant (7% vs 25%, respectively) (Figure 5.3) (Adamo *et al.* 2008). These results indicate that RFS-1 is not playing a role in the intersister pathway of meiotic recombination.

5.2.3 *rfs-1* suppression of *mus-81; him-9/xpf-1* meiotic catastrophe

One of the issues that arose from the work on HRR substrate generation at an ICL was the underlying cause of the synthetic lethality of *mus-81; him-9/xpf-1* double mutants. Either these mutants have problems in dealing with endogenously arising mitotic lesions or difficulties with the resolution of meiotic DSBs. An initial hypothesis was that MUS-81 and XPF-1 might be redundantly generating HRR substrates at ICLs, however, *him-9/xpf-1* was epistatic to *mus-81* with respect to RAD-51 loading following CDDP treatment (Figure 3.15). After examination of RAD-51 staining

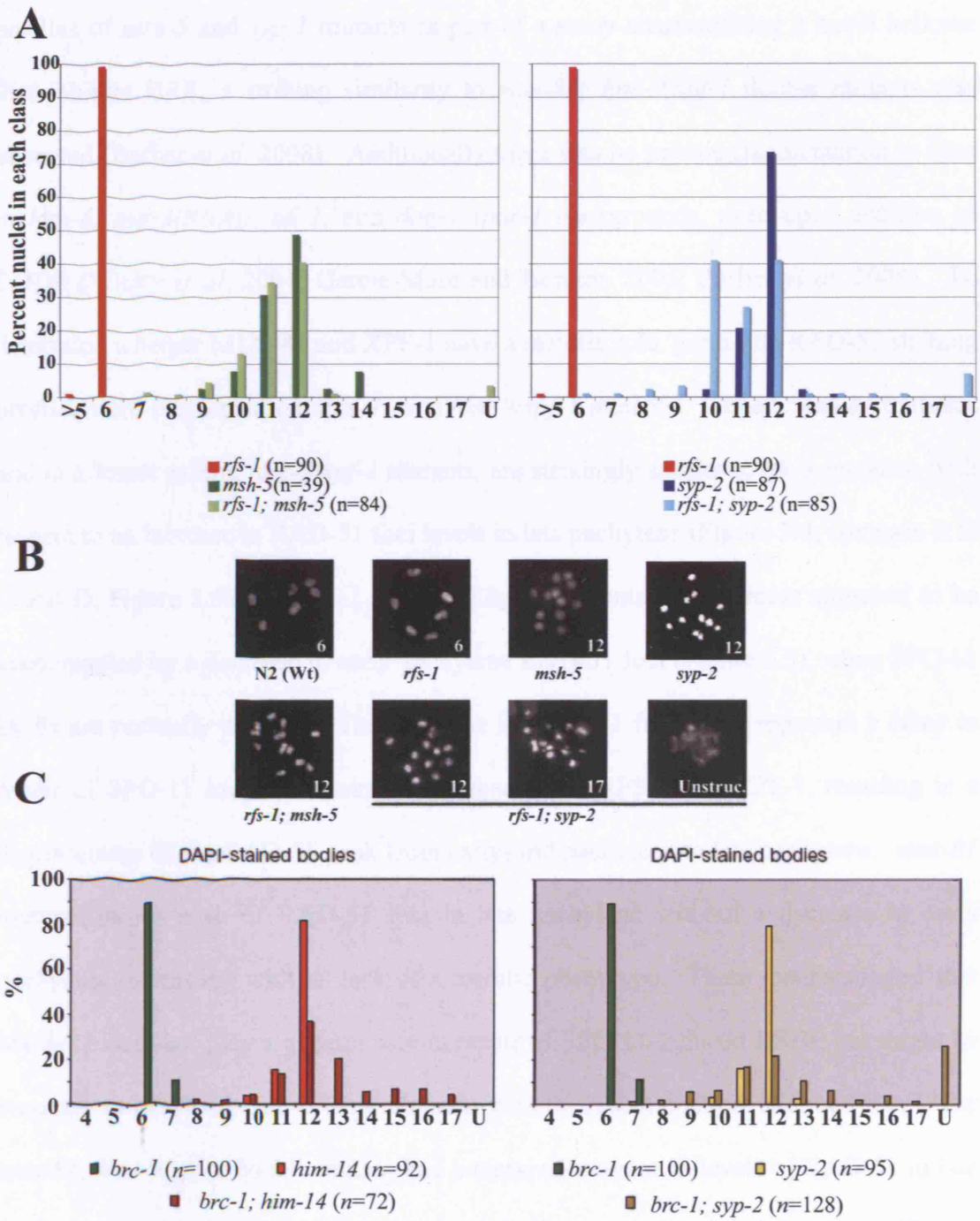

Figure 5.3. RFS-1 does not appear to play a role in the inter-sister pathway of meiotic DSB repair. (A) Diakinesis chromosomes were quantified as previously described (Adamo *et al.*, 2008). Histograms representing quantitation of DAPI-stained bodies in animals of the indicated genotype. The number of diakineses examined is in parentheses following the genotype. The *x*-axis indicates the number of DAPI-stained bodies in each class. The number of fragmented, unstructured diakineses is also indicated (U). The *y*-axis denotes the percentage of nuclei in each class. B) Representative images of diakinesis nuclei from animals of the indicated genotypes. The number of DAPI-stained bodies visible is noted in the bottom right corner of each image. (C) Quantitation of diakineses chromosomes in *brc-1; syp-2* and *brc-1; msh-5* animals from Adamo *et al.* (2008) Histograms were generated as described in (A). Figure 5.3C is courtesy of A. La Volpe.

profiles of *msh-5* and *syp-1* mutants as part of a study characterizing a novel helicase that inhibits HRR, a striking similarity to *mus-81; him-9/xpf-1* double mutants was observed (Barber *et al.* 2008). Additionally there was no mitotic fragmentation as seen in *him-6; top-3(RNAi)*, *atl-1*, and *dog-1 spar-1* backgrounds, even upon addition of CDDP (Wicky *et al.* 2004; Garcia-Muse and Boulton 2005; Barber *et al.* 2008). To determine whether MUS-81 and XPF-1 have a meiotic role, germ line RAD-51 staining profiles were performed on *mus-81* and *him-9/xpf-1* mutants. Indeed, *mus-81* mutants, and to a lesser extent, *him-9/xpf-1* mutants, are strikingly similar to *rfs-1* mutants, with respect to an increase in RAD-51 foci levels in late pachytene (Figure 5.4; compare B to C and D, Figure 5.5B). In *rfs-1* and *him-9/xpf-1* mutants, this increase appeared to be accompanied by a decrease in early pachytene RAD-51 foci (Figure 5.5), when SPO-11 DSBs are normally repaired. This decrease in RAD-51 foci could represent a delay in repair of SPO-11 induced breaks in the absence of RFS-1 and XPF-1, resulting in a displacement of the RAD-51 peak from early-mid pachytene to late pachytene. *mus-81* mutants had a peak of RAD-51 foci in late pachytene without a decrease in early pachytene, consistent with its lack of a meiotic phenotype. These results suggest that MUS-81 does not play a general role in repair of SPO-11-induced DSBs, but might be required to deal with late arising aberrant meiotic recombination intermediates. The *mus-81; him-9/xpf-1* double mutant had a massive increase in levels of RAD-51 in late pachytene, which when quantitated, is very similar to *syp-1* and *msh-5* mutants (Figure 5.4; compare E to G and H, Figure 5.5B) (Colaiacovo *et al.* 2003). Interestingly, the spontaneous mitotic RAD-51 focus formation observed in the *mus-81* mutant was not exacerbated in the *mus-81; him-9/xpf-1* double mutant, with approximately 30% RAD-51 positive mitotic nuclei in both strains (Figure 5.4; compare C and E, Figure 5.5B). When *rfs-1* was introduced into a *mus-81; him-9/xpf-1* double mutant to examine the consequences on CDDP-induced mitotic RAD-51 focus formation, a striking

Figure 5.4. *rfs-1* mutations suppress RAD-51 accumulation in *mus-81; him-9/xpf-1* animals. Representative images of RAD-51 staining (red) in fixed germ line nuclei in animals of the indicated genotypes. DNA was counterstained with DAPI (blue). The mitotic tip of the germ line is oriented to the left of each panel. For each genotype, RAD-51 staining is shown in the top of the panel, while a DAPI overlay is provided in the bottom of the panel. Images are composites of two separate, overlapping images. Scale bars, 40 μm.

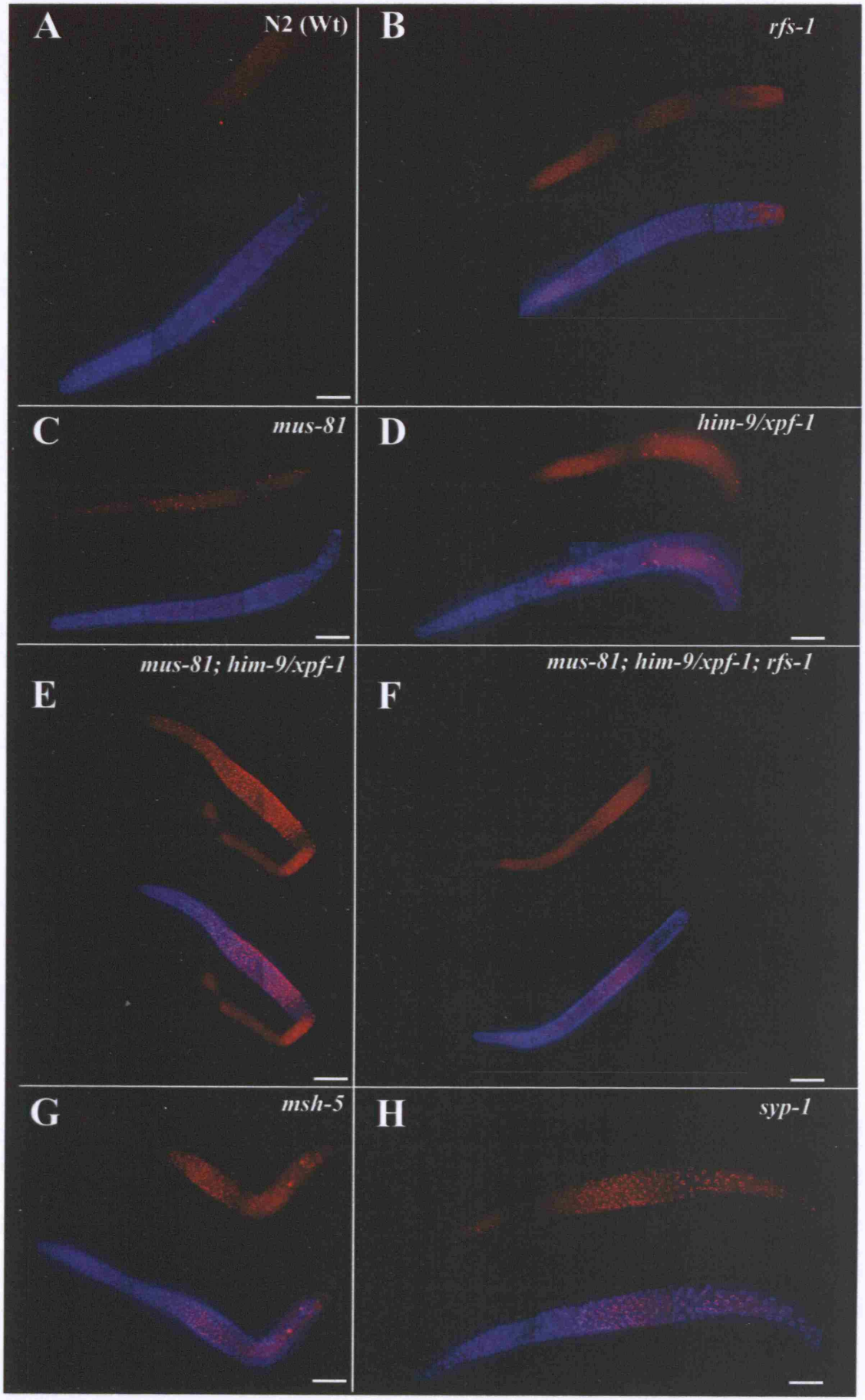

Figure 5.4. *rfs-1* mutations suppress RAD-51 accumulation in *mus-81; him-9/xpf-1* animals. For figure legend, see preceding page.

Figure 5.5. Elevation of late pachytene RAD-51 levels in *mus-81, rfs-1, him-9/xpf-1,* and *mus-81; him-9/xpf-1* animals. (A) Schematic of the regions of the germ line that correspond to each zone used in quantitation. (B) Histogram legend for the foci quantification. Foci were quantified in animals of the indicated genotype as previously described by Colaiacovo *et al.* (2003). The legend indicates which class (number of RAD-51 foci/nucleus) each colored column represents, the *x*-axis indicates the position within the germ line (zone) and the *y*-axis indicates the percentage of nuclei that fall in each class per zone. A minimum of seven animals was scored for each histogram. Representative images of germ lines from animals of each genotype are shown in Figure 5.4.

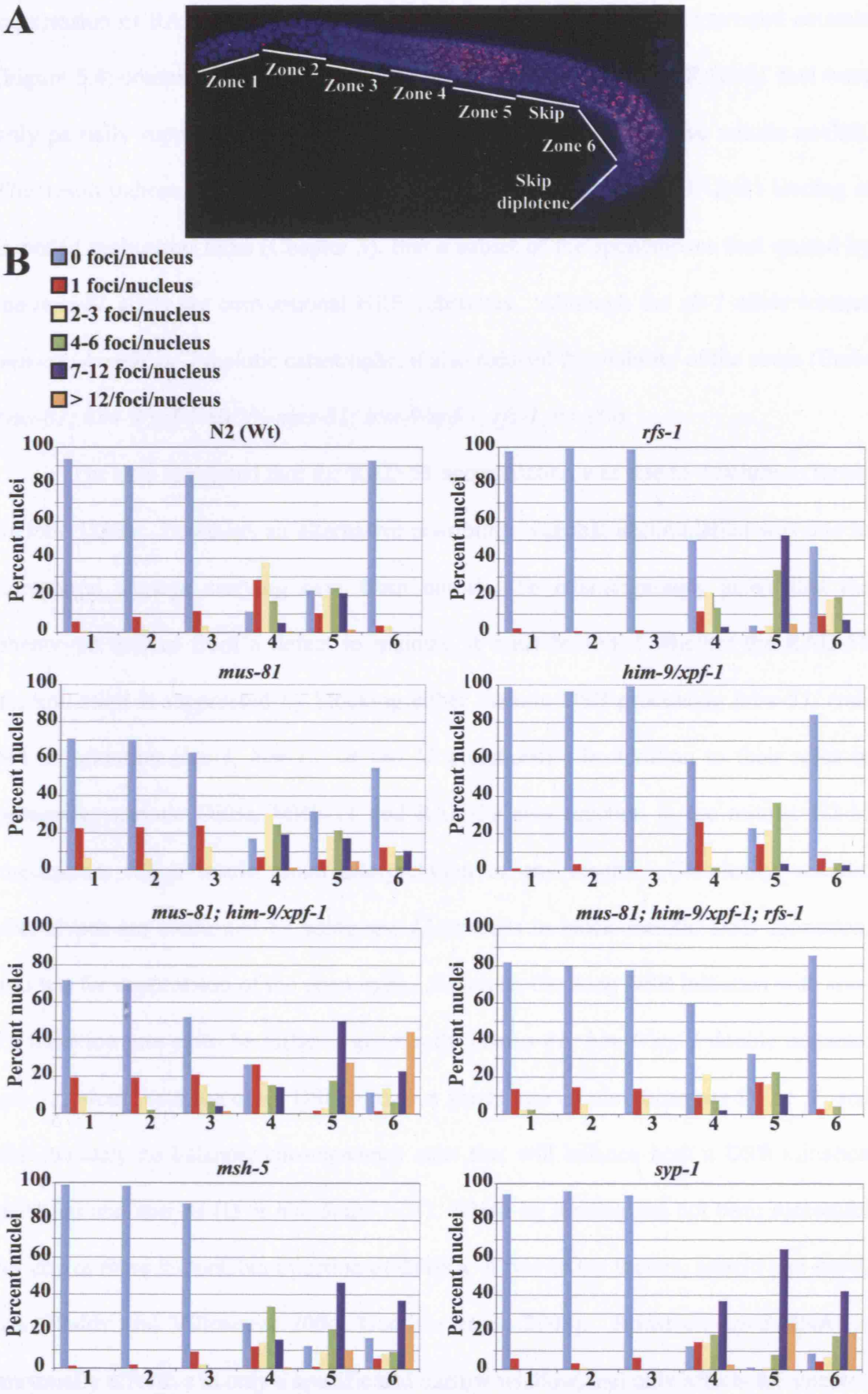

Figure 5.5. Elevation of late pachytene RAD-51 levels in *mus-81*, *him-9/xpf-1*, *rfs-1*, and *mus-81; him-9/xpf-1* animals. For figure legend, see preceding page.

suppression of RAD-51 accumulation in pachytene was observed in untreated animals (Figure 5.4; compare E and F, Figure 5.5). Importantly, the mitotic RAD-51 foci were only partially suppressed (approximately 10% fewer RAD-51 positive mitotic nuclei). This result indicates, given the specific role of RFS-1 in promoting RAD-51 loading at impeded replication forks (Chapter 3), that a subset of the spontaneous foci caused by the *mus-81* allele are conventional HRR substrates. Although the *rfs-1* allele rescues *mus-81; him-9/xpf-1* meiotic catastrophe, it also reduced the viability of the strain (Emb: *mus-81; him-9/xpf-1*-80.5% *mus-81; him-9/xpf-1; rfs-1*, 94.1%).

The data suggested that the RAD-51 accumulation was due to a failure to repair meiotic DSBs. However, an alternative possibility was that accumulation was due to unrepaired damage carrying over from mitosis. To unambiguously prove that the phenotype derives from a defect in meiosis, it must be tested whether the RAD-51 accumulation is suppressed by blocking either meiotic DSB processing (*mre-11, rad-50*) or initiation (*htp-3, him-17,* or *spo-11* mutations). In addition to their roles in processing meiotic DSBs, MRE-11 and RAD-50 also function in the mitotic G2-M checkpoint, which would cloud interpretation of any results. Classically, meiotic phenotypes are confirmed by using *spo-11* mutants to block meiotic DSB formation, and test for suppression of the phenotype. However, blocking DSB initiation with *spo-11* mutation proved to be difficult genetically in *mus-81; him-9/xpf-1* double mutants; *spo-11*, along with the other DSB initiation genes, are on chromosomes IV or V, and unfortunately no balancer chromosomes exist that will balance both a DSB initiation mutation and *mus-81* (I) or *him-9/xpf-1* (II). RNAi by feeding has not been successful for any of these factors, but injection of dsRNA of two of the factors, *him-17* and *htp-3,* has (Reddy and Villeneuve 2004; Goodyer *et al.* 2008). However, *htp-3* RNAi is maximally effective in only a specific and narrow window, and only affects the injected animal and not the F1 progeny (Zetka 2007). *him-17* injection was another possibility,

but the strong phenotype observed by Reddy *et al.* (2004) has not been reproducible. In an attempt to suppress the RAD-51 accumulation phenotype of *mus-81; him-9/xpf-1* animals, a *mus-81; him-9/mIn[gfp]; spo-11/+* strain was generated. All non-GFP progeny (*him-9* homozygotes) from this strain were dissected and RAD-51 immunostaining was performed. *spo-11* homozygotes were confirmed by the presence of 12 univalents at diakinesis. In animals with 12 univalents, the pachytene accumulation of RAD-51 was suppressed, providing very strong evidence that the recombination intermediates in *mus-81; him-9/xpf-1* animals are meiotic in origin (Figure 5.6A). However, there is a caveat to this conclusion; some animals with fewer than 12 univalents also displayed suppression of meiotic RAD-51 accumulation. These animals might correspond to partial rescue that would occur in *spo-11/+* heterozygotes, but there is no way to distinguish these animals from +/+ and therefore this belief cannot be confirmed. If the RAD-51 accumulation phenotype is, indeed, meiotic an alternative explanation is that the RAD-51 foci derive from a defect in homolog pairing. Mutations that abolish synaptonemal complex formation, such as *syp-1, syp-2*, and *him-3,* lead to increased RAD-51 staining in pachytene due a failure to repair SPO-11 induced DSBs while the barrier to HRR using the sister chromatid is in place (Colaiacovo *et al.* 2003). As expected, RAD-51 accumulation seen in *mus-81; him-9/xpf-1* double mutants does not appear to be due to defective chromosome pairing, since the synaptonemal complex is intact, evidenced by staining against the SC elements SYP-1 and HIM-3 (Figure 5.6B). Additionally, X chromosome pairing, monitored by marking the X pairing centre using HIM-8 staining, is also wild type (Figure 5.6B,C). It will be important to confirm this observation on at least one of the autosomes by examining the chromosomes themselves through fluorescence *in situ* hybridization. To confirm that the RAD-51 foci are formed in response to a meiotic repair defect, *htp-3* dsRNA injection will be performed to block meiotic DSB initiation.

Figure 5.6. RAD-51 accumulation in *mus-81;xpf-1* animals appears to arise from meiotic DSBs, but not through a defect in chromosome pairing. Representative images of RAD-51 staining (red) in fixed germ line nuclei in animals of the indicated genotypes. DNA was counterstained with DAPI (blue). Starting with a *mus-81; him-9/mIn[gfp]; spo-11/+* strain, all non-GFP progeny (*him-9/him-9*) were individually plated. All parental animals were dissected and stained with αRAD-51. Wells with approximately 100% embryonic lethality and 12 univalents at diakinesis were scored as *spo-11* homozygotes (right panel). Animals with six bivalents are either *spo-11/+* or +/+ (left panel). A representative image of diakinesis is shown in the inset white box. Numbers indicate the percentage of animals with >90% RAD-51 positive nuclei in late pachytene and the total number of animals scored. Images are composites of two separate, overlapping images. Scale bars, 40 μm. (B) Representative images of fixed nuclei of the indicated genotypes immunostained for the synaptonemal complex proteins SYP-1 (green) and HIM-3 (red), and for HIM-8 (green), which binds the X chromosome pairing centre. DNA was counterstained with DAPI (blue). (C) Quantification of X chromosome pairing throughout the germ line. The germ line was divided into six zones and X chromosome pairing was monitored by HIM-8 staining as described by Penkner *et al.* (2007). Single foci or overlapping foci for each nucleus were scored as paired. Three gonads were scored for each strain.

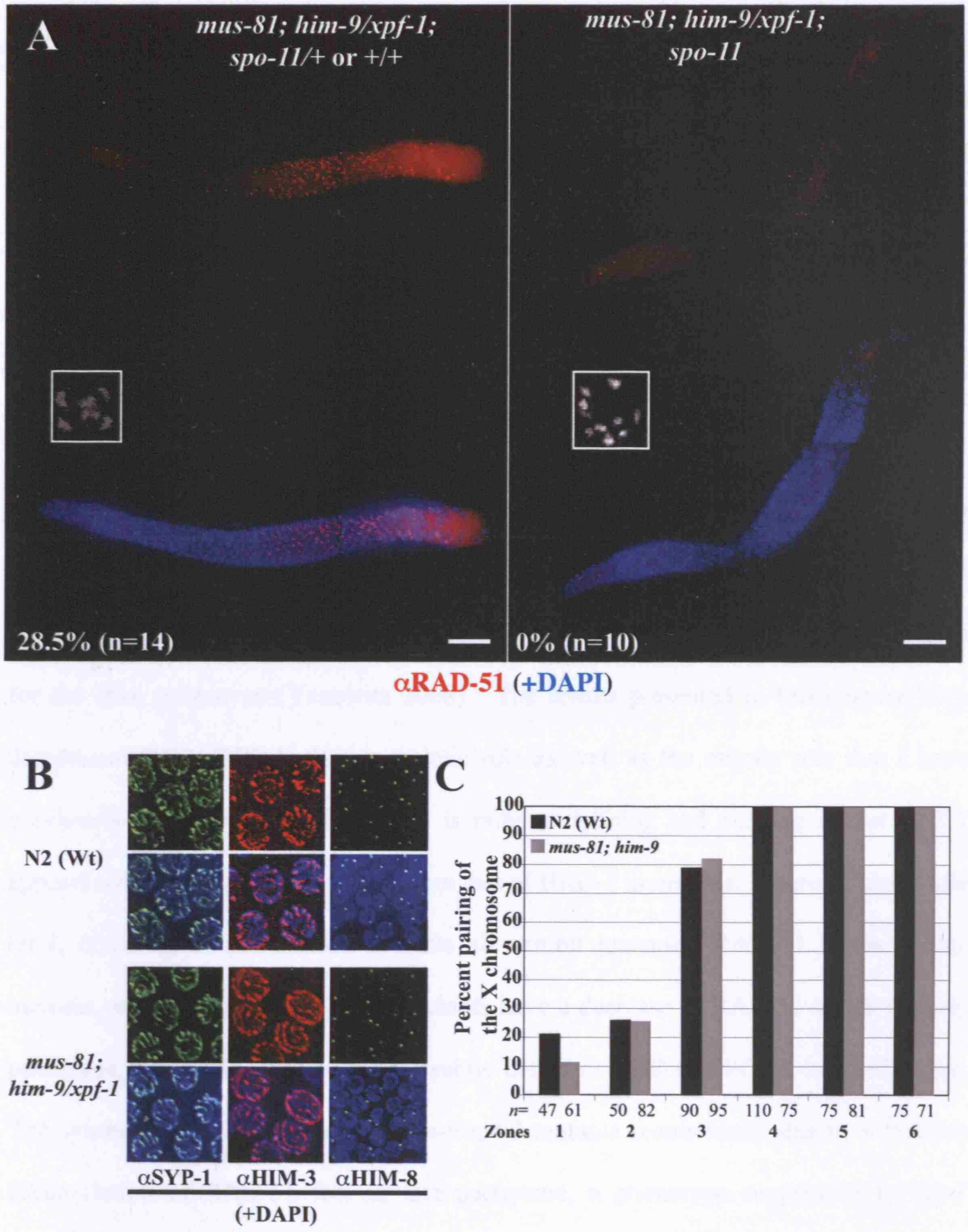

Figure 5.6. RAD-51 accumulation in *mus-81;him-9/xpf-1* animals appears to arise from meiotic DSBs, but not through a defect in chromosome pairing. For figure legend, see preceding page.

Although timing required for maximal RNAi effect is specific, it is not insurmountable. Suppression of RAD-51 accumulation and generation of 12 univalents in response to *htp-3* knockdown would conclusively demonstrate that the *mus-81; him-9/xpf-1* synthetic lethality is a meiotic phenotype.

5.2.4 Conclusions

The first allele of *rfs-1 (him-15)* was identified in a screen for chromosome non-disjunction mutants over 25 years ago (Hodgkin *et al.* 1979). Since the allele was a deficiency that deleted several genes, the molecular identity of *him-15* remained unknown until 2007 when it was found that the deletion in *rfs-1* was solely responsible for the Him phenotype (Yanowitz 2008). The results presented in this chapter have demonstrated that RFS-1 plays a meiotic role as well as the mitotic role that I have previously shown (Chapter 3). What is rather surprising and exciting is that RFS-1 appears to be playing a distinct role from that of BRC-1 in meiosis. Interestingly, while *rfs-1*, *him-9/xpf-1*, and *mus-81* mutants all exhibit increased RAD-51 levels in late meiosis, only *rfs-1* and *him-9/xpf-1* mutants have a decrease in RAD-51 levels in early pachytene, potentially indicative of a subtle defect in HRR of SPO-11-induced DSBs. The synthetic lethality of *mus-81; him-9/xpf-1* mutants seems likely due to a massive accumulation of RAD-51 foci in late pachytene, a phenotype suppressed by *rfs-1* mutations. The observation that *rfs-1* mutations only suppress the meiotic RAD-51 accumulation, but not the mitotic RAD-51 accumulation seen in *mus-81; him-9/xpf-1* double mutants supports two assertions: i; loss of MUS-81 leads to an increase in conventional HRR substrates in untreated animals, and ii; the pachytene RAD-51 accumulation is likely due to a defect in meiotic repair of DSBs, an idea supported by suppression of the accumulation by *spo-11* mutations.

A distinct role for RFS-1 in meiotic DSB repair from that of BRC-1 is unexpected and intriguing. This conclusion stemmed from the observation that *rfs-1; syp-2* and *rfs-1; msh-5* double mutants lack the degree of chromosome fragmentation observed in the corresponding *brc-1* double mutants (Figure 5.3). It will be important in the future to repeat the diakinesis quantification alongside a positive *brc-1; syp-2* or *brc-1; msh-5* control to definitively rule out RFS-1 as a sister chromatid repair factor. At this juncture, it is unclear what role RFS-1 plays in meiosis. It will be important to determine the effect of *rfs-1* mutations on CO frequencies at several loci to verify a detectable role in the crossover recombination pathway. Given the synthetic lethality observed with *him-6* mutants, it is possible that RFS-1 is redundantly promoting crossovers (Table 7). The fact that loss of either HIM-6 or RFS-1 can cause X chromosome non-disjunction supports this idea. Although its exact meiotic role is currently unclear, it appears that RFS-1 is not involved in sister chromatid repair.

The suppression of RAD-51 accumulation seen in *mus-81; him-9/xpf-1; rfs-1* mutants and delayed RAD-51 focus formation in *rfs-1* mutants suggests one of two possibilities: i; that RFS-1 is channelling a meiotic HRR substrate into a pathway on which MUS-81 and XPF-1 can then act, or ii; in the absence of MUS-81 and XPF-1 aberrant recombination intermediates collapse and RFS-1 is required to re-load RAD-51. The second scenario seems more probable, because CeBRC-2 plays such an essential role in promoting RAD-51 loading onto SPO-11 induced DSBs. RFS-1 is clearly not playing a similar role to CeBRC-2, for it has none of the phenotypes of Ce*brc-2* mutants (100% Emb, chromosome fragmentation at diakinesis), indicative of a critical function in meiotic RAD-51 loading. If RFS-1 is, indeed, promoting RAD-51 loading at SPO-11-induced DSBs, then this loading must only occur on a small subset of breaks. The level of RAD-51 accumulation and lethality in the absence of MUS-81 and XPF-1 suggests that these two proteins are acting on a major recombination

intermediate, rather than a minor RFS-1-dependent pathway of DSB repair. If RFS-1 is promoting RAD-51 reloading at sites of failed meiotic recombination, it will be important to determine whether this RFS-1-dependent HRR substrate resembles that which is generated at blocked replication forks; different substrates would argue distinct mitotic and meiotic role for RFS-1, while the converse would indicate a common function. A more comprehensive analysis of diakineses in *mus-81; him-9/xpf-1* and *mus-81; him-9/xpf-1; rfs-1* animals should also be performed to look for fragmentation or univalents. In superficial examination of diakineses, univalents have not been observed in either strain, suggesting that the crossover is not affected. However, an alternate possibility is an increase in fragmentation, similar to *Cebrc-2* and *rad-51* mutant diakineses, which would indicate a more global HRR defect (Alpi *et al.* 2003; Martin *et al.* 2005).

As Mus81 has been shown to resolve Holliday junctions in yeast, and both Mus81 and XPF are structure specific endonucleases, a possible explanation for the synthetic lethality is a redundant role in resolving meiotic HRR intermediates (Boddy *et al.* 2001; Gaskell *et al.* 2007). The Him phenotype of *him-9/xpf-1* mutants suggests a meiotic function; although HJ resolution could be the meiotic function of XPF-1, the expanded role of XPF in mammalian HRR means, alternatively, it could be involved in promoting DSB repair through gene conversion or SDSA (Al-Minawi *et al.* 2008). Either defective HJ resolution or impairment of the initial phases of DSB repair could explain the delay of RAD-51 focus accumulation in *him-9/xpf-1* mutants.

In contrast to *him-9/xpf-1* mutants, *mus-81* mutants do not have a Him phenotype. A collaborator on the MUS-81/XPF-1 work, Dr. Nigel O'Neil, has demonstrated that the increase in incidence of males and the lethality seen in hypomorphic mutants of the SC component *him-3* is suppressed by loss of *mus-81*. This suppression is accompanied by an increase in apoptosis, indicating increased

damage and revealing a role for MUS-81 in correcting faulty meiotic recombination. Thus, the increased RAD-51 levels in *mus-81* mutant pachytene chromosomes could be due to a failure to correct aberrant meiotic recombination intermediates. Perhaps XPF-1 is the *C. elegans* meiotic resolvase, with MUS-81 providing a backup function, as has been suggested in yeast (Gaskell *et al.* 2007). Alternatively, XPF-1 could be the CO pathway resolvase and MUS-81 could resolve NCO HJs, with partial redundancy between the two. Analysis of the effects of *mus-81* and *him-9/xpf-1* mutations on CO frequencies to place them in a meiotic HRR pathway will be important to distinguish between these possibilities.

Further insight into the role of RFS-1 in meiosis might also come from collaboration with Dr. Diego Muzzini, through analysis of a synthetic lethal interaction between *rfs-1* and *hel-308,* which encodes a DNA helicase homologous to *Drosophila mus308*. Initial interest in *hel-308* arose from the observation that *Drosophila mus308* mutants are profoundly sensitive to DNA cross-linking agents (Boyd *et al.* 1990). Thus, this work was part of a larger effort to characterize ICL repair in *C. elegans*. It was initially postulated that the nearly 100% embryonic lethality observed in *hel-308 rfs-1* double mutants would be due to mitotic issues but, similar to the *mus-81; him-9/xpf-1* double mutants, they displayed no discernible evidence of fragmentation or aberrations in mitosis. Instead, Diego observed persistent pachytene RAD-51 accumulation and chromosomal aberrations at diakinesis, which are reminiscent of *syp-2* and *rad-51* mutants, respectively (Alpi *et al.* 2003; Martin *et al.* 2005; Muzzini *et al.* 2008). *rfs-1; msh-5/nT1[gfp]* and *rfs-1; spo-11/nT1[gfp]* mutants have been created for Diego as a stepping stone for the generation of *hel-308 rfs-1; msh-5* and *hel-308 rfs-1; spo-11* triple mutants. Again, as was done with *mus-81; him-9/xpf-1*, *hel-308 rfs-1* double mutants must be tested for suppression by *spo-11* mutations to prove that synthetic lethality is due to a *bona fide* problem in meiosis. As this strain is technically difficult

to create and Diego has struggled to generate the triple mutant, *htp-3* dsRNA injection will be performed in *hel-308 rfs-1* double mutants as a parallel approach. If the phenotype is indeed meiotic, then *htp-3* RNAi should suppress the RAD-51 focus accumulation and chromosome fragmentation at diakinesis. Very interestingly, Diego has preliminary data demonstrating that the *hel-308 rfs-1* double mutant partially suppresses the *msh-5* diakinesis phenotype; fewer than 12 DAPI stained bodies are observed (Muzzini *et al.* 2008). This phenotype is very similar to that observed following *rad-51* depletion in *msh-5* mutants (Rinaldo *et al.* 2002). A major question emerging from this study surrounds the nature of the synthetic lethality: are RFS-1 and HEL-308 playing redundant roles in the same pathway or are they players in two overlapping pathways? Particularly intriguing is that loss of RFS-1 suppresses RAD-51 accumulation in *mus-81; him-9/xpf-1* animals, but conversely causes increased RAD-51 in *hel-308* animals, potentially suggesting two distinct functions for RFS-1 in meiotic recombination.

HEL-308 is similar to *S. cerevisiae* Mer3, a 3-5' helicase involved in crossover control (Nakagawa and Ogawa 1999; Nakagawa *et al.* 2001). *In vitro*, Mer3 has been shown to promote strand exchange, heteroduplex extension, second-end capture and Holliday junction resolution (Nakagawa and Kolodner 2002; Borner *et al.* 2004; Mazina *et al.* 2004). The chromosomal fragmentation in *hel-308 rfs-1* double mutants indicates that either an early stage of meiotic recombination, such as strand invasion, or an event affecting both CO and NCO pathways is defective; if both RFS-1 and HEL-308 were restricted to the CO pathway then double mutants would have 12 univalents, not fragmentation. Perhaps RFS-1 plays an accessory role in stabilizing invading RAD-51 nucleoprotein filaments (RAD-51 coated ssDNA tails) in the early stages of HRR, similar to yeast Rad55-Rad57. Therefore, RFS-1 would only be required for this function in the absence of HEL-308. An accessory role in stabilizing RAD-51 filaments

could explain the opposite effects of *rfs-1* mutations on RAD-51 foci in *mus-81; him-9/xpf-1* and *hel-308* mutant backgrounds. Alternatively, the increased lethality could be due to a failure to resolve Holliday junctions in the absence of HEL-308 and a paralog-associated resolvase. However, this author favours the first explanation, since the *mus-81; him-9/xpf-1* synthetic lethality and RAD-51 accumulation data supports MUS-81 and XPF-1 involvement in HJ-processing.

Cumulatively, the data presented in this section implicate RFS-1 in meiotic DSB repair, but its exact role remains elusive. It does not appear to play a role in repair through the sister chromatid, as has been shown for BRC-1. This assertion could be further tested by assessing the ability of *brc-1* mutants to rescue *mus-81; him-9/xpf-1* double mutant RAD-51 focus accumulation as well as testing for *brc-1* and *hel-308* synthetically lethality. While the *rfs-1* Him phenotype suggests that RFS-1 plays a role at some level in the CO pathway of recombination, what remains unclear is whether RFS-1 is also involved in the NCO pathway. The most significant question still to be resolved is: are RFS-1 mitotic and meiotic roles distinct or do they reflect a common process? The role for RFS-1 in promoting HRR at impeded forks at ssDNA in mitosis would argue for distinct roles. Although initiation of meiotic HRR has been suggested to occur in the absence of DSBs (i.e. at ssDNA gaps), it is a very infrequent event in *C. elegans*, as can be inferred from the lethality of *spo-11* mutants (Dernburg *et al.* 1998; Farah *et al.* 2005). Repair of non-DSB substrates would not account for the massive increase of RAD-51 foci in *mus-81; him-9/xpf-1* and *hel-308 rfs-1* animals. The meiotic data could also reflect additional roles for RFS-1 in mitosis, downstream of RAD-51 loading at the blocked fork. Alternatively, RFS-1 could be promoting RAD-51 loading at sites of failed recombination, which in turn could resemble the mitotic substrate to which RFS-1 responds. Although these results are preliminary, they are certainly interesting and warrant future study. Further exploration of the contributions of MUS-

81, XPF-1, HEL-308, and RFS-1 could provide important insight into the roles of these factors in higher metazoan meiotic recombination.

6 Chapter 6: Conclusions and Future Work

The main purpose of this work was to use a combination of genetics, cytology, and biochemistry in *C. elegans* to gain insight into the role of the Rad51 paralog proteins in homologous recombination. Work presented demonstrates that RFS-1 plays a specific role in promoting HRR at replication-blocking lesions but is dispensable for RAD-51 loading at conventional DSBs. Further, the dependence on RFS-1 for polyG/C tract stability in *dog-1* mutants confirms the notion that these tracts can form replication blocking lesions *in vivo*. The data for RFS-1 agrees well with genetic data from mammalian and DT40 cell lines showing that Rad51 paralog mutants are acutely sensitive to DNA cross-linking agents and only mildly sensitive to IR. Interestingly, RFS-1 was dispensable for RAD-51 loading following replication fork collapse in the absence of the S-phase checkpoint or through dNTP depletion by hydroxyurea treatment. These results imply that collapsed replication forks resemble conventional DSB substrates, such as those generated by IR. Two major questions from this work that need to be addressed involve the nature of the substrate onto which RFS-1 is promoting RAD-51 loading and whether RFS-1 does this loading directly. The RAD-51 foci defect in *rfs-1* mutants following UVC and CPT argues that ssDNA is a likely substrate for RFS-1, as are one-ended DSBs. The purification of RFS-1 protein for a number of assays will be important to provide a definitive answer to these questions. For example, binding of RFS-1 to these substrates can be tested and the ability of RFS-1 to load RAD-51 onto these substrates and catalyze strand exchange can also be examined. A requirement for interaction with CeBRC-2 for RAD-51 loading at RFBs would also reveal a direct role for RFS-1 in promoting HRR at impeded forks. Since CeBRC-2 is required for transport of RAD-51 into the nucleus, it is impossible to address this issue with the mutants that are currently available. These studies would require a *Cebrc-2* mutant with an intact nuclear localization signal and BRC domain,

which mediates the interaction with RAD-51, but a mutated OB-fold so it cannot bind ssDNA. This isoform could transport RAD-51 into the nucleus but would not target RAD-51 to DSBs. If RFS-1 played a direct, CeBRC-2-independent role in promoting HRR at non-DSB substrates, then RAD-51 foci should still form following UVC or ICL damage. Such a mutant might be obtained by TILLING, as discussed in Chapter 4. Alternatively, one could make use of the recently described *MosI* excision-induced transgene instructed gene conversion (*Mos*TIC) system, which is purported to be efficient at recombining DNA elements into the *C. elegans* genome; such a point mutation could be created by site-directed mutagenesis and directly introduced into the endogenous locus.

In an effort to determine the role of RFS-1 in HRR at blocked forks, a genome-wide Y2H screen was performed and identified the novel interactor RIP-1. Extension of these studies to the vertebrate system has been hampered by the fact that RIP-1 is an orphan protein with no obvious homologs based on primary sequence identity. *rip-1* mutants phenocopied *rfs-1* mutants with respect to embryonic sensitivity and increased apoptosis following HN2 treatment, as well as the RAD-51 loading defect in response to UVC and DNA cross-linking treatment but not IR or HU-treatment. This replication-specific role is akin to RecFOR in *E. coli* HRR at non-DSB substrates. Purification of RIP-1 and RFS-1 for detailed biochemical analyses, such as RAD-51 loading on gapped DNA, will be important to assess whether these proteins are in fact eukaryotic RecFOR analogs. As RFS-1 and RIP-1 are both small proteins (approximately 30 kDa and 24 kDa, respectively), structural analysis, either by X-ray crystallography or NMR, could provide even more information about the mechanistic functions of these proteins. Even though RIP-1 is not obviously conserved on the basis of sequence, it might be structurally conserved in other organisms. The peptide array data was very striking as it identified separate binding sites for RAD-51 and RIP-1 on RFS-1. Additionally, using

mutagenized arrays, interaction-dead peptides were generated by substitution of a single residue. In the case of the RIP-1-binding peptides, residues critical for interaction were identified, as binding was extremely sensitive to mutation of these positions. Similarly critical positions were not uncovered in the RAD-51 binding peptide, though binding was sensitive to alteration in two particular regions. This sensitivity could reflect two RAD-51 binding sites in the peptide and could possibly be addressed through a double substitution peptide array, where residues in each putative domain are sequentially mutated to all 400 possible substitutions of the 20 common amino acids. Dominant-negative peptide injection will allow selective blocking of RAD-51 and RIP-1 binding to RFS-1, and the biological consequences on functions such as damage-induced RAD-51 focus formation and apoptosis can then be examined. The effects of RIP-1 and RAD-51 interaction-deficient isoforms of RFS-1 on biochemical activities such as ATPase and strand exchange can also be explored.

A number of larger scale genetic and proteomic approaches are also feasible future directions for this work. Again, using *Mos*TIC, tandem affinity purification tagged RIP-1 and RFS-1 constructs could be introduced in the endogenous locus, circumventing the frequent silencing of transgenes by germ line co-suppression. Identification by mass spectroscopy of proteins that associate with RFS-1 and RIP-1 in the presence or absence of DNA damage could provide further insight into how RFS-1 and RIP-1 function in HRR. An RNAi screen for mutations that result in synthetic lethality when in combination with *rfs-1* and *rip-1* would uncover novel functions for the proteins and find new genetic interactions. Finally, as mentioned in the introduction, the recent characterization of a host of *C. elegans* RFB repair genes and the availability of viable mutants in all known ICL repair pathways provide the opportunity for a comprehensive genetic dissection of ICL repair in the nematode. Budding yeast have proven useful in the analysis of the mechanisms of ICL repair, but

the existence of factors specific to higher metazoans (BRCA1, BRCA2, FA proteins) somewhat limit the ability to extrapolate the yeast model to higher eukaryotes. To this end, a number of double mutant combinations of *rfs-1, brc-1, brd-1, dog-1, fcd-2, him-6, mus-81, him-9/xpf-1, xpa-1,* and *spar-1* have been created. Collaborators have generated other double mutant combinations (*mrt-1, mus-1, hel-308, pol-η, pol-κ,* etc.), so a concerted epistatic analysis of ICL repair is a glaring and enticing possibility that could provide extraordinarily valuable insight into the genetics of cross-link repair in metazoans.

Another very interesting area of inquiry is the nature of the endogenous substrate to which the Rad51 paralogs, Fanconi anaemia and XPF-1-ERCC1 proteins respond. It has been suggested that ICLs can form from lipid peroxidation products. The attempt to drive endogenous ICL formation using *daf-16* mutants was unsuccessful, though an interesting relationship between DAF-16 and HIM-6 does exist. Whether this interaction is occurring in germ cells or the soma is unclear. The effects of lipid peroxidation might be worth investigating by increasing poly-unsaturated fatty acids in the nematode diet as well as by using different mutants that directly impact on oxidative stress, such as mitochondrial or catalase mutants. An even more interesting avenue of future study is the mechanism underlying the connection between the DNA damage and IGF1 pathways. If DNA damage is able to promote DAF-16 translocation into the nucleus to drive expression of stress response genes, this translocation could be used as a readout for an RNAi screen performed to look for genes involved in this process. How the damage signal is transduced to the IGF1 pathway is completely unknown and the nematode would be an ideal model to complement the work done in mammalian systems conducted by Niedernhofer *et al.* (2006) and is an area this author hopes to explore in the future.

Finally, evidence was presented regarding the role of RFS-1 in meiosis. Although this work is very preliminary, it represents an interesting, though unrefined story. Loss of any of RFS-1, RIP-1, XPF-1, BRC-1, or BRD-1 causes mild Him phenotypes but low lethality, indicating that these proteins play accessory, non-essential roles in meiosis. Further, *rfs-1*, *brc-1*, *him-9/xpf-1*, and *mus-81* mutants all exhibit increased RAD-51 levels late in meiosis, indicating a defect or delay in HRR of meiotic DSBs. Although this evidence suggests that the recombination intermediate accumulation in *mus-81; him-9/xpf-1* double mutants derives from SPO-11-induced DSBs, blocking DSB formation with *htp-3* dsRNA injection will be important for confirmation. Likewise, though the genetic interaction of the *hel-308 rfs-1* double mutants with *msh-5* suggest that the synthetic lethality in the double mutant is a meiotic phenotype, unequivocal proof must be obtained by blocking meiotic DSB formation, an experiment currently underway.

The main purpose of this work was to gain insight into the biological role of the Rad51 paralogs. A specific role for the *C. elegans* RAD-51 paralog, RFS-1, in promoting HRR at impeded replication forks, but not at conventional DSB substrates was revealed. Strikingly, a novel RFS-1 interactor, RIP-1, also appears to be required for this impeded replication fork-specific HRR. A non-essential role for RFS-1 in promoting HRR in meiosis was also uncovered, though the specific function of RFS-1 in repair of SPO-11 DSBs remains elusive. It will be important in the future to refine the mechanism(s) through which RFS-1 promotes RAD-51 loading in both mitosis and meiosis and extend these studies to the mammalian Rad51 paralogs. This knowledge could impact on our understanding of how HRR functions in response to replication blocking damage, and how this serves to prevent genetic alterations that could lead to cancer.

Published work

Published work presented in this thesis:

Ward, J.D., Barber, L.J., Petalcorin, M.I., Yanowitz, J. and Boulton, S.J. (2007). **Replication blocking lesions present a unique substrate for homologous recombination.** *Embo J* **26**(14): 3384-3396.

This author performed all experiments and writing.

-J. Yanowitz contributed molecular identity of *him-15* allele of *rfs-1*

-M. Petalcorin aided with dsRNA microinjection

-L.J. Barber aided in development of DNA damage sensitivity assay

Goodyer, W., Kaitna, S., Couteau, F., Ward, J.D., Boulton, S.J. and Zetka, M. (2008). **HTP-3 Links DSB Formation with Homolog Pairing and Crossing Over during C. elegans Meiosis.** *Dev Cell* **14**(2): 263-274.

-this author generated the MRE-11 antibody, optimized it for use in immunofluorescence and provided it to the Zetka group

O'Neil, N.J., Ward, J.D., Youds, J.L., Boulton, S.J., Rose, A.M., and Kuwabara, P.K. **MUS-81 and EME-1 are involved in the repair of replication-associated DNA damage in *Caenorhabditis elegans*.** *Manuscript in preparation.*

This author performed/was involved in:

-immunofluorescence (germ line RAD-51 profiles and CDDP-induced RAD-51 focus formation analysis)

-diakinesis examination

-*mre-11* RNAi and *htp-3* and *him-17* dsRNA injection experiments

-strain generation

-manuscript revision

-experimental suggestion

Work contributed to not presented in thesis:

Adamo, A., Montemauri, P., Silva, N., Ward, J.D., Boulton, S.J. and La Volpe, A. (2008). **BRC-1 acts in the inter-sister pathway of meiotic double-strand break repair.** *EMBO Rep.* **9**(3): 287-292

This author performed/was involved in:

-mutant backcrossing

-experimental suggestions

- the writing and revising process

Collis, S.J., Barber, L.J., Clark, A.J., Martin, J.S., Ward, J.D. and Boulton, S.J. (2007). **HCLK2 is essential for the mammalian S-phase checkpoint and impacts on Chk1 stability.** *Nat Cell Biol* **9**(4): 391-401.

This author performed/was involved in:

-ICL sensitivity assays

-the writing and revising process

Collis, S.J., Barber, L.J., Ward, J.D., Martin, J.S. and Boulton, S.J. (2006). *C. elegans* **FANCD2 responds to replication stress and functions in interstrand cross-link repair.** *DNA Repair (Amst)* **5**(11): 1398-1406.

This author performed/was involved in:

- ICL sensitivity assays

-experimental suggestions

-the writing and revising process

Barber, L.J., Youds, J.L., Ward, J.D., O'Neil, N.J., Collis, S.J., Petalcorin, M.I., McIlwraith, M.J., Grabowski, M., Tissenbaum, H., Cantor, S., West, S.C., Rose, A.M. and Boulton, S.J. (2008). **SPAR-1 is a novel helicase that prevents illegitimate recombination.** *Manuscript in preparation.*

This author performed/was involved in:

-ICL sensitivity assays

-immunofluorescence analysis (germ line RAD-51 staining profiles)

-cytological analysis of chromosome integrity at diakinesis

-mutant generation

-brood size analysis

-experimental suggestions

-the writing and revising process

Muzzini, D., Ward, J.D., Martinez-Perez, E., Plevani, P., Cassata, G., Boulton, S.J. and Marini, F. (2008). ***hel-308* interacts with *rad-51* and its paralog *rfs-1* during meiotic crossing-over maturation in the nematode *C.elegans*.** *Manuscript in preparation.*

This author performed/was involved in:

-strain generation

-immunofluorescence (RAD-51 and RPA-1 staining profiles)

-*mre-11* RNAi feeding and *htp-3* and *him-17* dsRNA injection experiments

-*rfs-1; him-6* generation and characterization

-experimental suggestions

-the writing and revision process

Youds, J.L., Barber, L.J., Ward, J.D., Collis, S.J., O'Neil, N.J., Boulton, S.J. and Rose, A.M. (2008). **DOG-1 is the *Caenorhabditis elegans* BRIP1/FANCJ homologue and functions in interstrand cross-link repair.** *Mol Cell Biol* **28**(5): 1470-1479

This author performed/was involved in:

-cell cycle arrest assay (following HN2 treatment)

-ICL sensitivity assays

-immunofluorescence (mitotic RAD-51 staining ±ICL damage)

-the writing and revising process

References

Adamo, A., P. Montemauri, N. Silva, J. D. Ward, S. J. Boulton and A. La Volpe (2008). BRC-1 acts in the inter-sister pathway of meiotic double-strand break repair. *EMBO Rep* **9**(3): 287-292.

Adelman, R., R. L. Saul and B. N. Ames (1988). Oxidative damage to DNA: relation to species metabolic rate and life span. *Proc Natl Acad Sci U S A* **85**(8): 2706-8.

Ahmed, S., A. Alpi, M. O. Hengartner and A. Gartner (2001). *C. elegans* RAD-5/CLK-2 defines a new DNA damage checkpoint protein. *Curr Biol* **11**(24): 1934-44.

Al-Minawi, A. Z., N. Saleh-Gohari and T. Helleday (2008). The ERCC1/XPF endonuclease is required for efficient single-strand annealing and gene conversion in mammalian cells. *Nucleic Acids Res* **36**(1): 1-9.

Alpi, A., P. Pasierbek, A. Gartner and J. Loidl (2003). Genetic and cytological characterization of the recombination protein RAD-51 in *Caenorhabditis elegans*. *Chromosoma* **112**(1): 6-16.

Anderson, D. G. and S. C. Kowalczykowski (1997). The recombination hot spot chi is a regulatory element that switches the polarity of DNA degradation by the RecBCD enzyme. *Genes Dev* **11**(5): 571-81.

Anderson, D. G. and S. C. Kowalczykowski (1997). The translocating RecBCD enzyme stimulates recombination by directing RecA protein onto ssDNA in a chi-regulated manner. *Cell* **90**(1): 77-86.

Arthanari, H. and P. H. Bolton (2001). Functional and dysfunctional roles of quadruplex DNA in cells. *Chem Biol* **8**(3): 221-30.

Balajee, A. S. and V. A. Bohr (2000). Genomic heterogeneity of nucleotide excision repair. *Gene* **250**(1-2): 15-30.

Barber, L. J., T. A. Ward, J. A. Hartley and P. J. McHugh (2005). DNA interstrand cross-link repair in the *Saccharomyces cerevisiae* cell cycle: overlapping roles for PSO2 (SNM1) with MutS factors and EXO1 during S phase. *Mol Cell Biol* **25**(6): 2297-309.

Barber, L. J., J. L. Youds, J. D. Ward, N. J. O'Neil, S. J. Collis, M. I. Petalcorin, M. J. McIlwraith, M. Grabowski, H. Tissenbaum, S. Cantor, S. C. West, A. M. Rose and S. J. Boulton (2008). SPAR-1 is a novel helicase that prevents illegitimate recombination. *Manuscript in preparation*

Bardwell, A. J., L. Bardwell, A. E. Tomkinson and E. C. Friedberg (1994). Specific cleavage of model recombination and repair intermediates by the yeast Rad1-Rad10 DNA endonuclease. *Science* **265**(5181): 2082-5.

Batty, D. P. and R. D. Wood (2000). Damage recognition in nucleotide excision repair of DNA. *Gene* **241**(2): 193-204.

Bennett, R. J., H. J. Dunderdale and S. C. West (1993). Resolution of Holliday junctions by RuvC resolvase: cleavage specificity and DNA distortion. *Cell* **74**(6): 1021-31.

Berardini, M., P. L. Foster and E. L. Loechler (1999). DNA polymerase II (polB) is involved in a new DNA repair pathway for DNA interstrand cross-links in *Escherichia coli*. *J Bacteriol* **181**(9): 2878-82.

Bessler, J. B., K. C. Reddy, M. Hayashi, J. Hodgkin and A. M. Villeneuve (2007). A role for *Caenorhabditis elegans* chromatin-associated protein HIM-17 in the proliferation vs. meiotic entry decision. *Genetics* **175**(4): 2029-37.

Bhatia, P. K., R. A. Verhage, J. Brouwer and E. C. Friedberg (1996). Molecular cloning and characterization of *Saccharomyces cerevisiae* RAD28, the yeast homolog of the human Cockayne syndrome A (CSA) gene. *J Bacteriol* **178**(20): 5977-88.

Bi, B., N. Rybalchenko, E. I. Golub and C. M. Radding (2004). Human and yeast Rad52 proteins promote DNA strand exchange. *Proc Natl Acad Sci U S A* **101**(26): 9568-72.

Bishop, D. K., U. Ear, A. Bhattacharyya, C. Calderone, M. Beckett, R. R. Weichselbaum and A. Shinohara (1998). Xrcc3 is required for assembly of Rad51 complexes in vivo. *J Biol Chem* **273**(34): 21482-8.

Bishop, D. K. and D. Zickler (2004). Early decision; meiotic crossover interference prior to stable strand exchange and synapsis. *Cell* **117**(1): 9-15.

Boddy, M. N., P. H. Gaillard, W. H. McDonald, P. Shanahan, J. R. Yates, 3rd and P. Russell (2001). Mus81-Eme1 are essential components of a Holliday junction resolvase. *Cell* **107**(4): 537-48.

Borner, G. V., N. Kleckner and N. Hunter (2004). Crossover/noncrossover differentiation, synaptonemal complex formation, and regulatory surveillance at the leptotene/zygotene transition of meiosis. *Cell* **117**(1): 29-45.

Boulton, S. J., A. Gartner, J. Reboul, P. Vaglio, N. Dyson, D. E. Hill and M. Vidal (2002). Combined functional genomic maps of the *C. elegans* DNA damage response. *Science* **295**(5552): 127-31.

Boulton, S. J., J. S. Martin, J. Polanowska, D. E. Hill, A. Gartner and M. Vidal (2004). BRCA1/BARD1 orthologs required for DNA repair in *Caenorhabditis elegans*. *Curr Biol* **14**(1): 33-9.

Boyd, J. B., K. Sakaguchi and P. V. Harris (1990). *mus308* mutants of Drosophila exhibit hypersensitivity to DNA cross-linking agents and are defective in a deoxyribonuclease. *Genetics* **125**(4): 813-9.

Brenner, S. (1974). The genetics of *Caenorhabditis elegans*. *Genetics* **77**(1): 71-94.

Brosh, R. (2008). Personal communication.

Bugreev, D. V. and A. V. Mazin (2004). Ca2+ activates human homologous recombination protein Rad51 by modulating its ATPase activity. *Proc Natl Acad Sci U S A* **101**(27): 9988-93.

Burma, S., B. P. Chen and D. J. Chen (2006). Role of non-homologous end joining (NHEJ) in maintaining genomic integrity. *DNA Repair (Amst)* **5**(9-10): 1042-8.

Cantor, S. B., D. W. Bell, S. Ganesan, E. M. Kass, R. Drapkin, S. Grossman, D. C. Wahrer, D. C. Sgroi, W. S. Lane, D. A. Haber and D. M. Livingston (2001). BACH1, a novel helicase-like protein, interacts directly with BRCA1 and contributes to its DNA repair function. *Cell* **105**(1): 149-60.

Cassuto, E. (1984). Formation of covalently closed heteroduplex DNA by the combined action of gyrase and RecA protein. *Embo J* **3**(9): 2159-64.

Chen, P. L., C. F. Chen, Y. Chen, J. Xiao, Z. D. Sharp and W. H. Lee (1998). The BRC repeats in BRCA2 are critical for RAD51 binding and resistance to methyl methanesulfonate treatment. *Proc Natl Acad Sci U S A* **95**(9): 5287-92.

Cheung, I., M. Schertzer, A. Rose and P. M. Lansdorp (2002). Disruption of *dog-1* in *Caenorhabditis elegans* triggers deletions upstream of guanine-rich DNA. *Nat Genet* **31**(4): 405-9.

Chin, G. M. and A. M. Villeneuve (2001). *C. elegans mre-11* is required for meiotic recombination and DNA repair but is dispensable for the meiotic G(2) DNA damage checkpoint. *Genes Dev* **15**(5): 522-34.

Chow, K. H. and J. Courcelle (2004). RecO acts with RecF and RecR to protect and maintain replication forks blocked by UV-induced DNA damage in *Escherichia coli*. *J Biol Chem* **279**(5): 3492-6.

Christensen, M., A. Estevez, X. Yin, R. Fox, R. Morrison, M. McDonnell, C. Gleason, D. M. Miller, 3rd and K. Strange (2002). A primary culture system for functional analysis of *C. elegans* neurons and muscle cells. *Neuron* **33**(4): 503-14.

Ciccia, A., C. Ling, R. Coulthard, Z. Yan, Y. Xue, A. R. Meetei, H. Laghmani el, H. Joenje, N. McDonald, J. P. de Winter, W. Wang and S. C. West (2007). Identification of FAAP24, a Fanconi anemia core complex protein that interacts with FANCM. *Mol Cell* **25**(3): 331-43.

Clerici, M., D. Mantiero, G. Lucchini and M. P. Longhese (2005). The *Saccharomyces cerevisiae* Sae2 protein promotes resection and bridging of double strand break ends. *J Biol Chem* **280**(46): 38631-8.

Colaiacovo, M. P., A. J. MacQueen, E. Martinez-Perez, K. McDonald, A. Adamo, A. La Volpe and A. M. Villeneuve (2003). Synaptonemal complex assembly in *C. elegans* is dispensable for loading strand-exchange proteins but critical for proper completion of recombination. *Dev Cell* **5**(3): 463-74.

Cole, R. S. (1973). Repair of DNA containing interstrand crosslinks in *Escherichia coli*: sequential excision and recombination. *Proc Natl Acad Sci U S A* **70**(4): 1064-8.

Collis, S. J., L. J. Barber, A. J. Clark, J. S. Martin, J. D. Ward and S. J. Boulton (2007). HCLK2 is essential for the mammalian S-phase checkpoint and impacts on Chk1 stability. *Nat Cell Biol* **9**(4): 391-401.

Collis, S. J., L. J. Barber, J. D. Ward, J. S. Martin and S. J. Boulton (2006). *C. elegans* FANCD2 responds to replication stress and functions in interstrand cross-link repair. *DNA Repair (Amst)* **5**(11): 1398-406.

Connelly, J. C., L. A. Kirkham and D. R. Leach (1998). The SbcCD nuclease of *Escherichia coli* is a structural maintenance of chromosomes (SMC) family protein that cleaves hairpin DNA. *Proc Natl Acad Sci U S A* **95**(14): 7969-74.

Connolly, B. and S. C. West (1990). Genetic recombination in *Escherichia coli*: Holliday junctions made by RecA protein are resolved by fractionated cell-free extracts. *Proc Natl Acad Sci U S A* **87**(21): 8476-80.

Connor, F., D. Bertwistle, P. J. Mee, G. M. Ross, S. Swift, E. Grigorieva, V. L. Tybulewicz and A. Ashworth (1997). Tumorigenesis and a DNA repair defect in mice with a truncating Brca2 mutation. *Nat Genet* **17**(4): 423-30.

Constantinou, A., X. B. Chen, C. H. McGowan and S. C. West (2002). Holliday junction resolution in human cells: two junction endonucleases with distinct substrate specificities. *Embo J* **21**(20): 5577-85.

Courcelle, J. and P. C. Hanawalt (2001). Participation of recombination proteins in rescue of arrested replication forks in UV-irradiated *Escherichia coli* need not involve recombination. *Proc Natl Acad Sci U S A* **98**(15): 8196-202.

Couteau, F., K. Nabeshima, A. Villeneuve and M. Zetka (2004). A component of *C. elegans* meiotic chromosome axes at the interface of homolog alignment, synapsis, nuclear reorganization, and recombination. *Curr Biol* **14**(7): 585-92.

Couteau, F. and M. Zetka (2005). HTP-1 coordinates synaptonemal complex assembly with homolog alignment during meiosis in *C. elegans*. *Genes Dev* **19**(22): 2744-56.

Cox, M. M. (2001). Recombinational DNA repair of damaged replication forks in *Escherichia coli*: questions. *Annu Rev Genet* **35**: 53-82.

Cox, M. M. and I. R. Lehman (1982). recA protein-promoted DNA strand exchange. Stable complexes of recA protein and single-stranded DNA formed in the presence of ATP and single-stranded DNA binding protein. *J Biol Chem* **257**(14): 8523-32.

d'Adda di Fagagna, F., S. H. Teo and S. P. Jackson (2004). Functional links between telomeres and proteins of the DNA-damage response. *Genes Dev* **18**(15): 1781-99.

Dardalhon, M. and D. Averbeck (1995). Pulsed-field gel electrophoresis analysis of the repair of psoralen plus UVA induced DNA photoadducts in *Saccharomyces cerevisiae*. *Mutat Res* **336**(1): 49-60.

De Bont, R. and N. van Larebeke (2004). Endogenous DNA damage in humans: a review of quantitative data. *Mutagenesis* **19**(3): 169-85.

De Silva, I. U., P. J. McHugh, P. H. Clingen and J. A. Hartley (2000). Defining the roles of nucleotide excision repair and recombination in the repair of DNA interstrand cross-links in mammalian cells. *Mol Cell Biol* **20**(21): 7980-90.

De Silva, I. U., P. J. McHugh, P. H. Clingen and J. A. Hartley (2002). Defects in interstrand cross-link uncoupling do not account for the extreme sensitivity of ERCC1 and XPF cells to cisplatin. *Nucleic Acids Res* **30**(17): 3848-56.

De Stasio, E., C. Lephoto, L. Azuma, C. Holst, D. Stanislaus and J. Uttam (1997). Characterization of revertants of *unc-93(e1500)* in *Caenorhabditis elegans* induced by N-ethyl-N-nitrosourea. *Genetics* **147**(2): 597-608.

Deans, B., C. S. Griffin, P. O'Regan, M. Jasin and J. Thacker (2003). Homologous recombination deficiency leads to profound genetic instability in cells derived from Xrcc2-knockout mice. *Cancer Res* **63**(23): 8181-7.

Denver, D. R., S. Feinberg, C. Steding, M. Durbin and M. Lynch (2006). The relative roles of three DNA repair pathways in preventing *Caenorhabditis elegans* mutation accumulation. *Genetics* **174**(1): 57-65.

Dernburg, A. F., K. McDonald, G. Moulder, R. Barstead, M. Dresser and A. M. Villeneuve (1998). Meiotic recombination in *C. elegans* initiates by a conserved mechanism and is dispensable for homologous chromosome synapsis. *Cell* **94**(3): 387-98.

Dernburg, A. F., J. Zalevsky, M. P. Colaiacovo and A. M. Villeneuve (2000). Transgene-mediated cosuppression in the *C. elegans* germ line. *Genes Dev* **14**(13): 1578-83.

Derry, W. B., A. P. Putzke and J. H. Rothman (2001). *Caenorhabditis elegans* p53: role in apoptosis, meiosis, and stress resistance. *Science* **294**(5542): 591-5.

Dillingham, M. S., M. Spies and S. C. Kowalczykowski (2003). RecBCD enzyme is a bipolar DNA helicase. *Nature* **423**(6942): 893-7.

Dixon, D. A. and S. C. Kowalczykowski (1995). Role of the *Escherichia coli* recombination hotspot, chi, in RecABCD-dependent homologous pairing. *J Biol Chem* **270**(27): 16360-70.

Dronkert, M. L. and R. Kanaar (2001). Repair of DNA interstrand cross-links. *Mutat Res* **486**(4): 217-47.

Durkin, S. G. and T. W. Glover (2007). Chromosome Fragile Sites. *Annu Rev Genet.*

Ennis, D. G., S. K. Amundsen and G. R. Smith (1987). Genetic functions promoting homologous recombination in *Escherichia coli*: a study of inversions in phage lambda. *Genetics* **115**(1): 11-24.

Evans, E., J. G. Moggs, J. R. Hwang, J. M. Egly and R. D. Wood (1997). Mechanism of open complex and dual incision formation by human nucleotide excision repair factors. *Embo J* **16**(21): 6559-73.

Fabre, F., A. Chan, W. D. Heyer and S. Gangloff (2002). Alternate pathways involving Sgs1/Top3, Mus81/ Mms4, and Srs2 prevent formation of toxic recombination intermediates from single-stranded gaps created by DNA replication. *Proc Natl Acad Sci U S A* **99**(26): 16887-92.

Farah, J. A., G. Cromie, L. Davis, W. W. Steiner and G. R. Smith (2005). Activation of an alternative, *rec12* (*spo11*)-independent pathway of fission yeast meiotic recombination in the absence of a DNA flap endonuclease. *Genetics* **171**(4): 1499-511.

Fichtinger-Schepman, A. M., J. L. van der Veer, J. H. den Hartog, P. H. Lohman and J. Reedijk (1985). Adducts of the antitumor drug cis-diamminedichloroplatinum(II) with DNA: formation, identification, and quantitation. *Biochemistry* **24**(3): 707-13.

Fire, A., S. Xu, M. K. Montgomery, S. A. Kostas, S. E. Driver and C. C. Mello (1998). Potent and specific genetic interference by double-stranded RNA in *Caenorhabditis elegans*. *Nature* **391**(6669): 806-11.

Forget, A. L., B. T. Bennett and K. L. Knight (2004). Xrcc3 is recruited to DNA double strand breaks early and independent of Rad51. *J Cell Biochem* **93**(3): 429-36.

Fortini, P., B. Pascucci, E. Parlanti, M. D'Errico, V. Simonelli and E. Dogliotti (2003). The base excision repair: mechanisms and its relevance for cancer susceptibility. *Biochimie* **85**(11): 1053-71.

Francis, R., M. K. Barton, J. Kimble and T. Schedl (1995). *gld-1*, a tumor suppressor gene required for oocyte development in *Caenorhabditis elegans*. *Genetics* **139**(2): 579-606.

French, C. A., J. Y. Masson, C. S. Griffin, P. O'Regan, S. C. West and J. Thacker (2002). Role of mammalian RAD51L2 (RAD51C) in recombination and genetic stability. *J Biol Chem* **277**(22): 19322-30.

Friedberg, E. C. (2001). How nucleotide excision repair protects against cancer. *Nat Rev Cancer* **1**(1): 22-33.

Friedberg, E. C., G. C. Walker and W. Siede (1995). DNA repair and mutagenesis. Washington, D.C., ASM Press.

Fuller, L. F. and R. B. Painter (1988). A Chinese hamster ovary cell line hypersensitive to ionizing radiation and deficient in repair replication. *Mutat Res* **193**(2): 109-21.

Garcia-Muse, T. and S. J. Boulton (2005). Distinct modes of ATR activation after replication stress and DNA double-strand breaks in *Caenorhabditis elegans*. *Embo J* **24**(24): 4345-55.

Garcia-Muse, T. and S. J. Boulton (2007). Meiotic recombination in *Caenorhabditis elegans*. *Chromosome Res* **15**(5): 607-21.

Gaskell, L. J., F. Osman, R. J. Gilbert and M. C. Whitby (2007). Mus81 cleavage of Holliday junctions: a failsafe for processing meiotic recombination intermediates? *Embo J* **26**(7): 1891-901.

Gilchrist, E. J., N. J. O'Neil, A. M. Rose, M. C. Zetka and G. W. Haughn (2006). TILLING is an effective reverse genetics technique for *Caenorhabditis elegans*. *BMC Genomics* **7**: 262.

Glover, T. W., M. F. Arlt, A. M. Casper and S. G. Durkin (2005). Mechanisms of common fragile site instability. *Hum Mol Genet* **14 Spec No. 2**: R197-205.

Godthelp, B. C., F. Artwert, H. Joenje and M. Z. Zdzienicka (2002). Impaired DNA damage-induced nuclear Rad51 foci formation uniquely characterizes Fanconi anemia group D1. *Oncogene* **21**(32): 5002-5.

Goodyer, W., S. Kaitna, F. Couteau, J. D. Ward, S. J. Boulton and M. Zetka (2008). HTP-3 Links DSB Formation with Homolog Pairing and Crossing Over during C. elegans Meiosis. *Dev Cell* **14**(2): 263-74.

Grabowski, M. (2007). Unpublished data.

Greenwald, I. S. and H. R. Horvitz (1980). *unc-93(e1500)*: A behavioral mutant of *Caenorhabditis elegans* that defines a gene with a wild-type null phenotype. *Genetics* **96**(1): 147-64.

Greenwald, I. S. and H. R. Horvitz (1982). Dominant suppressors of a muscle mutant define an essential gene of *Caenorhabditis elegans*. *Genetics* **101**(2): 211-25.

Grossmann, K. F., A. M. Ward, M. E. Matkovic, A. E. Folias and R. E. Moses (2001). *S. cerevisiae* has three pathways for DNA interstrand crosslink repair. *Mutat Res* **487**(3-4): 73-83.

Gumienny, T. L., E. Lambie, E. Hartwieg, H. R. Horvitz and M. O. Hengartner (1999). Genetic control of programmed cell death in the *Caenorhabditis elegans* hermaphrodite germline. *Development* **126**(5): 1011-22.

Guzder, S. N., P. Sung, L. Prakash and S. Prakash (1996). Nucleotide excision repair in yeast is mediated by sequential assembly of repair factors and not by a pre-assembled repairosome. *J Biol Chem* **271**(15): 8903-10.

Habraken, Y., P. Sung, L. Prakash and S. Prakash (1995). Structure-specific nuclease activity in yeast nucleotide excision repair protein Rad2. *J Biol Chem* **270**(50): 30194-8.

Hanada, K., M. Budzowska, M. Modesti, A. Maas, C. Wyman, J. Essers and R. Kanaar (2006). The structure-specific endonuclease Mus81-Eme1 promotes conversion of interstrand DNA crosslinks into double-strands breaks. *Embo J* **25**(20): 4921-32.

Hayashi, M., G. M. Chin and A. M. Villeneuve (2007). *C. elegans* Germ Cells Switch between Distinct Modes of Double-Strand Break Repair During Meiotic Prophase Progression. *PLoS Genet* **3**(11): e191.

Henriques, J. A. and E. Moustacchi (1981). Interactions between mutations for sensitivity to psoralen photoaddition (*pso*) and to radiation (*rad*) in *Saccharomyces cerevisiae*. *J Bacteriol* **148**(1): 248-56.

Hodgkin, J., H. R. Horvitz and S. Brenner (1979). Nondisjunction Mutants of the Nematode *Caenorhabditis elegans*. *Genetics* **91**(1): 67-94.

Hoege, C., B. Pfander, G. L. Moldovan, G. Pyrowolakis and S. Jentsch (2002). RAD6-dependent DNA repair is linked to modification of PCNA by ubiquitin and SUMO. *Nature* **419**(6903): 135-41.

Hopfner, K. P., L. Craig, G. Moncalian, R. A. Zinkel, T. Usui, B. A. Owen, A. Karcher, B. Henderson, J. L. Bodmer, C. T. McMurray, J. P. Carney, J. H. Petrini and J. A. Tainer (2002). The Rad50 zinc-hook is a structure joining Mre11 complexes in DNA recombination and repair. *Nature* **418**(6897): 562-6.

Howlett, N. G., T. Taniguchi, S. Olson, B. Cox, Q. Waisfisz, C. De Die-Smulders, N. Persky, M. Grompe, H. Joenje, G. Pals, H. Ikeda, E. A. Fox and A. D. D'Andrea (2002). Biallelic inactivation of BRCA2 in Fanconi anemia. *Science* **297**(5581): 606-9.

Hsu, D. R., P. T. Chuang and B. J. Meyer (1995). DPY-30, a nuclear protein essential early in embryogenesis for *Caenorhabditis elegans* dosage compensation. *Development* **121**(10): 3323-34.

Huang, W., W. J. Feaver, A. E. Tomkinson and E. C. Friedberg (1998). The N-degron protein degradation strategy for investigating the function of essential genes: requirement for replication protein A and proliferating cell nuclear antigen proteins for nucleotide excision repair in yeast extracts. *Mutat Res* **408**(3): 183-94.

Ira, G., A. Malkova, G. Liberi, M. Foiani and J. E. Haber (2003). Srs2 and Sgs1-Top3 suppress crossovers during double-strand break repair in yeast. *Cell* **115**(4): 401-11.

Ivanov, E. L., N. Sugawara, J. Fishman-Lobell and J. E. Haber (1996). Genetic requirements for the single-strand annealing pathway of double-strand break repair in *Saccharomyces cerevisiae*. *Genetics* **142**(3): 693-704.

Ivanov, E. L., N. Sugawara, C. I. White, F. Fabre and J. E. Haber (1994). Mutations in XRS2 and RAD50 delay but do not prevent mating-type switching in *Saccharomyces cerevisiae*. *Mol Cell Biol* **14**(5): 3414-25.

Ivessa, A. S., B. A. Lenzmeier, J. B. Bessler, L. K. Goudsouzian, S. L. Schnakenberg and V. A. Zakian (2003). The *Saccharomyces cerevisiae* helicase Rrm3p facilitates replication past nonhistone protein-DNA complexes. *Mol Cell* **12**(6): 1525-36.

Ivessa, A. S., J. Q. Zhou, V. P. Schulz, E. K. Monson and V. A. Zakian (2002). *Saccharomyces* Rrm3p, a 5' to 3' DNA helicase that promotes replication fork progression through telomeric and subtelomeric DNA. *Genes Dev* **16**(11): 1383-96.

Ivessa, A. S., J. Q. Zhou and V. A. Zakian (2000). The *Saccharomyces* Pif1p DNA helicase and the highly related Rrm3p have opposite effects on replication fork progression in ribosomal DNA. *Cell* **100**(4): 479-89.

Iwasaki, H., M. Takahagi, T. Shiba, A. Nakata and H. Shinagawa (1991). *Escherichia coli* RuvC protein is an endonuclease that resolves the Holliday structure. *Embo J* **10**(13): 4381-9.

Jachymczyk, W. J., R. C. von Borstel, M. R. Mowat and P. J. Hastings (1981). Repair of interstrand cross-links in DNA of *Saccharomyces cerevisiae* requires two systems for DNA repair: the RAD3 system and the RAD51 system. *Mol Gen Genet* **182**(2): 196-205.

Jackson, A. L. and L. A. Loeb (2001). The contribution of endogenous sources of DNA damage to the multiple mutations in cancer. *Mutat Res* **477**(1-2): 7-21.

Jakupec, M. A., M. Galanski and B. K. Keppler (2003). Tumour-inhibiting platinum complexes--state of the art and future perspectives. *Rev Physiol Biochem Pharmacol* **146**: 1-54.

Jantsch, V., L. Tang, P. Pasierbek, A. Penkner, S. Nayak, A. Baudrimont, T. Schedl, A. Gartner and J. Loidl (2007). *Caenorhabditis elegans prom-1* Is Required for Meiotic Prophase Progression and Homologous Chromosome Pairing. *Mol Biol Cell* **18**(12): 4911-4920.

Johnson, R. D., N. Liu and M. Jasin (1999). Mammalian XRCC2 promotes the repair of DNA double-strand breaks by homologous recombination. *Nature* **401**(6751): 397-9.

Jones, N. J., R. Cox and J. Thacker (1987). Isolation and cross-sensitivity of X-ray-sensitive mutants of V79-4 hamster cells. *Mutat Res* **183**(3): 279-86.

Kadyrov, F. A., L. Dzantiev, N. Constantin and P. Modrich (2006). Endonucleolytic function of MutLalpha in human mismatch repair. *Cell* **126**(2): 297-308.

Kagawa, W., H. Kurumizaka, S. Ikawa, S. Yokoyama and T. Shibata (2001). Homologous pairing promoted by the human Rad52 protein. *J Biol Chem* **276**(37): 35201-8.

Kasai, H., N. Iwamoto-Tanaka and S. Fukada (1998). DNA modifications by the mutagen glyoxal: adduction to G and C, deamination of C and GC and GA cross-linking. *Carcinogenesis* **19**(8): 1459-65.

Kelly, K. O., A. F. Dernburg, G. M. Stanfield and A. M. Villeneuve (2000). *Caenorhabditis elegans msh-5* is required for both normal and radiation-induced meiotic crossing over but not for completion of meiosis. *Genetics* **156**(2): 617-30.

Kennedy, R. D. and A. D. D'Andrea (2005). The Fanconi Anemia/BRCA pathway: new faces in the crowd. *Genes Dev* **19**(24): 2925-40.

Kenyon, C. (2005). The plasticity of aging: insights from long-lived mutants. *Cell* **120**(4): 449-60.

Khasanov, F. K., A. F. Salakhova, O. V. Chepurnaja, V. G. Korolev and V. I. Bashkirov (2004). Identification and characterization of the *rlp1+*, the novel Rad51 paralog in the fission yeast *Schizosaccharomyces pombe*. *DNA Repair (Amst)* **3**(10): 1363-74.

Kim, J. M., Y. Kee, A. Gurtan and A. D. D'Andrea (2008). Cell cycle dependent chromatin loading of the fanconi anemia core complex by FANCM/FAAP24. *Blood*.

Kim, S. H., A. H. Holway, S. Wolff, A. Dillin and W. M. Michael (2007). SMK-1/PPH-4.1-mediated silencing of the CHK-1 response to DNA damage in early *C. elegans* embryos. *J Cell Biol* **179**(1): 41-52.

Kim, Y. C., M. H. Lee, S. S. Ryu, J. H. Kim and H. S. Koo (2002). Coaction of DNA topoisomerase IIIalpha and a RecQ homologue during the germ-line mitosis in *Caenorhabditis elegans*. *Genes Cells* **7**(1): 19-27.

Kim, Y. M., I. Yang, J. Lee and H. S. Koo (2005). Deficiency of Bloom's syndrome protein causes hypersensitivity of *C. elegans* to ionizing radiation but not to UV radiation, and induces p53-dependent physiological apoptosis. *Mol Cells* **20**(2): 228-34.

Kobayashi, T. (2003). The replication fork barrier site forms a unique structure with Fob1p and inhibits the replication fork. *Mol Cell Biol* **23**(24): 9178-88.

Kobayashi, T., D. J. Heck, M. Nomura and T. Horiuchi (1998). Expansion and contraction of ribosomal DNA repeats in *Saccharomyces cerevisiae*: requirement of replication fork blocking (Fob1) protein and the role of RNA polymerase I. *Genes Dev* **12**(24): 3821-30.

Kobayashi, T., M. Nomura and T. Horiuchi (2001). Identification of DNA cis elements essential for expansion of ribosomal DNA repeats in *Saccharomyces cerevisiae*. *Mol Cell Biol* **21**(1): 136-47.

Kowalczykowski, S. C. (2000). Initiation of genetic recombination and recombination-dependent replication. *Trends Biochem Sci* **25**(4): 156-65.

Kowalczykowski, S. C. and A. K. Eggleston (1994). Homologous pairing and DNA strand-exchange proteins. *Annu Rev Biochem* **63**: 991-1043.

Kraus, E., W. Y. Leung and J. E. Haber (2001). Break-induced replication: a review and an example in budding yeast. *Proc Natl Acad Sci U S A* **98**(15): 8255-62.

Krogh, B. O. and L. S. Symington (2004). Recombination proteins in yeast. *Annu Rev Genet* **38:** 233-71.

Kunkel, T. A. and D. A. Erie (2005). DNA mismatch repair. *Annu Rev Biochem* **74:** 681-710.

Kuzminov, A. (1999). Recombinational repair of DNA damage in *Escherichia coli* and bacteriophage lambda. *Microbiol Mol Biol Rev* **63**(4): 751-813, table of contents.

Kuznetsov, S., M. Pellegrini, K. Shuda, O. Fernandez-Capetillo, Y. Liu, B. K. Martin, S. Burkett, E. Southon, D. Pati, L. Tessarollo, S. C. West, P. J. Donovan, A. Nussenzweig and S. K. Sharan (2007). RAD51C deficiency in mice results in early prophase I arrest in males and sister chromatid separation at metaphase II in females. *J Cell Biol* **176**(5): 581-92.

Lambert, S., A. Watson, D. M. Sheedy, B. Martin and A. M. Carr (2005). Gross chromosomal rearrangements and elevated recombination at an inducible site-specific replication fork barrier. *Cell* **121**(5): 689-702.

Lee, K. Y., I. Yang, J. E. Park, O. R. Baek, K. Y. Chung and H. S. Koo (2007). Developmental stage- and DNA damage-specific functions of *C. elegans* FANCD2. *Biochem Biophys Res Commun* **352**(2): 479-85.

Lehmann, A. R. (2006). Translesion synthesis in mammalian cells. *Exp Cell Res* **312**(14): 2673-6.

Lengsfeld, B. M., A. J. Rattray, V. Bhaskara, R. Ghirlando and T. T. Paull (2007). Sae2 is an endonuclease that processes hairpin DNA cooperatively with the Mre11/Rad50/Xrs2 complex. *Mol Cell* **28**(4): 638-51.

Levitus, M., Q. Waisfisz, B. C. Godthelp, Y. de Vries, S. Hussain, W. W. Wiegant, E. Elghalbzouri-Maghrani, J. Steltenpool, M. A. Rooimans, G. Pals, F. Arwert, C. G. Mathew, M. Z. Zdzienicka, K. Hiom, J. P. De Winter and H. Joenje (2005). The DNA helicase BRIP1 is defective in Fanconi anemia complementation group J. *Nat Genet* **37**(9): 934-5.

Levran, O., C. Attwooll, R. T. Henry, K. L. Milton, K. Neveling, P. Rio, S. D. Batish, R. Kalb, E. Velleuer, S. Barral, J. Ott, J. Petrini, D. Schindler, H. Hanenberg and A. D. Auerbach (2005). The BRCA1-interacting helicase BRIP1 is deficient in Fanconi anemia. *Nat Genet* **37**(9): 931-3.

Li, X., J. Hejna and R. E. Moses (2005). The yeast Snm1 protein is a DNA 5'-exonuclease. *DNA Repair (Amst)* **4**(2): 163-70.

Limbo, O., C. Chahwan, Y. Yamada, R. A. de Bruin, C. Wittenberg and P. Russell (2007). Ctp1 is a cell-cycle-regulated protein that functions with Mre11 complex to control double-strand break repair by homologous recombination. *Mol Cell* **28**(1): 134-46.

Lio, Y. C., A. V. Mazin, S. C. Kowalczykowski and D. J. Chen (2003). Complex formation by the human Rad51B and Rad51C DNA repair proteins and their activities in vitro. *J Biol Chem* **278**(4): 2469-78.

Lisby, M., J. H. Barlow, R. C. Burgess and R. Rothstein (2004). Choreography of the DNA damage response: spatiotemporal relationships among checkpoint and repair proteins. *Cell* **118**(6): 699-713.

Litman, R., M. Peng, Z. Jin, F. Zhang, J. Zhang, S. Powell, P. R. Andreassen and S. B. Cantor (2005). BACH1 is critical for homologous recombination and appears to be the Fanconi anemia gene product FANCJ. *Cancer Cell* **8**(3): 255-65.

Liu, J. and K. J. Marians (1999). PriA-directed assembly of a primosome on D loop DNA. *J Biol Chem* **274**(35): 25033-41.

Liu, Y., J. Y. Masson, R. Shah, P. O'Regan and S. C. West (2004). RAD51C is required for Holliday junction processing in mammalian cells. *Science* **303**(5655): 243-6.

Liu, Y., M. Tarsounas, P. O'Regan and S. C. West (2007). Role of RAD51C and XRCC3 in genetic recombination and DNA repair. *J Biol Chem* **282**(3): 1973-9.

Lloyd, R. G. and G. J. Sharples (1993). Dissociation of synthetic Holliday junctions by *E. coli* RecG protein. *Embo J* **12**(1): 17-22.

Lobachev, K. S., D. A. Gordenin and M. A. Resnick (2002). The Mre11 complex is required for repair of hairpin-capped double-strand breaks and prevention of chromosome rearrangements. *Cell* **108**(2): 183-93.

Lozano, E., A. G. Saez, A. J. Flemming, A. Cunha and A. M. Leroi (2006). Regulation of growth by ploidy in *Caenorhabditis elegans*. *Curr Biol* **16**(5): 493-8.

Lundin, C., K. Erixon, C. Arnaudeau, N. Schultz, D. Jenssen, M. Meuth and T. Helleday (2002). Different roles for nonhomologous end joining and homologous recombination following replication arrest in mammalian cells. *Mol Cell Biol* **22**(16): 5869-78.

MacQueen, A. J., M. P. Colaiacovo, K. McDonald and A. M. Villeneuve (2002). Synapsis-dependent and -independent mechanisms stabilize homolog pairing during meiotic prophase in *C. elegans*. *Genes Dev* **16**(18): 2428-42.

MacQueen, A. J., C. M. Phillips, N. Bhalla, P. Weiser, A. M. Villeneuve and A. F. Dernburg (2005). Chromosome sites play dual roles to establish homologous synapsis during meiosis in *C. elegans*. *Cell* **123**(6): 1037-50.

Magana-Schwencke, N., J. A. Henriques, R. Chanet and E. Moustacchi (1982). The fate of 8-methoxypsoralen photoinduced crosslinks in nuclear and mitochondrial yeast DNA: comparison of wild-type and repair-deficient strains. *Proc Natl Acad Sci U S A* **79**(6): 1722-6.

Malkova, A., M. L. Naylor, M. Yamaguchi, G. Ira and J. E. Haber (2005). RAD51-dependent break-induced replication differs in kinetics and checkpoint responses from RAD51-mediated gene conversion. *Mol Cell Biol* **25**(3): 933-44.

Mankouri, H. W., H. P. Ngo and I. D. Hickson (2007). Shu proteins promote the formation of homologous recombination intermediates that are processed by Sgs1-Rmi1-Top3. *Mol Biol Cell* **18**(10): 4062-73.

Marnett, L. J. and J. P. Plastaras (2001). Endogenous DNA damage and mutation. *Trends Genet* **17**(4): 214-21.

Marti, T. M., E. Hefner, L. Feeney, V. Natale and J. E. Cleaver (2006). H2AX phosphorylation within the G1 phase after UV irradiation depends on nucleotide excision repair and not DNA double-strand breaks. *Proc Natl Acad Sci U S A* **103**(26): 9891-6.

Martin, J. S., N. Winkelmann, M. I. Petalcorin, M. J. McIlwraith and S. J. Boulton (2005). RAD-51-dependent and -independent roles of a *Caenorhabditis elegans* BRCA2-related protein during DNA double-strand break repair. *Mol Cell Biol* **25**(8): 3127-39.

Martin, V., C. Chahwan, H. Gao, V. Blais, J. Wohlschlegel, J. R. Yates, 3rd, C. H. McGowan and P. Russell (2006). Sws1 is a conserved regulator of homologous recombination in eukaryotic cells. *Embo J* **25**(11): 2564-74.

Martinez-Perez, E. and A. M. Villeneuve (2005). HTP-1-dependent constraints coordinate homolog pairing and synapsis and promote chiasma formation during *C. elegans* meiosis. *Genes Dev* **19**(22): 2727-43.

Masson, J. Y., A. Z. Stasiak, A. Stasiak, F. E. Benson and S. C. West (2001). Complex formation by the human RAD51C and XRCC3 recombination repair proteins. *Proc Natl Acad Sci U S A* **98**(15): 8440-6.

Masson, J. Y., M. C. Tarsounas, A. Z. Stasiak, A. Stasiak, R. Shah, M. J. McIlwraith, F. E. Benson and S. C. West (2001). Identification and purification of two distinct complexes containing the five RAD51 paralogs. *Genes Dev* **15**(24): 3296-307.

Mazin, A. V., E. Zaitseva, P. Sung and S. C. Kowalczykowski (2000). Tailed duplex DNA is the preferred substrate for Rad51 protein-mediated homologous pairing. *Embo J* **19**(5): 1148-56.

Mazina, O. M., A. V. Mazin, T. Nakagawa, R. D. Kolodner and S. C. Kowalczykowski (2004). *Saccharomyces cerevisiae* Mer3 helicase stimulates 3'-5' heteroduplex extension by Rad51; implications for crossover control in meiotic recombination. *Cell* **117**(1): 47-56.

Mazloum, N., Q. Zhou and W. K. Holloman (2007). DNA binding, annealing, and strand exchange activities of Brh2 protein from *Ustilago maydis*. *Biochemistry* **46**(24): 7163-73.

Mazloum, N., Q. Zhou and W. K. Holloman (2008). D-loop formation by Brh2 protein of *Ustilago maydis*. *Proc Natl Acad Sci U S A*.

McGlynn, P., R. G. Lloyd and K. J. Marians (2001). Formation of Holliday junctions by regression of nascent DNA in intermediates containing stalled replication forks: RecG stimulates regression even when the DNA is negatively supercoiled. *Proc Natl Acad Sci U S A* **98**(15): 8235-40.

McHugh, P. J., W. R. Sones and J. A. Hartley (2000). Repair of intermediate structures produced at DNA interstrand cross-links in *Saccharomyces cerevisiae*. *Mol Cell Biol* **20**(10): 3425-33.

McKee, A. H. and N. Kleckner (1997). A general method for identifying recessive diploid-specific mutations in *Saccharomyces cerevisiae*, its application to the isolation of mutants blocked at intermediate stages of meiotic prophase and characterization of a new gene SAE2. *Genetics* **146**(3): 797-816.

Meetei, A. R., J. P. de Winter, A. L. Medhurst, M. Wallisch, Q. Waisfisz, H. J. van de Vrugt, A. B. Oostra, Z. Yan, C. Ling, C. E. Bishop, M. E. Hoatlin, H. Joenje and W. Wang (2003). A novel ubiquitin ligase is deficient in Fanconi anemia. *Nat Genet* **35**(2): 165-70.

Meetei, A. R., S. Sechi, M. Wallisch, D. Yang, M. K. Young, H. Joenje, M. E. Hoatlin and W. Wang (2003). A multiprotein nuclear complex connects Fanconi anemia and Bloom syndrome. *Mol Cell Biol* **23**(10): 3417-26.

Memisoglu, A. and L. Samson (2000). Base excision repair in yeast and mammals. *Mutat Res* **451**(1-2): 39-51.

Meniel, V., N. Magana-Schwencke and D. Averbeck (1995). Preferential repair in *Saccharomyces cerevisiae rad* mutants after induction of interstrand cross-links by 8-methoxypsoralen plus UVA. *Mutagenesis* **10**(6): 543-8.

Michel, B., G. Grompone, M. J. Flores and V. Bidnenko (2004). Multiple pathways process stalled replication forks. *Proc Natl Acad Sci U S A* **101**(35): 12783-8.

Miller, K. A., D. Sawicka, D. Barsky and J. S. Albala (2004). Domain mapping of the Rad51 paralog protein complexes. *Nucleic Acids Res* **32**(1): 169-78.

Miller, K. A., D. M. Yoshikawa, I. R. McConnell, R. Clark, D. Schild and J. S. Albala (2002). RAD51C interacts with RAD51B and is central to a larger protein complex in vivo exclusive of RAD51. *J Biol Chem* **277**(10): 8406-11.

Miller, R. D., L. Prakash and S. Prakash (1982). Genetic control of excision of *Saccharomyces cerevisiae* interstrand DNA cross-links induced by psoralen plus near-UV light. *Mol Cell Biol* **2**(8): 939-48.

Modesti, M. and R. Kanaar (2001). Homologous recombination: from model organisms to human disease. *Genome Biol* **2**(5): REVIEWS1014.

Modrich, P. (2006). Mechanisms in eukaryotic mismatch repair. *J Biol Chem* **281**(41): 30305-9.

Mogi, S. and D. H. Oh (2006). gamma-H2AX formation in response to interstrand crosslinks requires XPF in human cells. *DNA Repair (Amst)* **5**(6): 731-40.

Montgomery, M. K., S. Xu and A. Fire (1998). RNA as a target of double-stranded RNA-mediated genetic interference in Caenorhabditis elegans. *Proc Natl Acad Sci U S A* **95**(26): 15502-7.

Moreno-Herrero, F., M. de Jager, N. H. Dekker, R. Kanaar, C. Wyman and C. Dekker (2005). Mesoscale conformational changes in the DNA-repair complex Rad50/Mre11/Nbs1 upon binding DNA. *Nature* **437**(7057): 440-3.

Murphy, C. T., S. A. McCarroll, C. I. Bargmann, A. Fraser, R. S. Kamath, J. Ahringer, H. Li and C. Kenyon (2003). Genes that act downstream of DAF-16 to influence the lifespan of *Caenorhabditis elegans*. *Nature* **424**(6946): 277-83.

Muzzini, D., J. D. Ward, E. Martinez-Perez, P. Plevani, G. Cassata, S. J. Boulton and F. Marini (2008). *hel-308* interacts with *rad-51* and its paralog *rfs-1* during meiotic crossing-over maturation in the nematode *C.elegans*. *Manuscript in preparation.*

Nakagawa, T., H. Flores-Rozas and R. D. Kolodner (2001). The MER3 helicase involved in meiotic crossing over is stimulated by single-stranded DNA-binding proteins and unwinds DNA in the 3' to 5' direction. *J Biol Chem* **276**(34): 31487-93.

Nakagawa, T. and R. D. Kolodner (2002). The MER3 DNA helicase catalyzes the unwinding of holliday junctions. *J Biol Chem* **277**(31): 28019-24.

Nakagawa, T. and H. Ogawa (1999). *The Saccharomyces cerevisiae* MER3 gene, encoding a novel helicase-like protein, is required for crossover control in meiosis. *Embo J* **18**(20): 5714-23.

Nakamura, M., R. Ando, T. Nakazawa, T. Yudazono, N. Tsutsumi, N. Hatanaka, T. Ohgake, F. Hanaoka and T. Eki (2007). Dicer-related *drh-3* gene functions in germ-line development by maintenance of chromosomal integrity in *Caenorhabditis elegans*. *Genes Cells* **12**(9): 997-1010.

New, J. H., T. Sugiyama, E. Zaitseva and S. C. Kowalczykowski (1998). Rad52 protein stimulates DNA strand exchange by Rad51 and replication protein A. *Nature* **391**(6665): 407-10.

Niedernhofer, L. J., J. S. Daniels, C. A. Rouzer, R. E. Greene and L. J. Marnett (2003). Malondialdehyde, a product of lipid peroxidation, is mutagenic in human cells. *J Biol Chem* **278**(33): 31426-33.

Niedernhofer, L. J., G. A. Garinis, A. Raams, A. S. Lalai, A. R. Robinson, E. Appeldoorn, H. Odijk, R. Oostendorp, A. Ahmad, W. van Leeuwen, A. F. Theil, W. Vermeulen, G. T. van der Horst, P. Meinecke, W. J. Kleijer, J. Vijg, N. G. Jaspers and J. H.

Hoeijmakers (2006). A new progeroid syndrome reveals that genotoxic stress suppresses the somatotroph axis. *Nature* **444**(7122): 1038-43.

Niedernhofer, L. J., A. S. Lalai and J. H. Hoeijmakers (2005). Fanconi anemia (cross)linked to DNA repair. *Cell* **123**(7): 1191-8.

Niedernhofer, L. J., H. Odijk, M. Budzowska, E. van Drunen, A. Maas, A. F. Theil, J. de Wit, N. G. Jaspers, H. B. Beverloo, J. H. Hoeijmakers and R. Kanaar (2004). The structure-specific endonuclease Ercc1-Xpf is required to resolve DNA interstrand cross-link-induced double-strand breaks. *Mol Cell Biol* **24**(13): 5776-87.

Niedzwiedz, W., G. Mosedale, M. Johnson, C. Y. Ong, P. Pace and K. J. Patel (2004). The Fanconi anaemia gene FANCC promotes homologous recombination and error-prone DNA repair. *Mol Cell* **15**(4): 607-20.

O'Connor, P. M. and K. W. Kohn (1990). Comparative pharmacokinetics of DNA lesion formation and removal following treatment of L1210 cells with nitrogen mustards. *Cancer Commun* **2**(12): 387-94.

O'Neil, N. J. (2008). Unpublished data.

Ogawa, T., X. Yu, A. Shinohara and E. H. Egelman (1993). Similarity of the yeast RAD51 filament to the bacterial RecA filament. *Science* **259**(5103): 1896-9.

Olive, P. L., J. P. Banath and R. E. Durand (1990). Heterogeneity in radiation-induced DNA damage and repair in tumor and normal cells measured using the "comet" assay. *Radiat Res* **122**(1): 86-94.

Ono, K. and S. Ono (2004). Tropomyosin and troponin are required for ovarian contraction in the *Caenorhabditis elegans* reproductive system. *Mol Biol Cell* **15**(6): 2782-93.

Page, S. L. and R. S. Hawley (2004). The genetics and molecular biology of the synaptonemal complex. *Annu Rev Cell Dev Biol* **20**: 525-58.

Park, H. K., J. S. Yook, H. S. Koo, I. S. Choi and B. Ahn (2002). The *Caenorhabditis elegans* XPA homolog of human XPA. *Mol Cells* **14**(1): 50-5.

Parsons, C. A., P. Baumann, E. Van Dyck and S. C. West (2000). Precise binding of single-stranded DNA termini by human RAD52 protein. *Embo J* **19**(15): 4175-81.

Patel, K. J., V. P. Yu, H. Lee, A. Corcoran, F. C. Thistlethwaite, M. J. Evans, W. H. Colledge, L. S. Friedman, B. A. Ponder and A. R. Venkitaraman (1998). Involvement of Brca2 in DNA repair. *Mol Cell* **1**(3): 347-57.

Peng, M., R. Litman, J. Xie, S. Sharma, R. M. Brosh, Jr. and S. B. Cantor (2007). The FANCJ/MutLalpha interaction is required for correction of the cross-link response in FA-J cells. *Embo J* **26**(13): 3238-49.

Penkner, A., Z. Portik-Dobos, L. Tang, R. Schnabel, M. Novatchkova, V. Jantsch and J. Loidl (2007). A conserved function for a *Caenorhabditis elegans* Com1/Sae2/CtIP protein homolog in meiotic recombination. *Embo J.*

Penkner, A., L. Tang, M. Novatchkova, M. Ladurner, A. Fridkin, Y. Gruenbaum, D. Schweizer, J. Loidl and V. Jantsch (2007). The nuclear envelope protein Matefin/SUN-1 is required for homologous pairing in *C. elegans* meiosis. *Dev Cell* **12**(6): 873-85.

Petalcorin, M. I., J. Sandall, D. B. Wigley and S. J. Boulton (2006). CeBRC-2 stimulates D-loop formation by RAD-51 and promotes DNA single-strand annealing. *J Mol Biol* **361**(2): 231-42.

Petukhova, G., S. Van Komen, S. Vergano, H. Klein and P. Sung (1999). Yeast Rad54 promotes Rad51-dependent homologous DNA pairing via ATP hydrolysis-driven change in DNA double helix conformation. *J Biol Chem* **274**(41): 29453-62.

Phillips, C. M. and A. F. Dernburg (2006). A family of zinc-finger proteins is required for chromosome-specific pairing and synapsis during meiosis in *C. elegans*. *Dev Cell* **11**(6): 817-29.

Phillips, C. M., C. Wong, N. Bhalla, P. M. Carlton, P. Weiser, P. M. Meneely and A. F. Dernburg (2005). HIM-8 binds to the X chromosome pairing center and mediates chromosome-specific meiotic synapsis. *Cell* **123**(6): 1051-63.

Picot, J. (2005). Human cell culture protocols. Totowa, N.J., Humana Press.

Pierce, A. J., R. D. Johnson, L. H. Thompson and M. Jasin (1999). XRCC3 promotes homology-directed repair of DNA damage in mammalian cells. *Genes Dev* **13**(20): 2633-8.

Pinkston, J. M., D. Garigan, M. Hansen and C. Kenyon (2006). Mutations that increase the life span of *C. elegans* inhibit tumor growth. *Science* **313**(5789): 971-5.

Pinto, A. L. and S. J. Lippard (1985). Binding of the antitumor drug cis-diamminedichloroplatinum(II) (cisplatin) to DNA. *Biochim Biophys Acta* **780**(3): 167-80.

Pittman, D. L., L. R. Weinberg and J. C. Schimenti (1998). Identification, characterization, and genetic mapping of Rad51d, a new mouse and human RAD51/RecA-related gene. *Genomics* **49**(1): 103-11.

Polanowska, J., J. S. Martin, T. Garcia-Muse, M. I. Petalcorin and S. J. Boulton (2006). A conserved pathway to activate BRCA1-dependent ubiquitylation at DNA damage sites. *Embo J* **25**(10): 2178-88.

Postow, L., C. Ullsperger, R. W. Keller, C. Bustamante, A. V. Vologodskii and N. R. Cozzarelli (2001). Positive torsional strain causes the formation of a four-way junction at replication forks. *J Biol Chem* **276**(4): 2790-6.

Prakash, S. and L. Prakash (2000). Nucleotide excision repair in yeast. *Mutat Res* **451**(1-2): 13-24.

Prinz, S., A. Amon and F. Klein (1997). Isolation of COM1, a new gene required to complete meiotic double-strand break-induced recombination in *Saccharomyces cerevisiae*. *Genetics* **146**(3): 781-95.

Ramirez, P., L. M. Del Razo, M. C. Gutierrez-Ruiz and M. E. Gonsebatt (2000). Arsenite induces DNA-protein crosslinks and cytokeratin expression in the WRL-68 human hepatic cell line. *Carcinogenesis* **21**(4): 701-6.

Raynard, S., W. Bussen and P. Sung (2006). A double Holliday junction dissolvasome comprising BLM, topoisomerase IIIalpha, and BLAP75. *J Biol Chem* **281**(20): 13861-4.

Reboul, J., P. Vaglio, J. F. Rual, P. Lamesch, M. Martinez, C. M. Armstrong, S. Li, L. Jacotot, N. Bertin, R. Janky, T. Moore, J. R. Hudson, Jr., J. L. Hartley, M. A. Brasch, J. Vandenhaute, S. Boulton, G. A. Endress, S. Jenna, E. Chevet, V. Papasotiropoulos, P. P. Tolias, J. Ptacek, M. Snyder, R. Huang, M. R. Chance, H. Lee, L. Doucette-Stamm, D. E. Hill and M. Vidal (2003). *C. elegans* ORFeome version 1.1: experimental verification of the genome annotation and resource for proteome-scale protein expression. *Nat Genet* **34**(1): 35-41.

Reddy, G., E. I. Golub and C. M. Radding (1997). Human Rad52 protein promotes single-strand DNA annealing followed by branch migration. *Mutat Res* **377**(1): 53-9.

Reddy, K. C. and A. M. Villeneuve (2004). *C. elegans* HIM-17 links chromatin modification and competence for initiation of meiotic recombination. *Cell* **118**(4): 439-52.

Reid, S., D. Schindler, H. Hanenberg, K. Barker, S. Hanks, R. Kalb, K. Neveling, P. Kelly, S. Seal, M. Freund, M. Wurm, S. D. Batish, F. P. Lach, S. Yetgin, H. Neitzel, H. Ariffin, M. Tischkowitz, C. G. Mathew, A. D. Auerbach and N. Rahman (2007). Biallelic mutations in PALB2 cause Fanconi anemia subtype FA-N and predispose to childhood cancer. *Nat Genet* **39**(2): 162-4.

Ridpath, J. R., A. Nakamura, K. Tano, A. M. Luke, E. Sonoda, H. Arakawa, J. M. Buerstedde, D. A. Gillespie, J. E. Sale, M. Yamazoe, D. K. Bishop, M. Takata, S. Takeda, M. Watanabe, J. A. Swenberg and J. Nakamura (2007). Cells deficient in the FANC/BRCA pathway are hypersensitive to plasma levels of formaldehyde. *Cancer Res* **67**(23): 11117-22.

Rijkers, T., J. Van Den Ouweland, B. Morolli, A. G. Rolink, W. M. Baarends, P. P. Van Sloun, P. H. Lohman and A. Pastink (1998). Targeted inactivation of mouse RAD52 reduces homologous recombination but not resistance to ionizing radiation. *Mol Cell Biol* **18**(11): 6423-9.

Rinaldo, C., P. Bazzicalupo, S. Ederle, M. Hilliard and A. La Volpe (2002). Roles for Caenorhabditis elegans rad-51 in meiosis and in resistance to ionizing radiation during development. *Genetics* **160**(2): 471-9.

Robert, V. and J. L. Bessereau (2007). Targeted engineering of the *Caenorhabditis elegans* genome following Mos1-triggered chromosomal breaks. *Embo J* **26**(1): 170-83.

Robison, J. G., J. Elliott, K. Dixon and G. G. Oakley (2004). Replication protein A and the Mre11.Rad50.Nbs1 complex co-localize and interact at sites of stalled replication forks. *J Biol Chem* **279**(33): 34802-10.

Robu, M. E., R. B. Inman and M. M. Cox (2001). RecA protein promotes the regression of stalled replication forks in vitro. *Proc Natl Acad Sci U S A* **98**(15): 8211-8.

Rodrigue, A., M. Lafrance, M. C. Gauthier, D. McDonald, M. Hendzel, S. C. West, M. Jasin and J. Y. Masson (2006). Interplay between human DNA repair proteins at a unique double-strand break in vivo. *Embo J* **25**(1): 222-31.

Rogakou, E. P., D. R. Pilch, A. H. Orr, V. S. Ivanova and W. M. Bonner (1998). DNA double-stranded breaks induce histone H2AX phosphorylation on serine 139. *J Biol Chem* **273**(10): 5858-68.

Roman, L. J., A. K. Eggleston and S. C. Kowalczykowski (1992). Processivity of the DNA helicase activity of *Escherichia coli* recBCD enzyme. *J Biol Chem* **267**(6): 4207-14.

Sarkar, S., A. A. Davies, H. D. Ulrich and P. J. McHugh (2006). DNA interstrand crosslink repair during G1 involves nucleotide excision repair and DNA polymerase zeta. *Embo J* **25**(6): 1285-94.

Sartori, A. A., C. Lukas, J. Coates, M. Mistrik, S. Fu, J. Bartek, R. Baer, J. Lukas and S. P. Jackson (2007). Human CtIP promotes DNA end resection. *Nature* **450**(7169): 509-14.

Sedgwick, B., P. A. Bates, J. Paik, S. C. Jacobs and T. Lindahl (2007). Repair of alkylated DNA: recent advances. *DNA Repair (Amst)* **6**(4): 429-42.

Sharan, S. K., M. Morimatsu, U. Albrecht, D. S. Lim, E. Regel, C. Dinh, A. Sands, G. Eichele, P. Hasty and A. Bradley (1997). Embryonic lethality and radiation hypersensitivity mediated by Rad51 in mice lacking Brca2. *Nature* **386**(6627): 804-10.

Sharples, G. J. and D. R. Leach (1995). Structural and functional similarities between the SbcCD proteins of *Escherichia coli* and the RAD50 and MRE11 (RAD32) recombination and repair proteins of yeast. *Mol Microbiol* **17**(6): 1215-7.

Shinohara, A., H. Ogawa and T. Ogawa (1992). Rad51 protein involved in repair and recombination in *S. cerevisiae* is a RecA-like protein. *Cell* **69**(3): 457-70.

Shinohara, A. and T. Ogawa (1998). Stimulation by Rad52 of yeast Rad51-mediated recombination. *Nature* **391**(6665): 404-7.

Shinohara, A., M. Shinohara, T. Ohta, S. Matsuda and T. Ogawa (1998). Rad52 forms ring structures and co-operates with RPA in single-strand DNA annealing. *Genes Cells* **3**(3): 145-56.

Shor, E., J. Weinstein and R. Rothstein (2005). A genetic screen for *top3* suppressors in *Saccharomyces cerevisiae* identifies *SHU1*, *SHU2*, *PSY3* and *CSM2*: four genes involved in error-free DNA repair. *Genetics* **169**(3): 1275-89.

Shu, Z., S. Smith, L. Wang, M. C. Rice and E. B. Kmiec (1999). Disruption of muREC2/RAD51L1 in mice results in early embryonic lethality which can Be partially rescued in a p53(-/-) background. *Mol Cell Biol* **19**(12): 8686-93.

Sigurdsson, S., S. Van Komen, W. Bussen, D. Schild, J. S. Albala and P. Sung (2001). Mediator function of the human Rad51B-Rad51C complex in Rad51/RPA-catalyzed DNA strand exchange. *Genes Dev* **15**(24): 3308-18.

Sladek, F. M., A. Melian and P. Howard-Flanders (1989). Incision by UvrABC excinuclease is a step in the path to mutagenesis by psoralen crosslinks in *Escherichia coli*. *Proc Natl Acad Sci U S A* **86**(11): 3982-6.

Sogo, J. M., M. Lopes and M. Foiani (2002). Fork reversal and ssDNA accumulation at stalled replication forks owing to checkpoint defects. *Science* **297**(5581): 599-602.

Somesh, B. P., J. Reid, W. F. Liu, T. M. Sogaard, H. Erdjument-Bromage, P. Tempst and J. Q. Svejstrup (2005). Multiple mechanisms confining RNA polymerase II ubiquitylation to polymerases undergoing transcriptional arrest. *Cell* **121**(6): 913-23.

Song, B. and P. Sung (2000). Functional interactions among yeast Rad51 recombinase, Rad52 mediator, and replication protein A in DNA strand exchange. *J Biol Chem* **275**(21): 15895-904.

Sonoda, E., M. S. Sasaki, J. M. Buerstedde, O. Bezzubova, A. Shinohara, H. Ogawa, M. Takata, Y. Yamaguchi-Iwai and S. Takeda (1998). Rad51-deficient vertebrate cells accumulate chromosomal breaks prior to cell death. *Embo J* **17**(2): 598-608.

Stasiak, A. Z., E. Larquet, A. Stasiak, S. Muller, A. Engel, E. Van Dyck, S. C. West and E. H. Egelman (2000). The human Rad52 protein exists as a heptameric ring. *Curr Biol* **10**(6): 337-40.

Stewart, L., M. R. Redinbo, X. Qiu, W. G. Hol and J. J. Champoux (1998). A model for the mechanism of human topoisomerase I. *Science* **279**(5356): 1534-41.

Strange, K., M. Christensen and R. Morrison (2007). Primary culture of *Caenorhabditis elegans* developing embryo cells for electrophysiological, cell biological and molecular studies. *Nat Protoc* **2**(4): 1003-12.

Strumberg, D., A. A. Pilon, M. Smith, R. Hickey, L. Malkas and Y. Pommier (2000). Conversion of topoisomerase I cleavage complexes on the leading strand of ribosomal DNA into 5'-phosphorylated DNA double-strand breaks by replication runoff. *Mol Cell Biol* **20**(11): 3977-87.

Sugawara, N. and J. E. Haber (1992). Characterization of double-strand break-induced recombination: homology requirements and single-stranded DNA formation. *Mol Cell Biol* **12**(2): 563-75.

Sugawara, N., G. Ira and J. E. Haber (2000). DNA length dependence of the single-strand annealing pathway and the role of *Saccharomyces cerevisiae* RAD59 in double-strand break repair. *Mol Cell Biol* **20**(14): 5300-9.

Sugawara, N., F. Paques, M. Colaiacovo and J. E. Haber (1997). Role of *Saccharomyces cerevisiae* Msh2 and Msh3 repair proteins in double-strand break-induced recombination. *Proc Natl Acad Sci U S A* **94**(17): 9214-9.

Sugawara, N., X. Wang and J. E. Haber (2003). In vivo roles of Rad52, Rad54, and Rad55 proteins in Rad51-mediated recombination. *Mol Cell* **12**(1): 209-19.

Sugiyama, T., J. H. New and S. C. Kowalczykowski (1998). DNA annealing by RAD52 protein is stimulated by specific interaction with the complex of replication protein A and single-stranded DNA. *Proc Natl Acad Sci U S A* **95**(11): 6049-54.

Sung, P. (1994). Catalysis of ATP-dependent homologous DNA pairing and strand exchange by yeast RAD51 protein. *Science* **265**(5176): 1241-3.

Sung, P. (1997). Function of yeast Rad52 protein as a mediator between replication protein A and the Rad51 recombinase. *J Biol Chem* **272**(45): 28194-7.

Sung, P., S. N. Guzder, L. Prakash and S. Prakash (1996). Reconstitution of TFIIH and requirement of its DNA helicase subunits, Rad3 and Rad25, in the incision step of nucleotide excision repair. *J Biol Chem* **271**(18): 10821-6.

Sunters, A., C. J. Springer, K. D. Bagshawe, R. L. Souhami and J. A. Hartley (1992). The cytotoxicity, DNA crosslinking ability and DNA sequence selectivity of the aniline mustards melphalan, chlorambucil and 4-[bis(2-chloroethyl)amino] benzoic acid. *Biochem Pharmacol* **44**(1): 59-64.

Takata, M., M. S. Sasaki, S. Tachiiri, T. Fukushima, E. Sonoda, D. Schild, L. H. Thompson and S. Takeda (2001). Chromosome instability and defective recombinational repair in knockout mutants of the five Rad51 paralogs. *Mol Cell Biol* **21**(8): 2858-66.

Takeuchi, Y., T. Horiuchi and T. Kobayashi (2003). Transcription-dependent recombination and the role of fork collision in yeast rDNA. *Genes Dev* **17**(12): 1497-506.

Tarsounas, M., P. Munoz, A. Claas, P. G. Smiraldo, D. L. Pittman, M. A. Blasco and S. C. West (2004). Telomere maintenance requires the RAD51D recombination/repair protein. *Cell* **117**(3): 337-47.

Thacker, J. (2005). The RAD51 gene family, genetic instability and cancer. *Cancer Lett* **219**(2): 125-35.

Thorslund, T., F. Esashi and S. C. West (2007). Interactions between human BRCA2 protein and the meiosis-specific recombinase DMC1. *Embo J* **26**(12): 2915-22.

Tijsterman, M., J. Pothof and R. H. Plasterk (2002). Frequent germline mutations and somatic repeat instability in DNA mismatch-repair-deficient *Caenorhabditis elegans*. *Genetics* **161**(2): 651-60.

Till, B. J., S. H. Reynolds, E. A. Greene, C. A. Codomo, L. C. Enns, J. E. Johnson, C. Burtner, A. R. Odden, K. Young, N. E. Taylor, J. G. Henikoff, L. Comai and S. Henikoff (2003). Large-scale discovery of induced point mutations with high-throughput TILLING. *Genome Res* **13**(3): 524-30.

Trujillo, K. M., D. H. Roh, L. Chen, S. Van Komen, A. Tomkinson and P. Sung (2003). Yeast Xrs2 binds DNA and helps target Rad50 and Mre11 to DNA ends. *J Biol Chem* **278**(49): 48957-64.

Tsai, C. J., S. A. Kim and G. Chu (2007). Cernunnos/XLF promotes the ligation of mismatched and noncohesive DNA ends. *Proc Natl Acad Sci U S A* **104**(19): 7851-6.

Tsubouchi, H. and H. Ogawa (1998). A novel *mre11* mutation impairs processing of double-strand breaks of DNA during both mitosis and meiosis. *Mol Cell Biol* **18**(1): 260-8.

Umezu, K., N. W. Chi and R. D. Kolodner (1993). Biochemical interaction of the *Escherichia coli* RecF, RecO, and RecR proteins with RecA protein and single-stranded DNA binding protein. *Proc Natl Acad Sci U S A* **90**(9): 3875-9.

Umezu, K. and R. D. Kolodner (1994). Protein interactions in genetic recombination in *Escherichia coli*. Interactions involving RecO and RecR overcome the inhibition of RecA by single-stranded DNA-binding protein. *J Biol Chem* **269**(47): 30005-13.

van Gool, A. J., R. Verhage, S. M. Swagemakers, P. van de Putte, J. Brouwer, C. Troelstra, D. Bootsma and J. H. Hoeijmakers (1994). RAD26, the functional *S. cerevisiae* homolog of the Cockayne syndrome B gene ERCC6. *Embo J* **13**(22): 5361-9.

Wakasugi, M. and A. Sancar (1998). Assembly, subunit composition, and footprint of human DNA repair excision nuclease. *Proc Natl Acad Sci U S A* **95**(12): 6669-74.

Walhout, A. J., G. F. Temple, M. A. Brasch, J. L. Hartley, M. A. Lorson, S. van den Heuvel and M. Vidal (2000). GATEWAY recombinational cloning: application to the cloning of large numbers of open reading frames or ORFeomes. *Methods Enzymol* **328**: 575-92.

Wang, W. (2007). Emergence of a DNA-damage response network consisting of Fanconi anaemia and BRCA proteins. *Nat Rev Genet* **8**(10): 735-48.

Webb, B. L., M. M. Cox and R. B. Inman (1997). Recombinational DNA repair: the RecF and RecR proteins limit the extension of RecA filaments beyond single-strand DNA gaps. *Cell* **91**(3): 347-56.

West, S. C. (2008). Personal communication.

West, S. C., E. Cassuto and P. Howard-Flanders (1981). recA protein promotes homologous-pairing and strand-exchange reactions between duplex DNA molecules. *Proc Natl Acad Sci U S A* **78**(4): 2100-4.

West, S. C. and B. Connolly (1992). Biological roles of the *Escherichia coli* RuvA, RuvB and RuvC proteins revealed. *Mol Microbiol* **6**(19): 2755-9.

Weterings, E. and D. J. Chen (2008). The endless tale of non-homologous end-joining. *Cell Res* **18**(1): 114-24.

Whitby, M. C., L. Ryder and R. G. Lloyd (1993). Reverse branch migration of Holliday junctions by RecG protein: a new mechanism for resolution of intermediates in recombination and DNA repair. *Cell* **75**(2): 341-50.

Whitby, M. C., S. D. Vincent and R. G. Lloyd (1994). Branch migration of Holliday junctions: identification of RecG protein as a junction specific DNA helicase. *Embo J* **13**(21): 5220-8.

Wicky, C., A. Alpi, M. Passannante, A. Rose, A. Gartner and F. Muller (2004). Multiple genetic pathways involving the *Caenorhabditis elegans* Bloom's syndrome genes *him-6*, *rad-51*, and *top-3* are needed to maintain genome stability in the germ line. *Mol Cell Biol* **24**(11): 5016-27.

Wiese, C., D. W. Collins, J. S. Albala, L. H. Thompson, A. Kronenberg and D. Schild (2002). Interactions involving the Rad51 paralogs Rad51C and XRCC3 in human cells. *Nucleic Acids Res* **30**(4): 1001-8.

Wiese, C., J. M. Hinz, R. S. Tebbs, P. B. Nham, S. S. Urbin, D. W. Collins, L. H. Thompson and D. Schild (2006). Disparate requirements for the Walker A and B ATPase motifs of human RAD51D in homologous recombination. *Nucleic Acids Res* **34**(9): 2833-43.

Wiltzius, J. J., M. Hohl, J. C. Fleming and J. H. Petrini (2005). The Rad50 hook domain is a critical determinant of Mre11 complex functions. *Nat Struct Mol Biol* **12**(5): 403-7.

Wojewodzka, M., I. Buraczewska and M. Kruszewski (2002). A modified neutral comet assay: elimination of lysis at high temperature and validation of the assay with anti-single-stranded DNA antibody. *Mutat Res* **518**(1): 9-20.

Wong, A. K., R. Pero, P. A. Ormonde, S. V. Tavtigian and P. L. Bartel (1997). RAD51 interacts with the evolutionarily conserved BRC motifs in the human breast cancer susceptibility gene brca2. *J Biol Chem* **272**(51): 31941-4.

Wu, L. and I. D. Hickson (2003). The Bloom's syndrome helicase suppresses crossing over during homologous recombination. *Nature* **426**(6968): 870-4.

Xia, B., J. C. Dorsman, N. Ameziane, Y. de Vries, M. A. Rooimans, Q. Sheng, G. Pals, A. Errami, E. Gluckman, J. Llera, W. Wang, D. M. Livingston, H. Joenje and J. P. de Winter (2007). Fanconi anemia is associated with a defect in the BRCA2 partner PALB2. *Nat Genet* **39**(2): 159-61.

Yamaguchi-Iwai, Y., E. Sonoda, J. M. Buerstedde, O. Bezzubova, C. Morrison, M. Takata, A. Shinohara and S. Takeda (1998). Homologous recombination, but not DNA repair, is reduced in vertebrate cells deficient in RAD52. *Mol Cell Biol* **18**(11): 6430-5.

Yang, H., Q. Li, J. Fan, W. K. Holloman and N. P. Pavletich (2005). The BRCA2 homologue Brh2 nucleates RAD51 filament formation at a dsDNA-ssDNA junction. *Nature* **433**(7026): 653-7.

Yanowitz, J. (2008). Genome Integrity Is Regulated by the C. elegans Rad51D homologue, rfs-1. *Genetics*.

Yokoyama, H., N. Sarai, W. Kagawa, R. Enomoto, T. Shibata, H. Kurumizaka and S. Yokoyama (2004). Preferential binding to branched DNA strands and strand-annealing activity of the human Rad51B, Rad51C, Rad51D and Xrcc2 protein complex. *Nucleic Acids Res* **32**(8): 2556-65.

Yonetani, Y., H. Hochegger, E. Sonoda, S. Shinya, H. Yoshikawa, S. Takeda and M. Yamazoe (2005). Differential and collaborative actions of Rad51 paralog proteins in cellular response to DNA damage. *Nucleic Acids Res* **33**(14): 4544-52.

Youds, J. L., L. J. Barber, J. D. Ward, S. J. Collis, N. J. O'Neil, S. J. Boulton and A. M. Rose (2008). DOG-1 Is the Caenorhabditis elegans BRIP1/FANCJ Homologue and Functions in Interstrand Cross-Link Repair. *Mol Cell Biol* **28**(5): 1470-1479.

Youds, J. L., N. J. O'Neil and A. M. Rose (2006). Homologous recombination is required for genome stability in the absence of DOG-1 in *Caenorhabditis elegans*. *Genetics* **173**(2): 697-708.

Zalevsky, J., A. J. MacQueen, J. B. Duffy, K. J. Kemphues and A. M. Villeneuve (1999). Crossing over during *Caenorhabditis elegans* meiosis requires a conserved MutS-based pathway that is partially dispensable in budding yeast. *Genetics* **153**(3): 1271-83.

Zdraveski, Z. Z., J. A. Mello, M. G. Marinus and J. M. Essigmann (2000). Multiple pathways of recombination define cellular responses to cisplatin. *Chem Biol* **7**(1): 39-50.

Zetka, M. (2007). Personal communication.

Zetka, M. C., I. Kawasaki, S. Strome and F. Muller (1999). Synapsis and chiasma formation in *Caenorhabditis elegans* require HIM-3, a meiotic chromosome core component that functions in chromosome segregation. *Genes Dev* **13**(17): 2258-70.

Zhang, N., X. Lu, X. Zhang, C. A. Peterson and R. J. Legerski (2002). hMutSbeta is required for the recognition and uncoupling of psoralen interstrand cross-links in vitro. *Mol Cell Biol* **22**(7): 2388-97.

Zwelling, L. A., T. Anderson and K. W. Kohn (1979). DNA-protein and DNA interstrand cross-linking by cis- and trans-platinum(II) diamminedichloride in L1210 mouse leukemia cells and relation to cytotoxicity. *Cancer Res* **39**(2 Pt 1): 365-9.

Appendix

Oligonucleotides used for this study (see following pages)

Table 8. Oligonucleotides used for PCR

Name	Sequence 5'-3'	Use	Product size	PCR program
atl-1 b atl-1 c	gagtcaactgtcttggctca ttcgtcccgtctatagacaa	Nested PCR-*atl-1(tm853)* genotyping-outer primer set	b+c then a+d Wt-2.5 kb; *tm853*-1.7kb	EL3 (55°C annealing, three minute extension)
atl-1 a atl-1 d	gaaacgtgtatcccatcgaa cgagtcatcgagagctactt	Nested PCR-*atl-1(tm853)* genotyping-inner primer set		"
brc-1 KO E1 brc-1 KO E2	tttcggtggcgccacatgga ctccgtagcttgaagtctca	Nested PCR-*brc-1(tm1145)* genotyping-outer primer set	E1+E2 then I1+I2 Wt-1.47 kb; *tm1145*-797 bp	KO-FCD-2 (55°C annealing, 2.5 minute extension)
brc-1 KO I1 brc-1 KO I2	tgtcgcatcgtcggcattaa aatataggcaccggcgggga	Nested PCR-*brc-1(tm1145)* genotyping-inner primer set		"
brc-1 KO E3 brc-1 KO I3	ctatagagtccagttttcca cgcagtccgctatgattttc	Nested PCR- Detecting Wt gene to identify homozygotes	E2+E3 then I2+I3: Wt 823 bp; *tm1145*-no product	"
daf-16 E1 daf-16 E2	acatagacgatttcgaaaagt acgacgatccaggaatcgaga	Nested PCR-*daf-16(mu86)* genotyping-outer primer set	E1+E2 then I1+I2 *mu86*-739 bp; Wt too large (11 720 bp)	KO-FCD-2 (55°C annealing, 2.5 minute extension)
daf-16 I1 daf-16 I2	tgaaaaatttgacgctcacct cggaaagatgatggaacgtta	Nested PCR-*daf-16(mu86)* genotyping-inner primer set		"
daf-16 E3 daf-16 I3	ggctttgaggtcttgattgct agaaaaagtgagaaatgcgtc	Nested PCR- Detecting Wt gene to identify homozygotes	E1+E3 then I1+I3 Wt-970 bp; *mu86*-no product	"

Underlines in the oligo sequence denote added restriction enzyme recognition sites, T7 RNA polymerase binding sites, and Gateway recombinational cloning sites.

Table 8. continued

Name	Sequence 5'-3'	Use	Product size	PCR program
dog-1 E1	tcgttcggtaattctcaggg	Nested PCR-*dog-1(gk10)*	E1+E2 then I1+I2	KO-FCD-2 (55°C annealing,
dog-1 E2	cgcggtgaaaatttgttttt	genotyping-outer primer set	Wt-3.4 kb; *gk10*- 1 kb	4 minute extension)
dog-1 I1	tgtccattgggcacagagta	Nested PCR-*dog-1(gk10)*		"
dog-1 I2	gttgtgaaagaggagcagcc	genotyping-inner primer set		
dog-1 E3	agaattccgtggacatcttc	Nested PCR- Detecting Wt gene	E1+E3 then I1+I3	KO-FCD-2 (55°C annealing,
dog-1 I3	aacacctgatccttgagatg	to identify homozygotes	Wt-1.1 kb; *gk10*-no product	2.5 minute extension)
him-6 E1	aatggtcacgatgaagagcc	Nested PCR-*him-6(ok412)*	E1+E2 then I1+I2	KO-FCD-2 (55°C annealing,
him-6 E2	accgaatatagccgttcgtg	genotyping-outer primer set	Wt-3.2 kb; *ok412*-1.5 kb	3.5 minute extension)
him-6 I1	atcgaccatcagagaatccg	Nested PCR-*him-6(ok412)*		"
him-6 I2	tgcatcctgctctgacattc	genotyping-inner primer set		
him-6 E3	gctcaggaaatccgtctata	Nested PCR- Detecting Wt gene	E2+E3 then I2+I3:	KO-FCD-2 (55°C annealing,
him-6 I3	ttttcatcagctcctttgtt	to identify homozygotes	Wt-1.7 kb; *ok412*-no product	2.5 minute extension)
mus-81 E1	cgctccacgatcaatagaga	Nested PCR-*mus-81(tm1937)*	E1+E2 then I1+I2	KO-FCD-2 (55°C annealing,
mus-81 E2	catcagctgtcggacccaag	genotyping-outer primer set	Wt-2.1 kb; *tm1937*-878 bp	2.5 minute extension)
mus-81 I1	aggtatttggcagacttacc	Nested PCR-*mus-81(tm1937)*		"
mus-81 I2	ggctgaatggaacacccgaa	genotyping-inner primer set		
mus-81 E3	aaattccaacatcaagagca	Nested PCR- Detecting Wt gene	E2+E3 then I2+I3:	"
mus-81 I3	attcgagattctgacaattg	to identify homozygotes	Wt-1619 bp; *tm1937*-no product	

Table 8. continued

Name	Sequence 5'-3'	Use	Product size	PCR program
rip-1 E1 rip-1 E2	acctcggcgttgttcagtgt ccgattcgtaacggattcac	Nested PCR-*rip-1(tm2948)* genotyping-outer primer set	E1+E2 then I1+I2: Wt-1146 bp; *tm2948*-478 bp	KO-FCD-2 (55°C annealing, 2.5 minute extension)
rip-1 I1 rip-1 I2	gtagtacgcgaggtggccta ggccacactcagagtagatc	Nested PCR-*rip-1(tm2948)* genotyping-inner primer set		"
rip-1 E3 rip-1 I3	tttcattttcagaatccctg gcgctctgcgaagaattcgc	Nested PCR- Detecting Wt gene to identify homozygotes	E1+E3 then I1+I3: Wt-594 bp; *tm2948*-no product	"
rfs-1 KO outer-L rfs-1 KO outer-R	cttccaaatcagcagcaaca tctggttgtcgaatgagcag	Nested PCR-*rfs-1(ok1372)*	outer L+R then inner L+R: Wt-2.2 kb; *ok1372*-1023 bp	KO-FCD-2 (55°C annealing, 2.5 minute extension)
rfs-1 KO inner-L rfs-1 KO inner-R	ttgcacaaatcgctaatcca tgggagtcttgtagtgggct	Nested PCR-*rfs-1(ok1372)*		"
rfs-1 cDNA-F rfs-1 cDNA-R1	gctatacatatggatccttctgaga atgtat gcctcgagtcattccactgctttga gtcctc	Nested PCR- Detecting Wt gene to identify homozygotes. Heterozygote product runs as doublet.	outer L+R then cDNA F+R: Wt-900bp; *ok1372*-1000 bp	"
spo-11 E1 spo-11 E2b	cgtgtttcccaagatgctc ctccattctctgcctctcctgga	Nested PCR-*spo-11(ok79)* genotyping-outer primer set	E1+E2b then I1+I2: Wt-2.9 kb; *ok79*-1.6 kb	KO-FCD-2 (55°C annealing, four minute extension)
spo-11 I1 spo-11 I2	ccgaacagcatattgaagagg gcgcatataaaacacggagac	Nested PCR-*spo-11(ok79)* genotyping-inner primer set		KO-FCD-2 (55°C annealing, three minute extension)
spo-11 E3 spo-11 I3	tcatttttttcttaaactagc tctgatatggtctatatctac	Nested PCR- Detecting Wt gene to identify homozygotes	E2b+E3 then I2+I3: Wt-516 bp; *ok79*-no product	KO-FCD-2 (55°C annealing, 2.5 minute extension)

Table 8. continued

Name	Sequence 5'-3'	Use	Product size	PCR program
syp-2 E1	tcgcgaaaaagagcacaa	Nested PCR-*syp-2(ok307)*	E1+E2 then I1+I2:	KO-FCD-2 (55°C annealing,
syp-2 E2	gtattttaatttgtcgggaa	genotyping-outer primer set	Wt-1225 bp; *ok307*-923 bp	2.5 minute extension)
syp-2 I1	cagaccaacacatggaaa	Nested PCR-*syp-2(ok307)*		"
syp-2 I2	gagtaaaaggaaactacgc	genotyping-inner primer set		
xpa-1 E1	tgagcgaggagaaagagagc	Nested PCR-*xpa-1(ok698)*	E1+E2 then I1+I2:	KO-FCD-2 (55°C annealing,
xpa-1 E2	aaaaacgacacgataacggc	genotyping-outer primer set	Wt-2132 bp; *ok698*-1218 bp	2.5 minute extension)
xpa-1 I1	agatagccggaatagctggc	Nested PCR-*xpa-1(ok698)*		
xpa-1 I2	ctggagccaatccaactgat	genotyping-inner primer set		
xpa-1 E3	cgagttctggaagtgcatgg	Nested PCR- Detecting Wt gene	E2+E3 then I2+I3:	"
xpa-1 I3	gacctcatactcacgaattc	to identify homozygotes	Wt-542 bp; *ok698*-no product	
NON50	ggacagtactctcggagatt	*him-9/xpf-1(e1487)* genotyping	NON50+NON53+NON87 triplex PCR	HIM-9/XPF (58°C annealing,
NON53	cgaactgtatcaaattggtctg	triplex PCR. Heterozygote	Wt-1 kb (NON50+53)	90 second extension)
NON87	cacattgtccgcttgtgtc	product will run as a doublet	*him-9(e1487)*-750 bp (NON50+NON87)	
vab-1 E1	cgattccaacaattggtaaatacc	Monitoring stability of	E1+E2 then I1+I2	vab-1 ext (58°C annealing,
vab-1 E2	aatatttgctaaacctattgttgcc	polyG/C tract in vab-1 locus	499 bp	90 second extension)
vab-1 I1	cgacgaaaaatgcagaatttggc			vab-1 ext (62°C annealing,
vab-1 I2	aggtgtgtgtgcatacctccg			60 second extension)

Table 8. continued

Name	Sequence 5'-3'	Use	Product size	PCR program
GW-stp-F	ggggacaagtttgtacaaaaaagcaggctggtagtagccctagtagtagt agccctagtag	Introducing stop codons to end of Gateway destination vectors to create expression controls.	~90 bp	EL1 (55°C annealing, one minute extension)
GW-stp-R	ggggaccactttgtacaagaaagctgggtcctactactagggctactacta ctagggctacta			
C30A5.3 GW-F	ggggacaagtttgtacaaaaaagcaggctgacggccgctacagaaaa	Gateway cloning C30A5.3 cDNA into an entry vector.	672 bp	EL1 (55°C annealing, one minute extension)
C30A5.3 GW-R	ggggaccactttgtacaagaaagctgggattgaaccgttgtttgttgttgt			
BamHI RIP-1 F	gcgcggatcctcagaatcgtgcaattcccta	Conventional cloning *rip-1* cDNA	630 bp	EL1 (55°C annealing, one minute extension)
XhoI RIP-1 R	gcgcctcgagctaaaaacaatttgaaaattttt			
top-3 RNAi-F	taatacgactcactatagggaaaagagccttatttgtggccg	Generating double stranded *top-3* transcription.	2.28 kb	EL3 (55°C annealing, three minutes extension)
top-3 RNAi-R	taatacgactcactatagggcccatttaaagaaattacatttttcag			
AD	cgcgtttggaatcactacaggg	Identifying Y2H interactors.		EL3 (55°C annealing, three minute extension)
Term	ggagacttgaccaaacctctggcg			
DB-B1	tagtaacaaaggtcaaagacagttgactgtatcgtcgaggttgtacaaaaa agcaggct	Universal Gateway primers.		EL programs (55°C annealing, one minute/kb extension)
B2-Term	aaatcataaatcataagaaattcgcccggaattagcttggttgtacaagaaa gctgggt	Monitoring cloning into entry vectors.		
M13 -21 Forward	tgtaaaacgacggccagt	Sequencing Gateway entry clones.		Sequencing (55°C annealing, four minute extension)
M13 reverse	caggaaacagctatgacc			

Underlines in the oligo sequence denote added restriction enzyme recognition sites, T7 RNA polymerase binding sites, and Gateway recombinational cloning sites.

Table 8. continued

Name	Sequence 5'-3'	Use
rfs-1 1 (1-19) F	ggggacaagtttgtacaaaa aagcaggctggatggatccttctgagaatgt	RFS-1 Y2H domain analysis. Fragments were generated through pairwise combinations of forward primers (1, 2, 4 and 6) and reverse primers (3, 5, 7, 8). The DNA sequence that the oligos recognize are in parentheses. Fragments were Gateway cloned into entry vectors, then transferred into Y2H vectors.
rfs-1 2 (181-200) F	ggggacaagtttgtacaaaaaagcaggctgg tactcatttgcggcgaaatt	
rfs-1 4 (361-380) F	ggggacaagtttgtacaaaaaagcaggctgg gattctttaactcgattttt	
rfs-1 6 (541-560) F	ggggacaagtttgtacaaaaaagcaggctgg attacacactggcgtgggta	
rfs-1 3 (181-201) R	ggggaccactttgtacaagaaagctgggtcctaaaatttcgccgcaaatgagta	
rfs-1 5 (361-381) R	ggggaccactttgtacaagaaagctgggtcctacaaaaatcgagttaaagaatc	
rfs-1 7 (541-561) R	ggggaccactttgtacaagaaagctgggtcctagtacccacgccagtgtgtaat	
rfs-1 8 (735-715) R	ggggaccactttgtacaagaaagctgggtcctattccactgctttgagtcctcg	
R01 1 (1-20) F	ggggacaagtttgtacaaaa aagcaggctggatgtcagaatcgtgcaattc	RIP-1 Y2H domain analysis. Fragments were generated through pairwise combinations of forward primers (1, 2, 4 and 6) and reverse primers (3, 5, 7, 8). The DNA sequence that the oligos recognize are in parentheses. Fragments were Gateway cloned into entry vectors, then transferred into Y2H vectors.
R01 2 (151-170) F	ggggacaagtttgtacaaaa aagcaggctgggaaatcgacgtggagttctc	
R01 4 (301-320) F	ggggacaagtttgtacaaaa aagcaggctggatcccgcaggactgcccgga	
R01 6 (451-470) F	ggggacaagtttgtacaaaa aagcaggctgggagaatgcgaattttctgga	
R01 3 (151-171) R	ggggaccactttgtacaagaaagctgggtcctacgagaactccacgtcgatttc	
R01 5 (301-321) R	ggggaccactttgtacaagaaagctgggtcctattccgggcagtcctgcggga	
R01 7 (451-471) R	ggggaccactttgtacaagaaagctgggtcctactccagaaaattcgcattctc	
R01 8 (607-621) R	ggggaccactttgtacaagaaagctgggtcctaaaaacaatttgaaaatttttc	

Because the Y2H domain primers used a series of pairwise combinations, no consistent product size was generated. To conserve space, the product size column was removed as the Gateway tagged primers are quite long. Also, all Y2H domain reactions used the EL1 PCR program and the PCR program column was removed. Underlined sequence indicates Gateway recombination cloning site.

Table 8. continued

Name	Sequence 5'-3'	Use
rfs-1 domain 3a-F	ggggacaagtttgtacaaaaaagcaggctgggaaaacattgacgctattctc	Further Y2H analysis of RFS-1 domain three. The domain was broken broken into four fragments using pairwise combinations of rfs-1 4-F, rfs-1 domain 3a, b, and c-F with rfs-1 7 R, rfs-1 domain 3a, b, and c-R. Fragments were Gateway cloned into entry vectors then transferred into Y2H vectors. rfs-1 4-F and rfs-1 7R were used to generate fragment three and are detailed on the preceeding page.
rfs-1 domain 3b-F	ggggacaagtttgtacaaaaaagcaggctggagatcaatgcaatctgatgtt	
rfs-1 domain 3c-F	ggggacaagtttgtacaaaaaagcaggctgggagattactgtgattttgaca	
rfs-1 domain 3a-R	ggggaccactttgtacaagaaagctgggtcctagagaatagcgtcaatgttttc	
rfs-1 domain 3b-R	ggggaccactttgtacaagaaagctgggtcctaaacatcagattgcattgatct	
rfs-1 domain 3c-R	ggggaccactttgtacaagaaagctgggtcctatgtcaaaatcacagtaatctc	
Helix 3-1 5gly F	ggggacaagtttgtacaaaaaagcaggctggggtggtggtggtggtaaaattg cggagcttcaggat	Further structural Y2H analysis of RFS-1 domain three . Domains were predicted based on modelling of the vertebrate paralogs structure (Miller *et al.*, 2004) . The fragments were Gateway cloned into an entry vector, then transferred into Y2H vectors. Glycine linkers (gly) were added to the forward primers to overcome any steric hindrance. All pairwise combinations of motifs in domain three were cloned.
Helix 3-1 F	ggggacaagtttgtacaaaaaagcaggctgg aaaattgcggagcttcaggat	
Helix 3-1 R	ggggaccactttgtacaagaaagctgggtccta ttgtagatttattgtatccaa	
Barrel 3-1 (WalkerB) 5gly F	ggggacaagtttgtacaaaaaagcaggctggggtggtggtggtggt caattggtgattgttgaaaac	
Barrel 3-1 (WalkerB) F	ggggacaagtttgtacaaaaaagcaggctgg caattggtgattgttgaaaac	
Barrel 3-1 (WalkerB) R	ggggaccactttgtacaagaaagctgggtccta agcgtcaatgttttcaacaat	

Table 8. continued

Name	Sequence 5'-3'	Use
Helix 3-2a 5gly F	ggggacaagtttgtacaaaaaagcaggctggggtggtggtggtggt attctccatgatactgtttat	Helix 3-1 amplifies KIAELQDSLTRFLDTINLQ
Helix 3-2a F	ggggacaagtttgtacaaaaaagcaggctggattctccatgatactgtttat	Barrel 3-1 (WalkerB) amplifies QLVIVENIDA
Helix 3-2b 5gly F	ggggacaagtttgtacaaaaaagcaggctggggtggtggtggtggttatcata aggaaatgggaaga	Helix 3-2a amplifies ILHDTVYHKEMGRSMQSDVVERIRK
Helix 3-2b F	ggggacaagtttgtacaaaaaagcaggctggtatcataaggaaatgggaaga	Helix 3-2b amplifies YHKEMGRSMQSDVVERIRK
Helix 3-2 R	ggggaccactttgtacaagaaagctgggtcctattttctgattctctcgacaac	Barrel 3-2 amplifies LEITVILTNHIT
Barrel 3-2 5gly F	ggggacaagtttgtacaaaaaagcaggctggggtggtggtggtggtttagaga ttactgtgattttg	Barrel 3-2 amplifies LEITVILTNHIT
Barrel 3-2 F	ggggacaagtttgtacaaaaaagcaggctggttagagattactgtgattttg	
Barrel 3-2 R	ggggaccactttgtacaagaaagctgggtcctatgtaatgtgatttgtcaaaat	

Reprints of papers to which this author has contributed (see following pages):

Ward, J.D., Barber, L.J., Petalcorin, M.I., Yanowitz, J. and Boulton, S.J. (2007). **Replication blocking lesions present a unique substrate for homologous recombination.** *Embo J* **26**(14): 3384-3396.

Goodyer, W., Kaitna, S., Couteau, F., Ward, J.D., Boulton, S.J. and Zetka, M. (2008). **HTP-3 Links DSB Formation with Homolog Pairing and Crossing Over during C. elegans Meiosis.** *Dev Cell* **14**(2): 263-274.

Adamo, A., Montemauri, P., Silva, N., Ward, J.D., Boulton, S.J. and La Volpe, A. (2008). **BRC-1 acts in the inter-sister pathway of meiotic double-strand break repair.** *EMBO Rep* **9**(3): 287-292.

Youds, J.L., Barber, L.J., Ward, J.D., Collis, S.J., O'Neil, N.J., Boulton, S.J. and Rose, A.M. (2008). **DOG-1 is the *Caenorhabditis elegans* BRIP1/FANCJ homologue and functions in interstrand cross-link repair.** *Mol Cell Biol* **28**(5): 1470-1479

Collis, S.J., Barber, L.J., Clark, A.J., Martin, J.S., Ward, J.D. and Boulton, S.J. (2007). **HCLK2 is essential for the mammalian S-phase checkpoint and impacts on Chk1 stability.** *Nat Cell Biol* **9**(4): 391-401.

Collis, S.J., Barber, L.J., Ward, J.D., Martin, J.S. and Boulton, S.J. (2006). ***C. elegans* FANCD2 responds to replication stress and functions in interstrand cross-link repair.** *DNA Repair (Amst)* **5**(11): 1398-1406.